UNIVERSITY OF CALIFORNIA
RIVERSIDE

Astrocyte Mediation of Neuronal Activity Through Cellular Volume Change

A Dissertation submitted in partial satisfaction
of the requirements for the degree of

Doctor of Philosophy

in

Biomedical Sciences

by

Erin Marie Walch

December 2021

Dissertation Committee:

Dr. Todd Fiacco, Chairperson
Dr. Devin Binder
Dr. Marcus Kaul

The Dissertation of Erin Marie Walch is approved:

_____

_____

_____

Committee Chairperson

University of California, Riverside

Acknowledgments

I would like to acknowledge my mentors and colleagues for their contributions to the data acquisition, analysis and writing showcased in this dissertation. Work from chapter 1 was previously published in ASN Neuro, the journal of the American Society for Neurochemistry, in September 2020. The co-authors of this work included: Dr. Thomas Murphy, Nicholas Cuvelier, Murad Aldoghmi, Cristine Morozova, Jordan Donohue, Gaby Young, Anjua Samant, Stacy Garcia, Camila Alvarez, Alex Bilas, David Davila, Dr. Devin Binder and Dr. Todd Fiacco.

My graduate studies were financially supported by UC Riverside through the Biomedical Sciences Pease Cancer Fellowship (2018), the Graduate Research Mentorship Program fellowship (2018), the Graduate Dean's Dissertation Research Grant (2021), and the Dissertation Year Program fellowship (2021).

Dedication

This dissertation is dedicated to my loving parents, Jill and Patrick Walch, who tirelessly supported my educational aspirations and made it possible for me to develop into the scientist I am today. I would not have attained a doctorate without your unwavering support over the last twenty-eight years.

ABSTRACT OF THE DISSERTATION

Astrocyte Mediation of Neuronal Activity Through Cellular Volume Change

by

Erin Marie Walch

Doctor of Philosophy, Graduate Program in Biomedical Sciences
University of California, Riverside, December 2021
Dr. Todd Fiacco, Chairperson

Astrocytes are a type of glial cell found in the CNS and play important physiological roles in maintaining homeostasis of the extracellular space. They are implicated in maintaining extracellular concentrations of certain ions and molecules, including the excitatory neurotransmitter glutamate. Astrocyte volume is strongly effected by changes in the extracellular environment, a phenomenon that is widely recognized and undisputed. Under both physiological and pathological circumstances, astrocyte volume changes can occur and have noticeable effects on the activity of adjacent neurons. This dissertation aimed to (1) characterize astrocyte volume increases that occur in the presence of elevated extracellular potassium, (2) isolate astrocyte- swelling-specific effects on neuronal excitability in a model of elevated extracellular potassium, and (3) ascertain the role of volume-regulated anion channel function in astrocyte volume change and alterations in neuronal excitability.

Table of Contents

Chapter 3

Chapter 4

List of Figures

Introduction

Chapter 1

Chapter 2

Appendix

Introduction

A little over thirty years ago, R.K. Orkand wrote: “the observations delineating glial membrane properties and processes that have given us a physiological basis for glial function have been made in a variety of model systems under admittedly unphysiological conditions” (Orkand, 1986). Since then, and despite progress made in imaging systems, transgenic lines, and *in vivo* models, the field has struggled to understand brain cell swelling and how best to measure it. Direct measurements are surprisingly lacking and therefore cell volume fluctuations have been inferred from measurements of the brain interstitial space in many instances. Knowledge of ion channels, pumps and transporters expressed by astrocytes has steadily grown, but understanding their roles in cell volume have proven difficult and controversial. Information about how water itself crosses cellular membranes is extremely limited and often not addressed in most studies. This likely stems from limitations in methods used to quantify cell volume and the many ways in which cell swelling has been modeled experimentally. In an effort to understand these divergences, we will provide a critical analysis of the methodologies and conclude with a summary model of proposed mechanisms underlying astrocyte volume changes with particular emphasis on processes hypothesized to control the movement of water molecules across astrocytic membranes.

Cell swelling: Why is it important?

Volume regulation is an essential process for all cells in the body. Fluctuating water content in cells can affect tightly regulated concentrations of cytosolic ions and molecules, triggering molecular pathways that maintain homeostasis (Jentsch, 2016). The phenomenon of cellular swelling can be linked to robust physiological responses orchestrated at the tissue level, but can also stem from unchecked pathological processes. In brain, glial cells in particular have been implicated in the swelling responses of nervous tissue under most physiological conditions, while the bulk of evidence suggests that neurons contribute to swelling of brain tissue in pathological situations including cortical spreading depression, energy failure and excitotoxicity.

Cell swelling modulates tissue excitability in a very significant way. Astrocytes play important housekeeping roles in maintenance of ion and neurotransmitter concentrations, and undergo transient or persistent volume changes in response to varying levels of neuronal activity. As astrocytes take up water, the volume of the extracellular space (ECS) decreases, limiting diffusion of ions, small molecules, and neurotransmitters. As the ECS shrinks, the effective concentration of the excitatory neurotransmitter glutamate increases (Ransom et al., 1986), increasing ionotropic glutamate receptor activation, neuronal depolarization and synchrony of neuronal firing (Lauderdale et al., 2015). Simply raising extracellular potassium concentration by ~5 mM decreases the size of the ECS and triggers electrographic seizure activity in the CA1 region of hippocampus (Traynelis and Dingledine, 1988). Even in conditions in which synaptic activity is blocked pre- and post-synaptically (low [Ca^{2+}], EGTA, DNQX, AP5), simply generating

tissue swelling with hypoosmotic ACSF can elicit epileptiform activity in slices (Dudek et al., 1990). This suggests a direct correlation between tissue swelling and excitability. Using a technique called fluorescence recovery after photobleaching (FRAP), the diffusional capacity of the ECS was quantified *in vivo* using anesthetized mice with open craniotomy. During either administration of water i.p. or the pro-convulsant drug PTZ, ECS diffusion was hindered in the mouse cortex, sometimes promoting dead-space microdomains in the cortical tissue that occurred *prior* to seizure initiation (Binder et al., 2004). In slices, application of hyperosmolar ACSF, which initiates expansion of the ECS, has been shown to reduce or completely block epileptiform activity brought on by hypoosmolar ACSF (Kilb et al., 2006) or high K^+ (Traynelis and Dingledine, 1989). In other models of epilepsy, such as low-[Mg^{2+}] ACSF application to hippocampal slices, decreases in osmolarity led to increased seizure duration, while increases in osmolarity produced the opposite effect (Shahar et al., 2009). The hypoosmolar model of cell swelling generates excitatory currents in CA1 hippocampal neurons, even in the presence of tetrodotoxin to block synaptic activity. These events, known as slow inward currents (SICs), are speculated to be the product of extrasynaptic NMDA receptor activation, as they are nearly abolished in the presence of the NR2B subunit selective NMDA receptor antagonist Ro 25-6981 (Lauderdale et al., 2015). Further single-cell imaging experiments in slices have shown that astrocyte swelling directly precedes the onset of SICs in the hypoosmolar model of acute cellular edema (Murphy et al., 2017).

Astrocyte swelling also occurs in a number of disease processes. The excessive energy demands of the brain require adequate flow of oxygen and glucose, which are

transported to cells via arterioles and capillaries. Minimal intercapillary distance (MID) is important for ensuring rich oxygenation and nutrient supply to tissues. With astrocyte swelling, distortion of the tissue landscape dramatically reduces neuronal access to the vasculature by increasing MID, putting a strain on the resources of nearby neurons and increasing the risk of hypoxia and necrosis (Bourke et al., 1980). In a mouse model of acute liver failure, the development of hyperammonemia leads to cerebral edema, largely mediated by the swelling of astrocytes (Lichter-Konecki et al., 2008). Cerebral edema is characterized by increasing intracranial pressure (ICP) and elevated brain water content, which enters the tissue through the astrocytic endfeet apposing the vasculature. These endfeet express water-passing channels (aquaporins) that aid in the movement of water, and their upregulation is known to increase the severity of vasogenic edema (Yang et al., 2008). After injury and during neurodegeneration, astrocytes are known to develop reactive phenotypes, which can undergo maladaptive dysregulation of key channels normally expressed at the endfeet, precipitating swelling (Wetherington et al., 2008). After ischemia in the retina, swollen astrocytes have been shown to down-regulate potassium conductance and redistribute Kir4.1 channels away from the vasculature (Pannicke et al., 2004). This swelling can be appreciated clinically with diffusion-weighted imaging, and is a hallmark in scans after traumatic brain injury (Badaut et al., 2011). In the rare megalencephalic leukoencephalopathy with subcortical cysts (MLC) disease, the defective MLC1 protein alters the ability of astrocytes to regulate their volume, with further progression leading to white matter swelling abnormalities (Bugiani et al., 2017). After transient ischemia, the widely-expressed volume regulated anion

channel (VRAC) is activated in astrocytes during swelling and releases glutamate, contributing to an excitotoxic environment. When delivered by intracisternal microdialysis, the VRAC inhibitor 4-[(2-Butyl-6,7-dichloro-2-cyclopentyl-2,3-dihydro-1-oxo-1*H*-inden-5-yl)oxy]butanoic acid (DCPIB) reduced glutamate in the CSF as well as infarct size in a model of stroke (Zhang et al., 2008). Similarly in a transgenic mouse model, conditional ablation of VRAC also effectively reduced infarct size following stroke (Yang et al., 2019). These studies illustrate the impacts of cell and brain tissue swelling in modulating neuronal excitability and overall health and survival of brain tissue in injury and disease.

Measurements of cell swelling

Prior to delving into possible mechanisms underlying acute astrocyte volume changes, it is useful to discuss the various techniques which have been used to measure cell volume along with their limitations. In the vast majority of publications the actual volume of the astrocytes (or neurons) is never measured. Cell volume alterations have been inferred indirectly by measuring intrinsic optical signals (IOS), changes in extracellular ion concentrations, or volume/resistance of the ECS. With ongoing improvement in microscopy, imaging tools and software-based analysis programs, the field has moved increasingly towards visualization of the astrocytes or neurons themselves to quantitatively assess their volume - although even these methodologies have their limitations. What implications this may have for the field are likely also rooted in how

data are analyzed, so that quantitative predictions contain minimal variability and are therefore more reproducible between groups.

Extracellular tissue resistance

One indicator of cell volume change is tissue resistance, recorded by microelectrodes placed within the ECS of intact brain tissue (Traynelis and Dingledine, 1989). According to Ohm's Law:

$V = IR$, where V refers to voltage, I refers to current and R refers to resistance.

Thus, to record changes in ECS resistance, a stimulating electrode generates electric current, while recording electrodes in the ECS measure ΔV between electrodes. With this information, tissue resistance can be calculated as:

$$\Delta R = \frac{\Delta V}{I}$$

Over time, this imparts information regarding the shrinkage or expansion of the ECS during an experiment. This technique was used by Traynelis and Dingledine (1988, 1989) to record the effects of elevated extracellular K^+ on seizure activity in rat hippocampal slices. These studies revealed the critical role of cell swelling (presumed to be astrocytic) in recurring ictal or seizure-like activity.

Membrane permeant & impermeant probes

Membrane impermeant probes are a useful tool that have been used to make measurements relative to space or concentration of units within a space. Modern studies continue to supplement experiments with these techniques, as they are a dependable method for making predictions about volume change occurring in bulk tissue. One such probe is the radioactive 3-O-methyl-D-glucose (3OMDG), which is a permeable molecule that crosses the membrane via the facilitated diffusion mechanism normally utilized by sugars. Because 3OMDG transport is entirely concentration dependent, flux will stop at equilibrium between the ECS and intracellular compartments. Therefore, bulk changes in radioactive content between compartments are the result of volume change in response to a treatment. This technique was used in cultured astrocytes to measure intracellular volume (Kletzien et al., 1975). However, flux of 3OMDG could be a confounding variable when measuring osmotic gradients during experiments, which lessens the appeal of this measurement approach. Application of phloretin can trap 3OMDG inside cells, a property that could be useful for retaining the current volume of a cell (Kletzien et al., 1975).

Another method relies on monitoring the concentration of the cation tetramethylammonium (TMA^+). Potassium-sensitive microelectrodes normally record changes of $[K^+]_o$ in intact tissue, but encounter strong electrical interference when exposed to TMA^+ solutions. The magnitude of this interference can be used to calculate relative $[TMA^+]$ in the ECS (Dietzel et al., 1980). The volume of the ECS is negatively correlated with $[TMA^+]$, as shrinkage of the ECS increases $[TMA^+]$. Importantly, TMA^+

cations are impermeable to cellular membranes on short timescales, allowing changes in [TMA^+] to faithfully represent changes in ECS volume. Choline (a similar agent) and TMA-sensitive electrodes have widely been used historically (Ransom et al., 1985; Ballanyi et al., 1990) and remain in use today (Haj-Yasein et al., 2012; Larsen et al., 2014; Larsen and MacAulay, 2017) to measure ECS volume changes. Tortuosity values can also be calculated using both [TMA^+] and diffusional capabilites in the ECS. Changes in tortuosity relate to changes in both the landscape and volume of the ECS, where diffusion of TMA^+ cations may be impeded by physical structures in the neuropil (Kilb et al., 2006). One unfortunate aspect of this technique requires insertion of the electrodes into tissue, thereby introducing damage into the site of observation prior to the start of experiments. Additionally, this measure does not give any information about swelling of different cell types that may be contributing to changes in ECS volume.

Another method enables the measurement of diffusion of high molecular-weight fluorescent dextrans in the ECS, which provides information about molecular constriction and crowding around astrocytes. The introduction of the fluorescein isothiocyanate (FITC)-labeled dextrans can be performed in a minimally-invasive and *in vivo* procedure (Binder et al., 2004). The ACSF-dissolved molecule is loaded onto the exposed dural surface of a mouse, post-craniectomy. Photobleaching of the FITC molecules is performed, and FRAP data is acquired over time points after the bleaching pulse. Slower FRAP values indicate reduced diffusion in the ECS, and subsequently can identify dead space microdomains. This is an important tool, as it can reveal differences in subcompartments of the ECS as opposed to ECS volume as a whole. Another advantage

of this technique includes the various molecular weights of dextrans that can be used to quantify information about how ECS diffusion is affected by swelling.

Membrane-permeant fluorescent probes have also been used to visualize and record changes in astrocyte volume based on changes in fluorescence intensity. Hansson (1994) used a pluronic acid buffer to solubilize the fluorophore fura-2/AM for passive uptake into cells; similarly, calcein-AM can be used (Gunnarson et al., 2008). Enzymatic cleavage of the AM ester yields it membrane impermeant once inside the cell. Once loaded, the cells can be measured for fluorescence intensity. Any changes in this value are proportional to changes in intracellular water content, such that fluorescence intensity decreases with increasing intracellular water content and vice-versa. This "dimming" of fluorescence intensity was used by Murphy et al. (2017) as an alternate method to measure volume changes of neurons located deep in tissue that was otherwise difficult to quantify using thresholding analysis.

Intrinsic optical signals (IOS)

While still controversial, many laboratories have relied on IOS as a reporter for morphological tissue changes in the brain. As cellular volume increases in the tissue, the amount of light scattering decreases, resulting in a change in IOS that corresponds to change in bulk cell volume. The measurements are taken at relatively low magnification and therefore provide an indication of bulk swelling (or shrinking) of cells at low resolution. The challenge in using IOS data involves making assumptions as to the physiological triggers of the optical phenomenon. Some groups attribute IOS to very

specific changes in the tissue, while others argue that the signals can be generated from multiple biological processes. In one of the early studies by Andrew and MacVicar (1994), it was shown that stronger IOS (increased light transmittance) could be generated during an experiment with hypotonic and high-potassium application to astrocytes. This provided early evidence that changes in IOS corresponded to increased light transmittance, and presumably cell swelling. Other groups have used this technique with apparent success (Holthoff and Witte, 1996), and the utility of an endogenous swelling reporter system saved time and resources. To measure astrocyte volume changes over time, a preliminary control image was first taken. This IOS signal was then subtracted from subsequent IOS images taken during the treatment application.

To critically evaluate the technique, another group compared IOS signals to [TMA^+] measurements in the ECS, as well as other relevant factors (Sykova et al., 2003). The authors found that in response to neuronal stimulation, TMA and IOS measurements of astrocyte swelling did not correspond temporally. The IOS signals did not appear to correlate with increasing potassium concentration, even though increasing potassium has been shown to increase swelling. Furthermore, IOS signals did not match other parameters used to assess swelling or ECS shrinkage, such as tortuosity or diffusion coefficients. A more recent study took a broader definition of IOS, and simply correlated changes in tissue light scattering as an output for cell morphological change (Kitaura et al., 2009). The challenge in using this form of measurement lies with the broad interpretation of IOS, its low resolution, lack of cell-specific volume estimates, and the lack of corroboration with other methods to measure cell volume.

Light microscopy and image analysis

The progression of fluorescence microscopy techniques and development of transgenic fluorescent tools has enabled groups to characterize astrocyte morphology with sufficient resolution to make definitive conclusions about cell volume changes in response to stimuli in real time. Current optical and analysis limitations dictate that conservative estimates be integrated into the analysis to prevent predictions of volume change of structures beyond the image resolution. Despite these challenges, current analysis methods are rapidly improving. A core common to many imaging protocols relies on taking stacks of images in the z-axis through the entire cell and recompiling them to perform analysis of volume change during treatments (Figure 1). In a study using differential interference contrast (DIC) optics, cross-sectional images were analyzed on the basis of soma area, and distance of (visible) processes from the soma (Su et al., 2002a). Changes in these areas or distances over the course of treatment were considered estimates of volume change. Encouragingly, a decrease in osmolarity of solutions applied to astrocyte cultures was correlated with an increase in the cross-sectional areas of astrocytes.

Confocal fluorescence microscopy provides the ability to label astrocytes with fluorescent dyes such as green fluorescent protein (GFP) or Sulforhodamine 101 (SR-101). In one study, when compiling a z-stack, a series of images was collected along the z-axis in rapid succession (Chvatal et al., 2007). This process was repeated over a desired time course, and the subsequently generated z-stacks were flattened and filtered by

imaging software. The soma and processes were then analyzed by a method called thresholding, wherein pixels above and below certain intensities are assigned grayscale values, thereby binning the pixels into manageable groups. After thresholding, the areas of the soma and processes were calculated using a method called edge detection, which involves software recognition of sharp changes in brightness within the image. At these points of contrast, lines are generated to form an edge, which presumably will define the area of the astrocyte. This procedure has been replicated by many labs using both confocal (Benesova et al., 2012; Murphy et al., 2017) and higher resolution two-photon laser scanning microscopy (Dibaj et al., 2007; Nase et al., 2008; Risher et al., 2009; Florence et al., 2012), with slight variations. With rapid scanning features, optical stacks through astrocytes can be generated in 15-20 s or less, enabling minute-by-minute assessment of rapid cell volume changes (Murphy et al., 2017; Walch et al., 2020). Availability of transgenic mice with fluorescent reporters expressed downstream of a cell-type specific promoter such as Thy-1-eGFP for pyramidal neurons or lox-stop-lox (lsl)-TdTomato for specific Cre lines offer improved signal-to-noise over bulk dyes or other cytoplasmic indicators.

Some protocols have used maximum intensity projections (Risher et al., 2009; Florence et al., 2012; Murphy et al., 2017) for the compilation of z-stacks, which allows for greater image dimensionality. This is a technique that is commonly used in radiology specialties such as positron emission tomography. In some cases a fixed space is defined in which apparent volume changes will be measured, while others manually draw regions of interest (ROIs) during the analysis process. This is a step in which group-to-group

variance may become amplified, and as such presents a problem for reproducibility of data. For example, Nase et al. (2008) chose to perform deconvolution on collected z-stacks and reassembled them into 3D formulations, where volume of the astrocyte could then be calculated in real-time. In the work of Kirov and colleagues (Andrew et al., 2007; Risher et al., 2009), four separate methods were used to measure cell volume: 1) Comparison of gray value pixel distributions, where an increase in the proportion of white pixels (representing GFP staining) signified an expansion of the imaged structure into adjacent space, assuming overall brightness remained constant; 2) Control profiles of somata in stacked images digitally traced by hand and filled to create a mask from behind, through which swelling could be discerned; 3) Overlay of pseudocolored control and experimental image stacks; and 4) Measurement of changes in a polygonal area drawn by linking cellular landmarks, where an expanding polygonal area indicated components moving apart in space (Andrew et al., 2007). Between their 2007 and 2009 studies, this research team shifted away from analysis of gray value pixel distributions in favor of overlay of pseudocolored maximum intensity projections (MIP), illustrating chronological improvements in analysis strategy that can make comparison of findings even within the same research team potentially difficult. This shift in strategy is noteworthy in that, using the preferred technique of overlay of thresholded MIP image stacks, Murphy et al. (2017) found clear evidence of rapid neuronal swelling in hypoosmolar conditions where Andrew et al. (2007) reported no neuronal volume change based on analysis of gray value pixel distributions. These differences are likely reflected

by the difference in analysis strategy, as some of the neuronal images from the 2007 study appear to show neuronal swelling.

Both the Kirov and Nase groups commented on the limitations of current microscopy technologies, given that most astrocyte processes are beyond the resolution of even two-photon microscopes. Another shared grievance involved the effects of tissue swelling on image distortion, wherein the astrocyte itself becomes harder to track and easily lost (Nase et al., 2008). As the field awaits improved image resolution, transgenic approaches and detection tools, an achievable goal may be to standardize the image analysis process, so that data can be more easily compared within and across labs with minimal bias.

Optical limitations & new directions to measure cell volume changes

Studies to date performing real-time volume imaging of fluorescent astrocytes to directly measure cell volume have been limited mainly to analysis of the soma. Some imaging of large astrocyte processes or a large field of smaller processes has been possible using strong swelling paradigms over longer timescales (10-20 min), but with increased variability of responses between selected regions of interest (Benesova et al., 2012; Chvatal et al., 2007; Dibaj et al., 2007). Su et al. (2002) measured the length of processes from the astrocyte soma *in vitro* as an indicator of relative volume change. However, a method capable of measuring the area of large flattened processes of cultured astroglia is unlikely to be useful to estimate volume changes in the much finer and more complex astrocyte processes in intact brain tissue. Dibaj et al. (2007) chose to only measure visible

processes within a fixed distance of the astrocyte soma. Their results after 10 minutes in 33% hypoosmolar ACSF suggested that Kir4.1 may play a role in volume regulation in the processes, but not in the soma. This suggests that the soma and processes may have differing expression of volume regulating mechanisms. Anderova, Sykova and colleagues were able to categorize different classes of astrocytes based on swelling phenotypes involving the processes and soma after either prolonged oxygen-glucose deprivation (OGD) or exposure to 33% hypoosmolar ACSF (Chvatal et al., 2007; Benesova et al., 2012). In "low-response astrocytes," swelling in the processes was the same as in the soma, whereas in "high-response astrocytes" the swelling of the processes was greater than in the soma. Beyond current reach is visualization of ultrafine structures in astrocytes, such as the fine branching processes in close proximity to synapses. While the soma is the largest contiguous part of the cell, the collective surface area of these other structures implicates their importance in the swelling process. Overall, the ability to reliably measure volume changes in astrocyte processes using physiological levels of stimulation has not been attainable and could greatly improve understanding of cell swelling and volume-regulating mechanisms.

Mechanisms of astrocyte swelling

Common experimental models used to induce cell swelling

In attempting to identify mechanisms underlying astrocyte swelling, there are notable discrepancies in results that likely stem from different swelling models and

methodologies of measurement. Astrocyte swelling has been induced using in a variety of experimental conditions spanning the physiological to pathological. This range of conditions runs from: 1) mild to moderate levels of synaptic activity modelled by stimulation of neuronal afferents such as the Schaffer collaterals in the hippocampus; 2) sustained bath increases in extracellular K^+ concentration within a physiological range from a few millimolar up to 10-15 mM, which approaches ceiling $[K^+]_o$ levels observed during seizure; 3) models of brain injury such as stroke by OGD; or 4) use of very high concentrations of extracellular $[K^+]_o$ which may occur in pathological situations including transiently during spreading depression, or more chronically in cases of energy failure or excitotoxicity. In the more pathological situations it is clear that neurons also participate in rapid swelling responses (Zhou et al. 2010, Rungta et al. 2015, Risher et al. 2007). The most commonly used model of cell swelling is application of hypoosmolar solution by simple dilution with distilled water or removal of NaCl from the extracellular medium. Hypoosmolar solutions have been described as ranging from mild to severe in terms of percent reduction (17% to up to 60%). This model is particularly intriguing in that it introduces an instantaneous osmotic gradient across the cell membrane, as opposed to an osmotic imbalance generated secondarily to application or movement of ions or small molecules. Severe hypoosmolarity provides a useful model for pathological situations such as of hyponatremia or water intoxication. For the scope of this review, we will focus on mechanisms of astrocyte volume change associated with elevated extracellular K^+ as would be expected to occur during varying levels of neuronal activity. Most of the transmembrane pathways theorized to contribute to astrocyte swelling in elevated $[K^+]_o$

are discussed individually but can be visually summarized in Figure 2. The hypoosmolar model will be revisited briefly in the context of how water actually traverses the cell membrane.

Early Theories on Potassium Buffering and effects on the brain extracellular space

Current knowledge of astrocyte swelling is built upon early studies characterizing ion composition of the ECS. Even in early studies, it was observed that neuronal excitation brought about increased K^+ permeability in neighboring glial cells (Lundandersen and Hertz, 1970). A coupling of sodium and potassium in the medium was observed to be necessary for an intracellular accumulation of potassium to trigger swelling (Lundandersen and Hertz, 1970). Similarly, it was observed that electrical stimulation of nerve cells could trigger glial swelling. In further experiments with sustained stimulation of neurons nearing epileptic bursting frequency, a continuous increase of potassium was measured in the extracellular space (Dietzel et al., 1980). This concentration of potassium was far above the "ceiling level" thought to border between 10-15 mM in the ECS. The way in which glia were thought to respond to such high concentrations of potassium was termed spatial buffering, a process in which $[K^+]$ itself does not change, but potassium ions are redistributed from sources to sinks (Orkand, 1986). There would be a conservation of ions and a displacement of their location from sites of high neuronal activity to glia in quiescent areas of the ECS. It was proposed that swelling might occur mainly via spatial buffering and the activity of the Na^+-K^+-ATP-ase (NKA) (Walz et al., 1984). Focus was placed on the theory that large water shifts might occur during the

coupled transit of sodium and potassium across the membrane in a mechanism yet to be elucidated (Walz and Hinks, 1985).

Detailed characterization of the biophysical properties of Müller cells in the retina provided seminal knowledge that later carried important implications for the conductance of glial cells in the CNS and provided evidence for the concept of spatial buffering. It was discovered that the endfeet of Müller glia possessed a higher resting conductance than other regions of the cell (Newman, 1986). This is perhaps one of the earliest indications that glia could differentially express transporters in a region-specific manner. Newman further argued that by using internal pathways of high to low conductance regions in the Müller cell, potassium ions are not so much spatially buffered, as much as siphoned. Spatial buffering lacked a directional relationship, while $[K^+]$ siphoning alluded to the push-pull relationship directing ionic currents. In the retina, siphoning directed potassium into the vitreous humor in a mechanism that might parallel how astrocytes direct excess potassium into the vasculature. This suggested that buffering is not simply a homogenous diffusive capacity of astrocytes, but an ability to direct potassium from individual sources to a shared 'sink', such as a nearby capillary.

It was proposed that potassium inwardly-rectifying (Kir) channels, and especially the main glial isoform Kir4.1, might be best suited to initiate siphoning of potassium into glia during physiological conditions based on their preferred conductance during hyperpolarization (Kofuji et al., 2000). Orkand supplemented Newman's hypothesis, proposing that the Nernst potential for potassium would affect the flux through Kir channels such that the initial influx of potassium would depolarize the surrounding

membrane enough to reduce—but not reverse—the inward driving force on potassium in the locally high $[K^+]_o$ region. As potassium would migrate through the astrocyte towards the endfoot region, the now depolarized membrane would direct the driving force for potassium outward through Kir and into the apposed vasculature (Orkand, 1986). After potassium movement into the vasculature, the maintenance of the membrane potential via NKA would be important to return to homeostatic conditions. This early work and the role of Kir channels in K^+ spatial buffering has become the prevailing theory behind extracellular K^+ regulation.

Kir4.1 and AQP4: A mechanism for K^+ and water entry or exit from astrocytes?

Work on potassium buffering and cell swelling was reinvigorated by a study detailing an impressive localization of the water channel aquaporin-4 (AQP4) to the endfeet bordering the vasculature in comparison to sparse expression facing the neuropil (Nielsen et al., 1997). The selective expression of AQP4 in astrocytes supported the complimentary theories of Newman and Orkand, as the Kir channels could provide the solute movement necessary to pull water into astrocytes via AQP4 channels to support K^+ spatial buffering, and give astrocytes a unique role in water handling in the brain in both physiological and pathological conditions.

However, subsequent work on Kir channels and AQP4 provides additional perspective on their roles in K^+ buffering and effects on ECS volume. The role of Kir in K^+ buffering was initially challenged by the work of Meeks and Mennerick (2007), who found that even though $BaCl_2$ at 100 μM blocked the stimulus-evoked K^+ current in

astrocytes, it did not affect local concentrations of extracellular K^+. More recently, Larsen and MacAulay (2014) reported that Ba^{2+} block of astrocytic Kir4.1 did not significantly affect extracellular K^+ kinetics or contribute to extracellular space volume reduction resulting from high frequency stimulation in the hippocampus. However, locally-applied K^+ by iontophoresis in the presence of Ba^{2+} consistently generated an increase in peak K^+ without affecting post-stimulus decay of $[K^+]_o$. Other studies suggest that in stronger swelling models, Kir appears to be involved in volume homeostasis/recovery rather than initiation of cell swelling. Using time-lapse two-photon microscopy in spinal cord slices, Dibaj et al. (2007) observed prominent swelling of larger astrocyte processes during co-application of hypotonic solution and Ba^{2+} to block Kir, but not in hypotonic solution alone. These observations were replicated in Kir4.1$^{-/-}$ mice, suggesting a role for Kir4.1 in *prevention* of glial process swelling during osmotic stress (Kofuji et al., 2000). Similar observations have been made in the retina. Wurm et al. (2006) found that swelling of Müller glia is dependent upon maturation of Kir4.1 channels. Immature glia that have not yet developmentally upregulated Kir4.1 expression exhibited prominent swelling, whereas mature Müller glia did not. Furthermore, upon pharmacologic block with Ba^{2+}, mature Müller cells swelled similarly to immature cells. The fact that immature glia that do not express Kir4.1 prominently swell is a strong indication that Kir4.1 is important for efflux of K^+ (and water) from the cell rather than uptake in these conditions. The authors concluded that functioning Kir channels are required for rapid osmotic volume *regulation* (Wurm et al., 2006), similar to what has been described for volume-regulated anion channels (Jentsch, 2016).

Similar observations have been made with regard to the role of AQP4 in water movement. A follow-up study to Nielsen et al. (1997) by the Ottersen group conducted in a glial fibrillary acidic protein (GFAP)-driven conditional knockout of AQP4 ($cAQP4^{-/-}$) showed that indeed, astrocytes express AQP4 and not the endothelial cells of the vasculature (Haj-Yasein et al., 2011). Water loading experiments in these mice showed $cAQP4^{-/-}$ astrocytes had decreased uptake of water, but the total brain water content was burdened in comparison to $AQP4^{+/+}$ mice. These findings suggested that AQP4 is important for both influx and efflux of water, and that astrocytes might act as a privileged gating mechanism to control the volumes of the ECS and vasculature. Another $AQP4^{-/-}$ brain slice experiment tested weak vs. strong stimulation of neurons to vary the potassium concentration physiologically (Strohschein et al., 2011). The $AQP4^{-/-}$ slices had reduced K^+ uptake near basal $[K^+]$ in comparison to wild-type slices, but stronger stimulation elicited similar levels of potassium uptake in $AQP4^{-/-}$ and wild-type slices. These experiments suggested that Kir4.1 and AQP4 may be more involved in K^+ and water entry around resting $[K^+]_o$ rather than at higher concentrations. Haj-Yasein et al. (2012) found that $AQP4^{-/-}$ astrocytes actually had more activity-induced ECS shrinkage in comparison to wild-type, suggesting increased cell swelling in $AQP4^{-/-}$ astrocytes. The authors suggested that this would occur if activity-coupled cotransport of water into perisynaptic glia normally is associated with a passive, AQP4-mediated water flux in the opposite direction. Recently it was published that selective inhibition of AQP4 with the drug TGN-020 failed to inhibit stimulus-induced extracellular space shrinkage in hippocampal slices (Toft-Bertelsen et al., 2021). In our own work, we have found that

AQP4 is not required for astrocyte volume increases in either hypoosmolar (Murphy et al., 2017) or raised extracellular K^+ conditions (Walch et al., 2020). Furthermore, AQP4$^{-/-}$ astrocytes swell more than wild type, suggesting a role for AQP4 in cell volume recovery in more extreme swelling conditions. Collectively, the above studies paint a picture suggesting a dual or bidirectional role for AQP4 and Kir4.1 in K^+ handling and volume regulation. During very local and transient increases in $[K^+]_o$ (illustrated in Figures 3A and 4A), Kir4.1 and AQP4 likely participate in K^+ and water uptake from the ECS that does not result in measurable changes in the ECS or cell swelling. During more sustained increases in $[K^+]_o$ (illustrated in Figure 4, C-D) resulting in measurable cell swelling or ECS constriction, the findings support a role for Kir4.1 and AQP4 in removal of K^+ and water from the cell to help regulate cell volume. This prediction is supported by the polarized distribution of Kir4.1 and AQP4 at the perivascular astrocyte endfeet, providing a convenient route to relieve excessive intracellular K^+ and water burden. With improved imaging capability, future studies may be able to detect more localized changes in astrocyte process volume associated with more transient fluxes in K^+.

NKCC and KCC

The conductance of potassium and chloride go hand-in-hand. Evidence of coupled transport of these ions has been known for decades. Co-transporters NKCC1 (sodium-potassium-chloride cotransporter type 1) and KCC (potassium-chloride cotransporter) are responsible for facilitating the movement of ions across the membrane while maintaining

electroneutrality. The net result of this transport affects intracellular osmolarity, with implications on cell volume.

The co-transporter NKCC1 displays an impressive electroneutral role in moving ions, which can trigger a shift in the osmotic gradient (Russell, 2000). Shifts in extra- or intracellular ion concentrations are known to have profound effects on the electrical repulsion and driving forces that manipulate ion movement across the plasma membrane. Simultaneously it is known that changes in the osmotic gradient can trigger water movement, independent of the electrical forces governing the movement of ions. Interestingly, the role of NKCC1 in potassium-induced astrocyte swelling may lie in its ability to transport water directly and in the direction of ion movement but independently of the overall osmotic gradient (Zeuthen, 2010). In an elegant series of experiments, Hamann et al. (2010) monitored the volume change of cultured epithelial cells expressing the co-transporter NKCC1. Using solutions of different ionic or osmotic composition, it became evident that a portion of water flux across the membrane was tied inextricably to movement of ions through NKCC1 (Hamann et al., 2010). This flux of water and ions were shown to be concomitant, suggesting permeability of NKCC1 to water itself. Importantly, through the use of an extracellular membrane-impermeable solute (mannitol), a fraction of water efflux occurred because of the increased osmotic gradient, while the remaining water influx followed the inward driving forces on Na^+ and Cl^-. Impressively, movement of water through NKCC1 directly opposed the energetic force of the osmotic gradient, due to dependence on these ionic driving forces (Hamann et al., 2010). Further work in *Xenopus* oocytes using solutions of elevated potassium and/or

urea confirmed that NKCC1 could ferry over 500 water molecules per protein turnover against a preexisting osmotic gradient (Zeuthen and Macaulay, 2012). Despite a unique role for NKCC1 in water movement, studies in various model systems suggest a contribution to cell swelling only in cases of very strong membrane depolarization at very high $[K^+]_o$.

Both NKCC1 and KCC have been studied in the scope of understanding mechanisms of regulatory volume increase (RVI) or decrease (RVD) in cultured astroglia and other cell types. Early experiments in primary astrocyte cultures revealed that a portion of K^+ uptake could be inhibited with the use of the loop diuretics furosemide and bumetanide, which block NKCC1 and KCC (Kimelberg and Frangakis, 1985). In another experiment, block of NKCC1/KCC prevented some of the astrocyte swelling normally triggered by the presence of hypotonic medium. Similarly in intact optic nerve, application of furosemide and bumetanide markedly depressed IOS signal normally corresponding to perfusion of elevated K^+ solution (MacVicar et al., 2002). In later studies, bumetanide block of NKCC1 in cultured astrocytes reduced potassium-induced swelling measured via DIC microscopy (MacVicar et al., 2002; Su et al., 2002a). Further experiments in astrocytes from NKCC1$^{-/-}$ mice clarified the need for NKCC1 activity to promote astrocyte swelling in elevated $[K^+]_o$ (Su et al., 2002b). However, it should be noted that this swelling occurred under extremely high potassium concentrations (75 mM K^+), far beyond the physiological limits for $[K^+]_o$ in the ECS of intact brain tissue. Therefore the relevance of these findings is up for debate.

While evidence for NKCC and KCC participation in swelling of cultured astroglia is apparent in conditions of strong membrane depolarization at very high $[K^+]_o$, their roles in more physiologically-relevant swelling models is less apparent. A more recent study found that NKCC1 did not play an obvious role in astrocyte K^+ buffering or astrocyte swelling in hippocampal slices post-stimulus (Larsen et al., 2014). Similarly with regard to KCC, its pharmacologic inhibition did not have any effect on ECS shrinkage in a stimulation-induced model of astrocyte swelling in hippocampal slices (Larsen and MacAulay, 2017).

Work in hippocampal slices from young and old mice produced conflicting results regarding the role of NKCC1 in swelling. In younger mice, block of NKCC1 reduced soma swelling in astrocytes, while only in older mice (18 months) did the block lead to a reduction in swelling of the processes (Kolenicova et al., 2020). Regardless of possible age-dependent changes in NKCC1 distribution and expression, astrocytes were exposed to 50 mM $[K^+]_o$ to induce swelling in these experiments, which is again far beyond physiological limits. In our recent study using 10.5 mM $[K^+]_o$ in hippocampal slices, application of the NKCC1-blocker bumetanide did not inhibit astrocyte swelling, suggesting that NKCC1 plays a relatively insignificant role in astrocyte swelling under more physiological concentrations of K^+ (Walch et al., 2020). Thus, our current perspective on the engagement of NKCC1 in the astrocyte swelling process may be heavily model dependent, as well as K^+ concentration specific.

NBCe1

As has been discussed, movement of K^+ ions is directly coupled to water movement and cell swelling, but a potassium-rich ECS can also prime astrocytes for swelling independently of K^+ influx. With bouts of neuronal activity, $[K^+]_o$ increases result in astrocytic membrane depolarization (Anderson et al., 1995). Sodium bicarbonate cotransporter (NBCe1) activity is generated under these depolarized conditions, triggering an inward flux of sodium and bicarbonate ions (Ruminot et al., 2011). The resulting alkalization and pH increases serve as an important signal for glycolysis (Bittner et al., 2011). The major byproducts of astrocytic glycolysis include ATP, pyruvate and lactate. Importantly, lactate released from astrocytes serves as an energy source for active neurons (Brown and Ransom, 2007). The crucial role of NBCe1 in mediating increases in astrocytic glycolysis has been explored in detail by the Barros group (2011). Upon inhibition of NBCe1, K^+-induced depolarization in astrocytes fails to initiate intracellular alkalinization and thus glycolysis (Ruminot et al., 2011). Interestingly, astrocytes from NBCe1 knock-out mice acidify in response to depolarization and intracellular glucose levels rise (Ruminot et al., 2011).

Bicarbonate ion flux through NBCe1 may directly bring about astrocyte swelling. While imaging astrocytes in brain slices, nearly a 20% increase in soma area occurred after dual exposure to potassium and bicarbonate-containing ACSF over an extended time period (~40 minutes) (Florence et al., 2012). In the absence of HCO_3^-, potassium-only exposure over the time period yielded merely a 5% increase in astrocyte soma area. Furthermore, this bicarbonate-mediated swelling could be reduced by nearly 10% with

co-application of 4,4'-Diisothiocyano-2,2'-stilbenedisulfonic Acid (DIDS, an inhibitor of NBCe1) (Florence et al., 2012). Bicarbonate-independent volume changes occurred within the first 10 minutes of K^+ exposure, while bicarbonate-dependent volume increases occurred over approximately 30 minutes of dual potassium-bicarbonate exposure (Florence et al., 2012).

More recently, the MacAulay group stimulated brain slices to induce increases in $[K^+]_o$ and subsequent shrinkage of the ECS (Larsen and MacAulay, 2017). They found that with application of DIDS, approximately 25% of the ECS shrinkage could be inhibited, suggesting that NBCe1 plays a partial role in astrocyte swelling during stimulation-evoked increases in $[K^+]_o$ (Larsen and MacAulay, 2017). In the past year, the Barros group (2019) turned to experiments using NBCe1 knock-out mice, showing that only wild-type astrocytes rapidly metabolized glucose in response to 12 mM $[K^+]_o$, while NBCe1 KO astrocytes did not alter glucose metabolism. Subsequent experiments in NBCe1 KO brain slices showed that stimulation of Schaffer collaterals failed to bring about the intracellular alkalinization and glucose depletion that occurs in astrocytes with functional NBCe1 (Ruminot et al., 2019). When slices were stimulated in the presence of TTX, astrocyte levels of glucose, pyruvate and lactate remained unaltered, reaffirming the role of neuronal K^+ release in priming astrocytes to swell with the uptake of HCO_3^- and enter a glycolytic state (Ruminot et al., 2019). In our own recent work, application of DIDS had no effect on direct astrocyte swelling measurements in 10.5 mM $[K^+]_o$ in acute hippocampal slices (Walch et al., 2020). While these results suggested no role for NBCe1 in astrocyte swelling, it is worthwhile to note that increases in extracellular potassium

were made directly by increasing $[K^+]_o$ in the ACSF, rather than by tissue stimulation. Thus, direct application of potassium may generate a different swelling response compared to stimulation of Schaffer collaterals which will produce a host of cellular responses (neurotransmitter release, ionotropic and metabotropic receptor activation, K^+ release, glutamate uptake, etc.). Overall, studies suggest that stimulation of neuronal afferents facilitates activity of NBCe1, which can lead to astrocyte volume increase. This NBCe1 swelling mechanism likely does not account for all of the astrocyte swelling induced by elevated $[K^+]_o$, given that multiple studies reported only modest reductions in swelling when NBCe1 was inhibited. However, any amount of ECS shrinkage might elevate extracellular glutamate concentration, and thus the activity of adjacent neurons.

Monocarboxylate transporters (MCTs)

Byproducts of glycolysis serve an important role in maintaining the astrocyte-neuron lactate shuttle, wherein astrocytes serve as lactate 'sources' and neurons 'sinks.' Lactate is commonly exchanged between astrocytes and neurons through MCTs in a process known as the "astrocyte-neuron lactate shuttle" (ANLS) (Pellerin et al., 1998; Mächler et al., 2016). Interactions between MCT and NBCe1 arise during shifts in intracellular pH. Elevations in extracellular $[K^+]_o$ activate NBCe1 and trigger inward fluxes of bicarbonate, alkalinizing the cell. In response, the rate of glycolysis and therefore the intracellular concentration of lactate, increase. MCT provide an outlet for this lactate load, in the proximity of adjacent neurons. In culture, oocytes expressing NBCe1 and MCT experienced more lactate flux in comparison to oocytes expressing MCT alone,

likely because the two channels cooperate in maintaining acid/base dynamics (Becker et al., 2004). Immunohistochemistry in mouse optic nerve showed MCT1 expression in astrocytes responsible for shuttling lactate and MCT2 on neurofilaments that actively uptake this energy source into neurons (Tekkok et al., 2005). In the same study, it was shown that in conditions without lactate or glucose, neurons encounter apparent energy failure and loss of action potentials. This implies the necessity of MCT function to support the ANLS, and thus the energetic needs of neurons.

Some evidence suggests a role for MCTs in astrocyte swelling responses. Indeed, early observations in bullfrog retinal epithelium indicated that a portion of water movement was tied to lactate permeability, such that water could be transported against osmotic gradients if coupled with lactate movement (Zeuthen et al., 1996). In healthy rat brain slice, concurrent stimulation of the Schaffer collaterals and block of MCT with α-cyano-4-hydroxycinnamic acid (4-CIN) limited changes in the volume of the ECS (Larsen and MacAulay, 2017). Normally, stimulation brings about shrinkage of the ECS as the astrocytes swell, but 4-CIN co-application mitigated ~25% of this volume change, suggesting a role for MCT in astrocytic swelling. Most recently, co-expression of MCT and AQP9 channels has been investigated in retinal ganglion cells after optic nerve crush injury (Mori et al., 2020). AQP9 is expressed by astrocytes, is said to be water and lactate permeable, and thus may contribute to the volume changes of astrocytes that are actively participating in the ANLS. Collectively, these studies suggest that lactate movement may be a key driver of astrocytic volume changes. However, it remains unclear how export of lactate from astrocytes could be tied to water movement into the cell to promote swelling.

Perhaps some of the volume changes ascribed to MCTs are driven by the synergistic activation of the NBCe1.

Glutamate transporters

Under physiological conditions, ambient glutamate has been estimated to range anywhere from 2 nM – 2 μM (Herman and Jahr, 2007). Nanomolar concentrations of glutamate are enough to tonically activate NMDARs, reinforcing the necessity of tight regulation of $[glutamate]_o$ in brain tissue. In astrocytes, excitatory amino acid transporters 1 (EAAT1) and 2 (rodent analogs GLAST and GLT-1, respectively) mediate uptake of glutamate from the ECS to balance tissue excitability and prevent excitotoxicity. *In vivo* inhibition of glutamate transporter synthesis in rats leads to elevated $[glutamate]_o$ and excitotoxicity, seen behaviorally as onset of paralysis (Rothstein et al., 1996). Thus, activity of glutamate transporters in response to neuronal excitatory synaptic transmission are nearly always active may mediate some of the volume changes in astrocytes.

In early work, direct application of glutamate to cultured C6 glioma cells triggered an increase in cell volume, which corresponded to an increase in glutamate uptake (Schneider et al., 1992). Similarly, glutamate application to Müller glia from rat *ex vivo* retinal tissue generated swelling (Izumi et al., 1999). This volume increase could be counteracted if glutamate was perfused in a sodium-free medium, suggesting involvement of the electrogenic glutamate transporters GLT-1 and GLAST in the swelling process (Izumi et al., 1999). In cultured rat astrocytes, cell swelling could also be triggered by application of a high-affinity glutamate transporter substrate called threo-

beta-hydroxyaspartate (TBHA), even in the absence of glutamate itself (Koyama et al., 2000). By expressing GLT-1 in *Xenopus laevis* oocytes, the Zeuthen lab was able to simultaneously record glutamate currents through the transporter as volume change was assessed in individual cells (MacAulay et al., 2001). They confirmed that: (1) glutamate uptake and cell swelling were positively correlated, (2) co-application of sodium and glutamate increased the water permeability of GLT-1, and (3) application of GLT-1 blocker DL-*threo*-β-benzyloxyaspartate (TBOA) reduced the water permeability (MacAulay et al., 2002). Molecular studies of GLT-1 mutants revealed important conformational changes upon glutamate binding that accommodated water molecules (Vandenberg et al., 2011). Thus, the water permeability of GLT-1 is not so much in question, but as to whether these transporters are responsible for substantial water movement into astrocytes during osmotic changes, remains to be seen.

The Na^+/K^+ ATPase (NKA)

The NKA performs a critical function necessary for cell survival, namely the maintenance of the sodium and potassium ionic gradients across the plasma membrane. Physiological processes like the firing of action potentials or sodium-dependent glutamate uptake by astrocytes rely on the NKA to sustain the resting membrane potential. Complete inhibition of the pump in astrocyte culture with ouabain (~1 mM) or barium chloride (~5 mM) can lead to severe health consequences over time (Walz et al., 1984; Larsen et al., 2014). Early work confirmed that NKA played a (partial) role in potassium uptake by astrocytes (Walz et al., 1984; Walz and Hinks, 1985; Kimelberg et

al., 1995). Walz et al. (1984) also reported that higher concentrations of barium chloride (50 μM - 5 mM) showed specific inhibition of NKA, an important consideration when using $BaCl_2$ with the intent to block K^+ channels specifically (Walch et al., 2020). Computational modeling of potassium uptake in conjunction with ECS shrinkage (from astrocyte swelling) suggested that the NKA itself could not account for all of the volume change occurring in astrocytes under conditions of elevated potassium (Ostby et al., 2009; Murakami and Kurachi, 2016). Interestingly, these models predicted different scenarios depending on the locality of other transporters and ion channels, the built-in conformity (or lack thereof) of the ECS, and the participation of neurons. For example, the locality of Kir4.1 channels regionally affects potassium buffering such that the role NKA plays is locally moderated (Murakami and Kurachi, 2016). In brain slice experiments, stimulation-induced increases in local potassium led to the finding that Kir4.1 channels play a small role in *local* potassium buffering, while block of NKA inhibited a large portion of post-stimulus potassium uptake (Larsen et al., 2014). Therefore, mechanisms of astrocyte potassium buffering and volume change are likely dependent on both the subcellular localization of the pumps, channels and transporters, as well as the region exposed to potassium itself.

More detailed studies of NKA molecular structure led to the discovery that most astrocytic NKA are of the $\alpha 2\beta 2$ isoform, which is far more sensitive to extracellular potassium increases compared to NKA isoforms expressed by neurons (Stoica et al., 2017). Somewhat surprisingly, Larsen et al. (2014) found that block of NKA in slices did not affect ECS volume changes, in contrast to the evident role the NKA plays in

sequestering potassium. Later work from the MacAulay group suggested that while NKA is responsible for potassium uptake, the NBCe1 and MCT transporters may actually participate in the water shifts occurring in the process of pH changes (Larsen and MacAulay, 2017). In our own work, we observed that ~75% of K^+-induced astrocyte swelling could be blocked by inhibition of the astrocytic NKA using ouabain (50 μM) (Walch et al., 2020). The remaining ~25% of astrocyte swelling remained unaccounted for in our experiments, suggesting involvement of other mechanisms. However, block of NBCe1, NKCC1/KCC and Kir4.1 failed to reduce any amount of astrocyte swelling. Overall, our findings suggested that the astrocyte NKA plays a predominant role in astrocyte swelling responses in moderately elevated $[K^+]_o$ conditions. It is valuable to again mention the possible differences that could arise from use of different experimental approaches. In our studies we performed volume measurements of astrocytes directly in response to a bath application of K^+, which would produce a more sustained activation of K^+ handling mechanisms within the cell compared to a stimulus-generated potassium elevation which might engage other more local K^+ buffering pathways and limit involvement of the NKA until those pathways become saturated. The different experimental conditions and approaches have been taken into account in our model summary of proposed astrocyte swelling mechanisms in elevated $[K^+]_o$ (Figure 4).

A Role for Cl^-

Chloride movement is also likely to be important for astrocyte volume responses. While studying cytotoxic edema in brain slices, the swelling of neurons after depolarization from sodium influx could be disrupted via knockdown of the voltage-gated chloride channel SLC26A11 (Rungta et al., 2015). Another group found that dendritic beading in brain slices resulting from spreading depression was in part mediated by the chloride cotransporters KCC2 and NKCC1, as well as the chloride-bicarbonate anion exchanger (AE3) (Steffensen et al., 2015). Blockage of these proteins almost entirely prevented dendritic beading, suggesting chloride as a main player in neuronal swelling. Shortly thereafter, the creation of two mathematical models for astrocyte and neuronal swelling substantiated these claims, once again providing evidence that chloride influx and cell volume are tightly intertwined (Dijkstra et al., 2016; Hübel and Ullah, 2016). Another voltage-gated chloride channel of note is ClC-2, which is expressed by astrocytes (Makara et al., 2003) and has been shown to be swelling-activated in other cell types (Comes et al., 2006). Finally, it is known that astrocytes exhibit tonic $GABA_A$ receptor currents from ambient extracellular GABA. The resulting chloride flux may represent a pathway to generating the osmotic shifts necessary for astrocyte swelling. Astrocytes express a number of $GABA_A$ receptor subunits that are specifically upregulated in comparison to other cell types, especially the subunits encoded by GABRg1, GABRa4, and GABRb1 (Zhang et al., 2014). Use of the $GABA_A$ receptor blocker bicuculline may provide information about its contribution to volume change in astrocytes during exposure to elevated extracellular potassium.

How does water enter the cell?

One of the most intriguing puzzles in all of the work on cellular volume changes is the issue of the water itself. Studies have focused on the various ion channels and transporters responsible for ion movements that generate an osmotic gradient which dictates a direction for water movement, but almost never is the issue of *how* the water gets into the cell addressed even in a speculative way. There are two general possibilities: Water either enters the cell through a specialized transmembrane protein that forms a water pore or channel, or water moves passively and directly across the lipid bilayer without need of a specialized protein. In both cases, the water will follow movement of ions or solutes, either together with the ions through the same cotransporter or following an osmotic gradient through another route. If the gradient is inward, water will flow into the cell, and if it is outward, water will move out. Dedicated studies in Xenopus oocytes and epithelial cells *in vitro* have identified several candidate water permeable cotransporters that are also expressed by astrocytes including NKCC, KCC and glutamate transporters (Zeuthen, 1994; MacAulay et al., 2001; Zeuthen and MacAulay, 2002, 2012). However, as detailed above, several recent studies in intact brain tissue have provided strong evidence that NKCC, KCC and activity-dependent glutamate uptake are not involved in ECS constriction or real-time astrocyte volume increases associated with mild- to moderate elevations in extracellular K^+. Of course, AQP4 was also touted as a key passive water entry pathway for astrocytes, responsible for astrocyte volume changes in hypoosmolar and high K^+ conditions, and also provided as an explanation for an inability to quantify such changes in neurons. This assertion has now been challenged on

many levels, and it is now clear that there is more to it than this simple explanation. Numerous studies using AQP4$^{-/-}$ mice and a variety of techniques to measure cell swelling have shown that not only is AQP4 not required for astrocyte swelling in hypoosmolar (Murphy et al., 2017) or elevated K^+ conditions (Walch et al., 2020), but further, that an important role for AQP4 (and Kir4.1) may be to *extrude* water (and ions) from the cell to assist in cellular volume maintenance or recovery.

As introduced above, a special water pore for dedicated water entry may not even be necessary for passive water movement into cells. Kimelberg reported that in most mammalian cells, plasma membranes have high water permeability, as water can diffuse relatively rapidly across the lipid bilayer, and that AQP expression is thought to be rate-limiting for fast water transport in a few, relatively water-impermeant cells such as epithelia (reviewed in Kimelberg, 2005). Application of hypoosmolar ACSF is especially noteworthy in this regard because osmotic gradients are generated for both neurons and astrocytes instantaneously by dilution of extracellular solute concentration. No ion-specific channels or transporters ever need to open to generate the osmotic gradient. Furthermore, neurons, which are thought to lack functional water channels, readily swell in these conditions (Aitken et al., 1998), and swell to an almost identical amount over a similar time course as astrocytes in intact brain tissue (Murphy et al., 2017). This is further evidence that AQP4, which is not expressed by neurons, is not a requirement for water movement into cells. These findings also suggest that neurons and astrocytes may share a common water entry mechanism in many experimental conditions. In the absence of a specialized pore, it seems probable that this water entry mechanism is simple

diffusion across the lipid bilayer. This passive water movement can be fast, as significant volume increases in neurons and astrocytes have been recorded within one minute in hypoosmolar conditions using standard solution perfusion rates (1-1.5 ml/min) (Lauderdale et al., 2015; Murphy et al., 2017). Alternately, an undiscovered (or not yet tested) water permeability pore expressed at similar levels by both neurons and astrocytes allows for water movement in these conditions.

In the case of rises in extracellular $[K^+]_o$, the inward osmotic gradient is provided by K^+ (and likely Cl^-) moving into the astrocytes as described above. Due to lack of mechanisms in neurons to move K^+ into the cell, neurons resist volume change in elevated $[K^+]_o$ as an inward osmotic gradient never occurs (Walch et al., 2020). Neurons are rather tuned to inward movement of Na^+ (and likely Cl^-) which provides the osmotic imbalance needed for neuronal swelling in more pathological situations (Rungta et al., 2015). Again, as to the water movement itself, it may be simple diffusion across the lipid bilayer occurring alongside the movement of K^+ into the astrocyte, similar to the water entry pathway proposed for neurons and astrocytes in hypoosmolar conditions. A dedicated pore route to consider for water entry into astrocytes in elevated $[K^+]_o$ are the glutamate transporters. Although experiments have provided little evidence in support of activity-dependent co-transport of water through glutamate transporters as a mechanism contributing to astrocyte swelling in elevated $[K^+]_o$, the transporters also express a passive water entry pathway driven entirely by the osmotic gradient (reviewed in MacAulay and Zeuthen, 2010). Glutamate transporters are abundantly expressed by astrocytes and are located in the same membrane domains as the astrocytic Na^+/K^+

ATPase (Cholet et al., 2002; Melone et al., 2019). In summary, more work is needed to identify mechanisms of water entry into astrocytes that leads to their swelling and associated consequences on brain tissue excitability.

Looking Ahead

As evidenced by the work above, the amount of conflicting results in this field of study is high. The mechanisms of volume regulation in astrocytes are likely to involve some amount of complexity, but poor ability to corroborate findings likely stems from differences in methodology, model systems, and measurements. While many groups are moving into *in vivo* experiments involving volume imaging in intact rodent brain, popularity of image analysis programming has revealed differences in protocols. This lack of standardization is sure to introduce variability between findings within and between studies. The field's increased interest in studying astrocyte processes will likely spur the development of new tools to record and study volume changes and their mechanisms in localized intracellular domains, which are likely to differ from those in the soma. With the advancement of new technologies that expand resolution of the astrocytic processes and endfeet, the field is poised to begin answering questions regarding the role of astrocyte processes in maintaining extracellular homeostasis, harboring water transiently due to local changes in excitability, and regulating the exchange of water and other byproducts with the vasculature.

References

Aitken PG, Borgdorff AJ, Juta AJ, Kiehart DP, Somjen GG, Wadman WJ (1998) Volume changes induced by osmotic stress in freshly isolated rat hippocampal neurons. Pflugers Arch 436:991-998.

Anderson S, Brismar T, Hansson E (1995) Effect of external K+, Ca2+, and Ba2+ on membrane potential and ionic conductance in rat astrocytes. Cell Mol Neurobiol 15:439-450.

Andrew RD, Labron MW, Boehnke SE, Carnduff L, Kirov SA (2007) Physiological evidence that pyramidal neurons lack functional water channels. Cereb Cortex 17:787-802.

Ballanyi K, Grafe P, Serve G, Schlue WR (1990) Electrophysiological measurements of volume changes in leech neuropile glial cells. Glia 3:151-158.

Becker HM, Bröer S, Deitmer JW (2004) Facilitated lactate transport by MCT1 when coexpressed with the sodium bicarbonate cotransporter (NBC) in Xenopus oocytes. Biophys J 86:235-247.

Benesova J, Rusnakova V, Honsa P, Pivonkova H, Dzamba D, Kubista M, Anderova M (2012) Distinct Expression/Function of Potassium and Chloride Channels Contributes to the Diverse Volume Regulation in Cortical Astrocytes of GFAP/EGFP Mice. Plos One 7.

Binder DK, Papadopoulos MC, Haggie PM, Verkman AS (2004) In vivo measurement of brain extracellular space diffusion by cortical surface photobleaching. J Neurosci 24:8049-8056.

Bittner CX, Valdebenito R, Ruminot I, Loaiza A, Larenas V, Sotelo-Hitschfeld T, Moldenhauer H, San Martín A, Gutiérrez R, Zambrano M, Barros LF (2011) Fast and reversible stimulation of astrocytic glycolysis by K+ and a delayed and persistent effect of glutamate. J Neurosci 31:4709-4713.

Brown AM, Ransom BR (2007) Astrocyte glycogen and brain energy metabolism. Glia 55:1263-1271.

Cholet N, Pellerin L, Magistretti PJ, Hamel E (2002) Similar perisynaptic glial localization for the Na+,K+-ATPase alpha 2 subunit and the glutamate transporters GLAST and GLT-1 in the rat somatosensory cortex. Cereb Cortex 12:515-525.

Chvatal A, Anderova M, Hock M, Prajerova I, Neprasova H, Chvatal V, Kirchhoff F, Sykova E (2007) Three-dimensional confocal morphometry reveals structural changes in astrocyte morphology in situ. J Neurosci Res 85:260-271.

Comes N, Abad E, Morales M, Borrás T, Gual A, Gasull X (2006) Identification and functional characterization of ClC-2 chloride channels in trabecular meshwork cells. Exp Eye Res 83:877-889.

Dibaj P, Kaiser M, Hirrlinger J, Kirchhoff F, Neusch C (2007) Kir4.1 channels regulate swelling of astroglial processes in experimental spinal cord edema. J Neurochem 103:2620-2628.

Dietzel I, Heinemann U, Hofmeier G, Lux HD (1980) Transient changes in the size of the extracellular space in the sensorimotor cortex of cats in relation to stimulus-induced changes in potassium concentration. Exp Brain Res 40:432-439.

Dijkstra K, Hofmeijer J, van Gils SA, van Putten MJ (2016) A Biophysical Model for Cytotoxic Cell Swelling. J Neurosci 36:11881-11890.

Florence CM, Baillie LD, Mulligan SJ (2012) Dynamic volume changes in astrocytes are an intrinsic phenomenon mediated by bicarbonate ion flux. PLoS One 7:e51124.

Gunnarson E, Zelenina M, Axehult G, Song Y, Bondar A, Krieger P, Brismar H, Zelenin S, Aperia A (2008) Identification of a molecular target for glutamate regulation of astrocyte water permeability. Glia 56:587-596.

Haj-Yasein NN, Jensen V, Østby I, Omholt SW, Voipio J, Kaila K, Ottersen OP, Hvalby Ø, Nagelhus EA (2012) Aquaporin-4 regulates extracellular space volume dynamics during high-frequency synaptic stimulation: a gene deletion study in mouse hippocampus. Glia 60:867-874.

Haj-Yasein NN, Vindedal GF, Eilert-Olsen M, Gundersen GA, Skare O, Laake P, Klungland A, Thoren AE, Burkhardt JM, Ottersen OP, Nagelhus EA (2011) Glial-conditional deletion of aquaporin-4 (Aqp4) reduces blood-brain water uptake and confers barrier function on perivascular astrocyte endfeet. Proceedings of the National Academy of Sciences of the United States of America 108:17815-17820.

Hamann S, Herrera-Perez JJ, Zeuthen T, Alvarez-Leefmans FJ (2010) Cotransport of water by the Na+-K+-2Cl(-) cotransporter NKCC1 in mammalian epithelial cells. J Physiol 588:4089-4101.

Herman MA, Jahr CE (2007) Extracellular glutamate concentration in hippocampal slice. J Neurosci 27:9736-9741.

Holthoff K, Witte OW (1996) Intrinsic optical signals in rat neocortical slices measured with near-infrared dark-field microscopy reveal changes in extracellular space. J Neurosci 16:2740-2749.

Hübel N, Ullah G (2016) Anions Govern Cell Volume: A Case Study of Relative Astrocytic and Neuronal Swelling in Spreading Depolarization. PLoS One 11:e0147060.

Izumi Y, Kirby CO, Benz AM, Olney JW, Zorumski CF (1999) Muller cell swelling, glutamate uptake, and excitotoxic neurodegeneration in the isolated rat retina. Glia 25:379-389.

Jentsch TJ (2016) VRACs and other ion channels and transporters in the regulation of cell volume and beyond. Nat Rev Mol Cell Biol 17:293-307.

Kilb W, Dierkes P, Sykova E, Vargova L, Luhmann H (2006) Hypoosmolar conditions reduce extracellular volume fraction and enhance epileptiform activity in the CA3 region of the immature rat hippocampus. Journal of Neuroscience Research 84:119-129.

Kimelberg HK (2005) Astrocytic swelling in cerebral ischemia as a possible cause of injury and target for therapy. Glia 50:389-397.

Kimelberg HK, Frangakis MV (1985) Furosemide- and bumetanide-sensitive ion transport and volume control in primary astrocyte cultures from rat brain. Brain Res 361:125-134.

Kimelberg HK, Rutledge E, Goderie S, Charniga C (1995) Astrocytic swelling due to hypotonic or high K+ medium causes inhibition of glutamate and aspartate uptake and increases their release. J Cereb Blood Flow Metab 15:409-416.

Kitaura H, Tsujita M, Huber VJ, Kakita A, Shibuki K, Sakimura K, Kwee IL, Nakada T (2009) Activity-dependent glial swelling is impaired in aquaporin-4 knockout mice. Neuroscience Research 64:208-212.

Kletzien RF, Pariza MW, Becker JE, Potter VR (1975) A method using 3-O-methyl-D-glucose and phloretin for the determination of intracellular water space of cells in monolayer culture. Anal Biochem 68:537-544.

Kofuji P, Ceelen P, Zahs KR, Surbeck LW, Lester HA, Newman EA (2000) Genetic inactivation of an inwardly rectifying potassium channel (Kir4.1 subunit) in mice: phenotypic impact in retina. J Neurosci 20:5733-5740.

Kolenicova D, Tureckova J, Pukajova B, Harantova L, Kriska J, Kirdajova D, Vorisek I, Kamenicka M, Valihrach L, Androvic P, Kubista M, Vargova L, Anderova M (2020) High potassium exposure reveals the altered ability of astrocytes to regulate their volume in the aged hippocampus of GFAP/EGFP mice. Neurobiology of Aging 86:162-181.

Koyama Y, Ishibashi T, Okamoto T, Matsuda T, Hashimoto H, Baba A (2000) Transient treatments with L-glutamate and threo-beta-hydroxyaspartate induce swelling of rat cultured astrocytes. Neurochem Int 36:167-173.

Larsen BR, MacAulay N (2017) Activity-dependent astrocyte swelling is mediated by pH-regulating mechanisms. Glia 65:1668-1681.

Larsen BR, Assentoft M, Cotrina ML, Hua SZ, Nedergaard M, Kaila K, Voipio J, MacAulay N (2014) Contributions of the Na^+/K^+-ATPase, NKCC1, and Kir4.1 to hippocampal K^+ clearance and volume responses. Glia 62:608-622.

Lauderdale K, Murphy T, Tung T, Davila D, Binder DK, Fiacco TA (2015) Osmotic Edema Rapidly Increases Neuronal Excitability Through Activation of NMDA Receptor-Dependent Slow Inward Currents in Juvenile and Adult Hippocampus. ASN Neuro 7.

Lundandersen H, Hertz L (1970) EFFECTS OF POTASSIUM AND OF GLUTAMATE ON SWELLING AND ON SODIUM AND POTASSIUM CONTENT IN BRAIN-CORTEX SLICES FROM ADULT RATS. Experimental Brain Research 11:199-+.

MacAulay N, Zeuthen T (2010) Water transport between CNS compartments: contributions of aquaporins and cotransporters. Neuroscience 168:941-956.

MacAulay N, Gether U, Klaerke DA, Zeuthen T (2001) Water transport by the human Na+-coupled glutamate cotransporter expressed in Xenopus oocytes. J Physiol 530:367-378.

MacAulay N, Gether U, Klaeke DA, Zeuthen T (2002) Passive water and urea permeability of a human Na(+)-glutamate cotransporter expressed in Xenopus oocytes. J Physiol 542:817-828.

MacVicar BA, Feighan D, Brown A, Ransom B (2002) Intrinsic optical signals in the rat optic nerve: Role for K+ uptake via NKCC1 and swelling of astrocytes. Glia 37:114-123.

Makara JK, Rappert A, Matthias K, Steinhauser C, Spat A, Kettenmann H (2003) Astrocytes from mouse brain slices express ClC-2-mediated Cl- currents regulated during development and after injury. Mol Cell Neurosci 23:521-530.

Meeks JP, Mennerick S (2007) Astrocyte membrane responses and potassium accumulation during neuronal activity. Hippocampus 17:1100-1108.

Melone M, Ciriachi C, Pietrobon D, Conti F (2019) Heterogeneity of Astrocytic and Neuronal GLT-1 at Cortical Excitatory Synapses, as Revealed by its Colocalization With Na+/K+-ATPase alpha Isoforms. Cereb Cortex 29:3331-3350.

Mori S, Kurimoto T, Miki A, Maeda H, Kusuhara S, Nakamura M (2020) Aqp9 Gene Deletion Enhances Retinal Ganglion Cell (RGC) Death and Dysfunction Induced by Optic Nerve Crush: Evidence that Aquaporin 9 Acts as an Astrocyte-to-Neuron Lactate Shuttle in Concert with Monocarboxylate Transporters To Support RGC Function and Survival. Mol Neurobiol 57:4530-4548.

Murakami S, Kurachi Y (2016) Mechanisms of astrocytic K(+) clearance and swelling under high extracellular K(+) concentrations. J Physiol Sci 66:127-142.

Murphy TR, Davila D, Cuvelier N, Young LR, Lauderdale K, Binder DK, Fiacco TA (2017) Hippocampal and Cortical Pyramidal Neurons Swell in Parallel with Astrocytes during Acute Hypoosmolar Stress. Frontiers in cellular neuroscience 11:275.

Mächler P, Wyss MT, Elsayed M, Stobart J, Gutierrez R, von Faber-Castell A, Kaelin V, Zuend M, San Martín A, Romero-Gómez I, Baeza-Lehnert F, Lengacher S, Schneider BL, Aebischer P, Magistretti PJ, Barros LF, Weber B (2016) In Vivo Evidence for a Lactate Gradient from Astrocytes to Neurons. Cell Metab 23:94-102.

Nase G, Helm PJ, Enger R, Ottersen OP (2008) Water entry into astrocytes during brain edema formation. Glia 56:895-902.

Newman EA (1986) Regional specialization of the membrane of retinal glial cells and its importance to K+ spatial buffering. Ann N Y Acad Sci 481:273-286.

Nielsen S, Nagelhus EA, AmiryMoghaddam M, Bourque C, Agre P, Ottersen OP (1997) Specialized membrane domains for water transport in glial cells: High-resolution immunogold cytochemistry of aquaporin-4 in rat brain. Journal of Neuroscience 17:171-180.

Orkand RK (1986) Glial-interstitial fluid exchange. Ann N Y Acad Sci 481:269-272.

Ostby I, Oyehaug L, Einevoll GT, Nagelhus EA, Plahte E, Zeuthen T, Lloyd CM, Ottersen OP, Omholt SW (2009) Astrocytic Mechanisms Explaining Neural-Activity-Induced Shrinkage of Extraneuronal Space. Plos Computational Biology 5.

Pellerin L, Pellegri G, Bittar PG, Charnay Y, Bouras C, Martin JL, Stella N, Magistretti PJ (1998) Evidence supporting the existence of an activity-dependent astrocyte-neuron lactate shuttle. Dev Neurosci 20:291-299.

Ransom BR, Yamate CL, Connors BW (1985) ACTIVITY-DEPENDENT SHRINKAGE OF EXTRACELLULAR-SPACE IN RAT OPTIC-NERVE - A DEVELOPMENTAL-STUDY. Journal of Neuroscience 5:532-535.

Risher WC, Andrew RD, Kirov SA (2009) Real-time passive volume responses of astrocytes to acute osmotic and ischemic stress in cortical slices and in vivo revealed by two-photon microscopy. Glia 57:207-221.

Rothstein JD, Dykes-Hoberg M, Pardo CA, Bristol LA, Jin L, Kuncl RW, Kanai Y, Hediger MA, Wang Y, Schielke JP, Welty DF (1996) Knockout of glutamate transporters reveals a major role for astroglial transport in excitotoxicity and clearance of glutamate. Neuron 16:675-686.

Ruminot I, Schmälzle J, Leyton B, Barros LF, Deitmer JW (2019) Tight coupling of astrocyte energy metabolism to synaptic activity revealed by genetically encoded FRET nanosensors in hippocampal tissue. J Cereb Blood Flow Metab 39:513-523.

Ruminot I, Gutiérrez R, Peña-Münzenmayer G, Añazco C, Sotelo-Hitschfeld T, Lerchundi R, Niemeyer MI, Shull GE, Barros LF (2011) NBCe1 mediates the acute stimulation of astrocytic glycolysis by extracellular K+. J Neurosci 31:14264-14271.

Rungta RL, Choi HB, Tyson JR, Malik A, Dissing-Olesen L, Lin PJ, Cain SM, Cullis PR, Snutch TP, MacVicar BA (2015) The cellular mechanisms of neuronal swelling underlying cytotoxic edema. Cell 161:610-621.

Russell JM (2000) Sodium-potassium-chloride cotransport. Physiol Rev 80:211-276.

Schneider GH, Baethmann A, Kempski O (1992) Mechanisms of glial swelling induced by glutamate. Can J Physiol Pharmacol 70 Suppl:S334-343.

Steffensen AB, Sword J, Croom D, Kirov SA, MacAulay N (2015) Chloride Cotransporters as a Molecular Mechanism underlying Spreading Depolarization-Induced Dendritic Beading. J Neurosci 35:12172-12187.

Stoica A, Larsen BR, Assentoft M, Holm R, Holt LM, Vilhardt F, Vilsen B, Lykke-Hartmann K, Olsen ML, MacAulay N (2017) The α2β2 isoform combination dominates the astrocytic Na. Glia 65:1777-1793.

Strohschein S, Huttmann K, Gabriel S, Binder DK, Heinemann U, Steinhauser C (2011) Impact of aquaporin-4 channels on K+ buffering and gap junction coupling in the hippocampus. Glia 59:973-980.

Su G, Kintner DB, Sun DD (2002a) Contribution of Na+-K+-Cl- cotransporter to high-K+ (o)-induced swelling and EAA release in astrocytes. American Journal of Physiology-Cell Physiology 282:C1136-C1146.

Su G, Kintner DB, Flagella M, Shull GE, Sun DD (2002b) Astrocytes from Na+-K+-Cl-cotransporter-null mice exhibit absence of swelling and decrease in EAA release. American Journal of Physiology-Cell Physiology 282:C1147-C1160.

Sykova E, Vargova L, Kubinova S, Jendelova P, Chvatal A (2003) The relationship between changes in intrinsic optical signals and cell swelling in rat spinal cord slices. Neuroimage 18:214-230.

Tekkok SB, Brown AM, Westenbroek R, Pellerin L, Ransom BR (2005) Transfer of glycogen-derived lactate from astrocytes to axons via specific monocarboxylate transporters supports mouse optic nerve activity. J Neurosci Res 81:644-652.

Toft-Bertelsen TL, Larsen BR, Christensen SK, Khandelia H, Waagepetersen HS, MacAulay N (2021) Clearance of activity-evoked K. Glia 69:28-41.

Traynelis SF, Dingledine R (1989) Role of extracellular space in hyperosmotic suppression of potassium-induced electrographic seizures. J Neurophysiol 61:927-938.

Vandenberg RJ, Handford CA, Campbell EM, Ryan RM, Yool AJ (2011) Water and urea permeation pathways of the human excitatory amino acid transporter EAAT1. Biochem J 439:333-340.

Walch E, Murphy TR, Cuvelier N, Aldoghmi M, Morozova C, Donohue J, Young G, Samant A, Garcia S, Alvarez C, Bilas A, Davila D, Binder DK, Fiacco TA (2020) Astrocyte-Selective Volume Increase in Elevated Extracellular Potassium Conditions Is Mediated by the Na. ASN Neuro 12:1759091420967152.

Walz W, Hinks EC (1985) Carrier-mediated KCl accumulation accompanied by water movements is involved in the control of physiological K+ levels by astrocytes. Brain Res 343:44-51.

Walz W, Shargool M, Hertz L (1984) Barium-induced inhibition of K+ transport mechanisms in cortical astrocytes--its possible contribution to the large Ba2+-evoked extracellular K+ signal in brain. Neuroscience 13:945-949.

Wurm A, Pannicke T, Iandiev I, Wiedemann P, Reichenbach A, Bringmann A (2006) The developmental expression of K+ channels in retinal glial cells is associated with a decrease of osmotic cell swelling. Glia 54:411-423.

Zeuthen T (1994) Cotransport of K+, Cl- and H2O by membrane proteins from choroid plexus epithelium of Necturus maculosus. J Physiol 478 (Pt 2):203-219.

Zeuthen T (2010) Water-transporting proteins. J Membr Biol 234:57-73.

Zeuthen T, MacAulay N (2002) Cotransporters as molecular water pumps. Int Rev Cytol 215:259-284.

Zeuthen T, Macaulay N (2012) Cotransport of water by Na(+)-K(+)-2Cl(-) cotransporters expressed in Xenopus oocytes: NKCC1 versus NKCC2. J Physiol 590:1139-1154.

Zeuthen T, Hamann S, la Cour M (1996) Cotransport of H+, lactate and H2O by membrane proteins in retinal pigment epithelium of bullfrog. J Physiol 497 (Pt 1):3-17.

Zhang Y, Zhang H, Feustel PJ, Kimelberg HK (2008) DCPIB, a specific inhibitor of volume regulated anion channels (VRACs), reduces infarct size in MCAo and the release of glutamate in the ischemic cortical penumbra. Exp Neurol 210:514-520.

Zhang Y, Chen K, Sloan SA, Bennett ML, Scholze AR, O'Keeffe S, Phatnani HP, Guarnieri P, Caneda C, Ruderisch N, Deng S, Liddelow SA, Zhang C, Daneman R, Maniatis T, Barres BA, Wu JQ (2014) An RNA-sequencing transcriptome and splicing database of glia, neurons, and vascular cells of the cerebral cortex. J Neurosci 34:11929-11947.

Figures

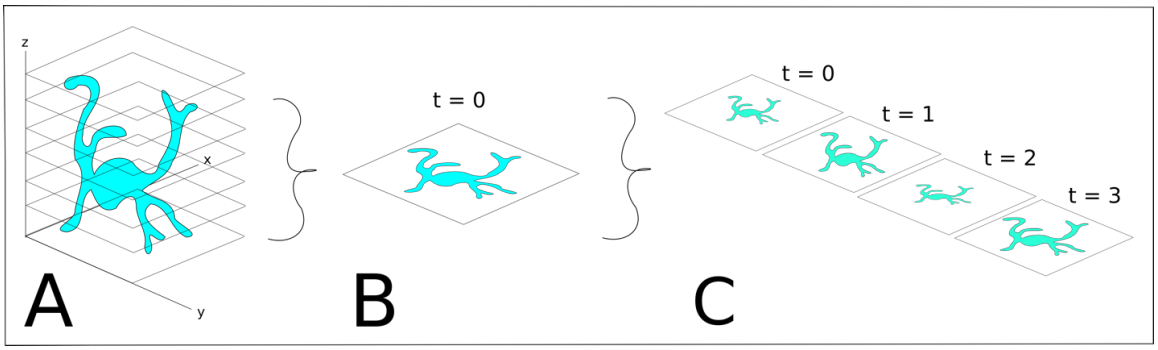

Figure 1.1. Real-time volume measurements. Morphometric analysis of fluorescently labeled cells begins with the collection of a z-stack of images at one point in time (A). Image processing allows for compression of the z-stack into a hyperstack (B), where all of the z-axis pixels are flattened onto a single plane. Hyperstacks are collected across individual timepoints (C), and methods such as edge detection after thresholding of average or maximum intensity projections are used to assess volume changes in real-time.

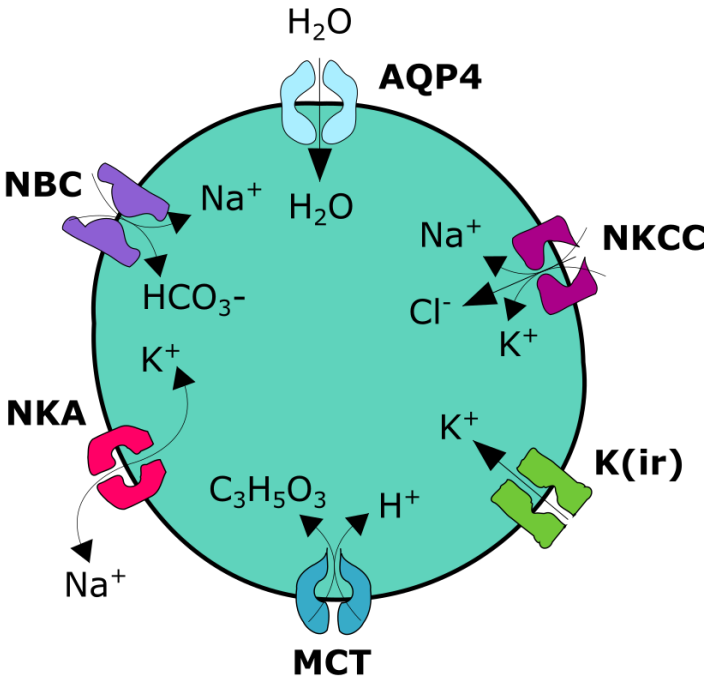

Figure 1.2. Transmembrane proteins involved in astrocyte swelling in elevated $[K^+]_o$, along with their substrates. All have the potential to move substrates outward as well under certain conditions. Aquaporin-4 has been tested in many *in vivo* models in comparison to the other proteins shown. Potassium inwardly rectifying channels are supported by the classical potassium siphoning hypothesis, while the sodium-potassium ATPase has received renewed attention in recent studies due to the uniquely K^+-sensitive isoform expressed by astrocytes. The sodium-potassium-chloride and potassium-chloride cotransporters are strongly supported by primary culture experiments performed using pathological potassium concentrations, but may be less physiologically relevant than the other proteins. Other evidence points to a role for the sodium bicarbonate cotransporter NBCe1 and monocarboxylate cotransporters (MCT1 and 4) at $[K^+]_o$ levels closer to basal $[K^+]_o$. Evidence supports the astrocyte sodium-potassium pump as the main K^+ entry pathway in more elevated and sustained extracellular K^+ conditions. Key: Aquaporin-4: (AQP4); sodium potassium chloride cotransporter: (NKCC1); inwardly rectifying potassium channel: (Kir); monocarboxylate transporters: (MCT); sodium-potassium ATPase: (NKA); sodium bicarbonate cotransporter: (NBCe1).

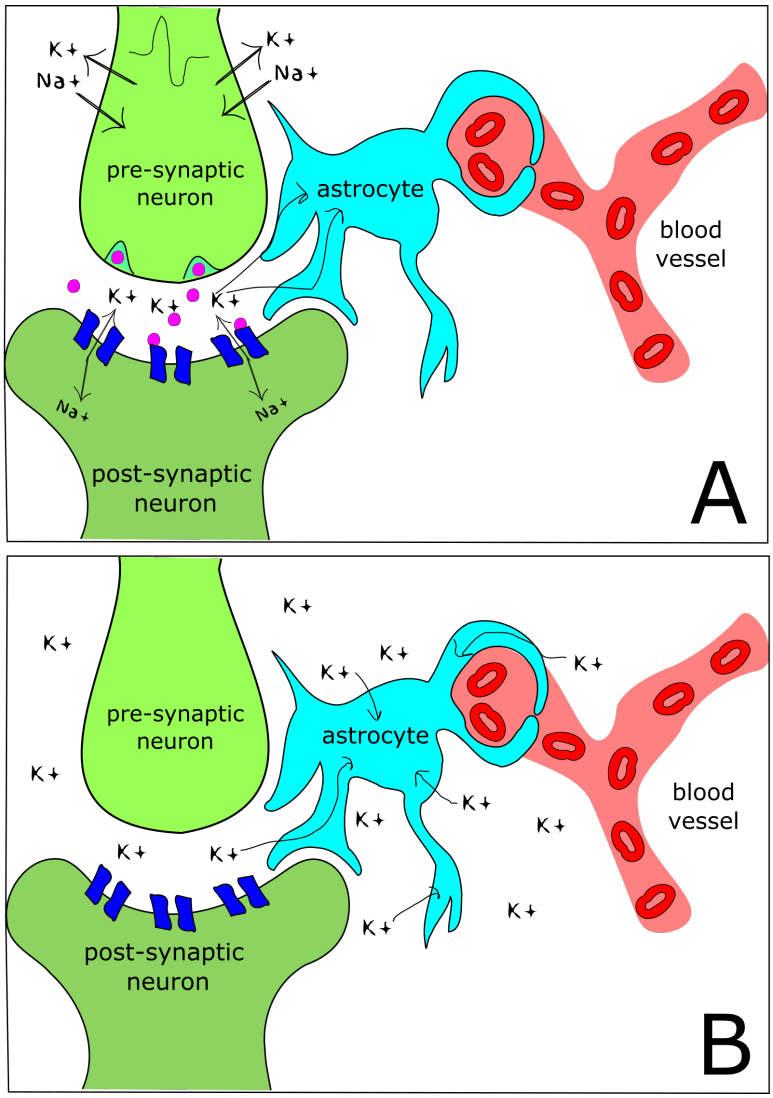
K+
Na+
K+
Na+
pre-synaptic neuron
astrocyte
blood vessel
K+
K+
K+
Na+
Na+
post-synaptic neuron
A
K+
K+
K+
K+
pre-synaptic neuron
astrocyte
K+
K+
blood vessel
K+
K+
K+
K+
K+
K+
post-synaptic neuron
B

Figure 1.3. Local/transient vs. sustained models of astrocyte swelling. (A) In many studies, low-level stimulation of neuronal afferents is used to generate local increases in $[K^+]_o$. Potassium is released pre-synaptically from voltage-gated potassium channels and post-synaptically from neurotransmitter-gated ion channels (receptors in dark blue, neurotransmitter in pink) resulting in transient and local increases in $[K^+]_o$. Extruded potassium ions will enter the perisynaptic astrocyte processes and dissipate into the larger volume of the astrocyte and/or released back into the ECS at areas of lower $[K^+]_o$. This local uptake and redistribution of potassium fits more closely with classical K^+-buffering/siphoning models and would likely result in transient local swelling of perisynaptic regions, which is not possible to measure directly using current imaging approaches. (B) Higher frequency or stronger stimulation of neurons or models using bath application of potassium will produce sustained and non-directional K^+ increases that will quickly engulf the cell. In these instances other K^+ handling mechanisms are activated and cell swelling is detectable using fluorescent imaging techniques. Specific swelling mechanisms are summarized in Figure 4.

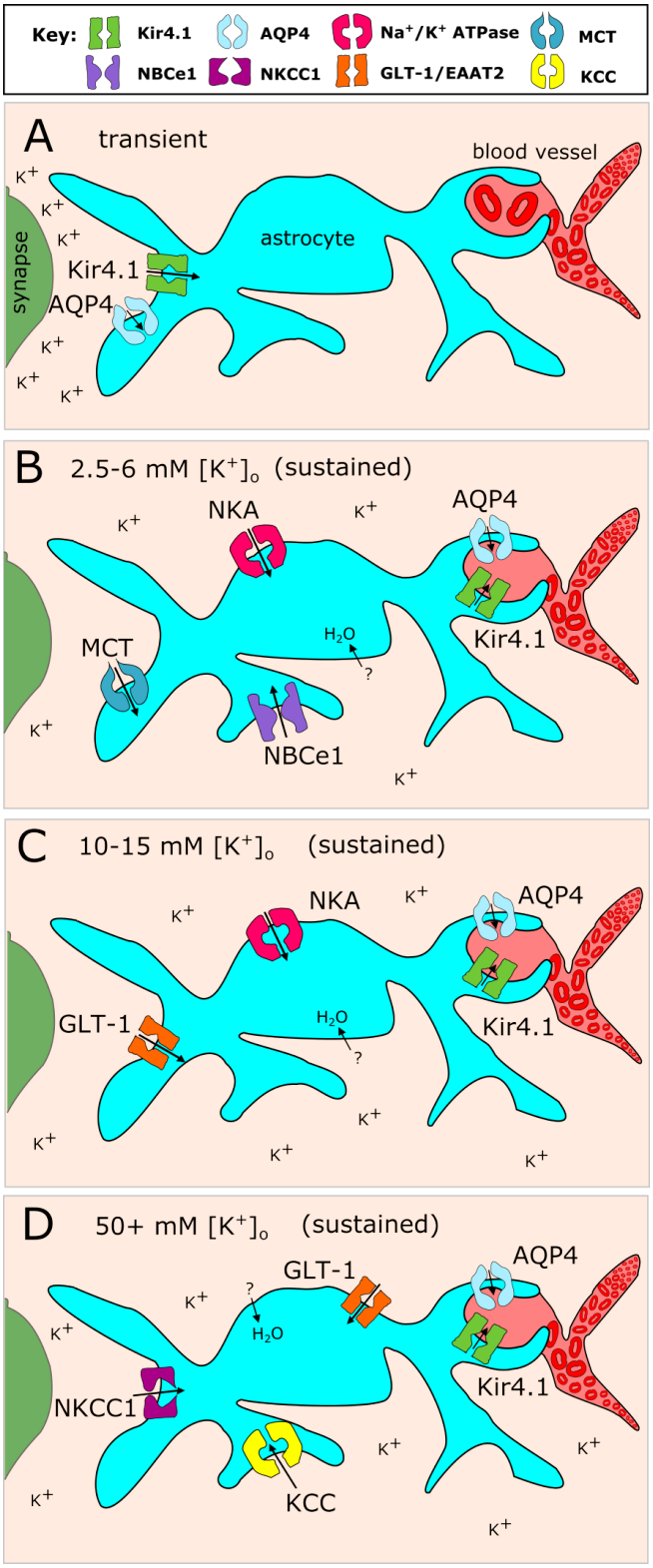
Key:
Kir4.1
AQP4
Na+/K+ ATPase
MCT
NBCe1
NKCC1
GLT-1/EAAT2
KCC
A
transient
blood vessel
astrocyte
synapse
Kir4.1
AQP4
K+
B
2.5-6 mM [K+]o (sustained)
NKA
AQP4
MCT
H2O
?
Kir4.1
NBCe1
C
10-15 mM [K+]o (sustained)
NKA
AQP4
GLT-1
H2O
?
Kir4.1
D
50+ mM [K+]o (sustained)
GLT-1
AQP4
?
H2O
Kir4.1
NKCC1
KCC

Figure 1.4. Summary of proposed mechanisms underlying astrocyte swelling and volume maintenance/recovery at different $[K^+]_o$. Conditions are shown along a range from A) Local/transient rises in $[K^+]_o$ near baseline levels through D) pathological levels of $[K^+]_o$. (**A**) Transient elevations in $[K^+]_o$ due to local synaptic activity may be siphoned into perisynaptic astrocyte processes via Kir4.1 along with water through AQP4. K^+ and water is redistributed locally to areas of lower activity. This model most closely approximates the K^+ buffering hypothesis proposed by Orkand and Newman, although evidence for it is limited by difficulty recording such local changes in $[K^+]_o$ and cell volume. (**B**) More sustained increases in $[K^+]_o$ up to 5-6 mM by bath application or repetitive stimulation of neuronal afferents likely affects a larger area of the astrocyte domain resulting in more widespread and observable changes in astrocyte and ECS volume. Monocarboxylate transporters, NBCe1, and the Na^+/K^+ ATPase may all contribute to ion movements coupled to astrocyte volume increases in these conditions. With the inward ion movements under the auspices of transporters and pumps, the role of Kir4.1 and AQP4 likely switches in these conditions to ease intracellular K^+ and water burden through efflux to areas of lower activity or at endfeet into the vasculature. (**C**) At more moderate K^+ approaching ceiling levels during seizure or high frequency stimulation, the Na^+/K^+ ATPase likely plays the primary role in sequestering $[K^+]_o$ into astrocytes. Influx of Cl^- through an as yet unidentified pathway seems necessary to create the osmotic imbalance required to direct water movement into the cell. (**D**) Strong cellular depolarization due to application of very high levels of $[K^+]_o$ (up to 100 mM) activates NKCC1 and reverses the direction of KCC, resulting in rapid ion influx and associated cell swelling. It is estimated that the astrocyte isoform of the Na^+/K^+ ATPase is effective at $[K^+]_o \leq$ ~12 mM and therefore would be rapidly overwhelmed in these conditions. In (**B**), (**C**), and (**D**), data from several labs suggest that AQP4 is not required for water entry into astrocytes, which may instead occur by diffusing directly across the lipid bilayer, by passing through other dedicated water pore proteins such as the glutamate transporters, or in the case of (D), directly through NKCC/KCC co-transporters themselves.

Chapter 1

Abstract

Astrocytes and neurons have been shown to swell across a variety of different conditions, including increases in extracellular potassium concentration (^$[K^+]_o$). The mechanisms involved in the coupling of K^+ influx to water movement into cells leading to cell swelling are not well understood and remain controversial. Here we set out to determine the effects of ^$[K^+]_o$ on rapid volume responses of hippocampal CA1 pyramidal neurons and stratum radiatum (s.r.) astrocytes using real-time confocal volume imaging. First, we found that elevating $[K^+]_o$ within a physiological range (to 6.5 mM and 10.5 mM from a baseline of 2.5 mM), and even up to pathological levels (26 mM), produced dose-dependent increases in astrocyte volume, with absolutely no effect on neuronal volume. In the absence of compensating for addition of KCl by removal of an equal amount of NaCl, neurons actually shrank in ^$[K^+]_o$, while astrocytes continued to exhibit rapid volume increases. Astrocyte swelling in ^$[K^+]_o$ was not dependent on neuronal firing, AQP4, Kir4.1, the sodium-bicarbonate cotransporter NBCe1, or the electroneutral cotransporter NKCC1, but was significantly attenuated in 1 mM $BaCl_2$ and by the Na^+/K^+ ATPase inhibitor ouabain. Effects of 1 mM $BaCl_2$ and ouabain applied together were not additive, and together with reports that $BaCl_2$ can inhibit the Na^+/K^+ ATPase at high concentrations, suggests a prominent role for the astrocyte Na^+/K^+ ATPase in rapid astrocyte volume increases occurring in ^$[K^+]_o$. These findings carry important

implications for understanding mechanisms of cellular edema, regulation of the brain ECS and brain tissue excitability.

Introduction

Astrocytes play a significant role in maintaining ion and neurotransmitter concentrations in the extracellular space. This includes uptake of glutamate and potassium ions that are released during synaptic transmission. Potassium influx into astrocytes during neuronal synaptic activity is redistributed through the glial syncytium to areas of lower potassium concentration, a process known as "potassium spatial buffering" (Walz, 2000; Kofuji and Newman, 2004). Potassium influx into astrocytes associated with K^+ spatial buffering is thought to be coupled to movement of water into the cell, leading to transient or prolonged fluxes in cellular volume (Pasantes-Morales and Schousboe, 1989; Walz, 1992; MacVicar et al., 2002; Risher et al., 2009). Volume changes in astrocytes have been measured in a number of different ways, both directly using fluorescence microscopy (Risher et al., 2009; Benesova et al., 2012) and inferred by recording changes in intracellular ion concentrations (Walz, 1992), light scattering (Andrew and MacVicar, 1994), or assessment of the size or composition of the ECS (Ransom et al., 1985; Traynelis and Dingledine, 1988; Binder et al., 2004; Larsen et al., 2014). While evidence suggests that elevated extracellular potassium leads to astrocyte volume increases, the mechanisms involved have remained controversial.

Astrocytes express an impressive array of potassium channels and cotransporters, including many not expressed by other cell types, that may be responsible for elevated K^+-induced astrocyte swelling. One such channel both highly expressed and unique to glial cells is Kir4.1, an inwardly-rectifying potassium channel that is thought to play a role in the spatial buffering of potassium (Kalsi et al., 2004; Kofuji and Newman, 2004). Interestingly, Kir4.1 has been linked to the astrocyte-specific water channel AQP4 (Connors et al., 2004; Nagelhus et al., 2004), providing a means for the coupling of K^+ fluxes to water movement. Another possible candidate is the sodium potassium chloride co-transporter, NKCC1. NKCC1 may contribute to potassium-mediated astrocyte swelling in the optic nerve (MacVicar et al., 2002), and it plays a clear role in $[K^+]_o$-induced astrocyte swelling *in vitro* (Su et al., 2002b). However, its role in intact tissue has been less convincing (Larsen et al., 2014). NKCC1 is especially compelling due to its high purported water permeability (Macaulay and Zeuthen, 2012). Finally, evidence suggests that the $\alpha_2\beta_2$ isoform of the Na^+/K^+ ATPase, which is highly expressed by astrocytes (Cholet et al., 2002; Stoica et al., 2017; Melone et al., 2019), is most sensitive to changes in extracellular potassium (Larsen et al., 2014), providing a route for K^+ influx into astrocytes that could couple to water movement.

While cellular volume increases have a powerful influence on neuronal and brain tissue excitability, the precise contribution of astrocyte swelling has not been clearly defined. In $[K^+]_o$ elevated to 8.5 mM, neurons generate synchronous ictal bursting activity that requires NMDA receptor activation and reduction of the ECS (Traynelis and Dingledine, 1988). In these conditions, although direct cell volume measurements were

not taken, it was speculated that the reduction of the ECS was due to astrocyte swelling tied to influx of K^+ (Traynelis et al., 1989). Therefore, astrocyte swelling may directly contribute to neuronal excitability and seizure generation.

The phenomenon of neuronal swelling is a topic of contention among groups studying cellular volume changes. Earlier work in acute slices demonstrated recordable changes in light transmittance (LT) after challenging slices with known triggers of tissue swelling - hypoosmolar and $\wedge[K^+]_o$ ACSF (Andrew and MacVicar, 1994). LT was said to positively correlate with swelling, although the authors did notice a relationship between neuronal activity and LT. With the advent of 2-photon laser microscopy (2PLSM), volume changes at the single-cell level could be estimated (Davies et al., 2007). Combining traditional LT and tissue resistance techniques with newly devised methods of 2PLSM image analysis, neurons were reported to swell under conditions of oxygen-glucose deprivation (OGD) and $\wedge[K^+]_o$, but not hypoosmolarity (Andrew et al., 2007). In another 2PLSM study (Rungta et al., 2015), neuronal swelling was observed after electrical stimulation intending to mimic the excitotoxicity that triggers primary Na^+ influx and later Cl^- influx. Induction of spreading depression via localized elevations in $[K^+]_o$ leads to apparent dendritic beading when visualized with 2PLSM (Steffensen et al., 2015; Sword et al., 2017). Interestingly, our past work recording cellular volume changes indicated that neurons do in fact swell under hypoosmolar conditions (Murphy et al., 2017). However, comparison of neuronal vs. astrocyte volume in varying concentrations of $\wedge[K^+]_o$ in a pathophysiological range has not been performed previously.

In this study, we set out to determine the effects of ^$[K^+]_o$ on volume of CA1 pyramidal cells and astrocytes in stratum radiatum using real-time confocal volume measurements of fluorescently-labeled cells in acute hippocampal slices. Slices were exposed to standard artificial cerebrospinal fluid, as well as ^$[K^+]_o$ ACSF at concentrations of 6.5, 10.5, or 26 mM. Two different conditions of ^$[K^+]_o$ were used, one in which addition of KCl was compensated for by removal of an equal amount of NaCl in order to maintain extracellular osmolarity, and the other in which only KCl was added without changing NaCl concentration. In both conditions, astrocytes dose-dependently increased their volume, while neurons either steadfastly maintained their volume or actually shrank significantly due to the increased extracellular osmolarity by addition of $[K^+]_o$. Even at 26 mM $[K^+]_o$, neurons completely resisted volume change, suggesting an inability to remove excess extracellular K^+. Astrocyte volume increases in ^$[K^+]_o$ were not due to AQP4, Kir4.1, NBCe1, NKCC1, or neuronal action potential generation, but were reduced significantly in 1 mM $BaCl_2$ and by the Na^+/K^+ ATPase inhibitor ouabain. Our findings are consistent with previous studies citing the importance of the Na^+/K^+ pump on astrocyte volume increases associated with influx of K^+ (Larsen et al., 2014).

Materials and Methods

All experiments were performed in accordance with National Institutes of Health guidelines for the care and use of laboratory animals, and approved by the Institutional Animal Care and Use Committee at the University of California, Riverside.

Slice Preparation

Hippocampal slices were prepared from C57Bl/6J mice or transgenic mice on the C57Bl6 background at 15-21 days of age as described previously (Xie et al., 2014). In some astrocyte imaging experiments, use of hippocampal slices from *mGFAP-Cre;Rosa26*$^{lsl\text{-}tdTomato}$ transgenic mice replaced C57Bl/6J mice. For experiments requiring neuronal imaging, Thy1-GFP-S or Thy1-GFP-M transgenic mice were used instead (#011070 and 007788 respectively; Jackson Laboratories, Bar Harbor, ME, USA). These mice have been repeatedly backcrossed to a C57Bl/6J background, and exhibit no obvious differences in phenotype compared to wild-type mice (Feng et al., 2000). Animals were anesthetized under isoflurane and rapidly decapitated, and brains were removed quickly into petri dishes containing oxygenated (Carbogen, 95% oxygen and 5% carbon dioxide), ice-cold slicing buffer. Standard slicing buffer contained (in mM): 125 NaCl, 2.5 KCl, 3.8 $MgCl_2$, 1.25 NaH_2PO_4, 26 $NaHCO_3$, 25 glucose, and 1.3 ascorbic acid. Parasagittal slices (350 μM thick) were cut using an automated vibrating blade microtome (VT1200S model; Leica Biosystems, Buffalo Grove, IL, USA) and transferred to a recovery chamber containing 36°C ACSF solution comprised of (in mM): 125 NaCl, 2.5 KCl, 2.5

$CaCl_2$, 1.3 $MgCl_2$, 1.25 NaH_2PO_4, 26 $NaHCO_3$, and 15 glucose. Slices were incubated for 45 minutes at 36°C, followed by a 15 minute recovery period at room temperature, before being used in experiments. In later experiments, the above protocol was modified slightly to improve slice recovery. Standard slicing buffer was substituted by a sucrose-based slicing buffer containing (mM): 87 NaCl, 75 sucrose, 10 glucose, 1.25 NaH_2PO_4, 2.5 KCl, 25 $NaHCO_3$, 1.3 ascorbic acid, 0.5 $CaCl_2$, 7 $MgCl_2$, 2 pyruvate, 3.5 MOPS, and 0.1 kynurenic acid. Sucrose slicing buffer was used in both slice preparation (as a partially-frozen "slush") and in the slice recovery chamber during incubation. After incubation and subsequent cooling to room temperature, slices were transferred to a second chamber containing normal ACSF and allowed to equilibrate for at least 15 minutes before use in experiments.

The transgenic *mGFAP-Cre;Rosa26*$^{lsl\text{-}tdTomato}$ mice express fluorescent tdTomato protein in astrocytes, which allows for imaging of astrocytes in hippocampal slices without exogenous fluorochromes. For astrocyte imaging in C57Bl/6J mice, astrocytes were incubated with sulforhodamine-101 (SR-101; Sigma-Aldrich, St. Louis, MO, USA) as described previously (Schnell et al., 2015; Murphy et al., 2017). In this case, slices were incubated in 1 μM SR-101 and a modified ACSF consisting of (in mM): 1.3 ascorbic acid, 125 NaCl, 15 glucose, 1.25 H_2PO_4, 2.5 KCl, 26 $NaHCO_3$, 0.5 $CaCl_2$, and 6 $MgCl_2$. After incubation (35-45 minutes at 36°C), slices were transferred to a chamber containing modified ACSF without SR-101 and incubated for an additional 10 minutes at 36°C. Slices were subsequently transferred to standard ACSF at room temperature for a minimum of 15 minutes prior to use in experiments. All experiments were then

performed at room temperature. Modified ACSF was replaced by sucrose slicing buffer following the protocol modifications described above.

Experimental Solutions and Pharmacology

To establish conditions of elevated extracellular potassium, we used either 6.5 mM, 10.5 mM, or 26 mM K^+ ACSF, progressing from a moderate challenge (6.5 mM K^+), to near ceiling levels reached during seizure (10.5 mM), to a concentration more closely linked to spreading depression models and which has been used in numerous studies previously (26 mM K^+). Initial ^$[K^+]_o$ ACSF solutions were kept isoosmolar (~300 mOsm) by equiosmolar omission of NaCl. In a second set of experiments, KCl was elevated with no corresponding change to the NaCl concentration ('non-isoosmolar') to deliberately examine effects of elevated solution hyperosmolarity by addition of K^+ on cellular volume changes. The osmolarities of these solutions were (in mOsm): 6.5 mM $[K^+]_o$: ~309; 10.5 mM $[K^+]_o$: ~317; 26 mM $[K^+]_o$: ~348. In order to study the mechanisms of astrocyte swelling in ^$[K^+]_o$, pharmacologic antagonists were diluted in standard ACSF or isoosmolar 10.5 mM K^+ ACSF. Drugs were added to the bath at the beginning of the 10-minute baseline period prior to the first application of isoosmolar ^$[K^+]_o$ ACSF and remained in the bath for the entire duration of the experiment. Barium chloride ($BaCl_2$) was used to block Kir4.1 channels at 100 μM (Djukic et al., 2007) and to non-selectively inhibit [K^+] channels at 1 mM (Benham et al., 1985; Miller et al., 1987). Disodium 4,4′-diisothiocyanatostilbene-2,2′-disulfonate (DIDS) was applied at a concentration of 300 μM, which is known to block the sodium-bicarbonate transporter (Lu and Boron, 2007;

Larsen and MacAulay, 2017). Bumetanide is a widely-used diuretic, and was applied at 10 μM to block the sodium potassium chloride cotransporter NKCC1 (Larsen et al., 2014). Complete block of the astrocyte sodium-potassium ATPase was achieved by applying 50 μM ouabain (Larsen et al., 2014). Higher ouabain concentrations are required to fully block the neuronal Na^+/K^+ pump isoform, but ouabain at high concentration can lead to slice health deterioration as reported by others (Larsen et al., 2014). In one experiment, tetrodotoxin (TTX) was administered to slices at 1 μM to block voltage-gated sodium channels and thus prevent the generation of action potentials.

Electrophysiology

Following recovery, slices were transferred to a recording chamber and continuously perfused with oxygenated ACSF at room temperature. Slices and individual CA1 pyramidal cells were visualized on a Leica DLMFSA upright microscope, with HCX APO L20x/0.50W U-V-I and HCX APO L63x/0.90W U-V-I submersion objectives and DIC optics (Leica Microsystems, Buffalo Grove, Il). Whole-cell patch clamp recordings were acquired using a Multiclamp 700B amplifier and Digidata 1550 digitizer, controlled with pClamp v.10.7.0.3 and Multiclamp Commander v.2.2.2.2 (Molecular Devices, Sunnyvale, CA, USA). Patch pipettes were pulled from thin-wall 1.5 mM borosilicate glass capillaries (WPI) using a Narishige PC-10 vertical micropipette puller (Narishige, Tokyo, Japan). Patch pipette resistances ranged from ~3-5 mOhm when filled with an internal solution containing (in mM): 140 K-gluconate, 4 $MgCl_2$, 0.4 EGTA, 4 Mg-ATP, 0.2 Na-GTP, 10 HEPES, and 10 phosphocreatine, pH 7.3 with KOH. CA1 pyramidal

neurons were identified using DIC optics based on their location in stratum pyramidale and their characteristic morphology including apical dendrites arborizing into the hippocampal molecular layer. Upon attaining the whole-cell configuration, the cell resting V_m and R_m were recorded and a voltage-step protocol was run to verify the presence of voltage-gated sodium and potassium currents. The cell was then placed into current "I=0" mode to continuously record membrane potential. After a 10-minute baseline recording, 10.5 mM $[K^+]_o$ isoosmolar ACSF was applied to measure effects on V_m and action potential generation, followed by a 10-minute wash period in control ACSF. Only a single neuronal current clamp recording was made per slice.

Imaging

Throughout our experiments, eGFP was excited using a 488 nm argon laser and detected with a 503-548 bandpass filter, and SR-101 was excited with a 559 nm semiconductor laser and detected with a 624 - 724 nm bandpass filter using an Olympus Fluoview FV1000 (FV10-ASW) confocal imaging system. The objective used was an Olympus LUMPlanFI 60x/0.90 W ∞/0 water immersion objective lens. Confocal laser settings were the same as described previously (Murphy et al., 2017). Output power for both lines was kept as low as possible (1.5%) to minimize the possibility for light-induced artifacts. Volume imaging of neurons and astrocytes was performed as described previously (Murphy et al., 2017). Briefly, z-stacks of 1 μm-thick images were collected at one-minute intervals over individual cell somata within 15 s, to ensure adequate coverage of the soma and main processes while at the same time preventing data loss caused by tissue

volume changes. Stacks were collected using a 2 - 3.5x zoom factor, with a scan ROI clipped close around the soma to increase imaging speed. Cell drift in the x-y-z planes was compensated using quick X-Y scans and X-Y-Z adjustments as necessary between time points. Briefly, imaging experiments consisted of 3 steps: (1) A 5 - 10 minute baseline period in standard ACSF, in which 2 - 3 z-stacks were acquired in succession at one-minute intervals and averaged to serve as the baseline comparison for later time points; (2) A 5 minute application of ^$[K^+]_o$ ACSF, during which z-stacks through the full thickness of the cell were collected each minute; (3) A 10 minute wash period in standard ACSF, during which an image was taken every 5 minutes. Steps 2 and 3 were then repeated once each, after which the slice was discarded. Fiji/Image J was used for thresholding of image stacks and subsequent volume analysis as previously described (Murphy et al., 2017). Area of compressed image stacks (used as a proxy for cell volume) was analyzed with cell volume changes reported as percent change from the averaged baseline.

Statistical Analysis

Statistical analysis was carried out using SPSS Statistics 24 software and Laerd Statistics methodology. For analysis of volume measurements, a two-way mixed ANOVA was used to check for significant interactions between the within-subject (time) and between-subjects (group/condition) factors. If a significant interaction was noted, a one-way ANOVA was conducted for the between-subjects factors, and a one-way repeated-measures ANOVA was used for the within-subjects factors. In cases where there was a

significant interaction between time and condition, a subsequent independent Student's t-test (two groups) or one way ANOVA (3 groups) was performed. Repeated measures ANOVA was utilized for all conditions of cell swelling, comparing two or more treatment groups. "Extreme" values in SPSS boxplots, and/or studentized residuals larger than ± 2.5 following a repeated measures ANOVA, were used as indicators of potential outliers. Outliers were only removed in cases where there were severe violations of normality or homogeneity, which were improved upon removal of that instance. Violations of normality were identified with the Shapiro-Wilk test, while homogeneity of variance (HOV) was assessed with Levene's test for equality of variance. Box's test established equality of covariances, and Mauchly's test determined sphericity of the dataset. The Greenhouse-Geiser estimation was used to determine significance in the two-way mixed ANOVA. At timepoints where the condition of normality was violated, non-parametric tests (Kruskal-Wallis or Mann-Whitney U) were used to determine significance. At timepoints with HOV violations, an unequal variance t-test (Welch test) was used to check for significance. After one-way ANOVA, post-hoc testing (Tukey or Games Howell) was performed in datasets with two or more groups. For repeated-measures ANOVA run for two or more comparisons, post-hoc testing (Holm-Bonferroni) accounted for the type-I error associated with multiple comparisons. Electrophysiology data were analyzed using a non-parametric one-way ANOVA (aka Kruskal Wallis H test) without removal of outliers in AP frequency or membrane potential. The distribution of values across treatment groups was not similar upon inspection of box plots. Accordingly, pairwise comparisons using Dunn's procedure (1964) were performed with

Bonferroni correction for multiple comparisons. For all experiments, each group contained N = 8 - 12 cells (numbers specified in each experiment), unless otherwise noted. Significance values are listed as: *p < 0.05, **p < 0.01, and ***p < 0.001.

Results

^$[K^+]_o$ ACSF Selectively Swells Astrocytes

We first recorded cellular volume of both CA1 pyramidal neurons and astrocytes within the stratum radiatum (s.r.) in response to 6.5, 10.5 and 26 mM $[K^+]_o$ ACSF. This ACSF was made isoosmolar by removal of NaCl (see Methods). Astrocytes were labeled with either Sulforhodamine 101 (SR-101) (Schnell et al., 2015) or by expression of TdTomato driven by the *mGFAP* promotor (*mGFAP-Cre;Rosa26*$^{lsl\text{-}tdTomato}$*)*. Astrocytes were identified by their characteristic bushy morphology with 1-3 main processes emerging from the cell soma, with subsequent branching into many increasingly smaller and finer processes. To image pyramidal neurons, slices were taken from Thy1-eGFP mice (Feng et al., 2000) where select CA1 neurons express eGFP. These mice express eGFP in a small proportion of CA1 pyramidal neurons, enabling easy visualization of individual cells. Pseudocolor images illustrate the increase in soma area over baseline in astrocytes exposed to ^$[K^+]_o$ (magenta outline in image overlays; Fig. 1A - C), as well as the persistent soma area in neurons unaffected by ^$[K^+]_o$ (Fig. 1D). Application of laser light alone had no effect on cell volume over time for either astrocytes or neurons (Fig. 1E).

Consistent with the role of astrocytes in potassium clearance, we found that astrocytes rapidly swelled in $\wedge[K^+]_o$ (within 1 minute), whereas there was little to no change in neurons (Fig. 1F - H). Astrocyte volume reached a maximum of 4.3% above baseline at 6.5 mM $[K^+]_o$, 6.6% at 10.5 mM $[K^+]_o$, and 15% at 26 mM $[K^+]_o$ after 5 minutes (the maximum $\wedge[K^+]_o$ exposure time) during the first application. Similar values were attained in the same astrocytes during a second application of $\wedge[K^+]_o$ after an intervening 10-minute wash period during which astrocytes recovered to baseline volume. Even in 6.5 mM $[K^+]_o$ ACSF, within one minute there was a significant increase in astrocyte volume in comparison to neurons which remained at or very near baseline (Fig. 1F, $^{**}p < 0.01$). Neuronal volume remained unchanged even in 26 mM $[K^+]_o$, which is far above estimated ceiling levels of K^+ during seizure (10 - 15 mM), but which may be reached during energy failure in conditions of stroke. The resilience of neurons to volume change in 26 mM $[K^+]_o$ is somewhat surprising, as similar levels of $[K^+]_o$ have been shown to swell neurons in previous studies (Andrew et al., 2007; Zhou et al., 2010; Tang et al., 2014). We attribute the lack of neuronal swelling to the absence of spreading depression (SD) in our conditions. Without the occurrence of SD, the elevated $[K^+]_o$ alone appears to swell astrocytes specifically, consistent with their role in K^+ homeostasis. To ensure that these CA1 neurons are capable of swelling, we performed experiments in which application of 10.5 mM $[K^+]_o$ was followed by application of 40% hypoosmolar ACSF. In line with our previous findings (Murphy et al., 2017), neurons rapidly swelled in hypoosmolar conditions, despite their resistance to volume change in $\wedge[K^+]_o$ (Fig. 1I).

Increased ACSF osmolarity due to addition of $[K^+]_o$ attenuates astrocyte swelling and leads to neuronal shrinking

Because elevations in $[K^+]_o$ would not normally be associated with an equiosmolar decrease in $[Na^+]_o$, we next assessed astrocyte and neuronal volume in $\wedge[K^+]_o$ solution without compensating by removal of NaCl. In these conditions, addition of K^+ to the ACSF increases the solution osmolarity relative to the control solution (see Methods). The elevated extracellular osmolarity is predicted to shrink cells, offsetting K^+-induced volume increases. We refer to these conditions as 'non-isoosmolar' to distinguish from the isoosmolar $\wedge[K^+]_o$ conditions used initially. Non-isoosmolar $\wedge[K^+]_o$ still resulted in clear expansion of the astrocyte soma over baseline (Fig. 2A, B). Neurons, however, did not exhibit any obvious change in volume relative to baseline in 10.5 mM $[K^+]_o$ (Fig. 2C), but cell shrinking was visibly apparent after 5 minutes in 26 mM $[K^+]_o$ (Fig. 2D). Although somewhat blunted compared to astrocyte volume increases in isoosmolar $\wedge[K^+]_o$, there were still significant increases in astrocyte volume over baseline at all concentrations of $\wedge[K^+]_o$ tested (Fig. 2E - G). Neurons actually exhibited significant shrinking at each $[K^+]_o$ in a dose- and time-dependent manner, with highly significant differences occurring at 26 mM $\wedge[K^+]_o$ (Fig 2E - G). These results re-affirm the key role astrocytes play in sequestering elevated $[K^+]_o$.

We next directly compared astrocyte and neuron volume in isoosmolar vs. non-isoosmolar $\wedge[K^+]_o$ to determine the effect of osmolarity on cell volume in $\wedge[K^+]_o$ (Fig. 3). The increase in osmolarity of 6.5 mM $\wedge[K^+]_o$ led to an insignificant, but noticeable decrease in the swelling of astrocytes, in comparison to swelling evoked in isoosmolar

6.5 mM ^$[K^+]_o$ (Fig. 3A). Neurons did not change their volume in isoosmolar 6.5 mM ^$[K^+]_o$, although there was a small but insignificant shrinking of neurons in non-isoosmolar 6.5 mM ^$[K^+]_o$ (Fig. 3A). In the first application of non-isoosmolar 10.5 mM ^$[K^+]_o$, astrocytes swelled significantly less at minutes two and three in comparison to isoosmolar 10.5 mM ^$[K^+]_o$ (Fig. 3B). Neurons maintained their original volume, regardless of the osmolarity of 10.5 mM ^$[K^+]_o$ (Fig. 3B). In the second application of non-isoosmolar 10.5 mM ^$[K^+]_o$, there were insignificant and nearly imperceptible changes in astrocyte swelling and neuron volume compared to those in isoosmolar 10.5 mM ^$[K^+]_o$ (Fig. 3B). Astrocyte swelling was significantly lower in non-isoosmolar compared to isoosmolar 26 mM ^$[K^+]_o$ (Fig. 3 C, D), likely due to hyperosmolarity-induced shrinking mitigating volume increases associated with K^+ influx. Surprisingly, neuronal shrinking in 26 mM non-isoosmolar ^$[K^+]_o$ was significant compared to isoosmolar 26 mM $[K^+]_o$ (Fig. 3C, E). Neuronal shrinking and reduced astrocyte swelling in non-isoosmolar ^$[K^+]_o$ suggested some amount of outward water movement due to solution hyperosmolarity.

Hyperosmolar ACSF by addition of mannitol shrinks both neurons and astrocytes

To verify that neurons and astrocytes are capable of shrinking in hyperosmolar solution, we raised the osmolarity of the ACSF by addition of mannitol. This manipulation has the advantage of altering solution osmolarity without changing extracellular ion concentrations. Application of 40% hyperosmolar ACSF by addition of mannitol shrank both astrocytes and neurons (Fig. 4), although astrocytes shrank significantly more than

neurons during the second + mannitol application (Fig. 4C, *p < 0.05, **p < 0.01 or ***p < 0.001). These findings suggest, together with our previous work (Murphy et al., 2017) and data in Fig. 1I, that neurons readily respond to changes in solution osmolarity with swelling or shrinking, but resist volume change in response to changes in $[K^+]_o$. Our data also support the idea that reduced astrocyte swelling and neuronal shrinking in non-isoosmolar ^$[K^+]_o$ ACSF is due to the increased osmolarity by addition of K^+, rather than possible alterations in volume regulatory mechanisms through changes in extracellular ion concentrations.

The co-transporter NKCC1 and the sodium bicarbonate cotransporter NBCe1 are not responsible for astrocyte swelling in ^$[K^+]_o$

We next considered the possibility that influx of bicarbonate ions induced by astrocyte depolarization (Larsen and MacAulay, 2017) could be responsible for astrocyte swelling in ^$[K^+]_o$ ACSF, as this has previously been demonstrated in astrocytes (Florence et al., 2012). In order to determine the contribution of the sodium bicarbonate cotransporter NBCe1, we utilized DIDS (300 μM) as an antagonist (Larsen and MacAulay, 2017). We observed no appreciable effect of DIDS on astrocyte swelling (Fig. 5A, E).

Previous work suggests that the electroneutral ion co-transporter NKCC1 is a key in K^+ influx pathway coupled to cellular volume changes (Mongin et al., 1994; MacVicar et al., 2002; Su et al., 2002b; Su et al., 2002a; Jayakumar and Norenberg, 2010). NKCC1 is especially intriguing not only because of its role as an ion cotransporter, but also because it has been shown to exhibit water permeability (Macaulay and Zeuthen, 2012).

Therefore, we probed the possible contribution of NKCC1 to astrocyte swelling in ^$[K^+]_o$ using the NKCC1 inhibitor bumetanide. Bumetanide (10 μM) had no effect on astrocytic swelling in ^$[K^+]_o$ ACSF (Fig. 5B, E), arguing against a role for NKCC1 in astrocyte swelling in our conditions. However it is worth noting that under hypotonic conditions, cultured astrocytes activate NKCC1 latently (approx. 5-7 min) after exposure (Mongin et al., 1994). This might suggest that NKCC1 could contribute to astrocyte swelling beyond the five minute period used in our experiments.

Astrocyte Swelling in ^$[K^+]_o$ is not due to K^+ influx via Kir4.1

We next set out to identify mechanism(s) underlying astrocyte swelling in ^$[K^+]_o$. In these and subsequent experiments, the isoosmolar ^$[K^+]_o$ protocol was used, which results in more pronounced astrocyte swelling compared to 'non-isoosmolar' ^$[K^+]_o$. The astrocyte-selective, inwardly rectifying K^+ channel Kir4.1 has long been considered a predominant K^+ influx pathway responsible for extracellular K^+ homeostasis (Kofuji and Newman, 2004; Nagelhus et al., 2004; Lichter-Konecki et al., 2008). Kir4.1-mediated inward potassium currents can be readily recorded in astrocytes (Djukic et al., 2007; Devaraju et al., 2013). The prevailing hypothesis is that water follows the osmotic gradient generated by the influx of K^+ ions into the astrocyte via Kir4.1, resulting in cellular volume changes. To determine any contribution of inwardly rectifying potassium channels to K^+-induced astrocyte swelling, we measured the astrocyte swelling profiles in the presence of 100 μM $BaCl_2$, a selective Kir channel blocker (Hille, 1978; Rudy, 1988). Surprisingly, astrocyte swelling in ^$[K^+]_o$ was not affected by application of 100 μM

$BaCl_2$ (n = 10) (Fig. 5C, F), arguing against a role for Kir4.1. Barium is also known to non-selectively block K^+ channels at concentrations of 1 mM or more (Benham et al., 1985; Miller et al., 1987). Therefore, to look for a more general role of astrocyte K^+ channels, experiments were performed in 1 mM $BaCl_2$ (Fig. 5D, F). Application of 1 mM $BaCl_2$ in $\wedge[K^+]_o$ significantly reduced astrocyte swelling to about 2% above baseline, compared to approximately 6% in $\wedge[K^+]_o$ alone. At 1 mM, $BaCl_2$ is considered to be a non-selective K^+ channel blocker (Walter et al., 2001), preventing identification of the specific K^+ channel(s) that possibly contribute to astrocytic volume increases. However, there is also a literature suggesting that barium at high concentrations nonselectively inhibits the Na^+/K^+ ATPase (NKA) (Walz et al., 1984; Elwej et al., 2017; Elwej et al., 2018). This led us to further explore the role of the NKA in $\wedge[K^+]_o$ astrocyte swelling in subsequent experiments.

Astrocyte swelling in $\wedge[K^+]_o$ is significantly attenuated by the Na^+/K^+ ATPase inhibitor ouabain

Previous work has reported an important role for the sodium-potassium pump as a K^+ influx pathway in astrocytes (Walz and Hinks, 1985; Mongin et al., 1994; Larsen et al., 2014; Larsen et al., 2016; Stoica et al., 2017). The Na^+/K^+ ATPase normally pumps potassium into the cell and sodium outside, against their concentration gradients. It has been shown previously that the astrocyte α2/β2 subunit isoform of the Na^+/K^+ pump is particularly sensitive to changes in extracellular K^+, which would make it uniquely suited to removing excess extracellular potassium (Larsen et al., 2014; Stoica et al., 2017).

Therefore, pumping of K^+ into astrocytes may be associated with the astrocyte volume increases observed in $\wedge[K^+]_o$. To test for a role of the Na^+/K^+ ATPase in $\wedge[K^+]_o$-induced astrocyte swelling, experiments were performed using the Na^+/K^+ ATPase inhibitor ouabain. A recent study found ouabain IC50 values of about 1-3 μM for the α2 isoform expressed in *Xenopus laevis* oocytes, with 200-300 μM for the α1 isoform, which is mainly expressed by neurons (Stoica et al., 2017). We used a concentration of 50 μM, which is predicted to completely block the astrocyte Na^+/K^+ ATPase in brain slices, with partial block of the neuronal isoform (Larsen et al., 2014). In the presence of 50 μM ouabain, astrocyte swelling was significantly diminished compared to control (Fig. 6A, B, D). Next, we reasoned that if the inhibitory effect of 1 mM $BaCl_2$ on astrocyte swelling was due to block of K^+ channels, then co-application of 1 mM $BaCl_2$ plus 50 μM ouabain would have an additive effect, reducing astrocyte swelling to near zero. However, there was no additional inhibition of astrocyte swelling in 50 μM ouabain + 1 mM $BaCl_2$ (Fig. 6C, E), suggesting that the effect of 1 mM $BaCl_2$ is likely due to off-target inhibition of the Na^+/K^+ ATPase as previously reported (Walz et al., 1984; Elwej et al., 2017; Elwej et al., 2018). Similarly, co-application of 100 μM $BaCl_2$ reduced swelling to the same extent as ouabain alone (data not shown). These data suggest that astrocyte swelling in conditions of $\wedge[K^+]_o$ is predominantly due to K^+ sequestration into astrocytes by the astrocyte Na^+/K^+ ATPase, although we cannot completely rule out a possible partial role for unidentified K^+ channels contributing to the astrocyte volume increase.

Astrocyte Swelling in ^$[K^+]_o$ occurs independently of the water channel AQP4

Aquaporin 4 (AQP4) is a functional water channel expressed by astrocytes, but not neurons (Nielsen et al., 1997; Nagelhus et al., 1998). In our previous study (Murphy et al., 2017), we found that astrocyte swelling was significantly *greater* in $AQP4^{-/-}$ mice in severe hypoosmolar conditions relative to controls, indicating that AQP4 is dispensable for swelling, and perhaps even important for extrusion of water. However, AQP4 has been shown to co-localize with Kir4.1, lending support to findings suggesting functional coupling of K^+ movement to AQP4-dependent water influx (Nagelhus et al., 1999; Wen et al., 1999; Nagelhus et al., 2004). Therefore, we performed experiments in hippocampal slices from $AQP4^{-/-}$ and control mice to assess any possible contribution of AQP4 to the water influx associated with astrocyte swelling in ^$[K^+]_o$. Surprisingly, we found an equal amount of swelling in $AQP4^{-/-}$ astrocytes compared to wild-type during the first application of 10.5 mM K^+ (Fig. 7A - C). $AQP4^{-/-}$ astrocytes then did not fully recover to baseline volume during the 10-minute wash period in normal ACSF, resulting in significantly higher peak swelling during the second ^$[K^+]_o$ application (Fig. 7C). These observations provide additional evidence that AQP4 may play an important role in water efflux to limit astrocyte swelling rather than serve as a required water entry pathway.

Block of neuronal firing does not affect astrocyte swelling in ^$[K^+]_o$

Raised extracellular K^+ depolarizes neurons and significantly increases neuronal action potential generation (Xie et al., 2012). It is possible that significant increases in neuronal firing could stimulate astrocytic receptors and elevate glutamate uptake, either of which

could modulate astrocyte swelling or volume regulatory mechanisms. Therefore, we performed experiments to determine the effects, if any, of neuronal firing on astrocyte swelling profiles in elevated $[K^+]_o$. We first performed current clamp recordings in CA1 pyramidal cells to determine the effect of 10.5 mM K^+ on neuronal V_m and action potential generation (Fig. 8). During the baseline period in 2.5 mM K^+ ACSF, neurons rested at an average V_m of -67.2 ± 1.2 mV and fired only occasional action potentials. Application of 10.5 mM K^+ depolarized neurons to -48.3 ± 1.0 mV and generated action potentials at high frequency over 10 minutes (baseline frequency 0.022 Hz; 10.5 mM $[K^+]_o$ 0.759 Hz; n = 11 neurons, 11 slices). Neuronal V_m and firing frequency returned to near baseline levels upon return to 2.5 mM $[K^+]_o$. To address whether neuronal firing affects astrocyte swelling, we recorded astrocyte volume in 10.5 mM $[K^+]_o$ ACSF with and without tetrodotoxin (TTX) (Fig. 8 D, E, F). The presence of TTX did not alter the swelling responses of astrocytes in $\wedge[K^+]_o$. These findings suggest that: a) astrocyte swelling is not due to water movement occurring through activity-dependent glutamate uptake; and b) possible stimulation of astrocytic receptors does not modulate the astrocyte swelling response in $\wedge[K^+]_o$.

Discussion

In this study, we found that elevated extracellular potassium (6.5, 10.5, or 26 mM) causes rapid (within 1 minute) and significant astrocyte swelling, up to ~ 6, 7, and 15% above

baseline volume, respectively, after five minutes. Astrocytes recovered to baseline volume within ten minutes after return to control 2.5 mM $[K^+]_o$ ACSF, and again swelled to a similar extent upon re-application of ^$[K^+]_o$ ACSF. Neuronal volume, on the other hand, remained largely unaffected by addition of K^+ to well above baseline values. These observations highlight the key role astrocytes play in regulating extracellular K^+ levels and provide direct evidence that astrocytes are the main cell type involved in cellular volume responses and associated constriction of the ECS in raised extracellular K^+ conditions. Astrocyte volume increases were significantly inhibited by 50 µM ouabain, implicating the astrocyte Na^+/K^+ ATPase. $BaCl_2$ at 100 µM had no effect on astrocyte volume increases, arguing against a role for Kir4.1. Inhibitors of other astrocytic channels and cotransporters often implicated in astrocyte swelling - including AQP4, NKCC1, and NBCe1 - had no effect. Overall, our findings suggest that the Na^+/K^+ ATPase plays a key role in astrocyte volume expansion occurring in elevated extracellular K^+ conditions, and provide further evidence that the astrocyte Na^+/K^+ pump isoform is unique in its sensitivity to rises in $[K^+]_o$.

The Na^+/K^+ pump inhibitor ouabain reduced the swelling of astrocytes to 0.90 percent above baseline after five minutes in 10.5 mM $[K^+]_o$ ACSF, compared to a 6.62 percent volume increase in ^$[K^+]_o$ alone. The slight amount of astrocyte swelling remaining in the presence of ouabain suggests an additional K^+ influx pathway may also play a small role in the K^+ clearance. Although the effects of 1 mM $BaCl_2$ support possible involvement of K^+ channels, $BaCl_2$ at this concentration non-selectively inhibits the Na^+/K^+ pump activity as previously reported (Walz et al., 1984). Application of 1 mM

$BaCl_2$ together with ouabain did not produce an additive effect, casting doubt on the specificity of barium for K^+ channels at this concentration. Based on these results, our findings are consistent with a prominent role for the astrocyte Na^+/K^+ ATPase in $\wedge[K^+]_o$ - induced astrocyte swelling. Our findings are in line with previous studies which have highlighted the unique Na^+/K^+ pump function of astrocytes and fit with the model of K^+ clearance proposed by Ransom et al. (2000) from their work in the rat optic nerve. Here they postulated (based upon their work as well as previous studies) that glial cells express an isoform of the Na^+/K^+ ATPase which is sensitive to changes in $[K^+]_o$ around the physiological concentration of 3 mM (i.e. low affinity) and that can adjust instantly to changes in $[K^+]_o$. The optic nerve axons, on the other hand, were assumed to express an isoform of the Na^+/K^+ ATPase that is insensitive to changes in K^+ but is sensitive to changes in $[Na^+]_o$, similar to other neurons. Subsequent studies have largely corroborated this model. Cholet et al. (2002) found similar perisynaptic glial localization of the Na^+/K^+ ATPase α2 subunit and the astrocyte glutamate transporters GLAST and GLT-1 in the rat somatosensory cortex, indicating that α2 is predominantly glial. The MacAulay group then went on to show that: a) the α2β2 isoform combination provides the low K^+ affinity and steep voltage sensitivity that render it kinetically geared to increase its activity in response to elevated extracellular K^+ (Larsen et al., 2014); and b) that astrocytic α2 pairs mainly with the β2 isoform at the protein level by proximity ligation assay (Stoica et al., 2017). Here we demonstrate that the astrocyte Na^+/K^+ ATPase is functionally involved in K^+ uptake in raised extracellular K^+ conditions, generating astrocyte swelling and compression of the ECS. Lack of neuronal swelling in $\wedge[K^+]_o$ may be due to their

predominant expression of the α1β1 isoform, which is largely insensitive to $[K^+]_o$ and responds instead to increases in intracellular Na^+.

Using real-time volume measurements similar to those used here, previous studies have observed rapid neuronal swelling in elevated K^+ conditions raised to 26 mM or higher (Andrew et al., 2007; Zhou et al., 2010). Neuronal swelling correlates with spreading depression (SD), which often occurs in elevated extracellular K^+ conditions, but not necessarily by raised extracellular K^+ per se. The work of Zhou et al. (2010) was particularly helpful in this regard. They found that neuronal volume only changed if $^[K^+]_o$ evoked spreading depression, but not when $^[K^+]_o$ failed to trigger SD. The two events were distinguishable by the intrinsic optical signals (IOS) they produced: successful SD produced an initial fast transient peak in light transmittance that appeared on top of a much slower IOS increase. When $^[K^+]_o$ failed to induce SD, there was no transient peak and no apparent propagation through the tissue; IOS showed only a gradual, non-propagating increase which was instead due to more gradual slice swelling. In reports of successful induction of SD using high $[K^+]_o$, almost invariably some combination of the following are used: 1) physiological recording temperature; 2) very fast perfusion speeds (3 - 8 ml/min); and 3) focal application of very high $[K^+]_o$ to a small area of tissue using microfluidic chambers or iontophoresis. Zhou and others (2010) found that slowing the perfusion rate alone was sufficient to prevent SD in 40 mM KCl at physiological temperature. Our combination of slow perfusion speeds (1.2 - 1.5 ml/min), recordings at room temperature, and bath application of K^+ were insufficient to promote SD, and therefore cell swelling changes in 26 mM $^[K^+]_o$ were effectively isolated to

astrocytes. The lower concentrations in the physiological range (6.5 and 10.5 mM) used in our studies were previously reported to be below the minimal K^+ concentration (~15 mM) needed to induce SD (Tang et al., 2014).

Elevated extracellular K^+ will depolarize neurons and increase neuronal action potential generation. Even a shift of 1-2 mM can lead to a significant increase in neuronal firing rates (Xie et al., 2012). We found that increasing $[K^+]_o$ to 10.5 mM greatly increases neuronal firing on a timescale that correlates with astrocyte swelling. The elevated synaptic transmission in $\wedge[K^+]_o$ could contribute to astrocyte swelling and/or volume regulation through uptake of released neurotransmitters into astrocytes, or activation of a broad array of astrocytic G protein-coupled receptors including the mGluRs, $GABA_B$Rs and P2YRs. Many GPCR subtypes have been reported to play a role in regulation of astrocyte transporters, K^+ channels and cell volume (Mongin and Kimelberg, 2002; Takano et al., 2005; Gunnarson et al., 2008; Devaraju et al., 2013), and could potentially modify astrocyte homeostatic functions. Despite these possibilities, astrocyte volume responses in 10.5 mM $[K^+]_o$ were nearly identical in the presence of TTX compared to control. These findings suggest that, at least acutely, elevated neuronal firing does not significantly contribute to astrocyte volume responses in $\wedge[K^+]_o$. It is possible that with more prolonged periods of neuronal firing, effects of astrocyte receptor activation on astrocyte volume responses or volume regulatory mechanisms could be uncovered.

Potassium-induced astrocyte swelling has been attributed to a host of different channels, pumps, and transporter systems in various studies. Early findings supported a

role for NKCC1 (MacVicar et al., 2002; Su et al., 2002b; Su et al., 2002a; Vázquez-Juárez et al., 2009). In many of these studies, the NKCC1 inhibitor bumetanide significantly attenuated astrocyte volume increases and reduced swelling-evoked release of osmolytes from astrocytes. However, most of these experiments were performed in culture, and in the presence of up to 75 mM potassium. Astrocytes in culture possess unique characteristics and only marginally resemble astrocytes in intact brain tissue, as has been well documented previously (Cahoy et al., 2008; Fiacco et al., 2009; Larsen and MacAulay, 2017). Our findings *in situ* using a lower range of K^+ concentrations are supported by those of Larsen et al. (2014), who found that while NKCC1 was important for swelling of cultured astrocytes, it did not contribute to ECS reduction in intact brain tissue. Furthermore, the activity of NKCC1 during application of extreme concentrations (75 mM) of potassium is unlikely to simulate a physiologically relevant build-up of potassium in the ECS. Interestingly, a recent study reported that age may also be a factor in the composition and activity of membrane proteins responsible for volume regulation in astrocytes. In hippocampal slices exposed to 50 mM potassium, NKCC1 played a greater role in swelling of astrocytes from young animals in comparison to older mice (Kolenicova et al., 2020). Considering the lack of NKCC1 activity contributing to astrocyte swelling in our experiments, which were performed in P15 - P21 mice, it seems unlikely that NKCC1 would play a role in astrocyte swelling in slices from older mice using the range of K^+ concentrations used in our study.

The inwardly-rectifying potassium channel Kir4.1 is another target traditionally associated with astrocyte potassium buffering and associated volume changes. In

hippocampal slices of this age, we and others have recorded significant Kir4.1 currents in astrocytes that are also blocked by 100 μM $BaCl_2$ (Djukic et al., 2007; Devaraju et al., 2013). Multiple studies have demonstrated morphological and functional association of Kir4.1 with the glial-specific water channel aquaporin 4 (AQP4) (Nagelhus et al., 1999; Wen et al., 1999; Manley et al., 2000; Nagelhus et al., 2004; Wurm et al., 2006; Strohschein et al., 2011). The working model, which has been supported by some findings, is that influx of potassium through Kir4.1 leads to corresponding inward water movement through AQP4, leading to glial swelling (Kitaura et al., 2009). In the present study, block of Kir4.1 by 100 μM $BaCl_2$ had no effect on astrocyte swelling in $\wedge[K^+]_o$, arguing against a role for Kir4.1 in removal of $[K^+]_o$ into astrocytes and subsequent volume changes. However, a recent immunohistochemical study demonstrated increased Kir4.1 signal in mouse hippocampus in P60 adult tissue, leaving open a possible role for Kir4.1 in astrocyte swelling in older mice (Moroni et al., 2015).

Like Kir4.1, AQP4 also appears unnecessary for astrocyte volume increases in $\wedge[K^+]_o$. Our findings are in line with a number of other studies which have found minimal to no role for Kir4.1 or AQP4 in clearance of extracellular K^+, cell swelling or contraction of the ECS (D'Ambrosio et al., 2002; Haj-Yasein et al., 2011; Haj-Yasein et al., 2012; Larsen et al., 2014; Toft-Bertelsen et al., 2020). For example, Haj-Yasein et al. (2011) reported that genetic deletion of Kir4.1 produced no change in stimulus-evoked shrinkage of the extracellular space (ECS). In subsequent work, the same group found that deletion of AQP4 actually *increased* ECS shrinkage, indicating a possible role for $AQP4^{-/-}$ in astrocyte volume regulation (Haj-Yasein et al., 2012). This is consistent with

our observations. In our previous work, we observed increased swelling of astrocytes in hippocampal slices from AQP4$^{-/-}$ mice compared to control in a hypoosmolar cell swelling model (Murphy et al., 2017). In the present study, AQP4$^{-/-}$ astrocytes exhibited a slower recovery to baseline volume during the wash period in-between ^$[K^+]_o$ applications, resulting in increased peak volume during the second ^$[K^+]_o$ application relative to control. Our data suggest that AQP4 is dispensable for astrocyte swelling, and in the absence of AQP4, astrocytes have impaired volume recovery. Based on both the present and past findings, we propose that during more elevated and sustained elevations in $[K^+]_o$, the main role of Kir4.1 and AQP4 is *redistribution* or *extrusion* of K^+ ions and water out of the astrocyte either into the vasculature or into areas of lower ^$[K^+]_o$, which aids in cell volume regulation. It is worth noting that our model exposes the tissue to potassium-enriched ACSF by bath application. Using this method, K^+ ions and water would presumably encounter most astrocytic compartments in a uniform and distributed manner. In contrast, many *in vivo* studies citing the importance of AQP4 in astrocyte swelling concern the volume transients through the endfeet of astrocytes abutting the vasculature (Manley et al., 2000; Amiry-Moghaddam et al., 2003; Badaut et al., 2011). Thus, the directionality of the water movement between vascular and interstitial compartments is an important consideration when comparing *in situ* to *in vivo* studies.

The NBCe1, monocarboxylate transporters MCT 1 and 4, and KCC are additional candidate pathways for astrocyte swelling in ^$[K^+]_o$. Astrocytic K^+-induced membrane depolarization has been shown to activate the NBCe1, resulting in influx of Na^+ and $HCO3^-$ and intracellular alkalinization (reviewed in Deitmer and Rose, 2010). Two

independent studies have supported a role for the NBCe1 in astrocyte swelling in conditions of elevated $^{[K^+]_o}$. Florence et al. (2012) observed astrocyte swelling 10 minutes after bath application of 5.5 mM $^{[K^+]_o}$ using 2-photon imaging of fluorescently labeled astrocytes in rat hippocampal slices. The astrocyte swelling was significantly attenuated by DIDS and after incubating slices in $HCO3^-$ free ACSF. Later, Larsen and MacAulay (2017) also found a role for the NBCe1 in stimulation-induced extracellular space shrinkage. Inhibition of the NBCe1 by DIDS (300 μM) reduced the ECS shrinkage by about 25%. In the present study, we found that 300 μM DIDS had no effect on the amount of astrocyte swelling occurring in $^{[K^+]_o}$. Although used mainly with the intention of blocking the NBCe1, DIDS is a general anion exchange inhibitor and would therefore also be expected to at least partially block KCC at these concentrations (Malek et al., 2003; Delpire and Weaver, 2016). Furthermore, DIDS is also an effective antagonist of the MCTs at similar concentrations as those used here (Dimmer et al., 2000). Therefore, our findings provide evidence that there is limited to no involvement of NBCe1, KCC, or MCTs in the astrocyte swelling observed in $^{[K^+]_o}$ in our experiments.

We explored astrocyte swelling mechanisms using $^{[K^+]_o}$ of 10.5 mM. This is in line with peak K^+ during intense electrical stimulation and nearing ceiling levels during seizure. It is right near the theoretical peak of $[K^+]_o$ that the α2β2 Na^+/K^+ ATPase isoform would saturate. Therefore, we cannot rule out possible involvement of other K^+-influx pathways such as NKCC and KCC at higher concentrations of $[K^+]_o$. The KCCs in particular are generally outwardly-directed but during heavy extracellular K^+ loads such as during ischemia and spreading depression, they may reverse and contribute to K^+

influx in pathological situations (reviewed in Macaulay and Zeuthen, 2012). Although we did not induce SD in our experiments, 26 mM $[K^+]_o$ may be high enough to involve KCC-mediated K^+ influx. On the other end of the K^+ concentration range, Florence et al. (2012) found a role for the NBCe1 at much lower $[K^+]_o$ values of 5.5 mM. The NBCe1 might therefore contribute to volume responses at lower $[K^+]_o$ but is then phased out by the Na^+/K^+ pump as $[K^+]_o$ levels continue to rise. Another methodological difference between studies has to do with the duration of exposure of the tissue to $\wedge[K^+]_o$. In the present study, astrocytes were imaged at one-minute intervals from the start of the $\wedge[K^+]_o$ application for a total of five minutes prior to returning to baseline $[K^+]_o$. In contrast, Florence et al. (2012) took the first volume measurement 10 minutes after the initial exposure to $\wedge[K^+]_o$ and continued recording for 40 minutes at 10-minute intervals. Thus, the concentration as well as the duration of exposure to $\wedge[K^+]_o$ may both be key variables influencing the role of different channels and transport pathways associated with astrocyte volume change.

In summary, our findings suggest that the Na^+/K^+ ATPase is the main contributor to potassium influx into astrocytes and the subsequent astrocyte swelling that occurs in elevated extracellular potassium conditions. Further study would be needed to pinpoint other candidate pathways responsible for the small amount of astrocyte swelling that remains during block of the Na^+/K^+ ATPase. A couple of key questions remain: 1) What is causing the cell swelling; and 2) how is the water getting into the cell? The Na^+/K^+ ATPase translocates 3 Na^+ out for every 2 K^+ in each cycle against the ion concentration gradients. Therefore, if water was simply following an osmotic gradient, water would

move outward in the same direction as the net outward movement of ions. We propose a role for Cl^- ions similar to their involvement in neuronal swelling as reported by Rungta et al. (2015) in cytotoxic edema. Neuronal swelling is initiated by influx of Na^+ ions through activation of glutamate receptors and Na^+/K^+ pump reversal during energy failure. The neuronal depolarization activates voltage-gated Cl^- channels (SLC26A11) leading to accumulation of NaCl inside the cell, providing the osmotic imbalance leading to water entry. In the case of astrocytes, depolarization is triggered by the increase in $[K^+]_o$ which could activate voltage-gated chloride channels. Cl^- influx would accompany K^+ ions being pumped into the cell by the astrocytic Na^+/K^+ ATPase, resulting in accumulation of intracellular KCl and the osmotic imbalance leading to influx of water. Future studies would be necessary to identify candidate Cl^- channels responsible for the Cl^- influx.

As to how the water crosses the cell membrane, there is no evidence that the sodium-potassium pumps themselves are water permeable. Numerous studies have provided compelling evidence that AQP4 is not necessary for astrocyte or neuronal swelling. Cotransporters and anion exchangers which have demonstrated water permeability, such as NKCC and KCC, have been shown to have limited to no role in the ECS dynamics or cell swelling following K^+ elevations within a physiological range. An intriguing candidate that warrants further investigation are the glutamate transporters. In addition to having an activity-dependent water permeability that can accompany glutamate uptake, the transporters also possess a parallel water pathway which is driven entirely by the osmotic gradient, analogous to the aquaporins (reviewed in MacAulay and

Zeuthen, 2010). Although the unit water permeability is manyfold smaller than that of AQP4, these are among the most abundantly expressed proteins in astrocytes and are localized throughout the astrocyte membrane including the perisynaptic region. Previous work has demonstrated almost complete co-distribution of the astrocytic Na^+/K^+ ATPase α2 subunit and the glutamate transporters GLAST and GLT-1 in glial leaflets surrounding dendritic spines and the dendritic and/or axonal elements at the ultrastructural level (Cholet et al., 2002). The glutamate transporters may therefore provide the passive water entry route responsible for astrocyte swelling in elevated $[K^+]_o$ conditions, in a manner reminiscent of what has been previously ascribed to AQP4.

References

Amiry-Moghaddam M, Otsuka T, Hurn PD, Traystman RJ, Haug FM, Froehner SC, Adams ME, Neely JD, Agre P, Ottersen OPT, Bhardwaj A (2003) An alpha-syntrophin-dependent pool of AQP4 in astroglial end-feet confers bidirectional water flow between blood and brain. Proceedings of the National Academy of Sciences of the United States of America 100:2106-2111.

Andrew RD, MacVicar BA (1994) Imaging cell volume changes and neuronal excitation in the hippocampal slice. Neuroscience 62:371-383.

Andrew RD, Labron MW, Boehnke SE, Carnduff L, Kirov SA (2007) Physiological evidence that pyramidal neurons lack functional water channels. Cereb Cortex 17:787-802.

Badaut J, Ashwal S, Adami A, Tone B, Recker R, Spagnoli D, Ternon B, Obenaus A (2011) Brain water mobility decreases after astrocytic aquaporin-4 inhibition using RNA interference. Journal of Cerebral Blood Flow and Metabolism 31:819-831.

Benesova J, Rusnakova V, Honsa P, Pivonkova H, Dzamba D, Kubista M, Anderova M (2012) Distinct Expression/Function of Potassium and Chloride Channels Contributes to the Diverse Volume Regulation in Cortical Astrocytes of GFAP/EGFP Mice. Plos One 7.

Benham CD, Bolton TB, Lang RJ, Takewaki T (1985) The mechanism of action of Ba2+ and TEA on single Ca2+-activated K+ -channels in arterial and intestinal smooth muscle cell membranes. Pflugers Arch 403:120-127.

Binder DK, Papadopoulos MC, Haggie PM, Verkman AS (2004) In vivo measurement of brain extracellular space diffusion by cortical surface photobleaching. J Neurosci 24:8049-8056.

Cahoy JD, Emery B, Kaushal A, Foo LC, Zamanian JL, Christopherson KS, Xing Y, Lubischer JL, Krieg PA, Krupenko SA, Thompson WJ, Barres BA (2008) A transcriptome database for astrocytes, neurons, and oligodendrocytes: a new resource for understanding brain development and function. J Neurosci 28:264-278.

Cholet N, Pellerin L, Magistretti PJ, Hamel E (2002) Similar perisynaptic glial localization for the Na+,K+-ATPase alpha 2 subunit and the glutamate transporters GLAST and GLT-1 in the rat somatosensory cortex. Cereb Cortex 12:515-525.

Connors N, Adams M, Froehner S, Kofuji P (2004) The potassium channel Kir4.1 associates with the dystrophin-glycoprotein complex via alpha-syntrophin in glia. Journal of Biological Chemistry 279:28387-28392.

D'Ambrosio R, Gordon DS, Winn HR (2002) Differential role of KIR channel and Na(+)/K(+)-pump in the regulation of extracellular K(+) in rat hippocampus. J Neurophysiol 87:87-102.

Davies ML, Kirov SA, Andrew RD (2007) Whole isolated neocortical and hippocampal preparations and their use in imaging studies. J Neurosci Methods 166:203-216.

Deitmer JW, Rose CR (2010) Ion changes and signalling in perisynaptic glia. Brain Res Rev 63:113-129.

Delpire E, Weaver CD (2016) Challenges of Finding Novel Drugs Targeting the K-Cl Cotransporter. ACS chemical neuroscience 7:1624-1627.

Devaraju P, Sun M, Myers T, Lauderdale K, Fiacco T (2013) Astrocytic group I mGluR-dependent potentiation of astrocytic glutamate and potassium uptake. Journal of Neurophysiology 109:2404-2414.

Dimmer KS, Friedrich B, Lang F, Deitmer JW, Broer S (2000) The low-affinity monocarboxylate transporter MCT4 is adapted to the export of lactate in highly glycolytic cells. Biochem J 350 Pt 1:219-227.

Djukic B, Casper KB, Philpot BD, Chin LS, McCarthy KD (2007) Conditional knock-out of Kir4.1 leads to glial membrane depolarization, inhibition of potassium and glutamate uptake, and enhanced short-term synaptic potentiation. J Neurosci 27:11354-11365.

Elwej A, Chaabane M, Ghorbel I, Chelly S, Boudawara T, Zeghal N (2017) Effects of barium graded doses on redox status, membrane bound ATPases and histomorphological aspect of the liver in adult rats. Toxicol Mech Methods 27:677-686.

Elwej A, Ghorbel I, Chaabane M, Soudani N, Mnif H, Boudawara T, Zeghal N, Sefi M (2018) Zinc and selenium modulate barium-induced oxidative stress, cellular injury and membrane-bound ATPase in the cerebellum of adult rats and their offspring during late pregnancy and early postnatal periods. Arch Physiol Biochem 124:237-246.

Feng G, Mellor R, Bernstein M, Keller-Peck C, Nguyen Q, Wallace M, Nerbonne J, Lichtman J, Sanes J (2000) Imaging neuronal subsets in transgenic mice expressing multiple spectral variants of GFP. Neuron 28:41-51.

Fiacco TA, Agulhon C, McCarthy KD (2009) Sorting out astrocyte physiology from pharmacology. Annu Rev Pharmacol Toxicol 49:151-174.

Florence CM, Baillie LD, Mulligan SJ (2012) Dynamic volume changes in astrocytes are an intrinsic phenomenon mediated by bicarbonate ion flux. PLoS One 7:e51124.

Gunnarson E, Zelenina M, Axehult G, Song Y, Bondar A, Krieger P, Brismar H, Zelenin S, Aperia A (2008) Identification of a molecular target for glutamate regulation of astrocyte water permeability. Glia.

Haj-Yasein NN, Jensen V, Vindedal GF, Gundersen GA, Klungland A, Ottersen OP, Hvalby O, Nagelhus EA (2011) Evidence that compromised K+ spatial buffering contributes to the epileptogenic effect of mutations in the human Kir4.1 gene (KCNJ10). Glia 59:1635-1642.

Haj-Yasein NN, Jensen V, Østby I, Omholt SW, Voipio J, Kaila K, Ottersen OP, Hvalby Ø, Nagelhus EA (2012) Aquaporin-4 regulates extracellular space volume dynamics during high-frequency synaptic stimulation: a gene deletion study in mouse hippocampus. Glia 60:867-874.

Hille B (1978) Ionic channels in excitable membranes. Current problems and biophysical approaches. Biophys J 22:283-294.

Jayakumar AR, Norenberg MD (2010) The Na-K-Cl Co-transporter in astrocyte swelling. Metab Brain Dis 25:31-38.

Kalsi AS, Greenwood K, Wilkin G, Butt AM (2004) Kir4.1 expression by astrocytes and oligodendrocytes in CNS white matter: a developmental study in the rat optic nerve. J Anat 204:475-485.

Kitaura H, Tsujita M, Huber VJ, Kakita A, Shibuki K, Sakimura K, Kwee IL, Nakada T (2009) Activity-dependent glial swelling is impaired in aquaporin-4 knockout mice. Neuroscience Research 64:208-212.

Kofuji P, Newman EA (2004) Potassium buffering in the central nervous system. Neuroscience 129:1045-1056.

Kolenicova D, Tureckova J, Pukajova B, Harantova L, Kriska J, Kirdajova D, Vorisek I, Kamenicka M, Valihrach L, Androvic P, Kubista M, Vargova L, Anderova M (2020) High potassium exposure reveals the altered ability of astrocytes to regulate their volume in the aged hippocampus of GFAP/EGFP mice. Neurobiology of Aging 86:162-181.

Larsen BR, MacAulay N (2017) Activity-dependent astrocyte swelling is mediated by pH-regulating mechanisms. Glia 65:1668-1681.

Larsen BR, Stoica A, MacAulay N (2016) Managing Brain Extracellular K(+) during Neuronal Activity: The Physiological Role of the Na(+)/K(+)-ATPase Subunit Isoforms. Frontiers in physiology 7:141.

Larsen BR, Assentoft M, Cotrina ML, Hua SZ, Nedergaard M, Kaila K, Voipio J, MacAulay N (2014) Contributions of the Na^+/K^+-ATPase, NKCC1, and Kir4.1 to hippocampal K^+ clearance and volume responses. Glia 62:608-622.

Lichter-Konecki U, Mangin J, Gordish-Dressman H, Hoffman E, Gallo V (2008) Gene expression profiling of astrocytes from hyperammonemic mice reveals altered pathways for water and potassium homeostasis in vivo. Glia 56:365-377.

Lu J, Boron WF (2007) Reversible and irreversible interactions of DIDS with the human electrogenic Na/HCO3 cotransporter NBCe1-A: role of lysines in the KKMIK motif of TM5. Am J Physiol Cell Physiol 292:C1787-1798.

MacAulay N, Zeuthen T (2010) Water transport between CNS compartments: contributions of aquaporins and cotransporters. Neuroscience 168:941-956.

Macaulay N, Zeuthen T (2012) Glial K^+ clearance and cell swelling: key roles for cotransporters and pumps. Neurochem Res 37:2299-2309.

MacVicar BA, Feighan D, Brown A, Ransom B (2002) Intrinsic optical signals in the rat optic nerve: Role for K+ uptake via NKCC1 and swelling of astrocytes. Glia 37:114-123.

Malek SA, Coderre E, Stys PK (2003) Aberrant chloride transport contributes to anoxic/ischemic white matter injury. J Neurosci 23:3826-3836.

Manley GT, Fujimura M, Ma TH, Noshita N, Filiz F, Bollen AW, Chan P, Verkman AS (2000) Aquaporin-4 deletion in mice reduces brain edema after acute water intoxication and ischemic stroke. Nature Medicine 6:159-163.

Melone M, Ciriachi C, Pietrobon D, Conti F (2019) Heterogeneity of Astrocytic and Neuronal GLT-1 at Cortical Excitatory Synapses, as Revealed by its Colocalization With Na+/K+-ATPase alpha Isoforms. Cereb Cortex 29:3331-3350.

Miller C, Latorre R, Reisin I (1987) Coupling of voltage-dependent gating and Ba++ block in the high-conductance, Ca++-activated K+ channel. J Gen Physiol 90:427-449.

Mongin AA, Kimelberg HK (2002) ATP potently modulates anion channel-mediated excitatory amino acid release from cultured astrocytes. Am J Physiol Cell Physiol 283:C569-578.

Mongin AA, Aksentsev SL, Orlov SN, Slepko NG, Kozlova MV, Maximov GV, Konev SV (1994) Swelling-induced K+ influx in cultured primary astrocytes. Brain Res 655:110-114.

Moroni RF, Inverardi F, Regondi MC, Pennacchio P, Frassoni C (2015) Developmental expression of Kir4.1 in astrocytes and oligodendrocytes of rat somatosensory cortex and hippocampus. Int J Dev Neurosci 47:198-205.

Murphy TR, Davila D, Cuvelier N, Young LR, Lauderdale K, Binder DK, Fiacco TA (2017) Hippocampal and Cortical Pyramidal Neurons Swell in Parallel with Astrocytes during Acute Hypoosmolar Stress. Frontiers in cellular neuroscience 11:275.

Nagelhus EA, Mathiisen TM, Ottersen OP (2004) Aquaporin-4 in the central nervous system: cellular and subcellular distribution and coexpression with KIR4.1. Neuroscience 129:905-913.

Nagelhus EA, Veruki ML, Torp R, Haug FM, Laake JH, Nielsen S, Agre P, Ottersen OP (1998) Aquaporin-4 water channel protein in the rat retina and optic nerve: polarized expression in Muller cells and fibrous astrocytes. J Neurosci 18:2506-2519.

Nagelhus EA, Horio Y, Inanobe A, Fujita A, Haug FM, Nielsen S, Kurachi Y, Ottersen OP (1999) Immunogold evidence suggests that coupling of K+ siphoning and water transport in rat retinal Müller cells is mediated by a coenrichment of Kir4.1 and AQP4 in specific membrane domains. Glia 26:47-54.

Nielsen S, Nagelhus EA, AmiryMoghaddam M, Bourque C, Agre P, Ottersen OP (1997) Specialized membrane domains for water transport in glial cells: High-resolution immunogold cytochemistry of aquaporin-4 in rat brain. Journal of Neuroscience 17:171-180.

Pasantes-Morales H, Schousboe A (1989) Release of taurine from astrocytes during potassium-evoked swelling. Glia 2:45-50.

Ransom BR, Yamate CL, Connors BW (1985) Activity-dependent shrinkage of extracellular space in rat optic nerve: a developmental study. J Neurosci 5:532-535.

Ransom CB, Ransom BR, Sontheimer H (2000) Activity-dependent extracellular K+ accumulation in rat optic nerve: the role of glial and axonal Na+ pumps. J Physiol 522 Pt 3:427-442.

Risher WC, Andrew RD, Kirov SA (2009) Real-time passive volume responses of astrocytes to acute osmotic and ischemic stress in cortical slices and in vivo revealed by two-photon microscopy. Glia 57:207-221.

Rudy B (1988) Diversity and ubiquity of K channels. Neuroscience 25:729-749.

Rungta RL, Choi HB, Tyson JR, Malik A, Dissing-Olesen L, Lin PJC, Cain SM, Cullis PR, Snutch TP, MacVicar BA (2015) The cellular mechanisms of neuronal swelling underlying cytotoxic edema. Cell 161:610-621.

Schnell C, Shahmoradi A, Wichert S, Mayerl S, Hagos Y, Heuer H, Rossner M, Hulsmann S (2015) The multispecific thyroid hormone transporter OATP1C1 mediates cell-specific sulforhodamine 101-labeling of hippocampal astrocytes. Brain Structure & Function 220:193-203.

Steffensen AB, Sword J, Croom D, Kirov SA, MacAulay N (2015) Chloride Cotransporters as a Molecular Mechanism underlying Spreading Depolarization-Induced Dendritic Beading. J Neurosci 35:12172-12187.

Stoica A, Larsen BR, Assentoft M, Holm R, Holt LM, Vilhardt F, Vilsen B, Lykke-Hartmann K, Olsen ML, MacAulay N (2017) The alpha2beta2 isoform combination dominates the astrocytic Na(+) /K(+) -ATPase activity and is rendered nonfunctional by the alpha2.G301R familial hemiplegic migraine type 2-associated mutation. Glia 65:1777-1793.

Strohschein S, Huttmann K, Gabriel S, Binder DK, Heinemann U, Steinhauser C (2011) Impact of aquaporin-4 channels on K+ buffering and gap junction coupling in the hippocampus. Glia 59:973-980.

Su G, Kintner DB, Sun DD (2002a) Contribution of Na+-K+-Cl- cotransporter to high-K+ (o)-induced swelling and EAA release in astrocytes. American Journal of Physiology-Cell Physiology 282:C1136-C1146.

Su G, Kintner DB, Flagella M, Shull GE, Sun DD (2002b) Astrocytes from Na+-K+-Cl-cotransporter-null mice exhibit absence of swelling and decrease in EAA release. American Journal of Physiology-Cell Physiology 282:C1147-C1160.

Sword J, Croom D, Wang PL, Thompson RJ, Kirov SA (2017) Neuronal pannexin-1 channels are not molecular routes of water influx during spreading depolarization-induced dendritic beading. J Cereb Blood Flow Metab 37:1626-1633.

Takano T, Kang J, Jaiswal JK, Simon SM, Lin JH, Yu Y, Li Y, Yang J, Dienel G, Zielke HR, Nedergaard M (2005) Receptor-mediated glutamate release from volume sensitive channels in astrocytes. Proc Natl Acad Sci USA 102:16466-16471.

Tang YT, Mendez JM, Theriot JJ, Sawant PM, Lopez-Valdes HE, Ju YS, Brennan KC (2014) Minimum conditions for the induction of cortical spreading depression in brain slices. J Neurophysiol 112:2572-2579.

Toft-Bertelsen TL, Larsen BR, Christensen SK, Khandelia H, Waagepetersen HS, MacAulay N (2020) Clearance of activity-evoked K(+) transients and associated glia cell swelling occur independently of AQP4: A study with an isoform-selective AQP4 inhibitor. Glia.

Traynelis SF, Dingledine R (1988) Potassium-induced spontaneous electrographic seizures in the rat hippocampal slice. J Neurophysiol 59:259-276.

Traynelis SF, Dingledine R, McNamara JO, Butler L, Rigsbee L (1989) Effect of kindling on potassium-induced electrographic seizures in vitro. Neurosci Lett 105:326-332.

Vázquez-Juárez E, Hernández-Benítez R, López-Domínguez A, Pasantes-Morales H (2009) Thrombin potentiates D-aspartate efflux from cultured astrocytes under conditions of K+ homeostasis disruption. J Neurochem 111:1398-1408.

Walter SJ, Shirley DG, Folkerd EJ, Unwin RJ (2001) Effects of the potassium channel blocker barium on sodium and potassium transport in the rat loop of Henle in vivo. Exp Physiol 86:469-474.

Walz W (1992) Mechanism of rapid K(+)-induced swelling of mouse astrocytes. Neurosci Lett 135:243-246.

Walz W (2000) Role of astrocytes in the clearance of excess extracellular potassium. Neurochemistry International 36:291-300.

Walz W, Hinks EC (1985) Carrier-mediated KCl accumulation accompanied by water movements is involved in the control of physiological K+ levels by astrocytes. Brain Res 343:44-51.

Walz W, Shargool M, Hertz L (1984) Barium-induced inhibition of K+ transport mechanisms in cortical astrocytes--its possible contribution to the large Ba2+-evoked extracellular K+ signal in brain. Neuroscience 13:945-949.

Wen H, Nagelhus EA, Amiry-Moghaddam M, Agre P, Ottersen OP, Nielsen S (1999) Ontogeny of water transport in rat brain: postnatal expression of the aquaporin-4 water channel. Eur J Neurosci 11:935-945.

Wurm A, Pannicke T, Iandiev I, Wiedemann P, Reichenbach A, Bringmann A (2006) The developmental expression of K+ channels in retinal glial cells is associated with a decrease of osmotic cell swelling. Glia 54:411-423.

Xie A, Lauderdale K, Murphy T, Myers T, Fiacco T (2014) Inducing Plasticity of Astrocytic Receptors by Manipulation of Neuronal Firing Rates. Jove-Journal of Visualized Experiments.

Xie AX, Sun MY, Murphy T, Lauderdale K, Tiglao E, Fiacco TA (2012) Bidirectional scaling of astrocytic metabotropic glutamate receptor signaling following long-term changes in neuronal firing rates. PLoS ONE 7:e49637.

Zhou N, Gordon G, Feighan D, MacVicar B (2010) Transient Swelling, Acidification, and Mitochondrial Depolarization Occurs in Neurons but not Astrocytes during Spreading Depression. Cerebral Cortex 20:2614-2624.

Figures

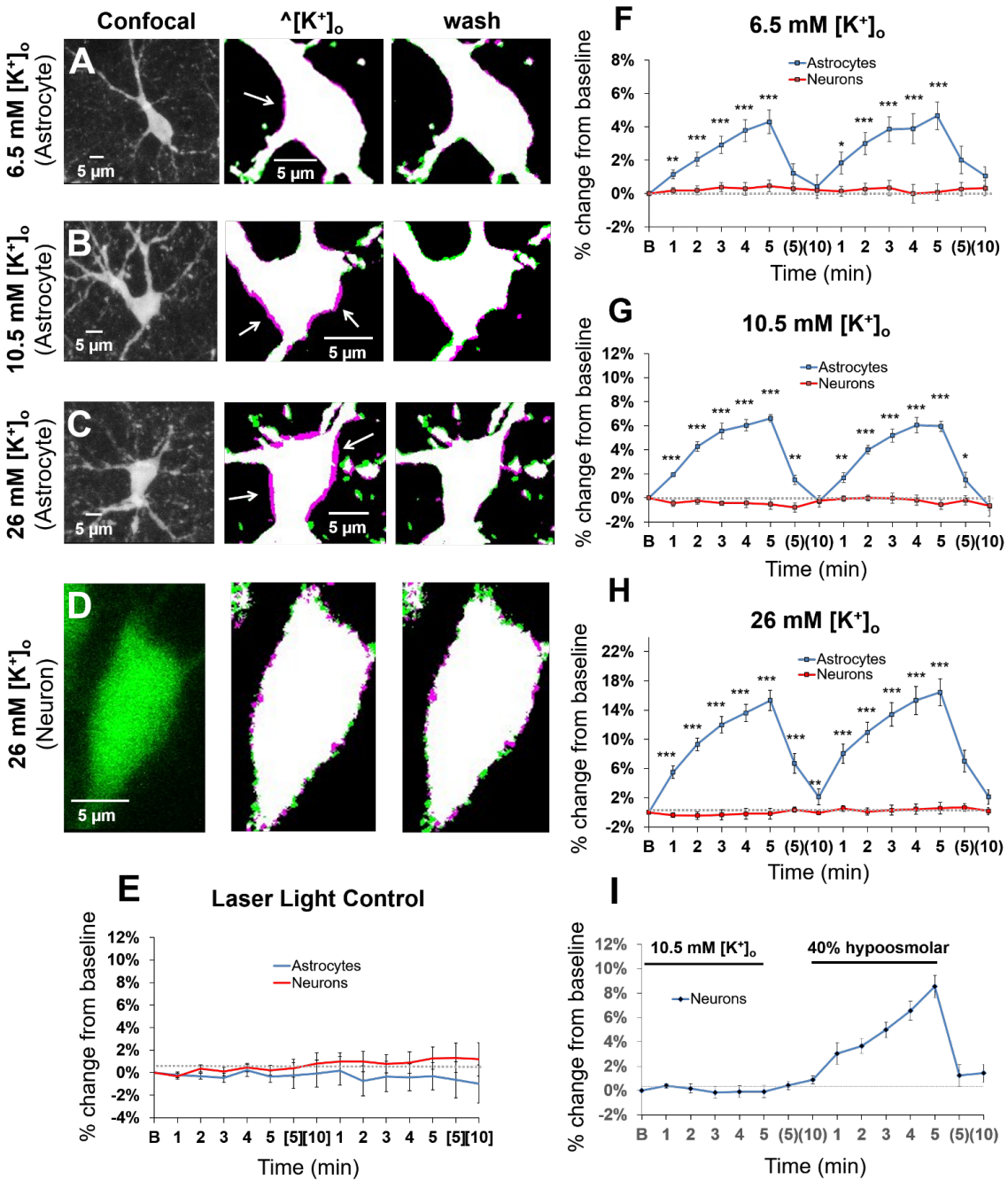
Confocal
^[K+]o
wash
A
6.5 mM [K+]o (Astrocyte)
B
10.5 mM [K+]o (Astrocyte)
C
26 mM [K+]o (Astrocyte)
D
26 mM [K+]o (Neuron)
5 µm
F
6.5 mM [K+]o
G
10.5 mM [K+]o
H
26 mM [K+]o
Astrocytes
Neurons
% change from baseline
Time (min)
B 1 2 3 4 5 (5)(10) 1 2 3 4 5 (5)(10)
E
Laser Light Control
B 1 2 3 4 5 [5][10] 1 2 3 4 5 [5][10]
I
10.5 mM [K+]o
40% hypoosmolar

Figure 2.1. Elevated $[K^+]_o$ ACSF selectively swells astrocytes. $[K^+]_o$ was raised from a baseline of 2.5 mM in control ACSF by addition of KCl, with removal of an equal amount of NaCl to preserve solution osmolarity (see Methods). **(A - D)** Representative confocal images of s.r. astrocytes **(A - C)** and a CA1 pyramidal neuron **(D)** in control ACSF show general cell morphology (left panels). Middle panels in **(A - D)** show thresholded, pseudocolor images of the same cells taken after 5 minutes in $^[K^+]_o$ at 6.5 mM **(A)**, 10.5 mM **(B)** or 26 mM **(C, D),** overlaid onto the baseline image. Increase in cell volume in the image overlays is indicated by a magenta outline (white arrows). "Wash" is the image taken after the first 10 minute wash period overlaid onto the baseline image (right panels) to show recovery of cell volume in control ACSF. **(E)** Application of laser light alone to acute slices perfused with control ACSF for the duration of an imaging experiment (20 min.) had no effect (± ~1%) on the volume of astrocytes (n = 6) or neurons (n = 6). **(F)** 6.5 mM $[K^+]_o$ increased the volume of astrocytes in a time-dependent manner, to approximately 4.3 - 4.6% above baseline after 5 minutes. Return to control ACSF (timepoints (5) and (10)) led to recovery of cell volume to near baseline. Neurons exposed to 6.5 mM $[K^+]_o$ did not undergo changes in volume (n = 7). At all timepoints tested, astrocyte volume was significantly greater than neuronal volume, which remained at or near baseline (*$p < 0.05$, **$p < 0.01$ or ***$p < 0.001$; n = 9 astrocytes, 7 neurons). **(G)** Application of 10.5 mM $[K^+]_o$ triggered astrocyte volume increase to ~6% above baseline, significantly greater than neuronal volume at all time points, which remained within 1% of baseline (**$p < 0.01$ or ***$p < 0.001$; n = 9 astrocytes, 7 neurons) . **(H)** 26 mM $^[K^+]_o$, increased astrocyte volume by up to 15%, significantly greater than neuronal volume at all timepoints (***$p < 0.001$; n = 8 astrocytes, 10 neurons). **(I)** Dose-response of astrocyte and neuronal volume at the 5 min. time point of the first application of $^[K^+]_o$. At each concentration, astrocyte volume was significantly greater than neurons, which steadfastly maintained their volume in elevated $^[K^+]_o$ (***$p < 0.001$).

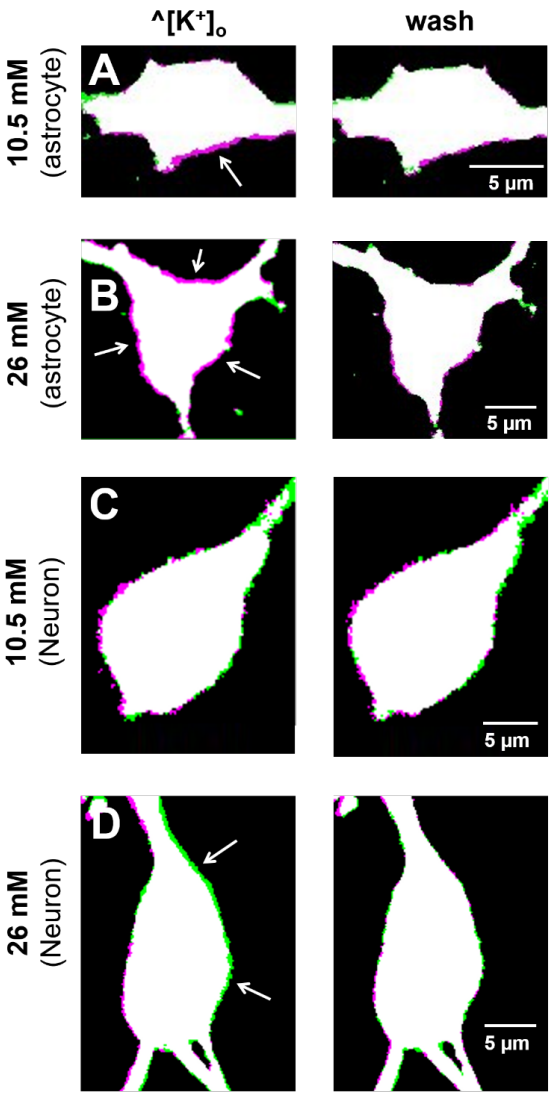
^[K+]o
wash
10.5 mM (astrocyte)
26 mM (astrocyte)
10.5 mM (Neuron)
26 mM (Neuron)
A
B
C
D
5 µm

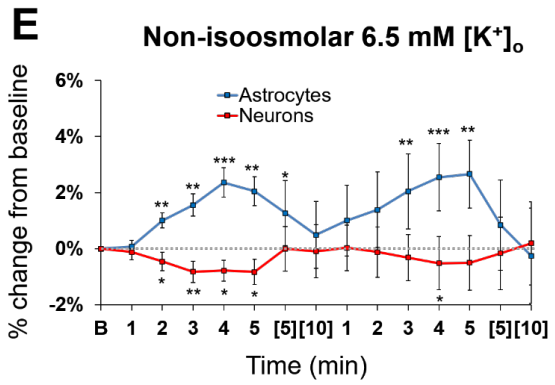
E
Non-isoosmolar 6.5 mM [K+]o
Astrocytes
Neurons
% change from baseline
Time (min)
B 1 2 3 4 5 [5][10] 1 2 3 4 5 [5][10]

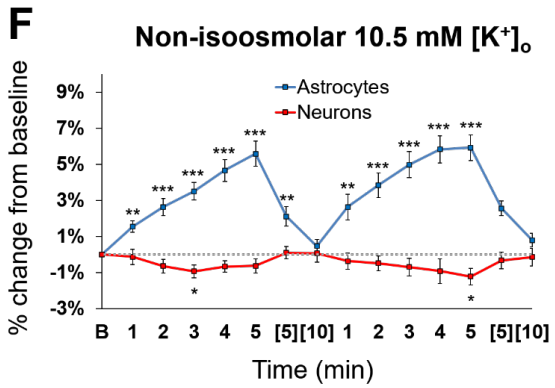
F
Non-isoosmolar 10.5 mM [K+]o
Astrocytes
Neurons
% change from baseline
Time (min)
B 1 2 3 4 5 [5][10] 1 2 3 4 5 [5][10]

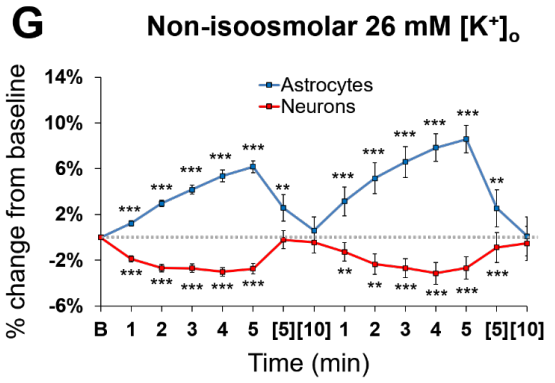
G
Non-isoosmolar 26 mM [K+]o
Astrocytes
Neurons
% change from baseline
Time (min)
B 1 2 3 4 5 [5][10] 1 2 3 4 5 [5][10]

Figure 2.2. Increased solution osmolarity by addition of K^+ attenuates astrocyte swelling and shrinks neurons. KCl was added to control ACSF to elevate $[K^+]_o$ from 2.5 mM without a corresponding removal of NaCl. The resulting 'non-isoosmolar' $^[K^+]_o$ was applied over 5 min. followed by a 10 min. 'wash' in control ACSF. **(A - D)** Representative thresholded images of astrocytes **(A, B)** and neurons **(C, D)** after 5 min in $^[K^+]_o$ overlaid onto the baseline image to show volume changes (left panels). The magenta outline reveals volume expansion while green indicates cell shrinking. Astrocytes in 10.5 mM **(A)** and 26 mM **(B)** non-isoosmolar $[K^+]_o$ swell while neuronal shrinking is visibly apparent at 26 mM $[K^+]_o$ but not at 10 mM $[K^+]_o$ after 5 minutes **(C, D)**. Any changes in cell volume recover to baseline during the "wash" period (right panels). **(E)** Dose-response of cell volume illustrates the peak volume change of both cell types after five minutes in non-isoosmolar $^[K^+]_o$. Dampening of astrocyte swelling and neuronal shrinking are most evident at the 26 mM $[K^+]_o$ dose. **(F - H)** Summary data of astrocyte and neuron volume changes at the different non-isoosmolar concentrations of $[K^+]_o$ relative to baseline volume. Astrocyte volume increased significantly over baseline at 6.5 mM $[K^+]_o$ (n = 11) **(F)**, 10.5 mM $[K^+]_o$ (n = 8) **(G)**, and 26 mM $[K^+]_o$ (n = 9). Neurons, however, exhibited significant shrinking in a dose- and time-dependent manner (6.5 mM $[K^+]_o$, n = 9; 10.5 mM $[K^+]_o$, n = 10; 26 mM $[K^+]_o$, n = 9) and recovered to baseline volume after 10 minutes in control ACSF ($^[K^+]_o$ wash). Significance is indicated as percent change from baseline within-cell at $*p < 0.05$, $**p < 0.01$ or $***p < 0.001$.

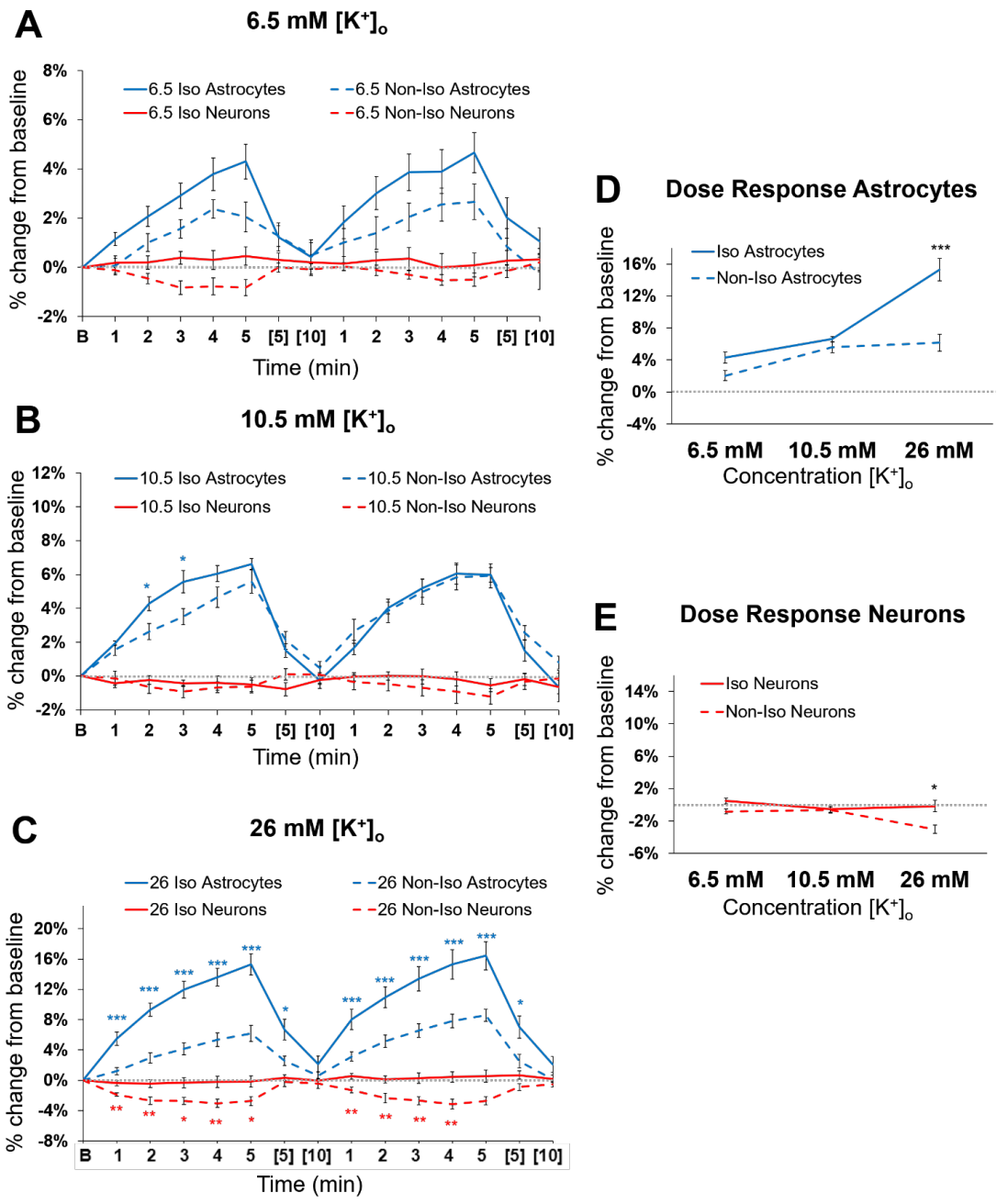
A
6.5 mM [K+]o
6.5 Iso Astrocytes
6.5 Non-Iso Astrocytes
6.5 Iso Neurons
6.5 Non-Iso Neurons
% change from baseline
Time (min)
B
10.5 mM [K+]o
10.5 Iso Astrocytes
10.5 Non-Iso Astrocytes
10.5 Iso Neurons
10.5 Non-Iso Neurons
% change from baseline
Time (min)
C
26 mM [K+]o
26 Iso Astrocytes
26 Non-Iso Astrocytes
26 Iso Neurons
26 Non-Iso Neurons
% change from baseline
Time (min)
D
Dose Response Astrocytes
Iso Astrocytes
Non-Iso Astrocytes
% change from baseline
6.5 mM 10.5 mM 26 mM
Concentration [K+]o
E
Dose Response Neurons
Iso Neurons
Non-Iso Neurons
% change from baseline
6.5 mM 10.5 mM 26 mM
Concentration [K+]o

Figure 2.3. Comparison of astrocyte and neuron volume in isoosmolar vs. non-isoosmolar ^$[K^+]_o$. Data from Fig. 1 and 2 have been reassembled to highlight effects of increased extracellular osmolarity on cell volume in ^$[K^+]_o$. At each concentration of $[K^+]_o$, cell types are specified by color (astrocytes blue, neurons red), and the ACSF osmolarity indicated by dotted (non-isoosmolar) or solid (isoosmolar) lines. Blue asterisks indicate significant differences between astrocyte volume across osmolarity treatments, with red asterisks indicating the same for neurons. **(A)** Although the effect of the increased osmolarity by addition of K^+ is readily apparent in reducing the volume of cells, the osmolarity of 6.5 mM $[K^+]_o$ treatment did not have a significant effect on the swelling of astrocytes or shrinkage of neurons. **(B)** At 10.5 mM $[K^+]_o$, the increase in osmolarity led to a small but significant reduction in astrocyte swelling at minutes 2 and 3 ($*p < 0.05$) during ^$[K^+]_o$ exposure. During the second 10.5 mM $[K^+]_o$ application, there was no difference in the swelling of astrocytes across treatments. Similarly, the osmolarity of 10.5 mM $[K^+]_o$ application had no significant effect on the volume of neurons. **(C)** Non-isoosmolar 26 mM $[K^+]_o$ ACSF significantly decreased astrocyte swelling ($***p < 0.001$) and significantly shrank neurons ($*p < 0.05$ or $**p < 0.01$) compared to isoosmolar treatment. **(D)** Dose-response of iso- vs. non-isoosmolar ^$[K^+]_o$ treatment in astrocytes shows minimal effect of osmolarity on astrocyte ^$[K^+]_o$-induced volume increases, except at the highest dose where the increase in osmolarity by 26 mM $[K^+]_o$ significantly dampened the volume change ($***p < 0.001$). **(E)** Overall, effects of $[K^+]_o$ and extracellular osmolarity on neuron volume are negligible at 6.5 and 10.5 mM. Only at 26 mM $[K^+]_o$ does the osmolarity increase trigger significant (~3%) shrinkage of neurons from baseline volume.

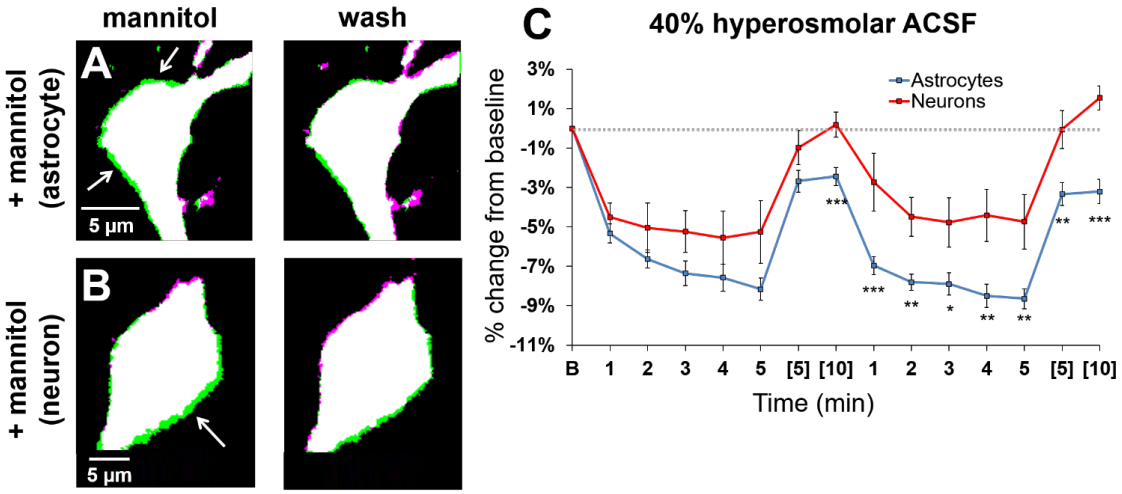

Figure 2.4. Hyperosmolar ACSF shrinks both neurons and astrocytes. Pseudocolor images of an astrocyte **(A)** and neuron **(B)** at baseline overlaid with the image taken after 5 min. in mannitol-supplemented ACSF ("mannitol"; left) and then after return to control ACSF for 10 min ("wash"). Green coloring (white arrows) indicates reduction in soma volume compared to the baseline image. **(C)** Application of 40% hyperosmolar ACSF (by addition of mannitol) led to shrinking of both astrocytes (n = 14) and neurons (n = 10) during both 5 min application periods. Upon return to control ACSF, neurons completely recovered their volume, while astrocytes remained at most 3.3% below baseline volume. Astrocyte shrinking was significantly greater than neurons at all timepoints during and after the second application of hyperosmolar ACSF (*$p < 0.05$, **$p < 0.01$ or ***$p < 0.001$).

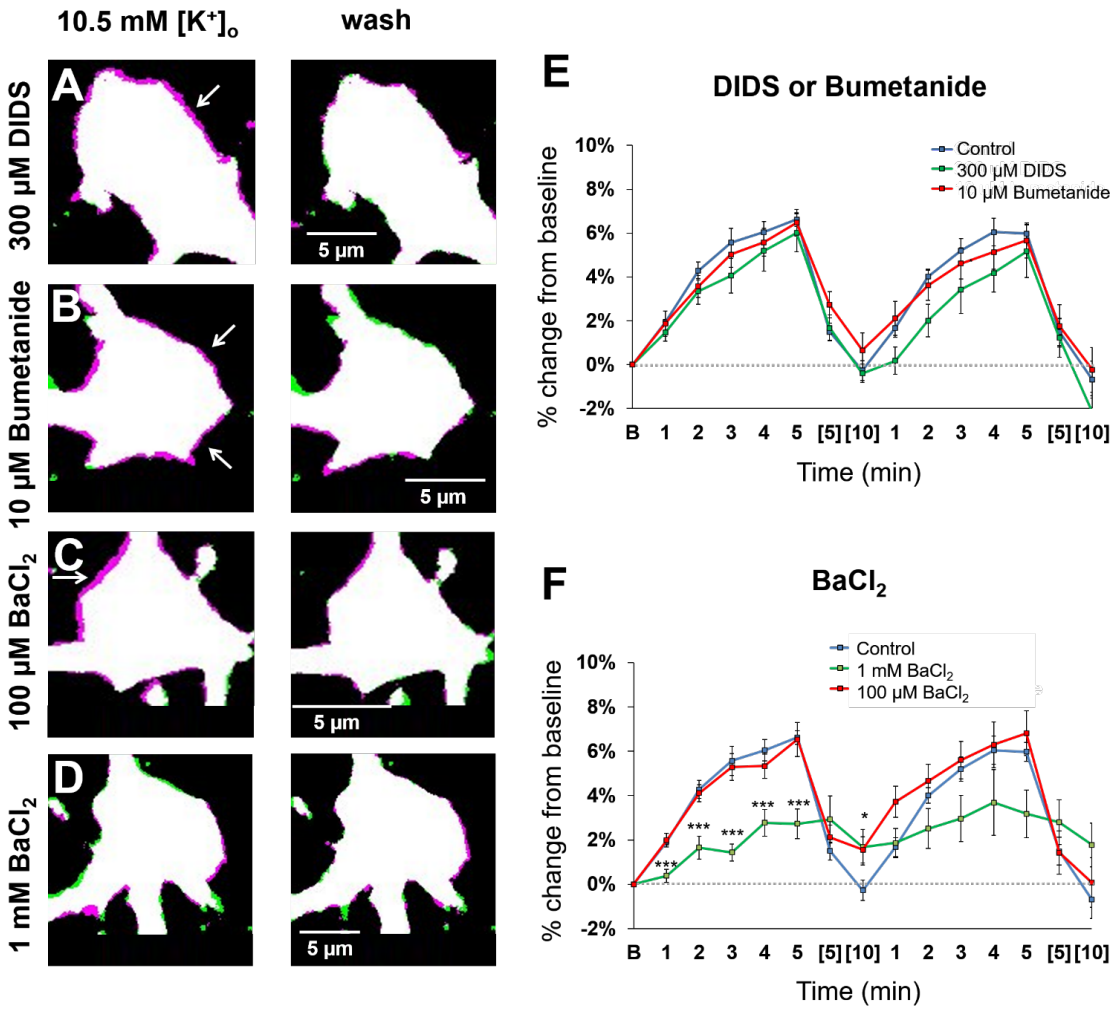

Figure 2.5. Astrocyte swelling in ^$[K^+]_o$ is not due to NBCe1, NKCC1 or Kir4.1. (A - D) Representative astrocyte images taken at 5 minutes overlaid onto the baseline image in isoosmolar 10.5 mM $[K^+]_o$ in the presence of antagonists for the NBCe1 (DIDS; 300 µM), NKCC (bumetanide; 10 µM), Kir4.1 ($BaCl_2$; 100 µM), or K^+ channels in general ($BaCl_2$; 1 mM) (left panels) followed by 10 min. wash (right panels). Note continued swelling of astrocytes in all conditions except 1 mM $BaCl_2$ as indicated by the magenta border (white arrows). **(E)** Summary data showing lack of effect of DIDS (n = 6) or bumetanide (n = 8) on astrocyte swelling profiles in 10.5 mM $[K^+]_o$ compared to control recordings in the absence of antagonists (n = 9). **(F)** $BaCl_2$ at 100 µM had no effect on astrocyte volume (n = 10), but significantly reduced astrocyte volume increases at 1 mM (n = 8), suggesting possible involvement of an unidentified K^+ channel.

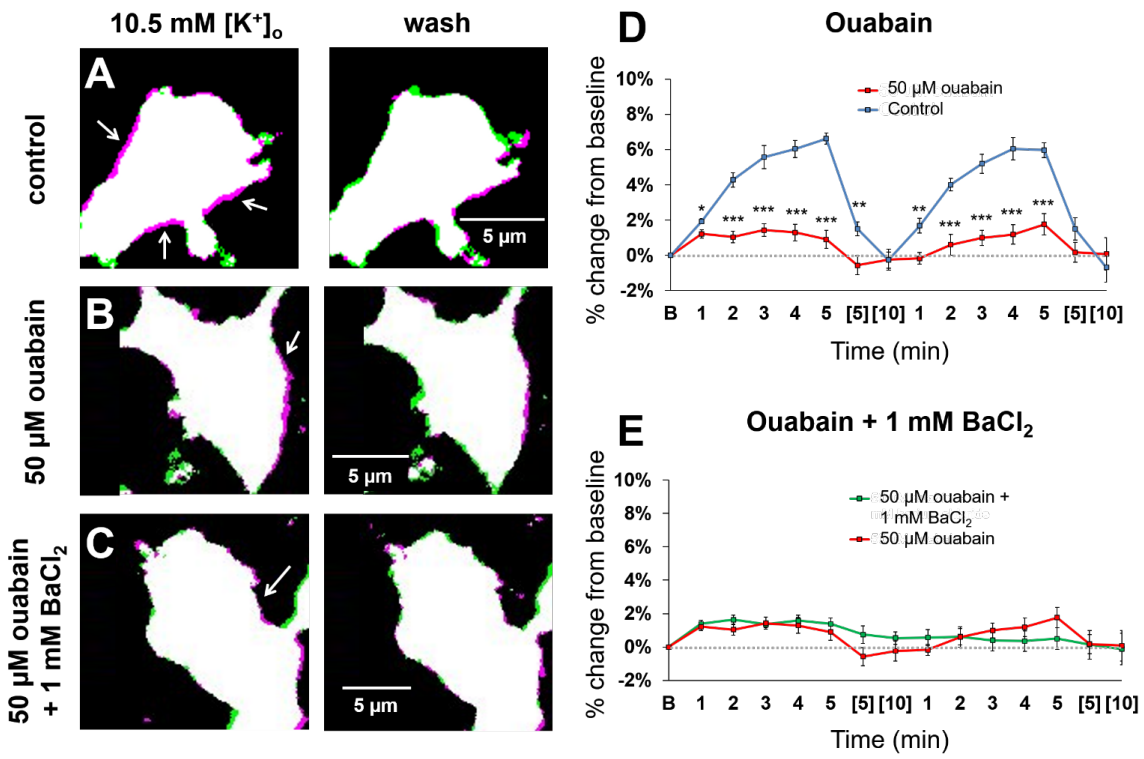

Figure 2.6. The Na^+/K^+ ATPase inhibitor ouabain significantly reduces astrocyte swelling in $^[K^+]_o$. (A - C) Representative astrocyte images taken at 5 minutes in isoosmolar 10.5 mM $[K^+]_o$ overlaid onto the baseline image for $^[K^+]_o$ only **(A)** or $^[K^+]_o$ in the presence of ouabain (50 µM) **(B)** or ouabain + 1 mM $BaCl_2$ **(C)** (left panels). Note the significant reduction in astrocyte swelling in the treatment groups compared to control as indicated by the magenta border around the cells (white arrows). Overlay of the astrocyte image taken after a 10 min. wash period in control ACSF with the baseline image shows recovery of volume to baseline (right panels). **(C)** Ouabain potently counteracted astrocyte swelling, which led to a significant reduction in astrocyte volume at all time points (n = 8; *p < 0.05, **p < 0.01, or ***p < 0.001). **(D)** The combination of 50 µM ouabain plus 1 mM $BaCl_2$ applied together was no different than + ouabain alone (n = 9) on suppressing astrocyte swelling in 10.5 mM $[K^+]_o$.

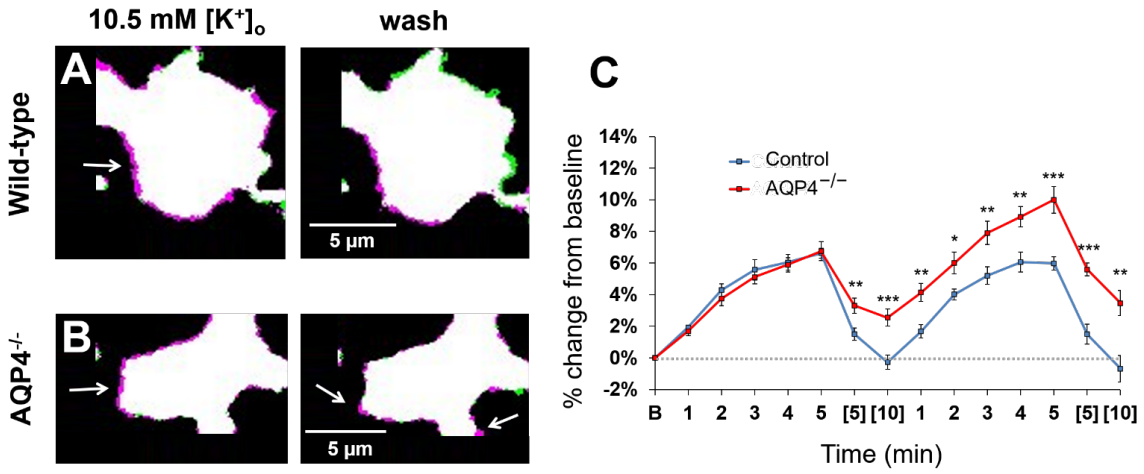

Figure 2.7. Astrocyte Swelling in ^$[K^+]_o$ occurs independently of the water channel AQP4. (A, B) The left panel shows a representative astrocyte image taken after 5 min. in isoosmolar 10.5 mM $[K^+]_o$ ACSF overlaid onto the baseline image for **(A)** wild type and **(B)** AQP4$^{-/-}$. On the right is the 10 min. wash image relative to baseline to show cell volume recovery. The magenta outline (white arrows) indicates volume expansion over baseline. **(C)** Wild-type (n = 9) and AQP4$^{-/-}$ (n = 8) astrocytes swelled at the same rate and to the same volume during the first exposure to ^$[K^+]_o$. Note that AQP4$^{-/-}$ astrocytes failed to return to initial baseline volume after the 10 min. wash period in control ACSF, and remained significantly swollen (**$p < 0.01$ or ***$p < 0.001$). The inability for AQP4$^{-/-}$ astrocytes to recover their volume in the wash period resulted in significantly higher volume increases in the AQP4$^{-/-}$ astrocytes relative to control during the second application of 10.5 mM $[K^+]_o$. These data suggest a possible role for AQP4 in water efflux from astrocytes, rather than a route for water entry.

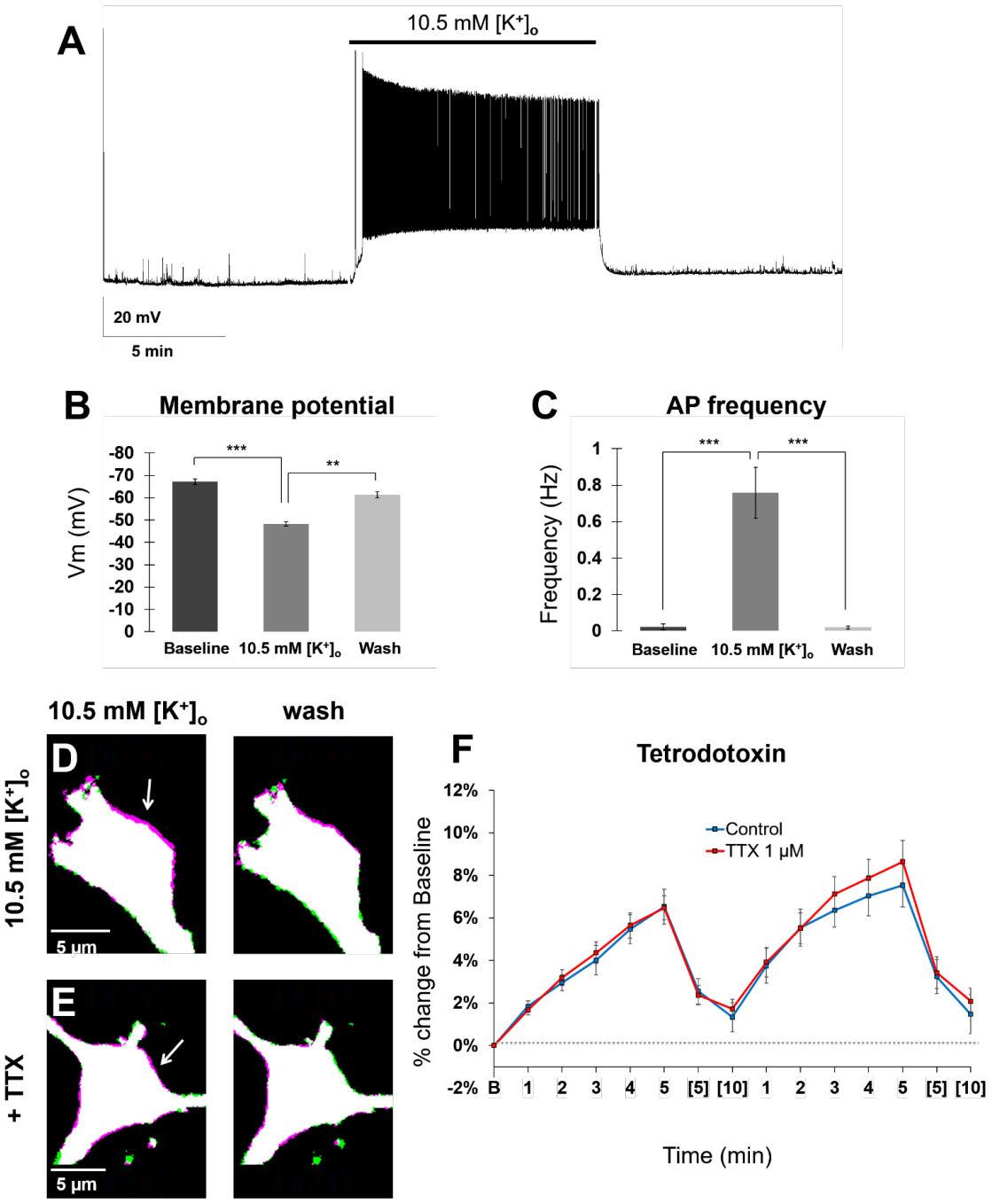
A
10.5 mM [K+]o
20 mV
5 min
B
Membrane potential
Vm (mV)
-80
-70
-60
-50
-40
-30
-20
-10
0
***
**
Baseline
10.5 mM [K+]o
Wash
C
AP frequency
Frequency (Hz)
1
0.8
0.6
0.4
0.2
0
***
***
Baseline
10.5 mM [K+]o
Wash
10.5 mM [K+]o
wash
D
10.5 mM [K+]o
5 µm
E
+ TTX
5 µm
F
Tetrodotoxin
% change from Baseline
12%
10%
8%
6%
4%
2%
0%
-2%
Control
TTX 1 µM
B
1
2
3
4
5
[5]
[10]
1
2
3
4
5
[5]
[10]
Time (min)

Figure 2.8. Block of neuronal firing has no effect on astrocyte swelling in elevated potassium. (A) Representative recording of a CA1 pyramidal neuron in 10.5 mM $[K^+]_o$. Application of 10.5 mM $[K^+]_o$ depolarized the cell by ~25 mV and resulted in generation of frequent action potentials within ~30s. In control ACSF (2.5 mM $[K^+]_o$), action potentials were absent in this cell, both during the baseline and wash periods. **(B)** On average, neurons rested at -67.2 mV and depolarized to -48.3 mV in the presence of 10.5 mM $[K^+]_o$. **(C)** Application of 10.5 mM $[K^+]_o$ significantly increased the frequency of action potentials in CA1 pyramidal cells on average. For (B) and (C), n = 11 neurons, **p < 0.01, ***p < 0.001. Pseudocolor images of astrocytes **(D, E)** depict cell volume at baseline overlaid with images taken after five minutes in isoosmolar 10.5 mM $[K^+]_o$ **(D)** or 10.5 mM $[K^+]_o$ plus 1 μM TTX **(E)** (left panels). "Wash" images (right panels) show cell baseline volume overlaid with volume post- ^$[K^+]_o$ reperfusion in control ACSF. The magenta outline (arrows) shows expansion of the cell soma over baseline volume. **(F)** Co-application of 1 μM TTX with 10.5 mM $[K^+]_o$ had no significant effect on astrocyte swelling compared to 10.5 mM $[K^+]_o$ alone (control n = 8; + TTX n = 10). TTX, like other antagonists, was applied 10 min. prior to addition of 10.5 mM $[K^+]_o$ + TTX and was present throughout the electrophysiology recordings and imaging measurements.

Chapter 2

Abstract

Rapid increases in cell volume reduce the size of the extracellular space (ECS) and are associated with elevated brain tissue excitability. We recently demonstrated that astrocytes swell selectively in elevated extracellular K^+ (^$[K^+]_o$) in concentrations up to 26 mM [Walch et al., 2020]. However, the effects of acute astrocyte volume fluctuations on neuronal excitability changes in elevated $[K^+]_o$ remain unclear. Here we set out to determine the effects of rapid astrocyte volume increases in raised $[K^+]_o$ on the excitability of hippocampal CA1 pyramidal neurons. Volume-specific excitability effects were isolated from direct depolarizing effects of elevated $[K^+]_o$ on neurons by application of TTX and recording neuronal ionotropic glutamate receptor currents in voltage-clamp mode. Elevating $[K^+]_o$ to 10.5 mM induced astrocyte swelling and resulted in significant increases in neuronal excitability in the form of miniature excitatory post-synaptic currents (mEPSCs) and large NMDA receptor-dependent slow inward currents (SICs). To better isolate volume-specific effects on neuronal excitability, experiments were performed using hyperosmolar ACSF to shrink cells during continued application of 10.5 mM $[K^+]_o$. Application of hyperosmolar ACSF in the continued presence of 10.5 mM K^+ forced shrinkage of both neurons and astrocytes, but more dramatically reduced astrocyte volume as astrocytes swell selectively in elevated $[K^+]_o$, while neurons do not. Addition of mannitol in high $[K^+]_o$ diminished the holding current and reduced the occurrence of

extremely large SICs, while mEPSC events persisted. Our findings suggest that a significant portion of increased neuronal excitability in high $[K^+]_o$ can be isolated from the direct depolarizing effects of elevated $[K^+]_o$ on neurons and is driven by cell swelling activation of NMDA receptors.

Introduction

Astrocytes play a significant role in maintaining ion and neurotransmitter concentrations in the extracellular space. This includes uptake of glutamate and potassium that is released during synaptic transmission. Potassium influx into astrocytes during neuronal synaptic activity is redistributed through the glial syncytium to areas of lower potassium concentration, a process known as "spatial buffering" (Walz, 2000; Kofuji & Newman, 2004). Potassium influx into astrocytes associated with K^+ spatial buffering generates an osmotic gradient coupled to movement of water into the cell, leading to transient or prolonged fluxes in cellular volume (Pasantes-Morales & Schousboe; Walz, 1992 MacVicar et al., 2002; Risher et al., 2009).

Cellular swelling tied to ion and water influx results in a transient decrease in the volume of the extracellular space, positively influencing neuronal excitability (Fiacco et al., 2007; Lauderdale et al., 2015; Yang et al., 2019). Dramatic reduction of the ECS also occurs prior to the generation of ictal (or seizure-like) discharges (Traynelis & Dingledine, 1989; Kilb et al., 2006; Shahar et al., 2009). In 8.5 mM $[K^+]_o$, neurons generate synchronous ictal bursting activity that requires NMDA receptor activation and

reduction of the ECS (Traynelis and Dingledine, 1988). In these conditions, although direct cell volume measurements were not taken, it was speculated that the reduction of the ECS was likely due to astrocyte swelling tied to influx of K^+ (Traynelis and Dingledine, 1989). Therefore, astrocyte swelling may directly influence neuronal excitability, contributing directly to seizure generation. However, because epileptiform activity is by definition synchronous neuronal bursting, it is difficult to dissociate possible influences of changes in cell volume from the direct effects of elevated extracellular potassium ($\wedge[K^+]_o$) on neuronal spiking.

We previously used a hypoosmolar model of acute cerebral edema to examine the effects of rapid cell swelling on neuronal activity (Lauderdale et al, 2015; Murphy et al, 2017). Cell swelling generated a burst of NMDA receptor-mediated slow inward currents (SICs) over the course of several minutes which correlated with increased action potentials and burst firing (Lauderdale et al, 2015). However, although the hypoosmolar model had previously been reported to swell only astrocytes due to selective expression of the water channel AQP4 (Manley et al, 2000; Solenov et al, 2004; Risher et al, 2009), we later found that neurons swell to a similar extent as astrocytes (Murphy et al, 2017). Therefore, it was not possible to define a specific contribution of astrocyte swelling to the neuronal excitability increases we observed. An advantage provided by the $\wedge[K^+]_o$ model is that it swells astrocytes selectively [Walch et al., 2020], presenting an alternative cell swelling model to determine effects of astrocyte swelling on neuronal excitability. In this study, we isolate cell swelling-specific effects on neuronal excitability by modifying astrocytic and neuronal osmotic gradients without altering $[K^+]_o$. By quantitative

comparison of event frequency and event characteristics occurring in ^$[K^+]_o$ before and during forced reduction of cell volume, a volume-dependent component of ^$[K^+]_o$-induced neuron excitability can be isolated from hyperosmolarity-induced forced vesicular fusion, which generates fast synaptic events. Our findings suggest that astrocyte swelling in ^$[K^+]_o$ increases neuronal excitability through the generation of slow inward currents that are abolished by astrocyte volume reduction and forced expansion of the ECS in the continued presence of ^$[K^+]_o$.

Materials and Methods

All experiments were performed in accordance with National Institutes of Health guidelines for the care and use of laboratory animals and approved by the Institutional Animal Care and Use Committee at the University of California, Riverside.

Slice Preparation

Hippocampal slices were prepared from C57Bl/6J mice or transgenic mice on the C57Bl6 background at 15 to 21 days of age as described previously (Xie et al., 2014). In some astrocyte imaging experiments, use of hippocampal slices from mGFAP-Cre;Rosa26$^{lsl\text{-}tdTomato}$ transgenic mice replaced C57Bl/6J mice. For experiments requiring neuronal imaging, Thy1-GFP-S or Thy1-GFP-M trans- genic mice were used instead (#011070

and 007788, respectively; Jackson Laboratories, Bar Harbor, ME, USA). These mice have been repeatedly backcrossed to a C57Bl/6J background and exhibit no obvious differences in phenotype compared with wild-type mice (Feng et al., 2000).

Animals were anesthetized under isoflurane and rapidly decapitated, and brains were removed quickly into a container of frozen and blended slicing buffer perfused with Carbogen (95% oxygen and 5% carbon dioxide) for 5 min before being bisected in a petri dish containing the same mixture. Slicing buffer contained (in mM) the following: 87 NaCl, 75 sucrose, 10 glucose, 1.25 NaH_2PO_4, 2.5 KCl, 25 $NaHCO_3$, 1.3 ascorbic acid, 0.5 $CaCl_2$, 7 $MgCl_2$, 2 pyruvate, and 0.1 kynurenic acid. Parasagittal slices (350 μm thick) were cut using an automated vibrating blade microtome (VT1200S model; Leica Biosystems, Buffalo Grove, IL, USA) and trimmed until only the hippocampus and immediately surrounding tissues remained. These mini-slices were transferred to a recovery chamber containing 36°C slicing buffer solution and incubated in a 36°C water bath for 45 min. After incubation, the slicing chamber was moved into room temperature (RT) conditions. After 15 min of rest at RT, slices were moved into another chamber containing control ACSF comprised (in mM) of the following: 125 NaCl, 2.5 KCl, 2.5 $CaCl_2$, 1.3 $MgCl_2$, 1.25 NaH_2PO_4, 26 $NaHCO_3$, and 15 glucose. Slices rested in ACSF for 15 min at RT before the start of the experiment.

The transgenic mGFAP-Cre;$Rosa26^{lsl\text{-}tdTomato}$ mice express fluorescent tdTomato protein in astrocytes, which allows for imaging of astrocytes in hippocampal slices without exogenous fluorochromes. For astrocyte imaging in C57Bl/6J mice, astrocytes were

incubated in 36°C slicing buffer supplemented with 1 μM sulforhodamine-101 (SR-101; Sigma-Aldrich, St. Louis, MO, USA) as described previously (Schnell et al., 2015; Murphy et al., 2017). After a 45 min incubation at 36°C, slices were transferred into room temperature (RT) conditions for 10 min of rest. Slices were subsequently transferred to a chamber containing ACSF without SR-101 and rested for an additional 10 min. Slices were subsequently transferred to another chamber of ACSF at room temperature and rested for a minimum of 10 min before the start of the experiment. All experiments were performed at room temperature.

Electrophysiology

Following recovery, slices were transferred to a recording chamber and continuously perfused with oxygenated ACSF at room temperature. Slices and individual CA1 pyramidal cells were visualized on a Leica DLMFSA upright microscope, with HCX APO L20x/0.50W U-V-I and HCX APO L63x/0.90W U-V-I submersion objectives and differential interference contrast optics (Leica Microsystems, Buffalo Grove, IL, USA). Whole-cell patch clamp recordings were acquired using a Multiclamp 700B amplifier and Digidata 1550 digitizer, controlled using pClamp v.10.7.0.3 and Multiclamp Commander v.2.2.2.2 software (Molecular Devices, San Jose, CA, USA). Patch pipettes were pulled from thin-wall 1.5 mM borosilicate glass capillaries World Precision Instruments using a Narishige PC-10 vertical micropipette puller (Narishige, Tokyo, Japan). Patch pipette resistances ranged from ~3-5 mOhm when filled with an internal solution containing the

following (in mM): 140 K-gluconate, 4 $MgCl_2$, 0.4 ethylene glycol- bis(b-aminoethyl ether)-N,N,N^0 ,N^0 -tetraacetic acid (EGTA), 4Mg-ATP, 0.2 Na-GTP, 10 2-[4-(2-hydroxyethyl)piperazin-1-yl]ethanesulfonic acid (HEPES), and 10 phosphocreatine, pH 7.3 with KOH. CA1 pyramidal neurons were identified using differential interference contrast optics based on their location in stratum pyramidale and their characteristic morphology including apical dendrites arborizing into the hippocampal molecular layer. Upon attaining the whole-cell configuration, the cell resting V_m and R_m were recorded, and a voltage-step protocol was run to verify the presence of voltage-gated sodium and potassium currents. In voltage clamp mode, neurons were held at the chloride reversal potential V_m = -70 mV during continuous recording of excitatory currents (I) in pA. Only a single neuronal recording was made per slice.

Experimental Solutions and Pharmacology

In addition to the isoosmolar (~300 mOsmo) control ACSF (2.5 mM K^+) described in slice preparation, some ACSF was altered to increase the concentration of potassium to 10.5 mM (^$[K^+]_o$) by addition of KCl, while reducing the concentration of NaCl by an equal amount so that the solution osmolarity was constant. Some isoosmolar 10.5 mM K^+ ACSF was made 40% hyperosmolar (~420 mOsmo) by the addition of D-mannitol (a sugar alcohol that is cell-membrane impermeable). The process of finding neurons and astrocytes for single-cell imaging was conducted under control ACSF conditions.

Similarly, neurons were patched in control ACSF before the start of the experiment. At the start of the recording or imaging and throughout the experiment, the slice was bathed in magnesium-free ACSF in order to record NMDAR-mediated excitatory activity and the drug tetrodotoxin (1 μM) was present to block voltage-gated sodium channels. Two different experimental protocols were used in this study. The first protocol consisted of an initial 10 min exposure to control ACSF (2.5 mM K^+), followed by a 5 min exposure to ^$[K^+]_o$ ACSF. This ACSF application sequence was repeated once more, and a final 10 min exposure to normal ACSF concluded the recording. The second protocol consisted of an initial 10 min exposure to control ACSF, followed by a 10 min exposure to ^$[K^+]_o$ ACSF. Following the exposure to ^$[K^+]_o$ ACSF, the slice was exposed to 40% hyperosmolar 10.5 mM K^+ ACSF for 10 min. This two-step sequence of 10 min ^$[K^+]_o$ exposure then 10 min hyperosmolar ^$[K^+]_o$ exposure was repeated once more before the conclusion of the experiment.

Event Analysis

Voltage-clamp recordings of CA1 pyramidal neurons were analyzed for individual events in the form of currents (pA). Clampfit software (Molecular Devices) was used to extract characteristics from individual events: peak amplitude, 10-90% rise time, time to peak and decay tau. For the purposes of this study, miniature excitatory post-synaptic currents (mEPSCs) were defined as events having a rise time < 10 ms, and slow inward currents (SICs) with rise times ≥ 10 ms and amplitudes ≥ 20 pA. The kinetics of mixed mEPSCs

recorded in this study are slower than the ~3 ms rise time of mEPSCs in other studies (Zhang et al., 2005). We attribute this difference to a combination of factors, including slower intrinsic kinetics of NMDA synaptic events, slice recording temperature, ACSF perfusion rate, rise time parameters (e.g. 10 - 90% vs. 20 - 80%), and use of different analysis software.

Two different methods were used to detect events. A threshold-based search was used to identify events using the following parameters: (1) negative-going event polarity; (2) event-finding trigger, -20 pA; (3) event-finding re-arm, -1e4 pA; (4) noise rejection, 1 ms; (5) pre-trigger length, 100 ms; (6) post-trigger length, 1000 ms; and (7) taus calculated at 10% of peak. Alternatively, a template-based search was used to detect events from a user-made representative event template from each recording. Creation of an event template consisted of averaging 5-6 events, each contained within an 80 ms duration of recording. This template was then used to detect all events in the recording. The parameters of the template were: (1) negative-going event polarity; (2) baseline set "in template"; (3) match threshold 5; and (4) taus calculated from 10% of peak. The template-based detection strategy was ineffective at detecting large events with slow kinetics; i.e. slow inward currents. Therefore, a final pool of events was comprised of threshold-detected events with amplitudes > 20 pA and template-detected events with amplitudes < 20 pA. This method prevented events from being double-counted.

Imaging

Throughout our experiments, enhanced green fluorescent protein (eGFP) was excited using a 488 nm argon laser and detected with a 503–548 nm bandpass filter, and SR-101 was excited with a 559 nm semiconductor laser and detected with a 624–724 nm bandpass filter using an Olympus Fluoview FV1000 (FV10-ASW) confocal imaging system. The objective used was an Olympus LUMPlanFI 60x/0.90 W 1/0 water immersion objective lens. Confocal laser settings were the same as described previously (Murphy et al., 2017). Output power for both lines was kept as low as possible (1.5%) to minimize the possibility of light-induced artifacts. Volume imaging of neurons and astrocytes was performed as described previously (Murphy et al., 2017). Briefly, z-stacks of 1-mm-thick images were collected at 1-min intervals over individual cell somata within 15 s to ensure adequate coverage of the soma and main processes while at the same time preventing data loss caused by tissue volume changes. Stacks were collected using a 2–3.5 zoom factor, with a scan area clipped close around the soma to increase imaging speed. Cell drift in the x-y-z planes was compensated using quick X-Y scans and X-Y-Z adjustments as necessary between time points. Imaging experiments consisted of three steps: (1) 10-min baseline period in normal ACSF, in which 2 to 3 z-stacks were acquired in succession at 1-min intervals and averaged to serve as the baseline comparison for later time points; (2) a 5-min application of ^$[K^+]_o$ ACSF, during which z-stacks through the full thickness of the cell were collected each minute; and (3) a 10-min exposure period in 40% hyperosmolar ^$[K^+]_o$ ACSF, during which an image was

taken every 5 min. Steps (2) and (3) were then repeated once each, after which the slice was discarded. Only a single cell was imaged per slice. Fiji/Image J was used for thresholding of image stacks and subsequent volume analysis as previously described (Murphy et al., 2017). Soma area of compressed image stacks (used as a proxy for cell volume) was analyzed with cell volume changes reported as percent change from the averaged baseline.

Statistical Analysis

Statistical analysis was carried out using SPSS Statistics 24 software and Laerd Statistics methodology. Datasets were first assessed for "extreme" outliers by inspection of SPSS boxplots and evaluation of studentized residuals. Outliers were rarely excluded from analysis due to the small sample size of our datasets. Secondly, the data was assessed for violations of normality with the Shapiro–Wilk test, which determined the selection of either a parametric or non-parametric statistical test. For analysis of volume measurements, a two-way mixed analysis of variance (ANOVA) was used to check for significant interactions between the within-subject (time) and between-subjects (group/condition) factors as previously described (Walch et al., 2020). Homogeneity of variance was assessed with Levene's test for equality of variance, Box's test established equality of covariances, and Mauchly's test determined sphericity of the data set. If the assumption of sphericity was violated, the Greenhouse–Geisser estimation was used to determine significance in the two-way mixed ANOVA. If a one-way repeated-measures

ANOVA was run for two or more comparisons, post hoc testing (Holm– Bonferroni) accounted for the type-I error associated with multiple comparisons. For analysis of electrophysiological data, nearly all datasets violated the assumption of normality, so non-parametric tests were used to determine significance. Within-subject changes in event amplitude, frequency, or percentage occurring across multiple treatments were assessed for significance by the Friedman test with a Bonferroni adjustment to pairwise comparison. Within-subject comparisons of only two groups were performed by the Wilcoxon signed rank test. For imaging experiments, each group (astrocytes or neurons) contained N = 8–12 cells (numbers specified in each experiment), unless otherwise noted. For electrophysiology experiments, the total number of neuron recordings per protocol consisted of both partial and complete recordings. The number of partial recordings per protocol consisted of at least N=8-12 cells, while the number of complete recordings was less. Error bars in all graphs indicate the standard error of the mean (SEM). Significance values are listed as follows: *p < .05, **p < .01, and ***p < .001.

Results

Neuronal excitability increases recorded in ^$[K^+]_o$ include a mix of synaptic and non-synaptic events

We first set out to quantify the excitable effects of ^$[K^+]_o$ ACSF on CA1 pyramidal neurons. Under baseline conditions in slice experiments, the concentration of extracellular potassium was set to 2.5 mM K^+, while K^+ was raised to 10.5 mM in ^$[K^+]_o$

ACSF. TTX (1 μM) was included in all solutions in order to minimize direct depolarizing effects of ^$[K^+]_o$ on neuronal firing and action potential-driven synaptic transmission, and Mg^{2+}-free ACSF was used to permit recording of NMDA receptor events. With the introduction of ^$[K^+]_o$ ACSF, the frequency of mixed AMPA/NMDA mEPSCs and slow inward currents (SICs) increased (Figure 1A). The change in frequency of mEPSCs was quantified during each phase of the experimental recording (Figure 1B). In 2.5 mM K^+ ACSF, the frequency of mEPSCs was approximately ~0.25 Hz, while ^$[K^+]_o$ ACSF triggered mEPSC frequencies over ~0.4 Hz in both the 1st and 2nd ^$[K^+]_o$ applications (Figure 1B). In comparison to mEPSCs, SIC events occurred much less frequently, with the highest recorded frequencies detected near ~0.15 Hz, during the application of ^$[K^+]_o$ ACSF (Figure 1C). Most notably, the initial baseline frequency of SICs was ~0.005 Hz, but after the 1st application of ^$[K^+]_o$ ACSF the SIC frequency remained elevated, even during subsequent periods of control ACSF exposure (Figure 1C). After the first application of ^$[K^+]_o$ ACSF, the frequency of SICs alternated between subsequent exposures of 2.5 mM and 10.5 mM $[K^+]_o$. Overall, the excitability of pyramidal neurons increased when exposed to ^$[K^+]_o$ ACSF in the form of increased frequency of mEPSCs and SICs in comparison to their respective baseline frequencies in 2.5 mM $[K^+]_o$.

Increasing osmolarity of ^$[K^+]_o$ ACSF leads to shrinking of astrocytes and neurons

After confirming the excitability increases of pyramidal neurons exposed to ^$[K^+]_o$ ACSF (Figure 1) and reflecting on the selective swelling of astrocytes in response to ^$[K^+]_o$ ACSF (Walch et al., 2020), we aimed to block or prevent astrocyte swelling in ^$[K^+]_o$ by

applying 40% hyperosmolar in the continued presence of ^$[K^+]_o$ (Figure 2). Astrocyte volume increased in response to ^$[K^+]_o$ as expected, while neuronal volume remained relatively constant (Figure 2). The selective swelling of astrocytes under ^$[K^+]_o$ conditions has been documented previously by our lab (Walch et al, 2020) and is a result of the unique isoform of the Na^+/K^+ ATPase expressed by astrocytes, which is activated by increases in extracellular K^+ (Walch et al., 2020). Next, in the continued presence of ^$[K^+]_o$, 40% hyperosmolar ACSF forced volume reduction of both astrocytes and neurons (Figure 2B). Despite astrocyte swelling > 5% from baseline in ^$[K^+]_o$ ($p<.01$), the increased extracellular osmolarity triggered a large astrocyte volume decrease (to ~-6%, $p<.001$). Neurons, which don't swell in ^$[K^+]_o$, also shrank in hyperosmolar conditions to ~5% below baseline volume ($p<.01$) after 5 min (Figure 2B). This was not surprising, as we previously found that neurons readily swell in hypoosmolar conditions (Murphy et al., 2017). While astrocyte and neuron volume dropped well below baseline in hyperosmolar ACSF in ^$[K^+]_o$, subsequent removal of mannitol over a 5 min period triggered an ~8% change ($p<.01$) in volume (ΔV) in astrocytes with >2% overshoot above baseline, while neuronal volume largely recovered to baseline (Figure 2B). Subsequent reintroduction of mannitol for 10 min forced both astrocytes and neurons to shrink to a volume approximately 5% below baseline (Figure 2B). The non-specific shrinkage of both cell types in response to hyperosmolar ^$[K^+]_o$ indicate that reduction of ECS volume cannot be attributed solely to astrocytes under these conditions, although the net change in volume of astrocytes is approximately double that of neurons, suggesting their volume change is likely the largest contributor to changes in ECS volume.

Hyperosmolar-induced cell shrinking isolates volume contribution to neuronal excitability in ^$[K^+]_o$

The stark effects of mannitol on astrocyte and neuron volume in the continued presence of ^$[K^+]_o$ (Figure 2) encouraged us to quantify changes in neuron excitability under these same conditions. During the first application of ^$[K^+]_o$, there was an evident inward shift in the holding current to maintain voltage-clamp at -70 mV followed by a reduction in the holding current in hyperosmolar ^$[K^+]_o$ (Figure 3A). Given earlier experiments that detail the increase in neuronal excitability in ^$[K^+]_o$ (Figure 1), the negative shift in holding current was not unexpected and was coupled with an increase in both mEPSC and SIC events in comparison to baseline (Figure 3C). With the introduction of mannitol, accompanying the positive shift in holding current was an increase in AMPA- and NMDA-dependent mEPSCs and a reduction in SICs (Figure 3C). The second application cycle proceeded in the same manner as the first, but with a more noticeable occurrence of large SIC-like events with the removal of mannitol (return to ^$[K^+]_o$ alone) (Figure 3A). This is likely due to the more pronounced ΔV upon mannitol removal because, even in the presence of mannitol and forced reduction of astrocyte volume, astrocytes are still pumping in K^+ into the cell, resulting in a more pronounced volume increase when mannitol is removed (~5% compared to ~8%; see Figure 2). Next, we aimed to quantify the effects of forced cellular volume reduction on mEPSCs and SICs.

The mEPSC frequency trended toward an increase in ^$[K^+]_o$ as observed in our initial experiment. The frequency of mEPSCs increased when ^$[K^+]_o$ was supplemented

with mannitol to force cellular volume reduction in ^$[K^+]_o$ ($p<.01$; Figure 4A). We attribute this to the effects of mannitol as a secretagogue forcing fusion of synaptic vesicles with the presynaptic terminal upon neuronal shrinking (Kettenmann and Grantyn, 1992). Interestingly, during the last five minutes of ^$[K^+]_o$ exposure in both the 1st and 2nd applications, mEPSC frequency slightly decreased in comparison to the first five minutes (Figure 4A), possibly due to exhaustion of the readily releasable "docked" pool of synaptic vesicles. In the 2nd application cycle, mEPSCs evoked in ^$[K^+]_o$ closely mirrored the frequencies in the 1st application; however the inclusion of mannitol a second time did not evoke nearly as many mEPSCs as during the first application (Figure 4A). We again interpret this as due to limited availability of docked synaptic vesicles, which may not have had time to restore following the first mannitol application (Marx et al., 2015). Hyperosmotic solutions have been shown to stimulate expenditure of this pool of docked vesicles in a calcium-independent mode of exocytosis (Kettenmann and Helmut, 1992; Rosenmund and Stevens, 1996). While the average frequency of mEPSCs changed between treatments, the average amplitude did not (Figure 4B), in line with a pre- vs. postsynaptic effect of mannitol acting as a secretagogue.

The pool of SIC events were analyzed separately from mEPSCs, as we've shown that SICs are evoked by cellular swelling (Lauderdale et al., 2015). Despite a low occurrence of SICs recorded throughout the experiment, there was a significant trend of increasing SIC frequency ^$[K^+]_o$ compared to baseline 2.5 mM $[K^+]_o$ ($p<.05$; Figure 5A). There was noticeable reduction in SIC amplitude in the presence of mannitol (when the ECS is expanding) compared to ^$[K^+]_o$ alone (Figure 5B). This mannitol-dependent

diminishment of SICs is similar in both the first and second application cycles (Figure 5B). SICs are known to occur with a variety of amplitudes, some near the size of synaptic events and others well over 100 pA (Kovács and Pál, 2017). Evidently, larger-amplitude SICs are more likely to occur while the ECS volume is constricted, decreasing the distance between neuronal and astrocytic membranes.

We further dissected the population of SICs occurring in each condition using cutoffs for amplitude and/or rise time. For example, when SIC events with 10 - 20 ms rise times were excluded from the larger SIC event pool, the frequency was no longer different between the first ^$[K^+]_o$ and hyperosmolar ^$[K^+]_o$ applications (Figure 6A). This is likely because this faster SIC population is likely grading into mEPSCs which include slower and noisier NMDA events. Shifting the cutoff to 30 ms, we see a trend towards a higher SIC frequency upon removal of mannitol compared to re-application of mannitol in ^$[K^+]_o$ (Figure 6B). In general, SIC events with rise times between 10-20 ms made up the largest portion of the SIC event pool across all treatments (Figure 7). There was also a trend towards slower SIC events making up less of the SIC event population across all treatments (Figure 7). Similarly to categorizing SICs on the basis of rise time, we sorted the SIC event pool into bins according to amplitude (Figure 8). Smaller-amplitude SICs (10-50 pA) made up a sizeable portion of the total SIC event pool (Figure 8A), just as faster-rise time SICs do (Figure 7A). It became apparent that very large-amplitude SICs (100-200 pA) occurred exclusively in ^$[K^+]_o$ (Figure 8C, 8D). In fact, SICs with amplitudes > 100 pA were completely abolished by the presence of mannitol (Figure 8C, 8D).

This is illustrated further by merging rise time bins and calculating the percentage of slower SIC events (> 30 ms) that occur during each 10-min treatment application (Figure 9A). Although there is no substantial difference between SICs > 30 ms when mannitol is applied compared to the first 10 minutes in $^{\wedge}[K^+]_o$, there is an increase in the prevalence of these events occurring in the 10 minutes in $^{\wedge}[K^+]_o$ after mannitol removal (first mannitol wash period) (Figure 9A). The 2nd application of mannitol then triggers a noticeable reduction in the proportion of SICs > 30 ms compared to the preceding 10 min in $^{\wedge}[K^+]_o$ alone (Figure 9A). Although there is an apparent difference in the effects of the first and second application cycles of hyperosmolar $^{\wedge}[K^+]_o$ compared to $^{\wedge}[K^+]_o$ alone, it is still useful to compare the proportion of SIC events > 30 ms that occurred across the total 20 minutes in $^{\wedge}[K^+]_o$ to the total 20-min application period in mannitol (Figure 9B). Indeed, the proportion of SIC events > 30 ms occurring in $^{\wedge}[K^+]_o$ alone is > 15% points higher ($p<.05$) than with co-application of mannitol (Figure 9B). Using a 50 ms cutoff reveals a similar effect between treatments. The proportion of SICs > 50 pA occurring in $^{\wedge}[K^+]_o$ is significantly greater than those that occur in hyperosmolar $^{\wedge}[K^+]_o$ conditions ($p<.05$; Figure 10B). The presence of mannitol reduces the occurrence of large SICs that are evoked by $^{\wedge}[K^+]_o$.

Overall these findings suggest that under conditions of astrocyte swelling (i.e. $^{\wedge}[K^+]_o$), larger and slower SIC events are preferentially generated over smaller amplitude, faster rise time SICs. Consequently, when the ECS volume expands with the simultaneous application of $^{\wedge}[K^+]_o$ and mannitol, the largest and slowest SIC events are almost completely abolished (Figures 7 and 8). Despite mannitol's positive modulation of

mEPSC activity (Figure 5), it negatively modulates the occurrence of large SICs, which are the most likely to synchronize activity among and between adjacent neurons (Fellin et al., 2004).

Discussion

Exposure of hippocampal slices to 10.5 mM $[K^+]_o$ ACSF leads to a depolarizing shift in the holding current, increased miniature synaptic activity and generation of SICs in CA1 pyramidal neurons. During this time, we know that astrocytes are swelling in response to ^$[K^+]_o$ while neuronal volume is relatively constant (shown in Figure 2, and in Walch et al., 2020). Even in the continued presence of ^$[K^+]_o$, mannitol shrinks astrocytes and neurons to well below their baseline volumes. As a result of this study, we know that larger and slower SIC events become less frequent as the extracellular space expands. The proximity of astrocytes and neurons decreases as cell volumes are reduced, with extracellular glutamate concentration lessening to the point where the likelihood of extracellular glutamate stimulating extrasynaptic NMDARs is very small.

Surprisingly, overall event frequency increased under these conditions. This result seemed to contradict the known relationship between tissue swelling and excitability, however multiple studies have described another interesting phenomenon where shrinkage of neuronal presynaptic terminals can lead to calcium-independent exocytosis (Bekkers and Stevens, 1992; Capogna et al, 1996; Rosenmund et al, 1996; Waseem et al,

2008). Since we saw about 1% shrinkage of the neuronal soma, it remains possible that there is also significant shrinking of the processes, which could trigger vesicular fusion from neurons due to mannitol acting as a secretagogue in this manner. There is also a peculiar report of mannitol being used to treat neuronal swelling in an *in vivo* traumatic brain injury model, where treatment increased seizure susceptibility in mice (Sawant-Pokam et al., 2020). Thus, we hypothesized the benefit of alleviating shrinkage in the ECS could be masked by mannitol's secretagogue effects. There is a way to determine if this assumption is correct. If we were to incubate our slices in bafilomycin (an inhibitor of vacuolar H^+-ATPase), we could empty the synaptic vesicles of neurotransmitter (Roseth et al, 1995; Fonnum et al, 1998). If under conditions of ^$[K^+]_o$ and bafilomycin, the application of mannitol resulted in a decrease in neuronal excitability in comparison to high potassium and mannitol alone, it would suggest that mannitol acted as a secretagogue in our experiments. Traynelis and Dingledine (1989) showed that application of sucrose—another known secretagogue—completely blocked NMDA receptor-dependent, spontaneously-occurring seizures. This points to the importance of extracellular space volume regulation as a mediator for neuronal excitability, and arguably plays a far more important role than even secretagogue-mediated vesicular release of glutamate. Even though it is likely that sucrose is increasing vesicular fusion in neurons, seizures stop due to the marked dilation of the extracellular space.

In our data, binning of events according to amplitude and rise time revealed a decrease in larger amplitude, slower rise time SICs in the presence of mannitol, suggesting they are preferentially generated during cell swelling. SICs have been shown

to be strongly evoked in swelling conditions such as hypoosmolar ACSF, and are thought to be due to extrasynaptic sources of glutamate (Angulo et al, 2004; Fellin et al, 2004; Fiacco et al, 2007; Lauderdale et al, 2015). If astrocyte swelling does induce glutamate release leading to hyperexcitability of neurons, how is the glutamate being released? The most likely and well-studied candidate would be VRAC, which has been dubbed a "frenemy" within the brain (Mongin, 2016). VRAC are thought to be stretch-sensitive, and have been implicated in the release of glutamate and various other ions and neutral molecules (Kimelberg et al, 1990; Rutledge et al, 1996; Mongin & Kimelberg, 2002; Kimelberg, 2005; Abdullaev et al, 2006) onto nearby extrasynaptic NMDARs (Gómez-Gonzalo et al., 2017). This mechanism alludes to the concept of "volume transmission," which describes intercellular communication facilitated by diffusion of substances through the extracellular space rather than "wired transmission" pathways like the synaptic cleft (Bach-y-Rita, 1993; Agnati et al., 1995). Slow, extrasynaptic diffusion of glutamate is likely a key factor contributing to the kinetics of SICs (Lozovaya et al., 2004).

On average, SICs have larger amplitudes and slower rise times in comparison to synaptic events (Rumbaugh and Vicini, 1999). Unlike synaptic ionotropic glutamate receptors (iGluRs), extrasynaptic receptors, which are predominantly NMDARs, do not have privileged access to pre-synaptic glutamate (Köhr, 2006). Glutamate migrating away from the synaptic cleft must traverse farther to stimulate these receptors, which might explain the slower kinetics of SICs (Conti and Weinberg, 1999). Unlike on the closely apposed pre- and post-synaptic membranes (~24 nm apart) (Peters et al., 1991;

Zuber et al., 2005), extrasynaptic NMDA receptors may be scattered on other parts of the neuron (Benke et al., 1993). Here, glutamate stimulation likely occurs in a wave-like manner, hitting some NMDARs earlier than others, thus prolonging event duration. Given the sparse astrocytic insulation of synapses in the hippocampus, glutamate spillover onto neighboring synapses is more common than in other parts of the brain (Rusakov and Kullmann, 1998; Ventura and Harris, 1999; Lozovaya et al., 1999). This might explain how so much glutamate escapes the industrious glutamate transporters highly expressed on astrocytes (Kullmann, Erdemli and Asztély, 1996). Finding the source of this extracellular glutamate is therefore of high priority and significance.

Recent work has identified the essential pore-forming subunit of VRAC as LRRC8A (Voss et al., 2014; Qiu et al, 2014), which is also necessary for glutamate release in conditions of swelling (Hyzinski-García et al, 2014). With this model, we can replicate the experimental procedures used in this study in the $VRAC^{-/-}$ mouse, and look at astrocyte swelling and changes in neuronal excitability in $\wedge[K^+]_o$. We would expect to see that $VRAC^{-/-}$ astrocytes continue to swell in elevated potassium, although these cells may not regulate their volume back to baseline during wash periods, if VRAC are responsible for water release during cell swelling. While VRAC can clearly contribute to excitotoxicity during tissue swelling, the cell-type responsible for the majority of VRAC-released glutamate is still unclear, as published transgenic VRAC cKO models did not ablate VRAC exclusively in astrocytes (Yang et al., 2019). If the expected increases in neuronal excitability in $\wedge[K^+]_o$ are depressed in our astrocyte VRAC cKO mice, we would attribute this to the role of VRAC in releasing glutamate during astrocyte swelling.

Aside from glutamate release via VRAC, it is also possible that astrocyte swelling simply shrinks the extracellular space, elevating ambient glutamate concentrations sufficiently to activate high-affinity extrasynaptic NMDA receptors, causing an increase in excitability. Both of these mechanisms may contribute significantly to the neuronal excitability increases seen in our model, making them intriguing subjects for future study. These results demonstrate the importance of astrocyte swelling in the control of neuronal and brain tissue excitability, while also highlighting the necessity for more specific tools to unravel the exact mechanisms involved in swelling-mediated excitability changes in intact tissue.

Conclusions

In this study, we have shown that (patho)physiologically relevant changes in extracellular potassium selectively swells astrocytes, and is correlated to an increase in neuronal excitability in the form of NMDA receptor-dependent slow inward currents. When astrocyte volume was forced back down to baseline levels by application of hyperosmolar ACSF in the continued presence of elevated potassium, larger and longer SICs were abolished, despite increases in synaptic activity. These SICs returned upon washout of mannitol, confirming the importance of cell swelling for the occurrence of these events. This could have profound implications for a variety of disease models, many of which manifest with changes in potassium levels in the CNS. These changes

very likely result in astrocyte volume fluctuations, which non-synaptically elevate neuronal excitability and could contribute to the generation of seizure activity.

Epileptiform bursting observed in previous studies occurred in 8.5 mM $[K^+]_o$, was NMDA receptor-dependent, and required constriction of the extracellular space (Traynelis & Dingledine, 1988). The presence of SICs, which have been discussed as synchronizing events that raise the excitability of neuronal populations (Wetherington et al, 2008), are particularly intriguing. Although their specific link to seizure activity has yet to be elucidated, their TTX insensitivity, NMDA receptor dependency, and slow kinetics have had them connected to astrocytes for some time (Perea & Araque, 2005; Carmignoto & Felling, 2006; Fiacco et al, 2007; Lauderdale et al, 2015). In the future, it would be prudent to continue to search for mechanisms to selectively manipulate astrocyte volume bidirectionally in order to isolate astrocyte volume contributions to changes in neuronal and brain tissue excitability.

Importantly, SICs are a hallmark feature of tissue-swelling induced excitability (Lauderdale et al., 2015; Yang et al., 2019). Their appearance has also been associated with increased neuronal synchrony (Fellin et al., 2004), a known characteristic of seizures. The generation of SICs may not be an explicit requirement for epileptiform activity (Fellin et al., 2006), but their presence will serve as a useful diagnostic. Thus, understanding the mechanisms that lead to the generation of SICs are stepping stones towards preventative strategies to treat epilepsy.

References

Abdullaev IF, Rudkouskaya A, Schools GP, Kimelberg HK, Mongin AA (2006) Pharmacological comparison of swelling-activated excitatory amino acid release and Cl- currents in cultured rat astrocytes. J Physiol 572:677-689.

Agnati LF, Zoli M, Strömberg I, Fuxe K (1995) Intercellular communication in the brain: wiring versus volume transmission. Neuroscience 69:711-726.

Angulo MC, Kozlov AS, Charpak S, Audinat E (2004) Glutamate released from glial cells synchronizes neuronal activity in the hippocampus. J Neurosci 24:6920-6927.

Bach-y-Rita P (1993) Neurotransmission in the brain by diffusion through the extracellular fluid: a review. Neuroreport 4:343-350.

Benke TA, Jones OT, Collingridge GL, Angelides KJ (1993) N-Methyl-D-aspartate receptors are clustered and immobilized on dendrites of living cortical neurons. Proc Natl Acad Sci U S A 90:7819-7823.

Capogna M, Gähwiler BH, Thompson SM (1996) Calcium-independent actions of alpha-latrotoxin on spontaneous and evoked synaptic transmission in the hippocampus. J Neurophysiol 76:3149-3158.

Carmignoto G, Fellin T (2006) Glutamate release from astrocytes as a non-synaptic mechanism for neuronal synchronization in the hippocampus. J Physiol Paris 99:98-102.

Conti F, Weinberg RJ (1999) Shaping excitation at glutamatergic synapses. Trends Neurosci 22:451-458.

Fellin T, Gomez-Gonzalo M, Gobbo S, Carmignoto G, Haydon PG (2006) Astrocytic glutamate is not necessary for the generation of epileptiform neuronal activity in hippocampal slices. J Neurosci 26:9312-9322.

Fellin T, Pascual O, Gobbo S, Pozzan T, Haydon PG, Carmignoto G (2004) Neuronal synchrony mediated by astrocytic glutamate through activation of extrasynaptic NMDA receptors. Neuron 43:729-743.

Feng G, Mellor R, Bernstein M, Keller-Peck C, Nguyen Q, Wallace M, Nerbonne J, Lichtman J, Sanes J (2000) Imaging neuronal subsets in transgenic mice expressing multiple spectral variants of GFP. Neuron 28:41-51.

Fiacco TA, Agulhon C, Taves SR, Petravicz J, Casper KB, Dong X, Chen J, McCarthy KD (2007) Selective stimulation of astrocyte calcium in situ does not affect neuronal excitatory synaptic activity. Neuron 54:611-626.

Fonnum F, Johnsen A, Hassel B (1997) Use of fluorocitrate and fluoroacetate in the study of brain metabolism. Glia 21:106-113.

Gómez-Gonzalo M, Zehnder T, Requie LM, Bezzi P, Carmignoto G (2018) Insights into the release mechanism of astrocytic glutamate evoking in neurons NMDA receptor-mediated slow depolarizing inward currents. Glia 66:2188-2199.

Hyzinski-García MC, Rudkouskaya A, Mongin AA (2014) LRRC8A protein is indispensable for swelling-activated and ATP-induced release of excitatory amino acids in rat astrocytes. J Physiol 592:4855-4862.

Kettenmann H, Grantyn R (1992) Practical electrophysiological methods : a guide for in vitro studies in vertebrate neurobiology. New York: Wiley-Liss.

Kilb W, Dierkes P, Sykova E, Vargova L, Luhmann H (2006) Hypoosmolar conditions reduce extracellular volume fraction and enhance epileptiform activity in the CA3 region of the immature rat hippocampus. Journal of Neuroscience Research 84:119-129.

Kimelberg HK (2005) Astrocytic swelling in cerebral ischemia as a possible cause of injury and target for therapy. Glia 50:389-397.

Kimelberg HK, Goderie SK, Higman S, Pang S, Waniewski RA (1990) Swelling-induced release of glutamate, aspartate, and taurine from astrocyte cultures. J Neurosci 10:1583-1591.

Kofuji P, Newman EA (2004) Potassium buffering in the central nervous system. Neuroscience 129:1045-1056.

Kovács A, Pál B (2017) Astrocyte-Dependent Slow Inward Currents (SICs) Participate in Neuromodulatory Mechanisms in the Pedunculopontine Nucleus (PPN). Front Cell Neurosci 11:16.

Kullmann DM, Erdemli G, Asztély F (1996) LTP of AMPA and NMDA receptor-mediated signals: evidence for presynaptic expression and extrasynaptic glutamate spill-over. Neuron 17:461-474.

Köhr G (2006) NMDA receptor function: subunit composition versus spatial distribution. Cell Tissue Res 326:439-446.

Lauderdale K, Murphy T, Tung T, Davila D, Binder DK, Fiacco TA (2015) Osmotic Edema Rapidly Increases Neuronal Excitability Through Activation of NMDA Receptor-Dependent Slow Inward Currents in Juvenile and Adult Hippocampus. ASN Neuro 7.

Lozovaya NA, Kopanitsa MV, Boychuk YA, Krishtal OA (1999) Enhancement of glutamate release uncovers spillover-mediated transmission by N-methyl-D-aspartate receptors in the rat hippocampus. Neuroscience 91:1321-1330.

Lozovaya NA, Grebenyuk SE, Tsintsadze TSh, Feng B, Monaghan DT, Krishtal OA (2004) Extrasynaptic NR2B and NR2D subunits of NMDA receptors shape 'superslow' afterburst EPSC in rat hippocampus. J Physiol 558:451-463.

MacVicar BA, Feighan D, Brown A, Ransom B (2002) Intrinsic optical signals in the rat optic nerve: Role for K+ uptake via NKCC1 and swelling of astrocytes. Glia 37:114-123.

Manley GT, Fujimura M, Ma TH, Noshita N, Filiz F, Bollen AW, Chan P, Verkman AS (2000) Aquaporin-4 deletion in mice reduces brain edema after acute water intoxication and ischemic stroke. Nature Medicine 6:159-163.

Marx MC, Billups D, Billups B (2015) Maintaining the presynaptic glutamate supply for excitatory neurotransmission. J Neurosci Res 93:1031-1044.

Mongin AA (2016) Volume-regulated anion channel--a frenemy within the brain. Pflugers Arch 468:421-441.

Mongin AA, Kimelberg HK (2002) ATP potently modulates anion channel-mediated excitatory amino acid release from cultured astrocytes. Am J Physiol Cell Physiol 283:C569-578.

Murphy TR, Davila D, Cuvelier N, Young LR, Lauderdale K, Binder DK, Fiacco TA (2017) Hippocampal and Cortical Pyramidal Neurons Swell in Parallel with Astrocytes during Acute Hypoosmolar Stress. Front Cell Neurosci 11:275.

Pasantes-Morales H, Schousboe A (1989) Release of taurine from astrocytes during potassium-evoked swelling. Glia 2:45-50.

Perea G, Araque A (2005) Properties of synaptically evoked astrocyte calcium signal reveal synaptic information processing by astrocytes. J Neurosci 25:2192-2203.

PETERS A (1991) A GUIDE TO THE CELLULAR STRUCTURE OF THE NERVOUS-SYSTEM - 2 CITATION-CLASSIC COMMENTARY ON THE FINE-STRUCTURE OF THE NERVOUS-SYSTEM - THE NEURONS AND

SUPPORTING CELLS BY PETERS,A., PALAY,S.L., AND WEBSTER,H.D. Current Contents/life Sciences:9-9.

Qiu Z, Dubin AE, Mathur J, Tu B, Reddy K, Miraglia LJ, Reinhardt J, Orth AP, Patapoutian A (2014) SWELL1, a plasma membrane protein, is an essential component of volume-regulated anion channel. Cell 157:447-458.

Risher WC, Andrew RD, Kirov SA (2009) Real-time passive volume responses of astrocytes to acute osmotic and ischemic stress in cortical slices and in vivo revealed by two-photon microscopy. Glia 57:207-221.

Rosenmund C, Stevens CF (1996) Definition of the readily releasable pool of vesicles at hippocampal synapses. Neuron 16:1197-1207.

Roseth S, Fykse EM, Fonnum F (1995) Uptake of L-glutamate into rat brain synaptic vesicles: effect of inhibitors that bind specifically to the glutamate transporter. J Neurochem 65:96-103.

Rumbaugh G, Vicini S (1999) Distinct synaptic and extrasynaptic NMDA receptors in developing cerebellar granule neurons. J Neurosci 19:10603-10610.

Rusakov DA, Kullmann DM (1998) Extrasynaptic glutamate diffusion in the hippocampus: ultrastructural constraints, uptake, and receptor activation. J Neurosci 18:3158-3170.

Rutledge EM, Kimelberg HK (1996) Release of [3H]-D-aspartate from primary astrocyte cultures in response to raised external potassium. J Neurosci 16:7803-7811.

Sawant-Pokam PA, Vail TJ, Metcalf CS, Maguire JL, McKean TO, McKean NO, Brennan KC (2020) Preventing neuronal edema increases network excitability after traumatic brain injury. J Clin Invest 130:6005-6020.

Schnell C, Shahmoradi A, Wichert S, Mayerl S, Hagos Y, Heuer H, Rossner M, Hulsmann S (2015) The multispecific thyroid hormone transporter OATP1C1 mediates cell-specific sulforhodamine 101-labeling of hippocampal astrocytes. Brain Structure & Function 220:193-203.

Shahar E, Derchansky M, Carlen P (2009) The role of altered tissue osmolality on the characteristics and propagation of seizure activity in the intact isolated mouse hippocampus. Clinical Neurophysiology 120:673-678.

Solenov E, Watanabe H, Manley GT, Verkman AS (2004) Sevenfold-reduced osmotic water permeability in primary astrocyte cultures from AQP-4-deficient mice,

measured by a fluorescence quenching method. Am J Physiol Cell Physiol 286:C426-432.

Traynelis SF, Dingledine R (1988) Potassium-induced spontaneous electrographic seizures in the rat hippocampal slice. J Neurophysiol 59:259-276.

Traynelis SF, Dingledine R (1989) Role of extracellular space in hyperosmotic suppression of potassium-induced electrographic seizures. J Neurophysiol 61:927-938.

Ventura R, Harris KM (1999) Three-dimensional relationships between hippocampal synapses and astrocytes. J Neurosci 19:6897-6906.

Voss FK, Ullrich F, Münch J, Lazarow K, Lutter D, Mah N, Andrade-Navarro MA, von Kries JP, Stauber T, Jentsch TJ (2014) Identification of LRRC8 heteromers as an essential component of the volume-regulated anion channel VRAC. Science 344:634-638.

Walch E, Murphy TR, Cuvelier N, Aldoghmi M, Morozova C, Donohue J, Young G, Samant A, Garcia S, Alvarez C, Bilas A, Davila D, Binder DK, Fiacco TA (2020) Astrocyte-Selective Volume Increase in Elevated Extracellular Potassium Conditions Is Mediated by the Na. ASN Neuro 12:1759091420967152.

Walz W (1992) Mechanism of rapid K(+)-induced swelling of mouse astrocytes. Neurosci Lett 135:243-246.

Walz W (2000) Role of astrocytes in the clearance of excess extracellular potassium. Neurochemistry International 36:291-300.

Waseem TV, Lapatsina LP, Fedorovich SV (2008) Influence of integrin-blocking peptide on gadolinium- and hypertonic shrinking-induced neurotransmitter release in rat brain synaptosomes. Neurochem Res 33:1316-1324.

Wetherington J, Serrano G, Dingledine R (2008) Astrocytes in the epileptic brain. Neuron 58:168-178.

Xie AX, Lauderdale K, Murphy T, Myers TL, Fiacco TA (2014) Inducing plasticity of astrocytic receptors by manipulation of neuronal firing rates. J Vis Exp.

Yang J, Vitery M, Chen J, Osei-Owusu J, Chu J, Qiu Z (2019) Glutamate-Releasing SWELL1 Channel in Astrocytes Modulates Synaptic Transmission and Promotes Brain Damage in Stroke. Neuron 102:813-+.

Zhang J, Yang Y, Li H, Cao J, Xu L (2005) Amplitude/frequency of spontaneous mEPSC correlates to the degree of long-term depression in the CA1 region of the hippocampal slice. Brain Res 1050:110-117.

Zuber B, Nikonenko I, Klauser P, Muller D, Dubochet J (2005) The mammalian central nervous synaptic cleft contains a high density of periodically organized complexes. Proc Natl Acad Sci U S A 102:19192-19197.

Figures

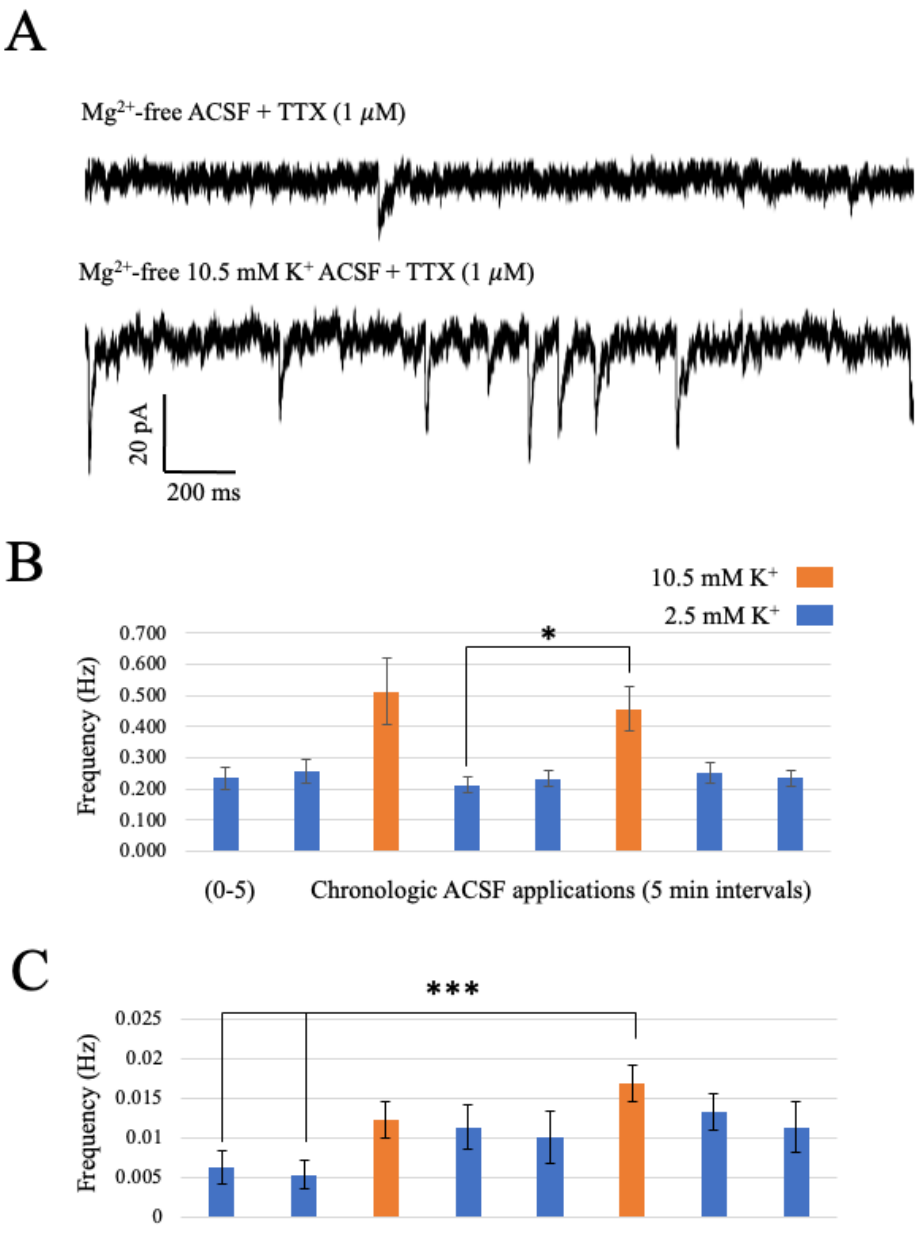
A
Mg2+-free ACSF + TTX (1 μM)
Mg2+-free 10.5 mM K+ ACSF + TTX (1 μM)
20 pA
200 ms
B
10.5 mM K+
2.5 mM K+
*
Frequency (Hz)
0.700
0.600
0.500
0.400
0.300
0.200
0.100
0.000
(0-5)
Chronologic ACSF applications (5 min intervals)
C
***
Frequency (Hz)
0.025
0.02
0.015
0.01
0.005
0

Figure 3.1: Exposure of hippocampal slice to ^$[K^+]_o$ ACSF leads to increases in neuron excitability. (A) Cropped sections of a gap-free recording from a representative CA1 pyramidal neuron during whole-cell patch clamp electrophysiology (voltage clamped at -70 mV) during exposure to Mg^{2+}-free ACSF (top) and Mg^{2+}-free ^$[K^+]_o$ ACSF (bottom). Tetrodotoxin (1μM) was continuously perfused throughout the experiment to block action potential generation in hippocampal neurons, but mEPSCs and SICs persisted. **(B)** Gap-free recordings (n=11) were analyzed for frequency of mEPSCs were calculated as events per second (Hz). Exposure to ^$[K^+]_o$ ACSF led to an increase in average mEPSC frequency during both the 1st and 2nd (5 min) applications, in comparison to the three (10 min; 0-5 min and 5-10 min) applications of control ACSF. **(C)** Gap-free recordings were analyzed for frequency of SICs calculated as events per second (Hz). Initial exposure to ^$[K^+]_o$ ACSF led to an increase in average SIC frequency in comparison to the baseline SIC frequency in control ACSF. This increased SIC frequency persisted throughout the remainder of the experiment, despite two subsequent (10 min) washes in control ACSF. N = 11 neuronal recordings; 1 recording per slice. *p < .05, **p < .01, and ***p < .001.

A

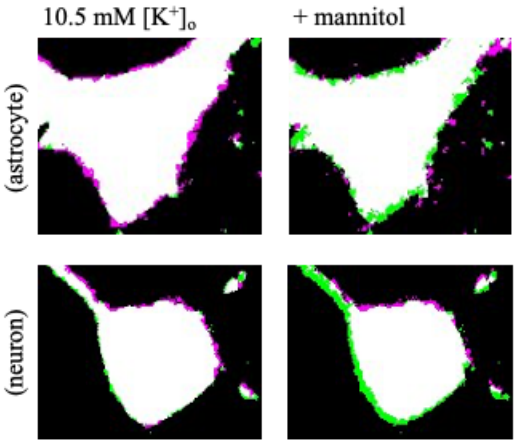

(Mg2+-free ACSF + 1 μM TTX)

B

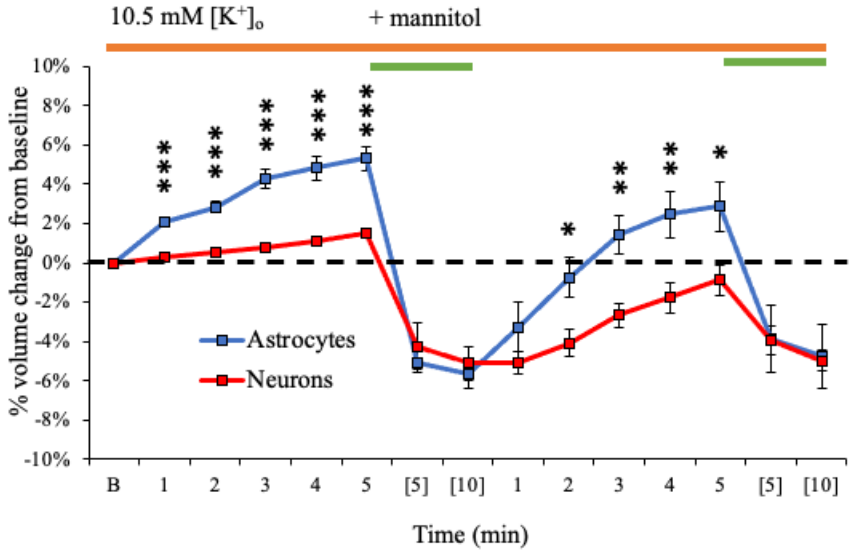

Figure 3.2: Application of mannitol in the presence of ^$[K^+]_o$ decreases the volume of both astrocytes and neurons. (A) The baseline volume of an astrocyte and neuron are depicted in thresholded images of the cell somas (in white). A magenta overlay indicates increased soma area, while green overlay indicates soma shrinkage beyond baseline area. The application of ^$[K^+]$ ACSF triggers noticeable astrocyte volume increase (top left) and minimal neuron volume change (bottom left). In the continued presence of ^$[K^+]_o$, the introduction of mannitol triggers astrocyte (top right) and neuron (bottom right) volume decrease. **(B)** Baseline soma volume was determined as the average soma area calculated from three z-stacks taken at minutes 8, 9, and 10 in control ACSF. Graph depicts average percent volume change from baseline ("B") of astrocytes (blue, N=9) and neurons (red, N=11) during continuous exposure to ^$[K^+]_o$ ACSF (orange bar) and two 10-min exposures to mannitol (green bar). One z-stack of the cell soma was collected every minute during exposure to ^$[K^+]_o$. During combined exposure to ^$[K^+]_o$ and mannitol, a z-stack was collected at minutes [5] and [10]. Note the significant shrinkage of astrocyte somas by nearly 10% ($p<.001$) compared to approximately 3% ($p<.01$) by neurons during the 1st application of dual exposure to ^$[K^+]_o$ and mannitol. Washout of mannitol resulted in a rebound of astrocyte volume to approximately 3% above baseline ($p<.01$), while neuron volume increased minimally. Only one cell was imaged per slice. Asterisks indicate a significant difference astrocyte and neuron volume at that timepoint. *$p < .05$, **$p < .01$, and ***$p < .001$.

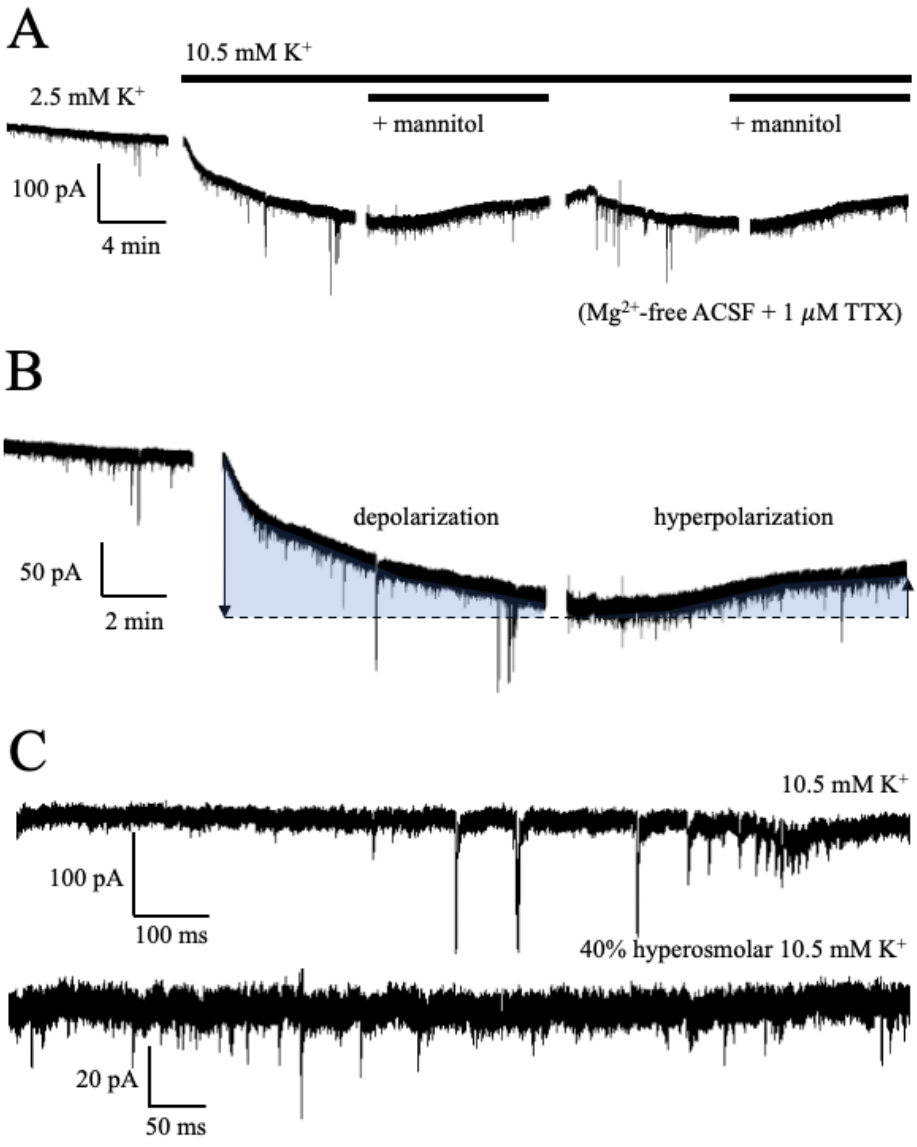
A
10.5 mM K+
2.5 mM K+
+ mannitol
+ mannitol
100 pA
4 min
(Mg2+-free ACSF + 1 μM TTX)
B
depolarization
hyperpolarization
50 pA
2 min
C
10.5 mM K+
100 pA
100 ms
40% hyperosmolar 10.5 mM K+
20 pA
50 ms

Figure 3.3: Application of hyperosmolar ^$[K^+]_o$ triggers changes in neuron membrane polarization and excitability. (A) Representative recording of a neuron voltage-clamped at -70 mV for the duration of an experiment in Mg^{2+}-free ACSF supplemented with TTX (1 μM). Gaps in recording coincide with periodic reassessment of patch-clamp quality between alternating 10-min ACSF treatments: (1^{st}) control ACSF, (2^{nd}) ^$[K^+]_o$, (3^{rd}) ^$[K^+]_o$ + mannitol, (4^{th}) ^$[K^+]_o$, and (5^{th}) ^$[K^+]_o$ + mannitol. **(B)** Partial 30-min section of recording shown at increased scale factor emphasizes changes in holding current during exposure to control ACSF, ^$[K^+]_o$ and hyperosmolar ^$[K^+]_o$. (C) Small ~1 min sections of recording showcasing individual events occurring during exposure to ^$[K^+]_o$ (top trace) and hyperosmolar ^$[K^+]_o$ (bottom trace). Note the prominence of large SIC events in ^$[K^+]_o$ and smaller mEPSC events in hyperosmolar ^$[K^+]_o$.

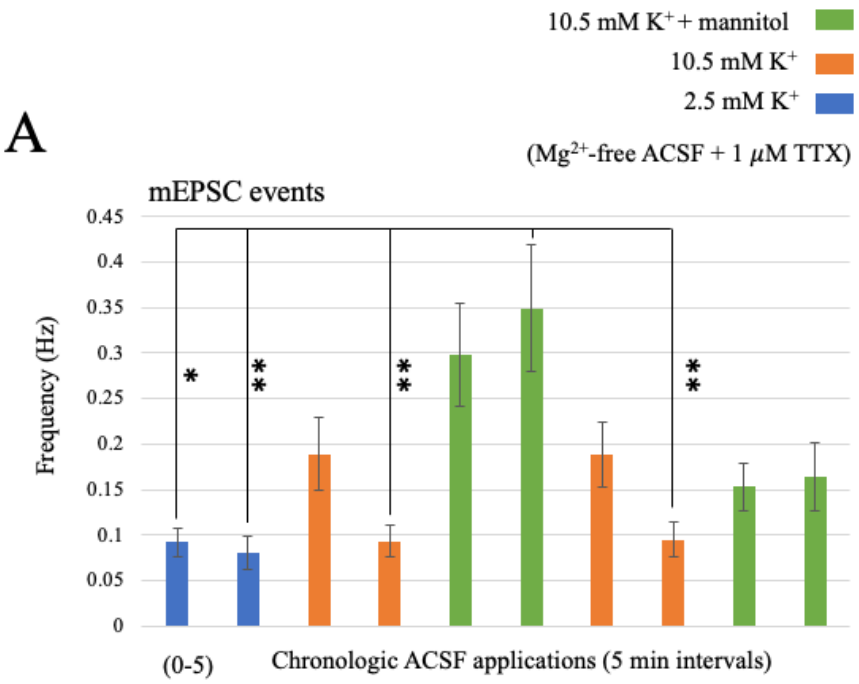
A
10.5 mM K+ + mannitol
10.5 mM K+
2.5 mM K+
(Mg2+-free ACSF + 1 μM TTX)
mEPSC events
Frequency (Hz)
0.45
0.4
0.35
0.3
0.25
0.2
0.15
0.1
0.05
0
*
**
**
**
(0-5)
Chronologic ACSF applications (5 min intervals)

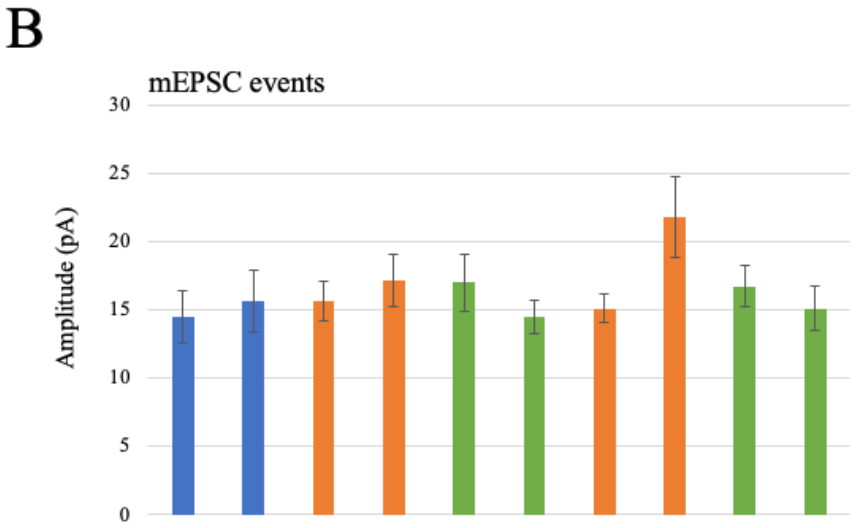
B
mEPSC events
Amplitude (pA)
30
25
20
15
10
5
0

Figure 3.4: mEPSC frequency increases in ^$[K^+]_o$ and hyperosmolar ^$[K^+]_o$ in comparison to baseline conditions. (A) The frequency of mEPSC events was calculated as events per second (Hz) during 5-min intervals of each 10-min treatment of either control ACSF (blue), ^$[K^+]_o$ (orange) or hyperosmolar ^$[K^+]_o$ (green). In the 1st application, note the trend of increasing mEPSC frequency as extracellular potassium increased, and when mannitol increased the osmolarity of the ECS under ^$[K^+]_o$ conditions. Although mEPSC frequency remained elevated in the 2nd application of ^$[K^+]_o$ in comparison to baseline conditions, the subsequent addition of mannitol did not dramatically increase frequency like it did in the 1st application cycle. **(B)** Over the course of exposure to the three different treatments, average mEPSC amplitude (pA) did not appreciably change, in comparison to average frequency. *$p < .05$, **$p < .01$, and ***$p < .001$.

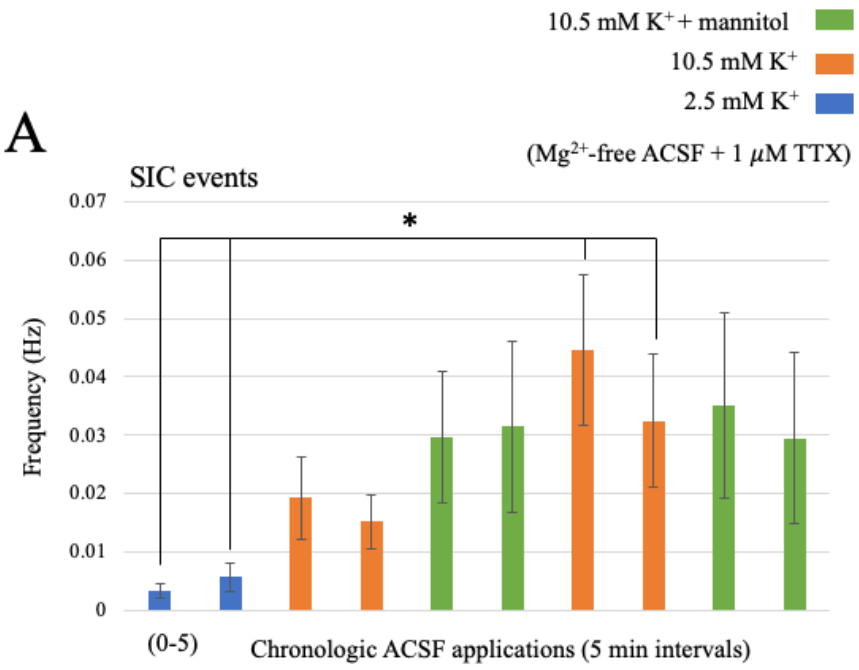
A
10.5 mM K+ + mannitol
10.5 mM K+
2.5 mM K+
(Mg2+-free ACSF + 1 μM TTX)
SIC events
*
Frequency (Hz)
0.07
0.06
0.05
0.04
0.03
0.02
0.01
0
(0-5)
Chronologic ACSF applications (5 min intervals)

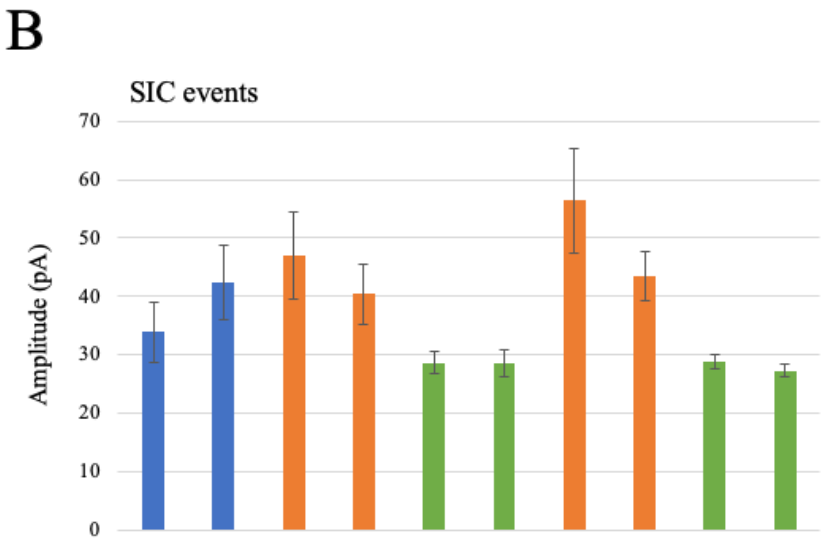
B
SIC events
Amplitude (pA)
70
60
50
40
30
20
10
0

Figure 3.5: SIC frequency and amplitude changes in ^$[K^+]_o$ when later exposed to mannitol. (A) The frequency of SIC events were calculated in five-minute intervals under three conditions: control ACSF (blue), ^$[K^+]_o$ (orange), and hyperosmolar ^$[K^+]_o$ (green). ^$[K^+]$ ACSF was perfused throughout the entire experiment, while mannitol was washed in and out of the recording chamber twice. During the 1st wash-in of mannitol, a noticeable increase in SIC frequency occurred within the first five minutes. Subsequent wash-out of mannitol did not significantly alter the frequency of SICs within five minutes of application, but after a total of 10 min the frequency trended toward a decrease. The final wash-in of mannitol affected SIC frequency minimally, unlike the first application. **(B)** The average amplitude of SIC events occurring under each condition was calculated. Note the slight decrease in average amplitude when mannitol is applied in the presence of ^$[K^+]_o$. This mannitol-dependent effect was consistent in both the 1st and 2nd application cycles with ^$[K^+]_o$. *$p < .05$, **$p < .01$, and ***$p < .001$.

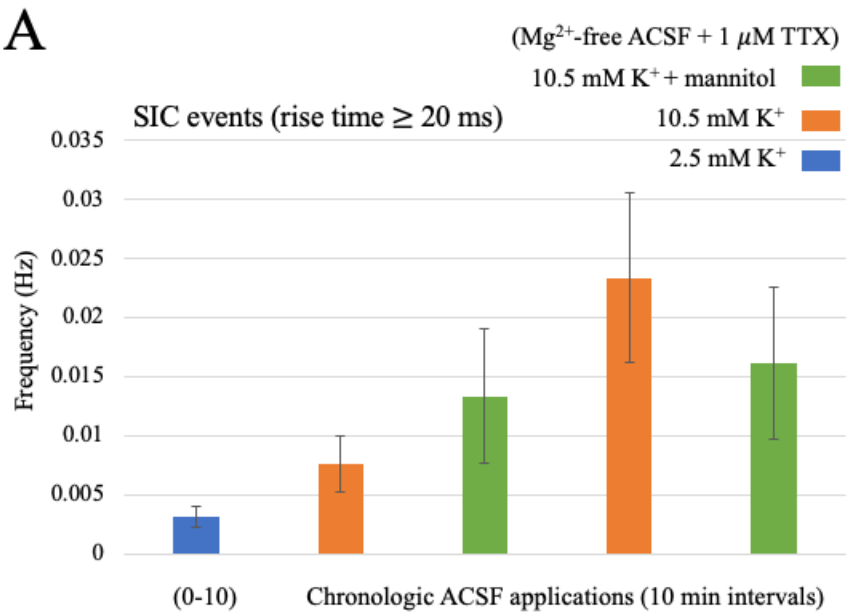
A
(Mg2+-free ACSF + 1 μM TTX)
10.5 mM K+ + mannitol
10.5 mM K+
2.5 mM K+
SIC events (rise time ≥ 20 ms)
Frequency (Hz)
0.035
0.03
0.025
0.02
0.015
0.01
0.005
0
(0-10)
Chronologic ACSF applications (10 min intervals)

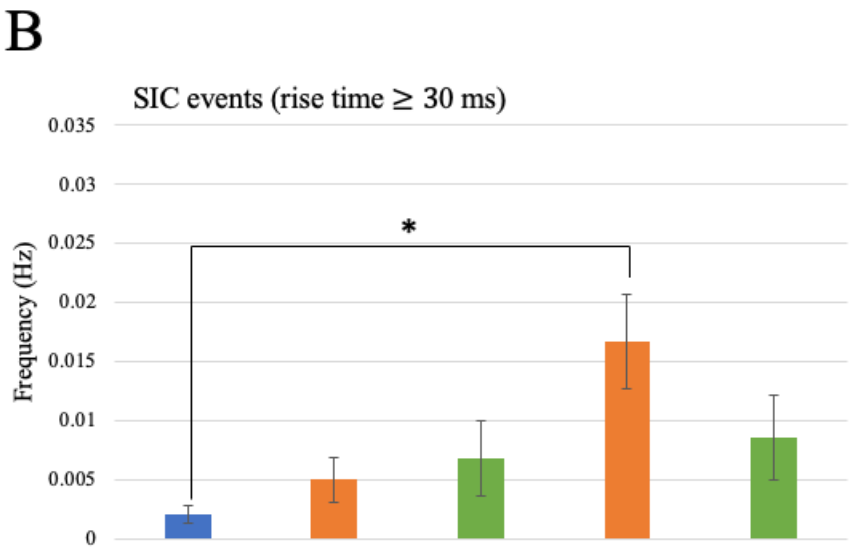
B
SIC events (rise time ≥ 30 ms)
Frequency (Hz)
0.035
0.03
0.025
0.02
0.015
0.01
0.005
0
*

Figure 3.6: Slower SIC events occurred more often in the presence of ^$[K^+]_o$. (A) The frequency of SIC events with rise times ≥ 20 ms that occurred during each 10 min treatment (control ACSF, ^$[K^+]_o$ or hyperosmolar ^$[K^+]_o$). **(B)** After the exclusion of events with rise times ≥ 30 ms, SIC frequency in the 2nd application appeared to slightly increase in the presence of ^$[K^+]_o$ compared to hyperosmolar ^$[K^+]_o$. *p < .05, **p < .01, and ***p < .001.

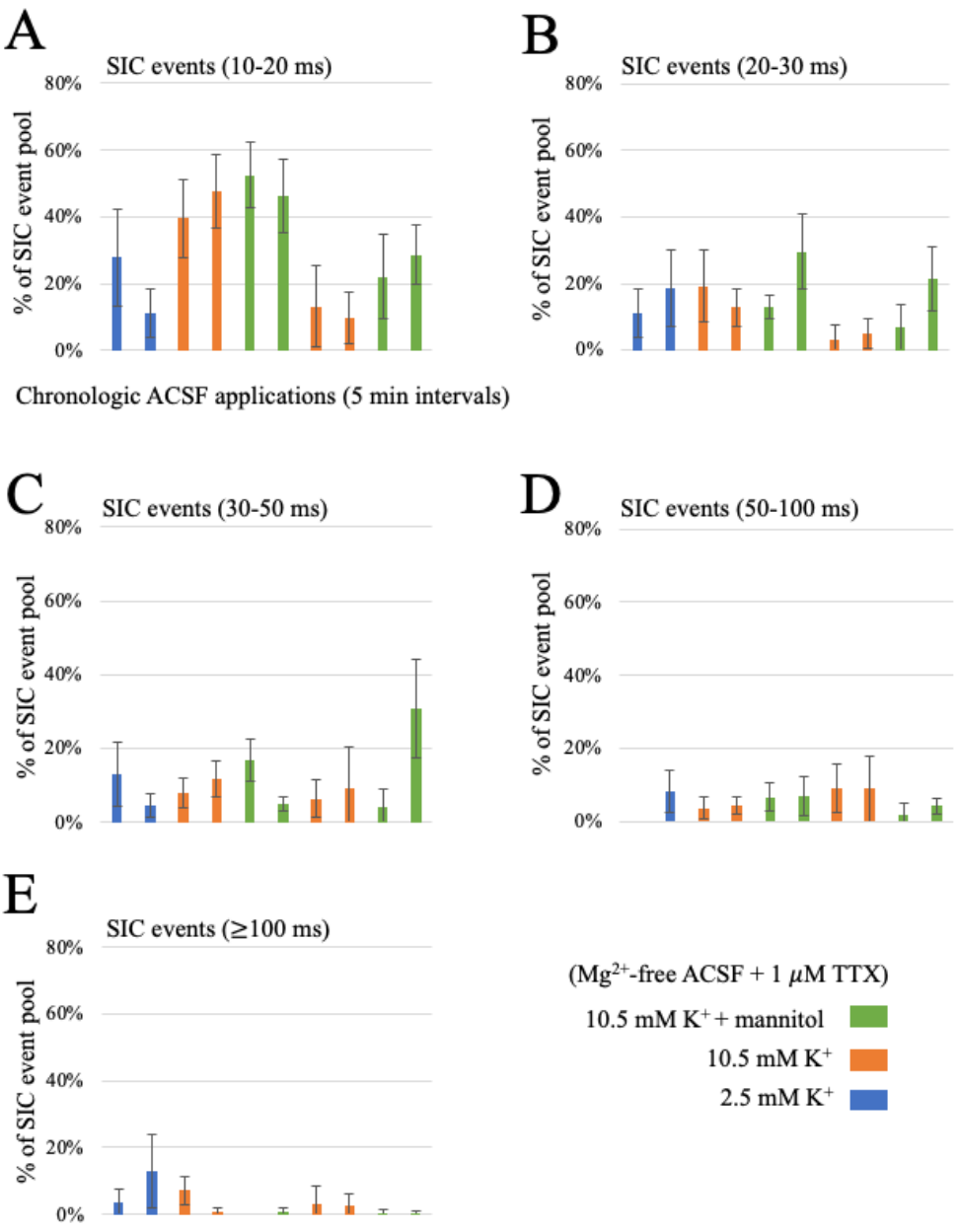
A
SIC events (10-20 ms)
% of SIC event pool
80%
60%
40%
20%
0%
B
SIC events (20-30 ms)
% of SIC event pool
80%
60%
40%
20%
0%
Chronologic ACSF applications (5 min intervals)
C
SIC events (30-50 ms)
% of SIC event pool
80%
60%
40%
20%
0%
D
SIC events (50-100 ms)
% of SIC event pool
80%
60%
40%
20%
0%
E
SIC events (≥100 ms)
% of SIC event pool
80%
60%
40%
20%
0%
(Mg2+-free ACSF + 1 μM TTX)
10.5 mM K+ + mannitol
10.5 mM K+
2.5 mM K+

Figure 3.7: SIC event rise times vary depending on ACSF treatment. All graphs show the percentage of SIC events that occurred during each treatment (control ACSF, $\wedge[K^+]_o$ or hyperosmolar $\wedge[K^+]_o$) that fall into a specific range of rise time values. SIC events occurring within 5-min treatment intervals were analyzed. **(A)** The proportion of SICs (out of the full SIC event pool) that had 10-20 ms rise times and occurred under a specific treatment are displayed. The proportion of SIC events occurring during each treatment with rise time values between either **(B)** 20-30 ms, **(C)** 30-50 ms, **(D)** 50-100 ms or **(E)** >100 ms are also displayed.

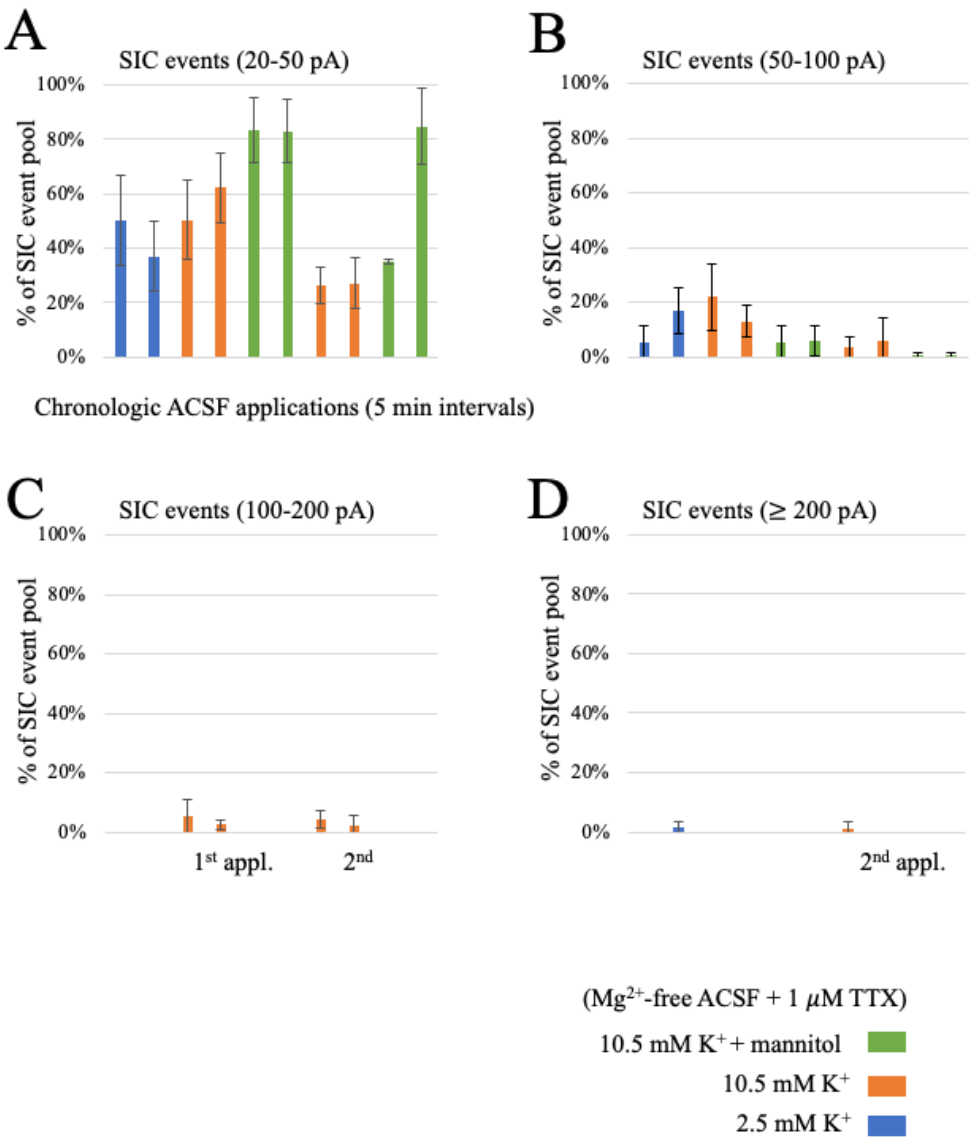
A
SIC events (20-50 pA)
100%
80%
60%
40%
20%
0%
% of SIC event pool
B
SIC events (50-100 pA)
100%
80%
60%
40%
20%
0%
% of SIC event pool
Chronologic ACSF applications (5 min intervals)
C
SIC events (100-200 pA)
100%
80%
60%
40%
20%
0%
% of SIC event pool
1st appl.
2nd
D
SIC events (≥ 200 pA)
100%
80%
60%
40%
20%
0%
% of SIC event pool
2nd appl.
(Mg2+-free ACSF + 1 μM TTX)
10.5 mM K+ + mannitol
10.5 mM K+
2.5 mM K+

Figure 3.8: SIC event amplitude varies depending on ACSF treatment. All graphs show the percentage of SIC events that occurred during each treatment (control ACSF, $\wedge[K^+]_o$ or hyperosmolar $\wedge[K^+]_o$) that fall into a specific range of amplitude values. SIC events occurring within 5-min treatment intervals were analyzed. **(A)** The proportion of SICs with 20-50 pA amplitude that occurred during specific treatments. The proportion of SIC events occurring during each treatment with amplitude values between either **(B)** 50-100 pA, **(C)** 100-200 pA, or **(D)** >100 pA are also displayed. Note the complete abolishment of >100 pA SICs in the presence of mannitol.

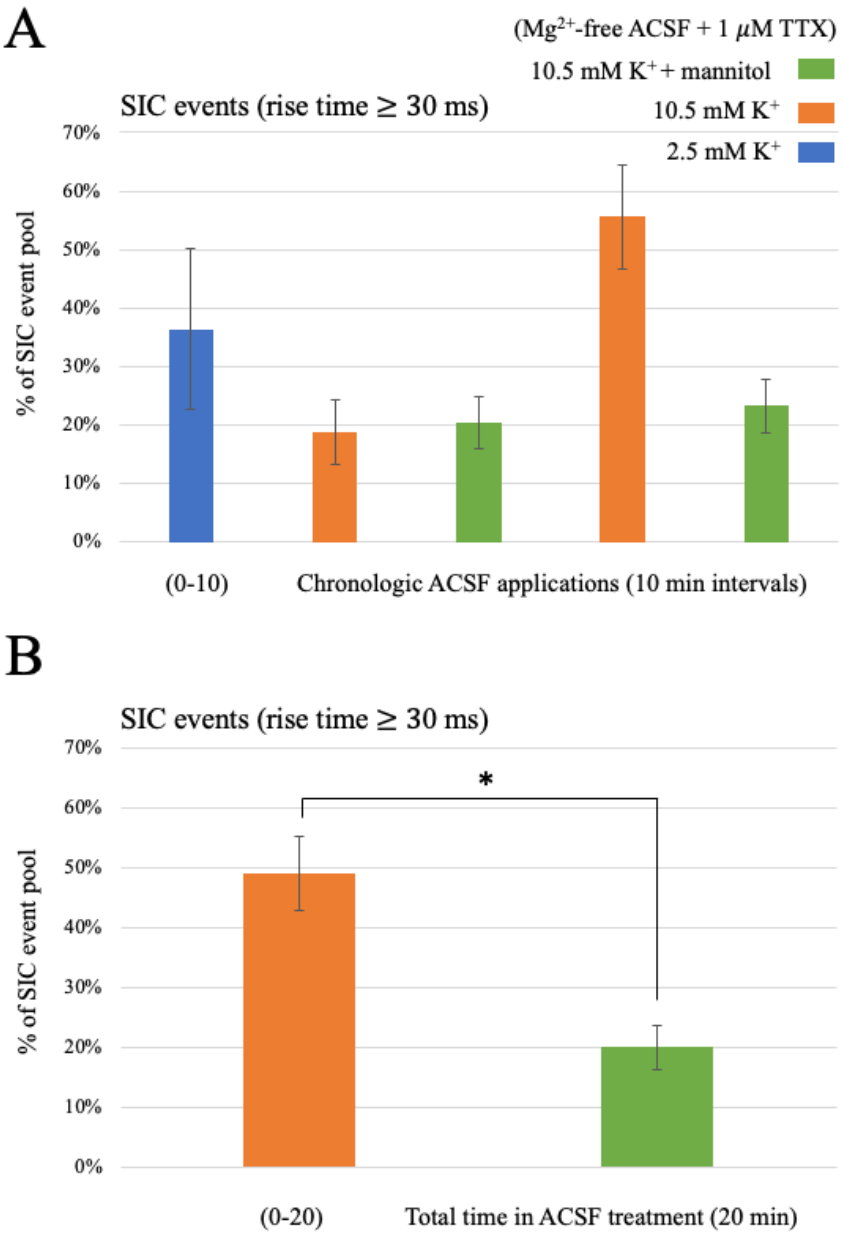
A
(Mg2+-free ACSF + 1 μM TTX)
10.5 mM K+ + mannitol
10.5 mM K+
2.5 mM K+
SIC events (rise time ≥ 30 ms)
% of SIC event pool
70%
60%
50%
40%
30%
20%
10%
0%
(0-10)
Chronologic ACSF applications (10 min intervals)
B
SIC events (rise time ≥ 30 ms)
% of SIC event pool
*
(0-20)
Total time in ACSF treatment (20 min)

Figure 3.9: Slower SICs predominate in the applications of ^$[K^+]_o$ in comparison to hyperosmolar ^$[K^+]_o$. (A) SIC events with rise time >30 ms made up a larger portion of the SIC event pool during the 2nd 10-min interval of ^$[K^+]_o$ treatment in contrast to both 10-min treatments of hyperosmolar ^$[K^+]_o$. **(B)** When SIC events occurring in the first and second 10-min applications of each treatment were summed, there was a readily apparent increase ($p<.05$) in slower SICs (>30 ms) in ^$[K^+]_o$, in comparison to the 20-min exposure to hyperosmolar ^$[K^+]_o$. *$p < .05$, **$p < .01$, and ***$p < .001$.

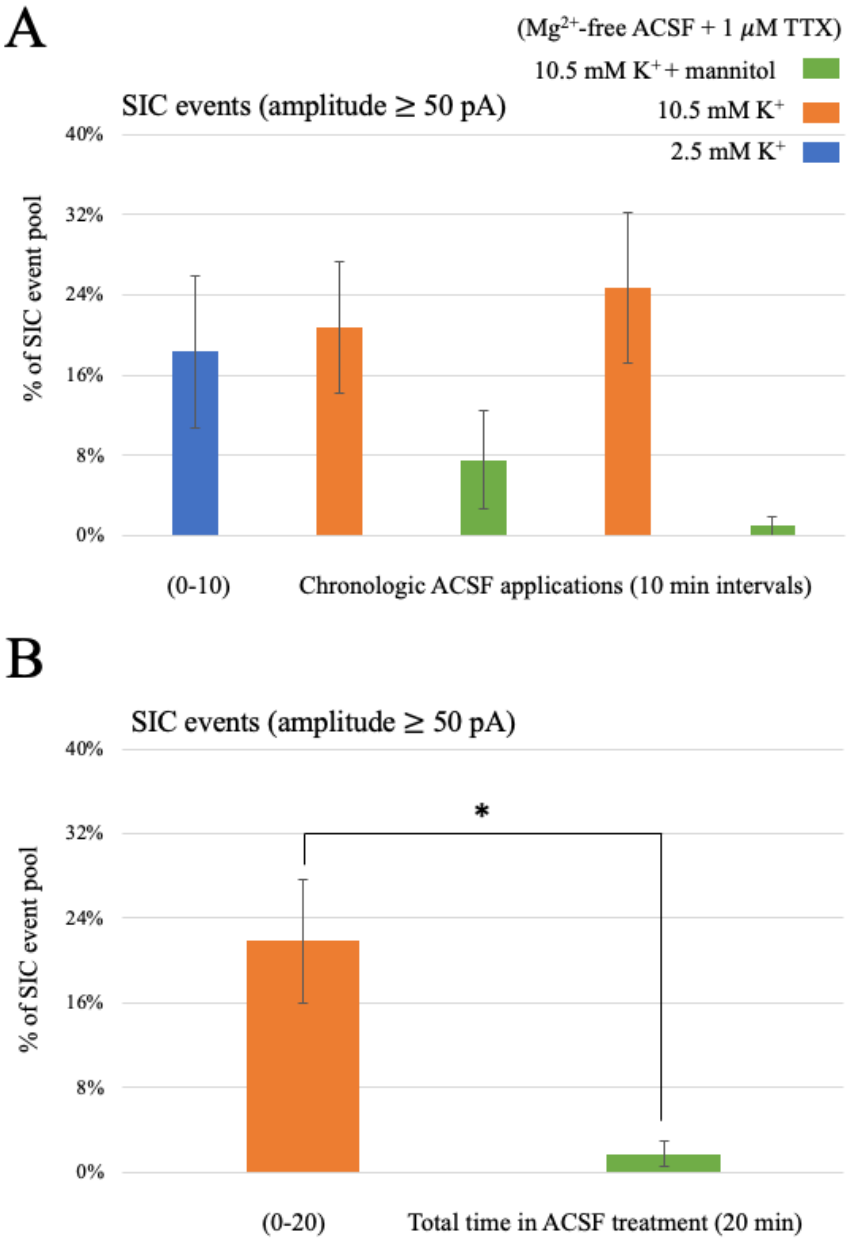
A
(Mg2+-free ACSF + 1 μM TTX)
10.5 mM K+ + mannitol
10.5 mM K+
2.5 mM K+
SIC events (amplitude ≥ 50 pA)
40%
32%
24%
16%
8%
0%
% of SIC event pool
(0-10)
Chronologic ACSF applications (10 min intervals)
B
SIC events (amplitude ≥ 50 pA)
40%
32%
24%
16%
8%
0%
*
% of SIC event pool
(0-20)
Total time in ACSF treatment (20 min)

Figure 3.10: Larger SICs predominate in the applications of ^$[K^+]_o$ in comparison to hyperosmolar ^$[K^+]_o$. (A) There was substantial variability in the occurrence of large SICs (>50 pA) in control ACSF and both applications of ^$[K^+]_o$, but there was a trend towards fewer large-amplitude SICs occurring in the presence of ^$[K^+]_o$ and mannitol. **(B)** When both 10-min intervals of each treatment were combined, the proportion of large SICs occurring in ^$[K^+]_o$ significantly dwarfed that of hyperosmolar ^$[K^+]_o$ by over 12% ($p<.05$). *$p < .05$, **$p < .01$, and ***$p < .001$.

Chapter 3

Abstract

In this project, we aimed to understand the role of volume regulated anion channels (VRAC) on brain tissue swelling and neuronal excitability. VRAC are activated in response to cell swelling, and release glutamate and other anions into the extracellular space in an effort to regulate cell volume. To study VRAC in the context of cell volume and excitability changes, we generated multiple transgenic mouse lines using Cre-lox technology to selectively ablate VRAC in specific cell types. Each Cre line was first characterized by crossing to a Rosa26-lsl-TdTomato reporter line to assess cell-type specific expression. The role of VRAC in astrocyte swelling was evaluated by recording real-time confocal volume responses of astrocytes in acute mouse hippocampal slices using two common models of tissue swelling - application of 40% hypoosmolar artificial cerebrospinal fluid or elevated-potassium ACSF (10.5 mM [K^+]). Data suggest that ablation of VRAC does not produce significant changes in short-term swelling profiles of astrocytes. To complement direct cell swelling models, we found that application of the pro-epileptic drug 4-AP resulted in less epileptiform activity in slices from *Nestin-Cre*$^{(+/-)}$*;SWELL*$^{fl/fl}$ mice in which VRAC was widely ablated from neural progenitors, in comparison to control slices. Interestingly, the ablation of astrocytic VRAC in *Aldh1l1-Cre*$^{ERT2(+/-)}$*;SWELL*$^{fl/fl}$ mice did not have any significant effects on epileptiform activity in

slices. Our findings thus far suggest that VRAC may play a role in mediating synchronous epileptiform activity.

Introduction

Excitatory neuronal activity results in release of K^+ and glutamate into the ECS, triggering astrocytes to uptake these molecules. In this environment, it has been shown by our lab and others (Walz and Hinks, 1985; Kimelberg et al., 1995; Su et al., 2002; Larsen et al., 2014; Larsen and MacAulay, 2017; Walch et al., 2020) that astrocytes rapidly swell due to concomitant water influx. Additionally, our lab has shown that both astrocytes and neurons swell in response to hypoosmotic ACSF applied to acute hippocampal slices, and this volume increase is associated with increased neuronal excitability (Lauderdale et al., 2015; Murphy et al., 2017). Swollen cells diminish the volume of the ECS, ultimately elevating $[glutamate]_o$. Understanding the mechanisms underlying changes in extracellular glutamate levels are fundamental to understanding the processes leading to brain excitotoxicity in neurological disorders including epilepsy and stroke. In culture, swelling of astrocytes decreases the uptake of excitatory amino acids (EAA) and increases their efflux (Kimelberg et al., 1995). Volume regulated anion channels (VRAC) are one of the most-promising candidates for swelling-activated glutamate release contributing to brain tissue excitability. VRAC have been identified on nearly every cell in the body, and are activated in conditions of cell swelling. The role of VRAC in cell

volume regulation is thought to be through regulatory volume decrease (RVD) that occurs in response to cell swelling. Cells efflux negatively charged osmolytes, triggering osmotic efflux of water. This function is well documented in cultured cells (Pasantes-Morales et al., 1994; Okada et al., 2001), but not in brain slice (Risher, Andrew and Kirov, 2009). Cultured astrocytes expressing VRAC have been shown to release radiolabeled aspartate (an analogue for glutamate) in response to swelling (Rutledge et al., 1998). Although pharmacologic inhibitors of VRAC have many off-target effects, their use has shown to be neuroprotective in multiple instances (Phillis, Song, and O'Regan, 1998; Zhang et al., 2008; Alibrahim et al., 2013).

Early use of tamoxifen (a known VRAC antagonist) in the rat brain *in vivo* reduced glutamate levels in cerebrospinal fluid after transient ischemia, suggesting a role for VRAC in this pathophysiological process (Phillis, Song, and O'Regan, 1998). In hippocampal slices, another pharmacological inhbitor of VRAC (NPPB) decreased glutamate release and reduced severity of spreading depression (Basarsky, Feighan and MacVicar, 1999). A whole-cell patch clamp study sought to abolish EAA release from swollen astrocytes, and did so successfully with DCPIB and tamoxifen, two of the most 'selective' inhibitors of VRAC (Abdullaev et al., 2006). In a rat model of stroke using middle cerebral artery occlusion (MCAo), it was found that pre-treatment with DCPIB lead to a large (~75%) and statistically significant decrease in infarct volume (Zhang et al., 2008). Samples of CSF collected from DCPIB-treated animals had reduced glutamate concentrations, in comparison to vehicle-treated controls (Zhang et al., 2008). In a later study, which measured the effects of DCPIB pre-treatment after an ischemic-hypoxic

injury, treated mice also experienced smaller infarct volumes and better functional recovery post-injury in comparison to controls (Alibrahim et al., 2013). This catalog of promising studies underscores the importance of VRAC in regulating excitotoxicity after severe brain injury. However, skeptics would be quick to comment on the promiscuity of pharmacologic antagonists on glutamate release pathways, such DCPIB's off-target effects on connexin hemichannels (Bowens et al., 2013) or carbenoxolone's off-target effects on VRAC (Ye et al., 2008). Thus without appropriate transgenic models, the role of VRAC in mediating glutamate excitotoxicity cannot be definitively answered if we continue to rely on pharmacology.

In 2014, two independent research groups identified leucine-rich repeat-containing protein 8A (LRRC8A) as the pore-forming subunit of the channel (Voss et al., 2014; Qiu et al., 2014). Because VRAC are ubiquitously expressed, and due to the lack of specific pharmacological reagents to target the channel (Bowens et al., 2013), a transgenic approach is required to enable targeted removal of VRAC in specific cell types. Most recently, the Qiu group has published promising findings using *mGFAP-Cre;SWELL*$^{fl/fl}$ mice, showing that removal of VRAC in astrocytes and some neurons can reduce infarct volume associated with transient MCAo (Yang et al., 2019). However, importantly, the field still has not generated and characterized VRAC cKO lines that would identify the specific role of VRAC in neurons vs. astrocytes, and no study to date has probed the role of VRAC in any capacity in epilepsy.

It is crucial to understand how VRAC in specific cell types may sculpt the brain's response to tissue swelling, as well as contribute to conditions of swelling-induced

excitability. It is possible that neurons and astrocytes differentially contribute to elevated glutamate concentrations within an already diminished ECS volume. It is not known whether there is heterogeneity of VRAC function from one cell type to another. For example, the degree of swelling required to activate VRAC may differ between neurons and glia. Furthermore, characteristics such as the sensitivity and duration of VRAC activation and amount of glutamate available for release might vary in different cell types. Accordingly, we have generated an astrocyte-specific model of VRAC ablation and two additional knockout lines that target a variety of cell types. These mice are being used in hippocampal slice experiments to understand the role of VRAC in astrocyte swelling and neuronal excitability.

Materials and Methods

All experiments were performed in accordance with National Institutes of Health guidelines for the care and use of laboratory animals and approved by the Institutional Animal Care and Use Committee at the University of California, Riverside.

Generation of Transgenic Mouse Lines

Using Cre-lox technology, we generated three transgenic mouse models with cell-selective ablation of LRRC8A gene. LRRC8A protein is an essential subunit of the volume regulated anion channel (VRAC) that is required for pore-formation and

trafficking of the channel to the membrane (Formaggio et al., 2018). We acquired mice with loxP sites flanking both allelic copies of LRRC8A ($SWELL^{fl/fl}$) and bred them to mice with promoter driven-Cre-recombinases (mGFAP-Cre, Nestin-Cre, and Aldh1l1-Cre^{ERT2}) purchased from Jackson Laboratories (Bar Harbor, ME). Breeding ensued until the homozygous knockout genotype was achieved ($Cre^{(+/-)};SWELL^{fl/fl}$), along with Cre-negative littermate controls ($Cre^{(-/-)};SWELL^{fl/fl}$). Genotypes were confirmed by PCR and electrophoresis of toeclip tissue samples. All mice were bred over the C57Bl6 background. Our VRAC conditional knockout models (VRAC cKO) do not carry an endogenous reporter for recombination, so we also crossed our Cre lines to $Rosa26^{lsl-tdTomato}$ mice, to assess the efficiency and selectively of recombination in the different Cre.

To induce Cre-recombinase activation in $Aldh1l1\text{-}Cre^{ERT2};SWELL^{fl/fl}$ mice, tamoxifen was administered via oral gavage. Tamoxifen binds a mutated estrogen receptor on Cre, which allows for temporal translocation of Cre-recombinase into the nucleus. Oral gavage of tamoxifen dissolved in corn oil (150 µg tamoxifen/g mouse) was administered to 6-7 week old adult mice, three times over the course of one week (1 mL syringe, 18G feeding needle). A period of 2 weeks post-gavage allows for sufficient time for tamoxifen to be metabolized from the system (about 24 hr) and for VRAC protein turnover from the membrane. Proteins in the mouse brain are degraded on average every nine days, and membrane-bound proteins exhibit shorter than average lifetimes, in comparison to synaptic and mitochondrial proteins (Price et al., 2010; Dörrbaum et al., 2018). With the exception of $Nestin\text{-}Cre;SWELL^{fl/fl}$ mice, all animals were sacrificed for experiments between 8-12 weeks of age. The Nestin-Cre-driven knockout of VRAC resulted in an

early mortality phenotype (death by ~7 weeks old), so *Nestin-Cre;SWELL*$^{fl/fl}$ mice were sacrificed between 6-8 weeks of age.

Immunohistochemistry & Slide Imaging

Mice were sacrificed via CO_2 asphyxiation at either P15-P21 (mGFAP-Cre), 6-8 weeks old (Nestin-Cre) or 8-12 weeks old (mGFAP-Cre and Aldh1l1-Cre^{ERT2}). Once signs of life were absent, mouse tissue was fixed via transcardial perfusion with paraformaldehyde using the procedure outlined in JoVE (Gage, Kipke, and Shain, 2012). Extracted whole brain tissue underwent postfixation at 4°C in 4% PFA for ~4 hrs with gentle agitation, then brains were transferred into 1x PBS (recipe outlined in Polleux and Ghosh, 2002). Subsequently, agar-mounted brains were submerged in PBS to make parasagittal slices (160 μm thick) using an automated vibrating blade microtome (VT1200S model; Leica Biosystems, Buffalo Grove, IL, USA). Primary antibodies (ThermoFisher GFAP rat monoclonal, 1:1000; Takara dsRed rabbit polyclonal, 1:500) and secondary antibodies (AlexaFluor488 goat anti-rat IgG, 1:1000; AlexaFluor546 goat anti-rabbit IgG, 1:400) were diluted in permeabilization solution supplemented with 5% normal goat serum to block non-specific binding. Floating slice immunohistochemistry protocol was adapted from a previously published procedure (Polleux and Ghosh, 2002). Briefly, slices were incubated overnight at 4°C in permeabilization solution (recipe outlined in Polleux and Ghosh, 2002). Slices were then incubated overnight at 4°C in diluted primary antibody solution with gentle agitation. Afterwards, slices were washed

for 15 min, 8x with 1x PBS, before being transferred into diluted secondary antibody solution. Slices were incubated in this solution overnight at 4°C with gentle agitation. Post-incubation, slices were washed for 15 min, 4x with 1x PBS before being mounted on glass slides and dried for 30 min. Afterwards, mounting medium (Prolong Glass Antifade Mountant) was applied to each brain slice before covering the tissue with a glass coverslip. Z-stack images were acquired from prepared slides using a laser scanning confocal microscope (Leica SPEII) at 10x and 20x objectives.

Acute Slice Preparation

Acute hippocampal slices were prepared from VRAC cKO (*Cre*$^{(+/-)}$*;SWELL*$^{fl/fl}$) or littermate control (*Cre*$^{(-/-)}$*;SWELL*$^{fl/fl}$) mice at 8-12 weeks of age, with the exception of *Nestin-Cre;SWELL*$^{fl/fl}$ mice sacrificed at 6-8 weeks of age, due to early mortality. Animals were anesthetized under isoflurane and rapidly decapitated, and brains were removed quickly into a container of frozen and blended slicing buffer perfused with Carbogen (95% oxygen and 5% carbon dioxide) for 5 min before being bisected in a petri dish containing the same mixture. Slicing buffer contained (in mM) the following: 87 NaCl, 75 sucrose, 10 glucose, 1.25 NaH_2PO_4, 2.5 KCl, 25 $NaHCO_3$, 1.3 ascorbic acid, 0.5 $CaCl_2$, 7 $MgCl_2$, 2 pyruvate, and 0.1 kynurenic acid. Parasagittal slices (350 μm thick) were cut using an automated vibrating blade microtome and trimmed until only the hippocampus and immediately surrounding tissues remained. These mini-slices were transferred to a recovery chamber containing 36°C slicing buffer solution and incubated in a 36°C water bath for 45 min. After incubation, the slicing chamber was moved into

room temperature (RT) conditions. After 15 min of rest at RT, slices were moved into another chamber containing control ACSF comprised (in mM) of the following: 125 NaCl, 2.5 KCl, 2.5 $CaCl_2$, 1.3 $MgCl_2$, 1.25 NaH_2PO_4, 26 $NaHCO_3$, and 15 glucose. Slices rested in ACSF for 15 min at RT before the start of the experiment.

For astrocyte imaging, astrocytes were incubated in 36°C slicing buffer supplemented with 4 μM sulforhodamine-101 (SR-101; Sigma-Aldrich, St. Louis, MO, USA) as described previously (Murphy et al., 2017). After a 45 min incubation at 36°C, slices were transferred into room temperature (RT) conditions for 10 min of rest. Slices were subsequently transferred to a chamber containing ACSF without SR-101 and rested for an additional 10 min. Once more before the start of the experiment, slices were transferred again to another chamber of ACSF to remove any residual SR-101 from slices. All experiments were performed at room temperature.

Experimental Solutions and Pharmacology

In addition to the isoosmolar (~300 mOsmo) control ACSF (2.5 mM K^+) described in slice preparation, some ACSF was altered to increase the concentration of potassium to 10.5 mM (^$[K^+]_o$) by addition of KCl, while reducing the concentration of NaCl by an equal amount so that the solution osmolarity was constant. Some control ACSF was diluted with DI water to generate 40% hypoosmotic ACSF (~180 mOsmo) while keeping all other ingredients the same. In other experiments, pre-made control ACSF was supplemented with 4-aminopyridine (4-AP, Sigma Aldrich), a pharmacological blocker

of voltage-gated potassium channels. Aliquots of 4-AP (~50 uL, dissolved in DI water) were added to 50 mL tubes of ACSF for perfusion of either 200 or 500 μM 4-AP during experiments. Tamoxifen gavage solution (15 mg/mL) was generated by adding solid tamoxifen (Sigma Aldrich, T-5648) to warmed and constantly shaken corn oil, and dissolved over a period of 12-24 hrs in a glass scintillation vial protected from light.

Electrophysiology

Following recovery, slices were transferred to a recording chamber and continuously perfused with oxygenated ACSF at room temperature. Slices and individual CA1 pyramidal cells were visualized on a Leica DLMFSA upright microscope, with HCX APO L20x/0.50W U-V-I and HCX APO L63x/0.90W U-V-I submersion objectives and differential interference contrast optics (Leica Microsystems, Buffalo Grove, IL, USA). Whole-cell patch clamp recordings were acquired using a Multiclamp 700B amplifier and Digidata 1550 digitizer, controlled using pClamp v.10.7.0.3 and Multiclamp Commander v.2.2.2.2 software (Molecular Devices, San Jose, CA, USA). Patch pipettes were pulled from thin-wall 1.5 mM borosilicate glass capillaries World Precision Instruments using a Narishige PC-10 vertical micropipette puller (Narishige, Tokyo, Japan). Patch pipette resistances ranged from ~3-5 mOhm when filled with an internal solution containing the following (in mM): 140 K-gluconate, 4 $MgCl_2$, 0.4 ethylene glycol- bis(b-aminoethyl ether)-N,N,N^0 ,N^0 -tetraacetic acid (EGTA), 4Mg-ATP, 0.2 Na-GTP, 10 2-[4-(2-hydrox-

yethyl)piperazin-1-yl]ethanesulfonic acid (HEPES), and 10 phosphocreatine, pH 7.3 with KOH. CA1 pyramidal neurons were identified using differential interference contrast optics based on their location in stratum pyramidale and their characteristic morphology including apical dendrites arborizing into the hippocampal molecular layer. Upon attaining the whole-cell configuration, the cell resting V_m and R_m were recorded, and a voltage-step protocol was run to verify the presence of voltage-gated sodium and potassium currents. In voltage clamp mode, neurons were held at the chloride reversal potential V_m = -70 mV during continuous recording of excitatory currents (I) in pA. Only one recording protocol was used to apply alternating treatments of control ACSF and 4-AP-supplemented ACSF (concentration specified per experiment). An initial 5-min exposure to control ACSF was followed by a 10-min exposure to 4-AP, which was followed by a 5-min wash in control ACSF before a longer 30-min application of 4-AP. This was followed by a final 5-min wash in control ACSF. Gaps in recordings occurred when the perfusion was being switched between treatments.

Analysis of Large Epileptiform Events

Voltage-clamp recordings of CA1 pyramidal neurons were analyzed for individual events in the form of currents (pA). Clampfit software (Molecular Devices) was used to extract characteristics from individual events. While recordings of 4-AP-exposed neurons contained numerous interesting event-types on differing scales of magnitude, “large epileptiform events” were chosen as the main metric for assessing seizure-like activity.

We define these “large epileptiform events” as having amplitudes ≥1000 pA and durations ≥ 30 sec. All such events were counted, regardless of treatment condition, as others have reported generation of ictal-like events after washout of 4-AP (Salah and Perkins, 2011). Occasionally, these events occurred during gaps in recording acquisition, but their long duration enabled us to infer full event characteristics from most partially captured events. Such events were still counted towards the total event number and frequency, but only the event duration captured within the recording was counted towards the total epileptiform duration per cell. We evaluated the severity of epileptiform activity in neurons using the average event number, average event frequency, average total epileptiform duration (the sum of all event durations per recording) and the total epileptiform duration across cells within the same group (VRAC cKO or littermate control). This total epileptiform duration metric is analogous to the “total time in seizure” metric that is often used to score the severity of epilepsy between treatment groups (for examples, see Lu et al., 2010 and Liu et al., 2016).

Imaging for Ex-Vivo Experiments

In our imaging experiments, SR-101 was excited with a 559 nm semiconductor laser and detected with a 624–724 nm bandpass filter using an Olympus Fluoview FV1000 (FV10-ASW) confocal imaging system. The objective used was an Olympus LUMPlanFI 60x/0.90 W 1/0 water immersion objective lens. Confocal laser settings were the same as described previously (Murphy et al., 2017). Output power for both lines was kept as low

as possible (1.5%) to minimize the possibility of light-induced artifacts. Volume imaging of astrocytes was performed as described previously (Murphy et al., 2017). Briefly, z-stacks of 1-mm-thick images were collected at 1-min intervals over individual cell somata within 15 s to ensure adequate coverage of the soma and main processes while at the same time preventing data loss caused by tissue volume changes. Stacks were collected using a 2–3.5 zoom factor, with a scan area clipped close around the soma to increase imaging speed. Cell drift in the x-y-z planes was compensated using quick X-Y scans and X-Y-Z adjustments as necessary between time points. Imaging experiments consisted of three steps: (1) 10-min baseline period in control ACSF, in which 2 to 3 z-stacks were acquired in succession at 1-min intervals and averaged to serve as the baseline comparison for later time points; (2) a 5-min application of 10.5 mM K^+ ACSF (or 40% hypoosmotic ACSF), during which z-stacks through the full thickness of the cell were collected each minute; and (3) a 10-min exposure period of control ACSF, during which an image was taken every 5 min. Steps (2) and (3) were then repeated once each, after which the slice was discarded. Only a single cell was imaged per slice. Fiji/Image J was used for thresholding of image stacks and subsequent volume analysis as previously described (Murphy et al., 2017). Soma area of compressed image stacks (used as a proxy for cell volume) was analyzed with cell volume changes reported as percent change from the averaged baseline.

Statistical Analysis

Statistical analysis was carried out using SPSS Statistics 24 software and Laerd Statistics methodology. Datasets were first assessed for "extreme" outliers by inspection of SPSS boxplots and evaluation of studentized residuals. Outliers were rarely excluded from analysis due to the small sample size of our datasets. Secondly, the data was assessed for violations of normality with the Shapiro–Wilk test, which determined the selection of either a parametric or non-parametric statistical test. For analysis of volume measurements, datasets most often did not violate normality, so a two-way mixed analysis of variance (ANOVA) was used to check for significant interactions between the within-subject (time) and between-subjects (group/condition) factors as previously described (Walch et al., 2020). Homogeneity of variance (HOV) was assessed with Levene's test for equality of variance, Box's test established equality of covariances, and Mauchly's test determined sphericity of the dataset. If the assumption of sphericity was violated, the Greenhouse–Geisser estimation was used to determine significance in the two-way mixed ANOVA. If a one-way repeated-measures ANOVA was run for two or more comparisons, post hoc testing (Holm–Bonferroni) accounted for the type-I error associated with multiple pairwise comparisons. For analysis of 4-AP epileptiform activity, the average event number, event frequency and total epileptiform duration were compared between the VRAC cKO and littermate control groups using a parametric independent samples t-test if the assumption of data normality was met or a non-parametric Mann-Whitney U-test if the data violated normality. For an independent samples comparison, Levene's test was used to assess HOV, while Mann-Whitney

significance values were confirmed by manual inspection of data population pyramids for symmetry between groups. In calculating the total epileptiform duration across cells, epileptiform duration was summed across cells within the same group. Thus, the presented values are "group sums" rather "group means," and therefore could not be statistically assessed. For imaging experiments, each group (astrocytes or neurons) contained N = 8–12 cells (numbers specified in each experiment), unless otherwise noted. For electrophysiology experiments, the total number of neuron recordings per protocol contained N = 7–8 cells (numbers specified in each experiment). Only one astrocyte was imaged per slice or only one neuron was recorded from. Error bars in all graphs indicate the standard error of the mean (SEM). Significance values are listed as follows: *p < .05, **p < .01, and ***p < .001.

Results

Immunohistochemistry in Rosa26-lsl-TdTomato reporter mice reveals the expression profiles of three Cre-recombinases in hippocampus

In the process of developing three conditional VRAC-knockout models ($Cre^{(+/-)};SWELL^{fl/fl}$), Rosa26-lsl-TdTomato reporter mice ($Cre^{(+/-)};Rosa26^{lsl\text{-}tdTomato}$) were used for brain slice immunohistochemistry to confirm the cell-type specificity of three promoter-driven Cre-recombinases. In juvenile $mGFAP\text{-}Cre^{(+/-)};Rosa26^{lsl\text{-}tdTomato}$ hippocampus,

overlay of GFAP and Tdtomato signals showed colocalization in astrocytes (Figure 1A). Beyond the rare Tdtomato-labeling of a few dentate gyrus or CA1 pyramidal neurons, most $Cre^{(+/-)}$ cells were isolated to the astrocyte population (Figure 1A). In comparison, in adult 8-12 week tissue, *mGFAP-Cre*$^{(+/-)}$*;Rosa26*$^{lsl\text{-}tdTomato}$ showed less colocalization of GFAP and Tdtomato signals in stratum radiatum (Figure 1B). Surprisingly, many neurons also expressed Tdtomato in adult tissue compared to juvenile. By visual inspection alone, it appeared that nearly 40% of the pyramidal neurons were $Cre^{(+/-)}$ (Figure 1B). Thus, it is important to note that mGFAP-Cre-driven ablation of LRRC8A will not be astrocyte-specific in adult *mGFAP-Cre*$^{(+/-)}$*;SWELL*$^{fl/fl}$ mice. In *Aldh1l1-Cre*^{ERT2}*; Rosa26*$^{lsl\text{-}tdTomato}$ tissue there was excellent colocalization of GFAP and Tdtomato signals in stratum lacunosum moleculare (Figure 2A), suggesting astrocyte-specific LRRC8A ablation should occur in *Aldh1l1-Cre*$^{ERT2(+/-)}$*;SWELL*$^{fl/fl}$ animals. Finally, *Nestin-Cre*$^{(+/-)}$*;Rosa26*$^{lsl\text{-}tdTomato}$ brain slice retained widespread and diffuse Tdtomato signal in seemingly all of the neurons in dentate gyrus and CA1 pyramidal layer (Figure 2B), as well the neuropil near stratum lacunosum moleculare (Figure 2B). There are also blank circles amidst Tdtomato signal in the neuropil, where a non-neural progenitor cell-type must reside (Figure 2B). These are likely to be microglia, which do not arise from neuroepithelial stem cells (Zimmerman et al., 1994).

VRAC does not play a role in elevated $[K^+]_o$-driven swelling of astrocytes

We imaged SR101-labeled astrocytes from *mGFAP-Cre;SWELL$^{fl/fl}$* mice during 10.5 mM $[K^+]$-driven astrocyte swelling as we have done previously (Walch et al., 2020). Like littermate controls, VRAC cKO astrocyte somas swell within five minutes of 10.5 mM $[K^+]$ ACSF exposure (Figure 3). Similarly, both types of astrocytes shrink back to approximately their baseline volume when exposed to 2.5 mM $[K^+]$ ACSF for 5 minutes. Indeed, minute-by-minute quantification of volume change over five minutes of 10.5 mM $[K^+]$ ACSF exposure show no significant difference in volume change between *mGFAP-Cre;SWELL$^{fl/fl}$* control and knockout astrocytes (Figure 3B). During the five-minute application of 10.5 mM $[K^+]$ ACSF, astrocytes swell to ~5% above their baseline volume in both the 1st and 2nd exposures (Figure 3B). When $[K^+]_o$ is reduced back to 2.5 mM, astrocyte volume decreases to approximately 99% of their baseline volume in the 1st 10-minute application and ~98% in the 2nd (Figure 3B). These data indicate that VRAC ablation in astrocytes does not affect their volume-change response in oscillating levels of $[K^+]_o$.

VRAC does not play a role in hypoosmotic-driven swelling in astrocytes

Next we tested the role of VRAC in astrocyte swelling, driven by changes in extracellular osmolarity. Imaging astrocytes from *mGFAP-Cre;SWELL$^{fl/fl}$* mice, we measured percent volume change during exposure to solutions of differing osmolarity (Figure 4). Control

and VRAC knockout astrocytes display the same degree of soma swelling after 5 minutes of exposure to 40% hypoosmotic ACSF (Figure 4A). Reperfusion of isoosmolar ACSF for 5 minutes triggered soma shrinkage of control and knockout astrocytes near their baseline volume (Figure 4A). A preliminary dataset shows nearly identical volume changes of control and VRAC knockout astrocytes in alternating applications of hypoosmotic and isoosmotic ACSF (Figure 4B). After the first five minutes of exposure to hypoosmotic ACSF, astrocytes had swollen to ~8% above their baseline volume, while return to isoosmotic ACSF triggered shrinkage to ~2% below their baseline volume (Figure 4B). In the 2nd application of hypoosmotic ACSF, astrocytes underwent ~10% volume change in relation to their previous volume, and sat ~8% above their baseline (Figure 4B). There is some non-significant variation in the volume of control and knockout astrocytes during minutes 2 and 3 of the 2nd hypoosmotic exposure, but there was otherwise no difference in the net volume increase between groups (Figure 4B). By the end of the 2nd 10-min application of isoosmotic ACSF, all astrocytes had undergone ~13% change in volume and settled at a volume approximately 5% below their original baseline (Figure 4B). These preliminary data suggest, like in the model of elevated $[K^+]_o$ astrocyte swelling, that VRAC plays no significant role in the volume change mechanisms of astrocytes exposed to fluctuating osmotic gradients (Figure 4).

To confirm that VRAC does not play a role in astrocyte swelling under hypoosmotic extracellular conditions, we performed the same 40% hypoosmotic ACSF experiment in *Aldh1l1-Cre^{ERT2};SWELL$^{fl/fl}$* brain slices (Figure 5). Given that VRAC is ablated from astrocytes in both the mGFAP and Aldh1l1 driven Cre lines, the swelling

profiles of control and knockout astrocytes from the *Aldh1l1-Cre^{ERT2};SWELL$^{fl/fl}$* line should be similar.

Indeed, control and VRAC knockout astrocytes swell to the same degree in hypoosmotic ACSF after five minutes (Figure 5A). Five-minute reperfusion of isoosmotic ACSF triggered volume reduction such that both control and knockout astrocyte somas recovered to baseline volume (Figure 5A). The volume changes of control and knockout astrocytes in the 1st and 2nd exposures to hypoosmotic ACSF are not statistically different, although the net percent increase in volume of astrocytes is slightly larger in the 2nd exposure compared to the 1st (Figure 5B). Consequently, the volume decreases of control and knockout astrocytes during exposure to isoosmotic ACSF are not significantly different. The 1st exposure to isoosmotic ACSF triggers ~10% decrease in volume of all astrocytes, while the 2nd reperfusion of isoosmotic ACSF forces a net volume reduction closer to 12% (Figure 5B). Collectively, this volume-change data from *Aldh1l1-Cre^{ERT2};SWELL$^{fl/fl}$* mice confirm our data from *mGFAP-Cre;SWELL$^{fl/fl}$* mice that indicate VRAC do not play a role in the mechanism of volume change in astrocytes exposed to changing osmotic gradients (Figures 4 and 5).

It is important to note that the magnitude of cell swelling is consistent between control and knockout astrocytes (of the same transgenic line) when exposed to hypoosmotic ACSF. However, there is a slight difference in the magnitude of astrocyte swelling in hypoosmotic ACSF across transgenic lines (*mGFAP-Cre;SWELL$^{fl/fl}$* versus *Aldh1l1-Cre^{ERT2};SWELL$^{fl/fl}$*). The most likely explanation for this involves (1) batch-to-batch variability in solution osmolarity and (2) long-term changes in the speed of solution

perfusion. Given that littermate control data were gathered in the same time period as knockout data, these internal controls are more reliable indicators of true differences between groups.

Past evidence suggests that VRAC may play a role in RVD of astrocytes in culture (Sánchez-Olea et al., 1993), but to-date there have not been any reports of a RVD occurring in brain slice. In our previous studies, we found no evidence of a RVD in *wild-type* hippocampal astrocytes when swelling was stimulated by either hypoosmotic or elevated $[K^+]_o$ conditions (Murphy et al., 2017; Walch et al., 2020). Here we report that in two models of astrocytic VRAC ablation, there was no evidence of astrocyte RVD occurring in either elevated $[K^+]$ or hypoosmotic ACSF (Figures 3, 4, 5). Similarly, volume change of astrocytes in differing levels of $[K^+]_o$ or extracellular osmolarity were also not affected by the ablation of VRAC (Figures 3, 4, 5).

Astrocyte-specific ablation of VRAC has no effect on 4-aminopyridine-evoked epileptiform activity in *Aldh1l1-Cre^{ERT2};SWELL$^{fl/fl}$* mice

Epileptiform activity can be reliably evoked in hippocampal slice neurons with exposure to submillimolar concentrations of 4-aminopyridine (4-AP), an antagonist of voltage-gated potassium channels (Perreault and Avoli, 1989; Gonzalez-Sulser et al., 2012). Although concentrations as low as 50 μM 4-AP have been known to induce epileptiform activity, we purposely employed higher concentrations in these studies (up to 500 μM) to

evoke substantial seizure-like events in VRAC conditional-knockout and littermate control brain slices. This experimental strategy did not pan out as hoped, because in our hands 4-AP did not evoke large epileptiform events in a dose-dependent manner. There is some evidence of this in hippocampal slice literature, where 4-AP concentration has been nonlinearly plotted against both the slope of field excitatory post synaptic potentials (Gu, Ge and Ruan, 2004) and the frequency of epileptiform bursting (Myers et al., 2018).

Adult *Aldh1l1-Cre^{ERT2};SWELL$^{fl/fl}$* hippocampal slices were exposed to 200 μM 4-AP during a 55-min recording of a single CA1 pyramidal neuron (Figure 6A). The first 10-min exposure to 4-AP acted as a priming step for the generation of epileptiform activity, prior to the onset of a longer 30-min exposure to the drug. Often-times during intermittent wash periods in control ACSF, epileptiform events were occurring, even in the absence of direct 4-AP perfusion (Figure 6A). This washout phenomenon has been discussed in the literature (Salah and Perkins, 2011). In addition to their massive amplitudes and long durations, these large epileptiform events bear substantial resemblance to the "giant depolarizing potentials" recorded from CA3 pyramidal neurons exposed to 100 μM 4-AP (Luhmann, Dzhala and Ben-Ari, 2000). Furthermore, epileptic activity in the form of ictal discharges and interictal events have been thoroughly characterized in CA1 neurons exposed to 4-AP (Avoli et al., 2013). These studies suggest that the "large epileptiform events" we observe in whole-cell voltage-clamp recordings could be described as seizure-like activity.

When quantified, the severity of 200 μM 4-AP-evoked epileptiform activity in *Aldh1l1-Cre$^{ERT2(+/-)}$;SWELL$^{fl/fl}$* slices was not significantly different from littermate

controls (Figure 7). On average, neurons from control littermate and VRAC knockout slices generated approximately the same number of large epileptic events (~2) during the 55-min recording period (Figure 7A), which resulted in a frequency of ~0.036 large epileptiform events per minute (Figure 7B). On average, the combined duration of these epileptiform events lasted almost 3 minutes per recording in both knockout and control slices (Figure 7C). When total epileptiform duration was summed across cells (n=8 per group), the littermate control slices endured over 22 minutes of epileptiform activity in comparison to VRAC knockout slices, which collectively lasted for ~15 minutes (Figure 7D). With the exception of total epileptiform duration data across cells, VRAC knockout slices experienced similar levels of seizure-like activity in comparison to littermate controls. This suggests that glutamate released from astrocytic VRAC does not majorly enhance epileptiform activity of hippocampal neurons.

Aldh1l1-Cre^{ERT2};SWELL$^{fl/fl}$ slices were subjected to a higher concentration of 4-AP (500 μM) in order to increase epileptiform activity. Neuron recordings from littermate control and VRAC knockout slices displayed similar levels of epileptiform activity (Figure 8A). At higher resolution, individual epileptiform events looked similar in both control and knockout slices (Figure 8B). Indeed when quantified, control and knockout slices exposed to 500 μM 4-AP experienced the same average number of epileptiform events (~1.8, Figure 9A) and approximate frequencies (~0.03 events per minute, Figure 9B). The average total epileptiform duration per cell was the same in both control and knockout slices (~2.8 min, Figure 9C), and the total epileptiform duration summed across all cells (n=7 per group) was highly similar (~18.5 min, Figure 9D).

Collectively, 4-AP-evoked epileptiform activity was not significantly different in control or knockout slices from *Aldh1l1-Cre^{ERT2};SWELL$^{fl/fl}$* mice, which was demonstrated at two different concentrations of 4-AP (200 μM, 500 μM). This is interesting, considering that recent studies have touted the importance of astrocytic VRAC in mediating the severity of stroke infarct volume in *mGFAP-Cre;LRRC8A$^{fl/fl}$* transgenic mice (Yang et al., 2019). Given the lack of cell-type specific VRAC knockout in our adult *mGFAP-Cre;SWELL$^{fl/fl}$* animals, it is possible that neuronal VRAC are also releasing glutamate under excitotoxic conditions like seizure or stroke.

CNS-wide ablation of VRAC significantly reduces 4-AP-evoked epileptiform activity in *Nestin-Cre;SWELL$^{fl/fl}$* mice

VRAC ablation in our *Nestin-Cre$^{(+/-)}$;SWELL$^{fl/fl}$* animals should be broad (affecting neurons and glia) according to the literature (Zimmerman et al., 1994; Tronche et al., 1999). Our IHC images from *Nestin-Cre$^{(+/-)}$;Rosa26$^{lsl\text{-}tdTomato}$* slices confirm this recombination pattern in hippocampal tissue (Figure 2B). Interestingly, neurons from *Nestin-Cre$^{(+/-)}$;SWELL$^{fl/fl}$* slices displayed increased sensitivity to 500 μM 4-AP in comparison to littermate controls (Figure 10). Upon inspection, large epileptiform events in VRAC knockout slices (Figure 10A) looked like those in control slices (Figure 10A), with extremely large amplitudes and durations usually over a minute long. However, it was immediately evident that neurons from knockout slices were experiencing a larger number of epileptiform events in comparison to controls (Figure 10A). Analysis exposed

a significant difference in the average number of large epileptiform events occurring in 4-AP, between control (~2.8 events) and VRAC knockout (~1 event) slices ($p<.01$; Figure 11A). This translated into a trend of increased event frequencies in control slices (~0.04 large epileptiform events per minute) compared to knockout tissue (~0.015 events per minute) (Figure 11B). Furthermore, the average total epileptiform duration in control slices was ~2.75 minutes, which was significantly greater than the ~1.5 minute duration in knockout slices ($p<.05$; Figure 11C). When the total epileptiform duration was summed across cells (n=8 per group), littermate control slices had collectively endured over 15 minutes of epileptiform activity, in contrast to the much quieter VRAC knockout slices with less than 10 minutes of these seizure-like events (Figure 11D). These data impart evidence that broad CNS VRAC ablation significantly decreased the amount of 4-AP-evoked epileptiform activity in *Nestin-Cre$^{(+/-)}$;SWELL$^{fl/fl}$* slices in comparison to littermate controls. Revisiting 4-AP exposure data from *Aldh1l1-Cre^{ERT2};SWELL$^{fl/fl}$* slices, it is interesting that astrocytic VRAC ablation did not significantly reduce the level of epileptiform activity in knockout slices compared to littermate controls. Although astrocytic VRAC are thought to be a major contributor of swelling-induced glutamate release, it seems that VRAC in other cells of the CNS (ex. neurons or microglia) also play a role in the generation of epileptiform activity.

Discussion

In this study, we generated three Cre-recombinase driven knockout lines of VRAC. The constitutive *mGFAP-Cre;SWELL$^{fl/fl}$* line drives broad ablation of VRAC in hippocampus in an age-specific manner, while inducible *Aldh1l1-Cre^{ERT2};SWELL$^{fl/fl}$* line allows for temporal control of astrocyte-specific ablation of VRAC. In contrast, the constitutive *Nestin-Cre;SWELL$^{fl/fl}$* line drives recombination in most neurons and glial cells of the CNS. We used the mGFAP- and Aldh1l1- Cre-driven knockout mice to test the role of VRAC in astrocyte volume change using two different swelling models (elevated $[K^+]_o$ and hypoosmotic ACSF). In *mGFAP-Cre;SWELL$^{fl/fl}$* mice, ablation of VRAC did not change the swelling profiles of astrocytes exposed to elevated $[K^+]_o$ ACSF in comparison to littermate controls. Furthermore, the use of 40% hypoosmotic ACSF in *mGFAP-Cre;SWELL$^{fl/fl}$* and *Aldh1l1-Cre^{ERT2};SWELL$^{fl/fl}$* mice did not alter astrocyte swelling profiles in comparison to controls. These data suggest that VRAC does not play a role in astrocyte volume change triggered by two different swelling models.

The lack of astrocyte RVD seen in both control and VRAC cKO tissue aligns with previous observations from our lab regarding astrocyte volume change in acute brain slices (Murphy et al., 2017; Walch et al., 2020). In comparison to the readily seen RVD mechanism in cultured astrocytes (Sánchez-Olea et al., 1993), the occurrence of RVD in intact brain tissue is likely a complex phenomenon, if it occurs at all. While cultured astrocytes lie adjacent to other cells and the extracellular space, astrocytes in slices are making physical connections between other cell types and the vasculature. When

movement of water is not restricted to merely the intra- and extra-cellular compartments of tissue, there may not be a necessity for a process like RVD, especially in astrocytes. In culture, astrocytic VRAC are known to be triggered by hypoosmotic conditions and release osmolytes into the extracellular space to trigger an outward osmotic gradient and subsequent volume decrease (Formaggio et al., 2019). In intact tissue, water movement intro astrocyte soma or processes can be redirected towards the astrocytic endfeet and released via AQP4 channels into blood vessels.

Another factor to consider when discussing the phenomenon of RVD is the timescale at which RVD changes have been shown to occur. In our astrocyte swelling experiments, we see rapid volume changes within a minute after perfusion of hypoosmotic or ^$[K^+]_o$ ACSF (Murphy et al., 2017; Walch et al., 2020). In contrast, in one of the rare observations of RVD in hippocampal slices, tissue swelling occurred over the span of 15-20 min of exposure to hypoosmotic ACSF, and the actual mechanism of RVD was not witnessed until at least 60 min of exposure (Kreisman and Olson, 2003). RVD may be mediated by multiple factors, including the severity of the osmotic gradient imposed upon intact tissue and the perfusion rate at which it replaces isoosmolar ACSF. Interestingly, in work from two studies where RVD was witnessed in hippocampal slices, experimental conditions were such that the osmolarity of perfused ACSF was gradually reduced over long timescales (Quesada et al., 2000; Franco, Quesada and Pasantes-Morales, 2000). Such data suggests that astrocyte RVD could occur in our experiments if these parameters were appropriately adjusted. Finally, much of the evidence for RVD in hippocampal slices comes in the form of intrinsic optical signal (IOS) data, which is a

technique that relies on endogenous changes in tissue light transmittance (Andrew, Jarvis and Obeidat, 1999). In some studies, IOS signals are said to correspond to tissue swelling (MacVicar and Hochman, 1991; Holthoff and Witte, 1996), while in others they vary according to neuron excitability (Syková et al., 2003). Thus, the origins of IOS make any tissue light transmittance data difficult to analyze and compare across studies. Collectively, work on RVD has occurred under a myriad of experimental conditions that increase or decrease the likelihood of observing the phenomenon. Therefore, before altering these conditions in subsequent experiments with VRAC cKO slices, we cannot definitively say whether VRAC plays a role in the mechanism of RVD.

Regardless of whether RVD is truly VRAC-dependent, the glutamate being released by VRAC may contribute to changes in tissue excitability. There is much work to be done to understand the role VRAC-released glutamate could play under physiological swelling conditions, or pathologic conditions such as epilepsy. To test the role of VRAC in epilepsy, we used the pharmacological blocker 4-AP to induce seizure-like activity in hippocampal slices. 4-AP is thought to exert pro-convulsant effects in brain and muscle tissue through the inhibition of voltage-gated K^+ channels on neurons to prolong action potentials (Yeh et al., 1976; Kirsch et al., 1993). When we exposed *Aldh1l1-Cre*^{ERT2}*;SWELL*$^{fl/fl}$ slices to the drug 4-AP at two concentrations (200, 500 μM), epileptiform activity was seen in both knockout and control slices, without a significant difference in severity.

Interestingly, 4-AP application to *Nestin-Cre;SWELL*$^{fl/fl}$ slices triggered more severe epileptiform activity in the control tissue, suggesting that more widespread VRAC ablation may be necessary to measure an effect on brain tissue excitability. The data also suggest that neuronal VRAC play an important role in the regulation of neuronal excitability. Data to support this hypothesis is lacking in comparison to astrocytic VRAC, which has already been shown to mediate the severity of cerebral ischemia in VRAC cKO mice (Yang et al., 2019). Astrocytes upregulate uptake of glutamate in response to rising $[glutamate]_o$ (Duan et al., 1999). Accumulated glutamate could then be released via VRAC when astrocytes swell in response to high levels of potassium generated by neuronal activity (Walch et al., 2020). This is assuming that VRAC's swelling-induced glutamate release is the mechanism by which VRAC predispose the tissue to epileptiform activity. Since 4-AP is not a commonly used model of tissue swelling, it is inappropriate to assume how VRAC are contributing to epileptiform activity. It will be important to gather electrophysiological data from Aldh1l1- and NEX- Cre-driven VRAC knockouts using common models of tissue swelling. For example, if there is a decrease in slow inward current (SIC) activity in *Aldh1l1-Cre*$^{ERT2(+/-)}$*;SWELL*$^{fl/fl}$ slices compared to controls, it would indicate that astrocytic VRAC are playing a role in swelling-induced glutamate release. Similarly, if SIC activity is decreased in *NEX-Cre*$^{(+/-)}$*;SWELL*$^{fl/fl}$ slices in comparison to controls, neuronal VRAC may also play an important role in swelling-induced excitability. Given that VRAC ablation is not neuron-specific in *Nestin-Cre;SWELL*$^{fl/fl}$ slices, we cannot comfortably attribute reduced epileptiform activity to neuronal VRAC ablation. Nestin is an intermediate filament expressed in neuroepithelial

stem cells, which are known give rise to neurons and glia in the mature brain (Zimmerman et al., 1994). It has been readily used to target CNS-wide genetic alterations (Tronche et al., 1999), however newer embryonic studies of Nestin-Cre reporter mice indicate recombination reaches beyond the neuroectoderm to somite-derived tissues and the kidneys (Dubois et al., 2006). Thus, the early mortality phenotype seen in our *Nestin-Cre;SWELL*$^{fl/fl}$ mice could be due to VRAC ablation effects in other tissues beyond the CNS.

Finally, there is also some evidence for the involvement of other channels in swelling-induced glutamate release. A study in culture used inhibitors known to affect gap junctions, and saw inhibition of glutamate efflux (Ye et al., 2003). However, due to the nonspecificity of inhibitors (such as carbenoxolone and 18-α-glycyrrhetinic acid), the individual contributions of pannexin and connexin hemichannels could not be concluded, nor the exclusion of VRAC. More importantly, there is newer literature suggesting that agents such as DCPIB, known to block VRAC, can also inhibit glutamate release from connexin hemichannels *in vitro* (Bowens et al., 2013). By merging transgenic and pharmacological approaches in the future, we will be able to differentiate the role of VRAC from other suspected glutamate release pathways activated during tissue swelling. For instance, the drug bafilomycin (an inhibitor of vacuolar-type H^+ -ATPase) prevents loading of neurotransmitter into vesicles. Once incubated with this, neurons in acute slices are not able to release pre-synaptic glutamate even in the presence of stimulation. Using bafilomycin in VRAC cKO slices and exposing them to hypoosmolar ACSF, the contributions of synaptic glutamate will be eliminated, as well as any VRAC-released

glutamate. Any activity that remains must then be the result of glutamate released from another source.

Conclusions

Our experiments indicate that widespread VRAC ablation reduces 4-AP-evoked epileptiform activity. Further experiments in *NEX-Cre$^{(+/-)}$;SWELL$^{fl/fl}$* mice are necessary to tease apart the cell type-specific VRAC contributions, but data thus far suggest that astrocytic VRAC may not be playing as significant a role as previously hypothesized. Regardless, VRAC ablation did correlate with a reduction in epileptiform activity in our *Nestin-Cre$^{(+/-)}$;SWELL$^{fl/fl}$* slices and other labs have shown that *mGFAP-Cre;SWELL$^{fl/fl}$* mice are partially neuroprotected in the MCAo model of stroke (Yang et al., 2019). The role of VRAC in pathology versus physiology may differ. Our experimental mice were not subjected to pro-convulsant drugs prior to being sacrificed, which may substantially alter the role that VRAC plays in naïve tissue in comparison to epilepsy or stroke. It is of interest to us and our collaborators that these VRAC cKO mice be challenged by disease models prior to the onset of slice experiments. Furthermore, it will be important to track the expression-level of VRAC in naïve vs pathological tissues.

The immediate next steps in this project involve the *NEX-Cre$^{(+/-)}$;SWELL$^{fl/fl}$* and *Aldh1l1-Cre^{ERT2};SWELL$^{fl/fl}$* mouse lines, which provide targeted ablation of VRAC in neurons and astrocytes. We will expose 4-AP to slices from *NEX-Cre$^{(+/-)}$;SWELL$^{fl/fl}$* mice

and observe whether neuronal VRAC are playing a key role in the development of epileptiform activity. Additionally, we will expose *Aldh1l1-Cre^{ERT2};SWELL$^{fl/fl}$* brain slices to hypoosmotic and elevated $[K^+]_o$ ACSF and record neuronal activity, to clarify whether VRAC-released glutamate is a major mechanism by which astrocytes contribute to swelling-induced changes in excitability.

References

Abdullaev IF, Rudkouskaya A, Schools GP, Kimelberg HK, Mongin AA (2006) Pharmacological comparison of swelling-activated excitatory amino acid release and Cl- currents in cultured rat astrocytes. J Physiol 572:677-689.

Alibrahim A, Zhao LY, Bae CY, Barszczyk A, Sun CL, Wang GL, Sun HS (2013) Neuroprotective effects of volume-regulated anion channel blocker DCPIB on neonatal hypoxic-ischemic injury. Acta Pharmacol Sin 34:113-118.

Andrew RD, Jarvis CR, Obeidat AS (1999) Potential sources of intrinsic optical signals imaged in live brain slices. Methods 18:185-196, 179.

Avoli M, Panuccio G, Herrington R, D'Antuono M, de Guzman P, Lévesque M (2013) Two different interictal spike patterns anticipate ictal activity in vitro. Neurobiol Dis 52:168-176.

Basarsky TA, Feighan D, MacVicar BA (1999) Glutamate release through volume-activated channels during spreading depression. J Neurosci 19:6439-6445.

Bowens NH, Dohare P, Kuo YH, Mongin AA (2013) DCPIB, the proposed selective blocker of volume-regulated anion channels, inhibits several glutamate transport pathways in glial cells. Mol Pharmacol 83:22-32.

Duan S, Anderson CM, Stein BA, Swanson RA (1999) Glutamate induces rapid upregulation of astrocyte glutamate transport and cell-surface expression of GLAST. J Neurosci 19:10193-10200.

Dubois NC, Hofmann D, Kaloulis K, Bishop JM, Trumpp A (2006) Nestin-Cre transgenic mouse line Nes-Cre1 mediates highly efficient Cre/loxP mediated recombination in the nervous system, kidney, and somite-derived tissues. Genesis 44:355-360.

Dörrbaum AR, Kochen L, Langer JD, Schuman EM (2018) Local and global influences on protein turnover in neurons and glia. Elife 7.

Formaggio F, Saracino E, Mola M, Rao S, Amiry-Moghaddam M, Muccini M, Zamboni R, Nicchia G, Caprini M, Benfenati V (2019) LRRC8A is essential for swelling-activated chloride current and for regulatory volume decrease in astrocytes. Faseb Journal 33:101-113.

Franco R, Quesada O, Pasantes-Morales H (2000) Efflux of osmolyte amino acids during isovolumic regulation in hippocampal slices. J Neurosci Res 61:701-711.

Gage GJ, Kipke DR, Shain W (2012) Whole animal perfusion fixation for rodents. J Vis Exp.

Gonzalez-Sulser A, Wang J, Queenan BN, Avoli M, Vicini S, Dzakpasu R (2012) Hippocampal neuron firing and local field potentials in the in vitro 4-aminopyridine epilepsy model. J Neurophysiol 108:2568-2580.

Gu Y, Ge SY, Ruan DY (2004) Effect of 4-aminopyridine on synaptic transmission in rat hippocampal slices. Brain Res 1006:225-232.

Holthoff K, Witte OW (1996) Intrinsic optical signals in rat neocortical slices measured with near-infrared dark-field microscopy reveal changes in extracellular space. J Neurosci 16:2740-2749.

Kimelberg HK, Rutledge E, Goderie S, Charniga C (1995) Astrocytic swelling due to hypotonic or high K+ medium causes inhibition of glutamate and aspartate uptake and increases their release. J Cereb Blood Flow Metab 15:409-416.

Kirsch GE, Shieh CC, Drewe JA, Vener DF, Brown AM (1993) Segmental exchanges define 4-aminopyridine binding and the inner mouth of K+ pores. Neuron 11:503-512.

Kreisman NR, Olson JE (2003) Taurine enhances volume regulation in hippocampal slices swollen osmotically. Neuroscience 120:635-642.

Larsen BR, MacAulay N (2017) Activity-dependent astrocyte swelling is mediated by pH-regulating mechanisms. Glia 65:1668-1681.

Larsen BR, Assentoft M, Cotrina ML, Hua SZ, Nedergaard M, Kaila K, Voipio J, MacAulay N (2014) Contributions of the Na^+/K^+-ATPase, NKCC1, and Kir4.1 to hippocampal K^+ clearance and volume responses. Glia 62:608-622.

Lauderdale K, Murphy T, Tung T, Davila D, Binder DK, Fiacco TA (2015) Osmotic Edema Rapidly Increases Neuronal Excitability Through Activation of NMDA Receptor-Dependent Slow Inward Currents in Juvenile and Adult Hippocampus. ASN Neuro 7.

Liu SJ, Zheng P, Wright DK, Dezsi G, Braine E, Nguyen T, Corcoran NM, Johnston LA, Hovens CM, Mayo JN, Hudson M, Shultz SR, Jones NC, O'Brien TJ (2016) Sodium selenate retards epileptogenesis in acquired epilepsy models reversing changes in protein phosphatase 2A and hyperphosphorylated tau. Brain 139:1919-1938.

Lu X, Roberts E, Xia F, Sanchez-Alavez M, Liu T, Baldwin R, Wu S, Chang J, Wasterlain CG, Bartfai T (2010) GalR2-positive allosteric modulator exhibits anticonvulsant effects in animal models. Proc Natl Acad Sci U S A 107:15229-15234.

Luhmann HJ, Dzhala VI, Ben-Ari Y (2000) Generation and propagation of 4-AP-induced epileptiform activity in neonatal intact limbic structures in vitro. Eur J Neurosci 12:2757-2768.

MacVicar BA, Hochman D (1991) Imaging of synaptically evoked intrinsic optical signals in hippocampal slices. J Neurosci 11:1458-1469.

Murphy TR, Davila D, Cuvelier N, Young LR, Lauderdale K, Binder DK, Fiacco TA (2017) Hippocampal and Cortical Pyramidal Neurons Swell in Parallel with Astrocytes during Acute Hypoosmolar Stress. Front Cell Neurosci 11:275.

Myers TL, Gonzalez OC, Stein JB, Bazhenov M (2018) Characterizing Concentration-Dependent Neural Dynamics of 4-Aminopyridine-Induced Epileptiform Activity. Epilepsy J 4.

Okada Y, Maeno E, Shimizu T, Dezaki K, Wang J, Morishima S (2001) Receptor-mediated control of regulatory volume decrease (RVD) and apoptotic volume decrease (AVD). J Physiol 532:3-16.

Pasantes-Morales H, Murray RA, Lilja L, Morán J (1994) Regulatory volume decrease in cultured astrocytes. I. Potassium- and chloride-activated permeability. Am J Physiol 266:C165-171.

Perreault P, Avoli M (1989) Effects of low concentrations of 4-aminopyridine on CA1 pyramidal cells of the hippocampus. J Neurophysiol 61:953-970.

Phillis JW, Song D, O'Regan MH (1998) Tamoxifen, a chloride channel blocker, reduces glutamate and aspartate release from the ischemic cerebral cortex. Brain Res 780:352-355.

Polleux F, Ghosh A (2002) The slice overlay assay: a versatile tool to study the influence of extracellular signals on neuronal development. Sci STKE 2002:pl9.

Price JC, Guan S, Burlingame A, Prusiner SB, Ghaemmaghami S (2010) Analysis of proteome dynamics in the mouse brain. Proc Natl Acad Sci U S A 107:14508-14513.

Qiu Z, Dubin AE, Mathur J, Tu B, Reddy K, Miraglia LJ, Reinhardt J, Orth AP, Patapoutian A (2014) SWELL1, a plasma membrane protein, is an essential component of volume-regulated anion channel. Cell 157:447-458.

Quesada O, Franco R, Hernández-Fonseca K, Tuz K (2000) Isovolumic regulation in nervous tissue: a novel mechanism of cell volume regulation. Adv Exp Med Biol 483:219-225.

Risher WC, Andrew RD, Kirov SA (2009) Real-time passive volume responses of astrocytes to acute osmotic and ischemic stress in cortical slices and in vivo revealed by two-photon microscopy. Glia 57:207-221.

Rutledge EM, Kimelberg HK (1996) Release of [3H]-D-aspartate from primary astrocyte cultures in response to raised external potassium. J Neurosci 16:7803-7811.

Salah A, Perkins KL (2011) Persistent ictal-like activity in rat entorhinal/perirhinal cortex following washout of 4-aminopyridine. Epilepsy Res 94:163-176.

Su G, Kintner DB, Sun DD (2002) Contribution of Na+-K+-Cl- cotransporter to high- K+ (o)-induced swelling and EAA release in astrocytes. American Journal of Physiology-Cell Physiology 282:C1136-C1146.

Syková E, Vargová L, Kubinová S, Jendelová P, Chvátal A (2003) The relationship between changes in intrinsic optical signals and cell swelling in rat spinal cord slices. Neuroimage 18:214-230.

Sánchez-Olea R, Peña C, Morán J, Pasantes-Morales H (1993) Inhibition of volume regulation and efflux of osmoregulatory amino acids by blockers of Cl- transport in cultured astrocytes. Neurosci Lett 156:141-144.

Tronche F, Kellendonk C, Kretz O, Gass P, Anlag K, Orban PC, Bock R, Klein R, Schütz G (1999) Disruption of the glucocorticoid receptor gene in the nervous system results in reduced anxiety. Nat Genet 23:99-103.

Voss FK, Ullrich F, Münch J, Lazarow K, Lutter D, Mah N, Andrade-Navarro MA, von Kries JP, Stauber T, Jentsch TJ (2014) Identification of LRRC8 heteromers as an essential component of the volume-regulated anion channel VRAC. Science 344:634-638.

Walch E, Murphy TR, Cuvelier N, Aldoghmi M, Morozova C, Donohue J, Young G, Samant A, Garcia S, Alvarez C, Bilas A, Davila D, Binder DK, Fiacco TA (2020) Astrocyte-Selective Volume Increase in Elevated Extracellular Potassium Conditions Is Mediated by the Na. ASN Neuro 12:1759091420967152.

Walz W, Hinks EC (1985) Carrier-mediated KCl accumulation accompanied by water movements is involved in the control of physiological K+ levels by astrocytes. Brain Res 343:44-51.

Yang J, Vitery M, Chen J, Osei-Owusu J, Chu J, Qiu Z (2019) Glutamate-Releasing SWELL1 Channel in Astrocytes Modulates Synaptic Transmission and Promotes Brain Damage in Stroke. Neuron 102:813-+.

Ye ZC, Wyeth MS, Baltan-Tekkok S, Ransom BR (2003) Functional hemichannels in astrocytes: a novel mechanism of glutamate release. J Neurosci 23:3588-3596.

Ye ZC, Oberheim N, Kettenmann H, Ransom BR (2009) Pharmacological "cross-inhibition" of connexin hemichannels and swelling activated anion channels. Glia 57:258-269.

Yeh JZ, Oxford GS, Wu CH, Narahashi T (1976) Interactions of aminopyridines with potassium channels of squid axon membranes. Biophys J 16:77-81.

Zhang Y, Zhang H, Feustel PJ, Kimelberg HK (2008) DCPIB, a specific inhibitor of volume regulated anion channels (VRACs), reduces infarct size in MCAo and the release of glutamate in the ischemic cortical penumbra. Exp Neurol 210:514-520.

Zimmerman L, Parr B, Lendahl U, Cunningham M, McKay R, Gavin B, Mann J, Vassileva G, McMahon A (1994) Independent regulatory elements in the nestin gene direct transgene expression to neural stem cells or muscle precursors. Neuron 12:11-24.

Figures

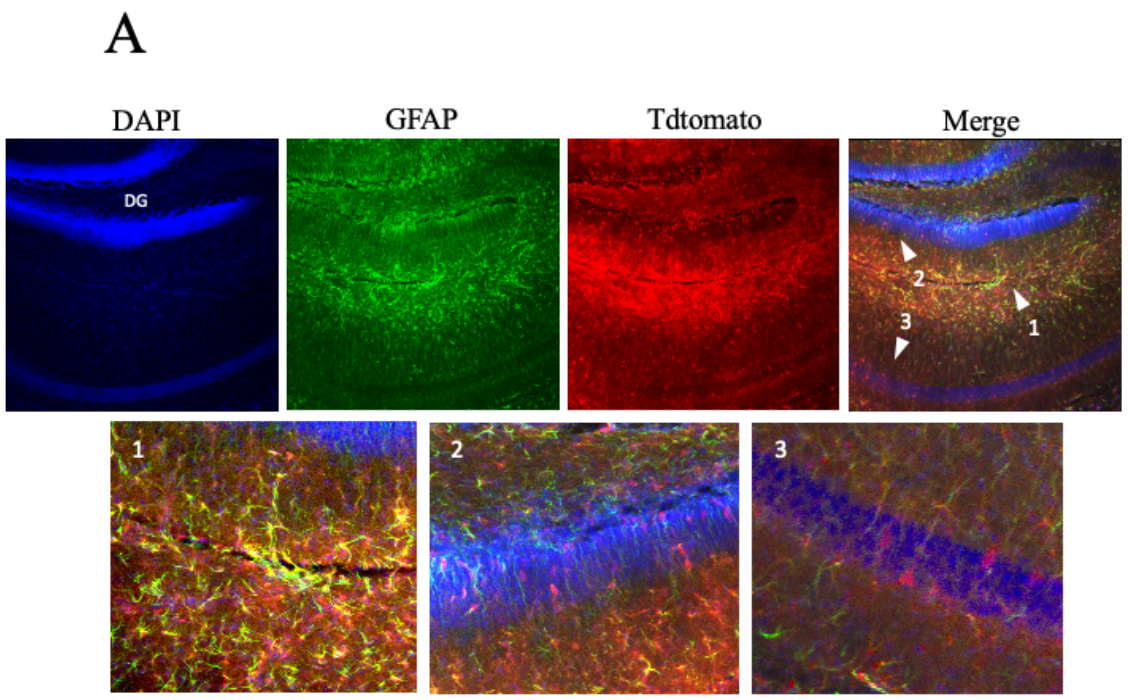
A
DAPI
GFAP
Tdtomato
Merge
DG
1
2
3
1
2
3

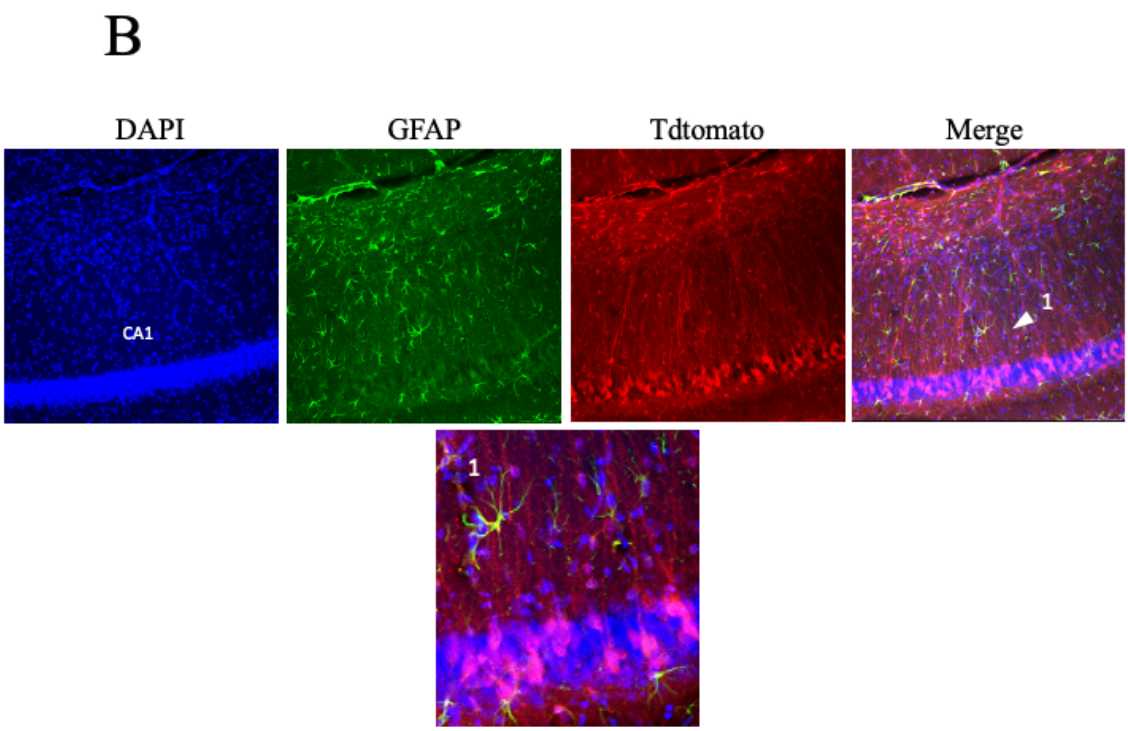
B
DAPI
GFAP
Tdtomato
Merge
CA1
1
1

Figure 4.1: mGFAP-Cre driven recombination in hippocampus is astrocyte-specific in juvenile, but not adult *mGFAP-Cre$^{(+/-)}$;Rosa26$^{lsl\text{-}tdTomato}$* mice. (A) In juvenile *mGFAP-Cre$^{(+/-)}$;Rosa26$^{lsl\text{-}tdTomato}$* hippocampus, DAPI-stained nuclei of dentate gyrus (DG) and CA1 pyramidal layer are apparent (blue), while GFAP-stained astrocytes (green) in stratum lacunosem moleculare co-localize well with Tdtomato signal (zoom image 1). Note the occasional Tdtomato^{+} neurons in DG (zoom image 2) and CA1 (zoom image 3) regions. **(B)** In contrast, adult *mGFAP-Cre$^{(+/-)}$;Rosa26$^{lsl\text{-}tdTomato}$* CA1 region reveals reduced colocalization of GFAP and Tdtomato signals, with most Tdtomato signal originating from the apical dendrites and soma of many CA1 pyramidal neurons (zoom image 1). Note a particularly large GFAP-stained astrocyte in stratum radiatum lacking colocalization with Tdtomato (zoom image 1). *mGFAP-Cre$^{(+/-)}$;Rosa26$^{lsl\text{-}tdTomato}$* images confirm astrocyte-specific recombination in juvenile hippocampus, with astrocyte and neuron inclusive recombination in adult hippocampus.

A

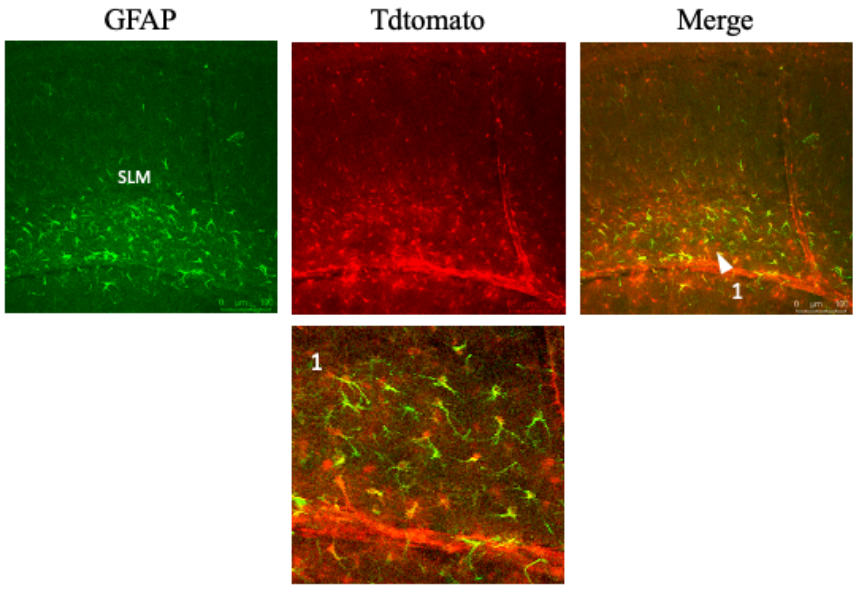
GFAP
Tdtomato
Merge
SLM
1
1

B

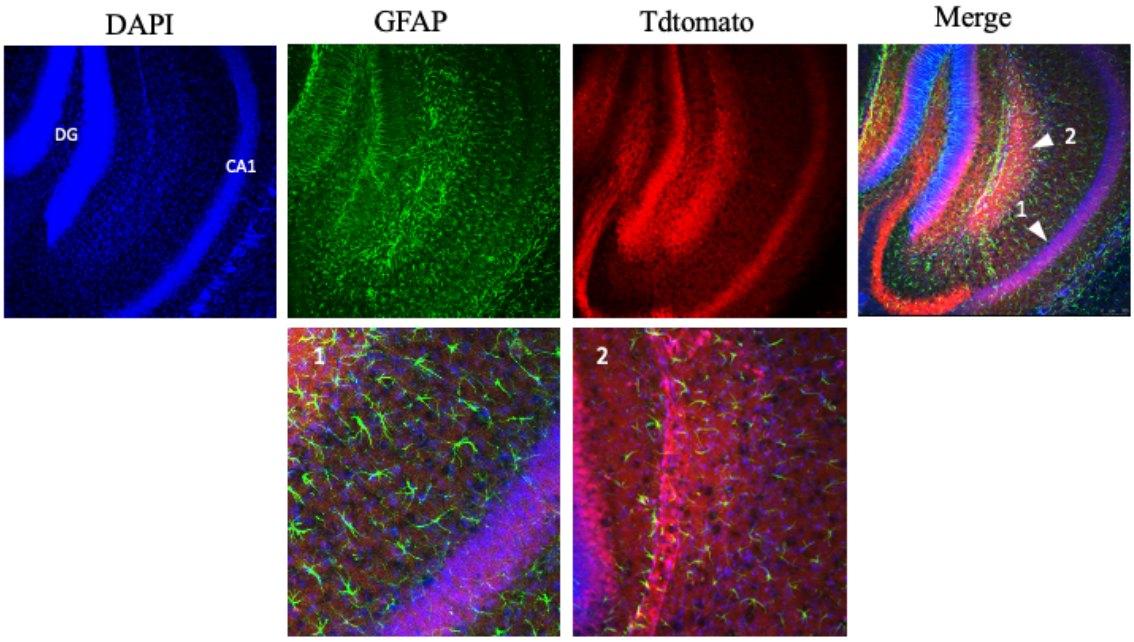
DAPI
GFAP
Tdtomato
Merge
DG
CA1
2
1
1
2

Figure 4.2: Aldh1l1-Cre^{ERT2} driven recombination in hippocampus is astrocyte-specific, while Nestin-Cre driven recombination affects most hippocampal neurons in Rosa26-lsl-TdTomato reporter mice. (A) Image of stratum lacunosum moleculare in *Aldh1l1-Cre$^{(+/-)}$; Rosa26$^{lsl\text{-}tdTomato}$* hippocampus denotes strong colocalization of GFAP-stained astrocytes and Tdtomato^{+} cells. Astrocytic processes are labeled only by GFAP (zoom image 1). Note the prominent blood vessel labeled by Tdtomato^{+} astrocytes. **(B)** Strong Tdtomato signal is evident in neurons of CA1 (zoom image 1), CA3 and dentate gyrus in *Nestin-Cre$^{(+/-)}$;Rosa26$^{lsl\text{-}tdTomato}$* hippocampus, while part of the neuropil near stratum lacunosum moleculare retains Tdtomato signal except for small unstained circles (zoom image 2) that might colocalize with cells not-descended from neural progenitors.

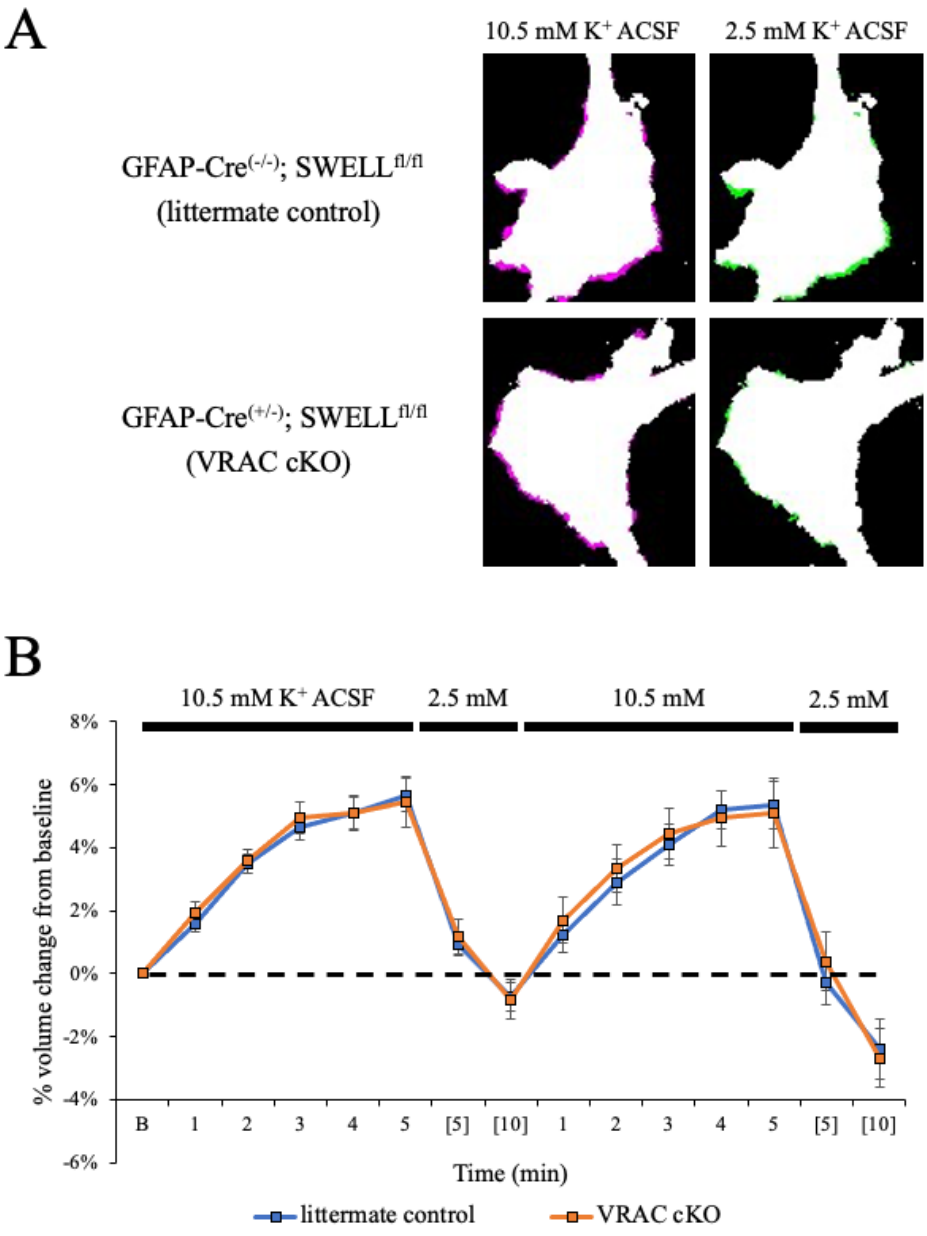
A
10.5 mM K+ ACSF
2.5 mM K+ ACSF
GFAP-Cre(-/-); SWELLfl/fl
(littermate control)
GFAP-Cre(+/-); SWELLfl/fl
(VRAC cKO)
B
10.5 mM K+ ACSF
2.5 mM
10.5 mM
2.5 mM
% volume change from baseline
8%
6%
4%
2%
0%
-2%
-4%
-6%
B
1
2
3
4
5
[5]
[10]
1
2
3
4
5
[5]
[10]
Time (min)
littermate control
VRAC cKO

Figure 4.3: $[K^+]_o$-driven astrocyte volume changes are not affected by the ablation of VRAC in *mGFAP-Cre;SWELL$^{fl/fl}$* mice. (A) Pseudocolor images of astrocytes show the soma at baseline volume (white), when swollen (magenta) or shrunk (green). In control ($Cre^{(-/-)}$, top left) and VRAC knockout ($Cre^{(+/-)}$, bottom left) representative astrocytes, soma area increases beyond baseline volume when exposed to 10.5 mM $[K^+]$ ACSF. Reperfusion of 2.5 mM $[K^+]$ ACSF triggers volume recovery in both control (top right) and knockout (bottom right) astrocytes to slightly less than their baseline volumes. **(B)** Quantification of average astrocyte volume change from baseline during every minute of a 5-min application of 10.5 mM $[K^+]$ ACSF, then volume change after five and ten minutes of exposure to 2.5 mM $[K^+]$ ACSF. A 2nd application cycle immediately follows the first. Astrocytes swell to a maximal volume ~6% above baseline and shrink to a minimum of ~2% below baseline. Note there is no significant difference in volume changes of either control (n=11) or VRAC knockout (n=11) astrocytes during the entire protocol. Only one astrocyte was imaged per brain slice.

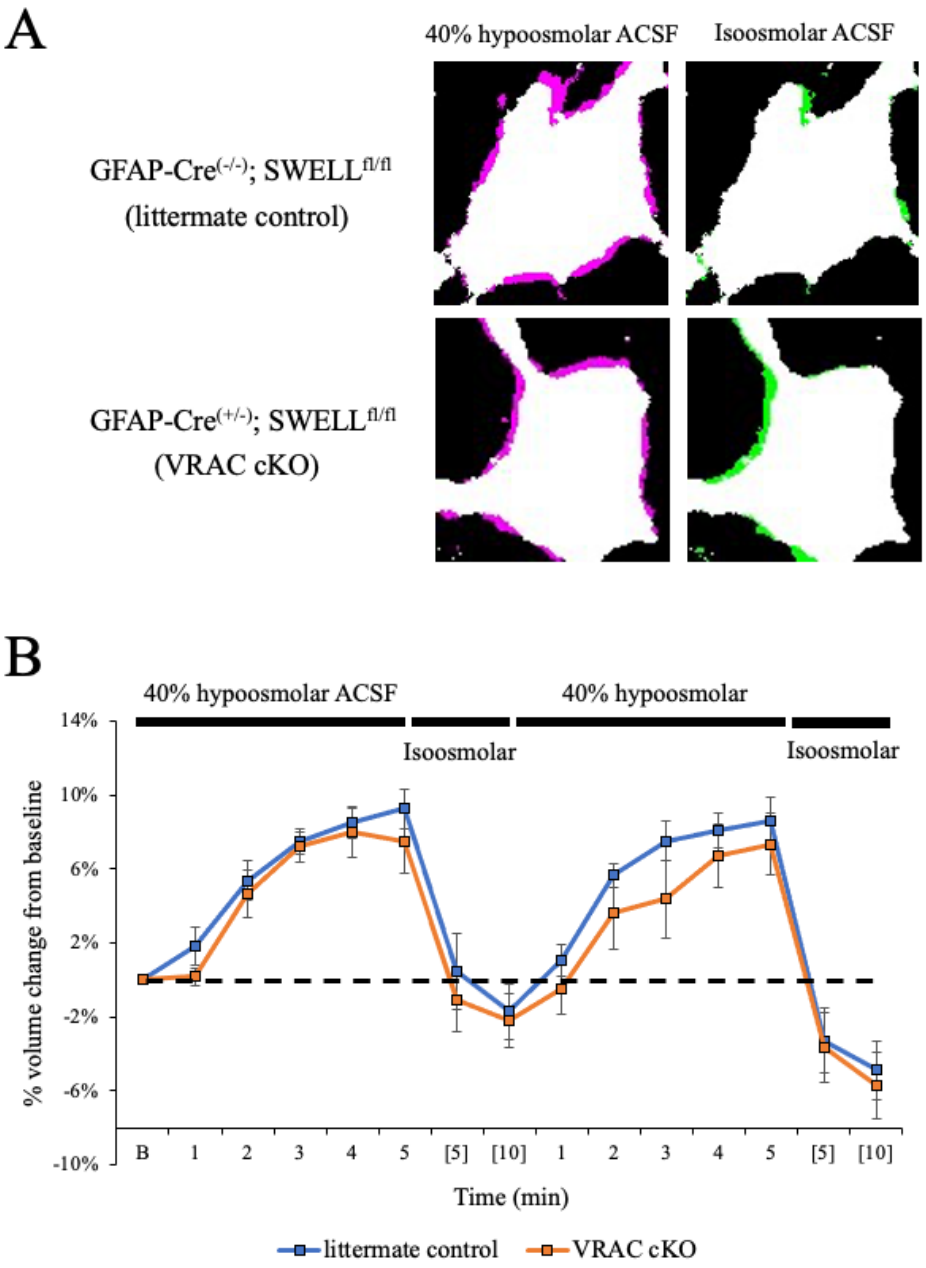
A
40% hypoosmolar ACSF
Isoosmolar ACSF
GFAP-Cre(-/-); SWELLfl/fl
(littermate control)
GFAP-Cre(+/-); SWELLfl/fl
(VRAC cKO)
B
40% hypoosmolar ACSF
40% hypoosmolar
Isoosmolar
Isoosmolar
14%
10%
6%
2%
-2%
-6%
-10%
% volume change from baseline
B
1
2
3
4
5
[5]
[10]
1
2
3
4
5
[5]
[10]
Time (min)
littermate control
VRAC cKO

Figure 4.4: Osmotic-driven astrocyte volume changes are not affected by the ablation of VRAC in *mGFAP-Cre;SWELL$^{fl/fl}$* mice. (A) Pseudocolor images show the soma at baseline volume (white), when swollen (magenta) or shrunk (green). In control (Cre$^{(-/-)}$, top left) and VRAC knockout (Cre$^{(+/-)}$, bottom left) representative astrocytes, soma area increases beyond baseline volume when exposed to 40% hypoosmolar ACSF. Reperfusion of isoosmolar ACSF (~300 mOsmo) triggers volume recovery in both control (top right) and knockout (bottom right) astrocytes to slightly less than their baseline volumes. **(B)** Quantification of average astrocyte volume change from baseline during every minute of a 5-min application of hypoosmotic ACSF, then volume changes after five and ten minutes of exposure to isoosmotic ACSF. After the 1st 5-min exposure to hypoosmotic ACSF, both groups of astrocytes swell to ~8% above their baseline volume and shrink by ~9% after 10 min of perfusion in isoosmotic ACSF. A 2nd application cycle immediately follows the first, with a minimal amount of variability occurring between control and knockout astrocyte volume at minutes 2 and 3 of hypoosmotic ACSF exposure. The final reperfusion of isoosmotic ACSF triggers more intense shrinkage of astrocytes, which rest at ~5% below their original baseline volume after 10 min. Note in this preliminary dataset, there is a trend towards no difference in volume change of control (n=7) or knockout (n=5) astrocytes during exposure to hypoosmotic or isoosmotic ACSF. Only one astrocyte was imaged per brain slice.

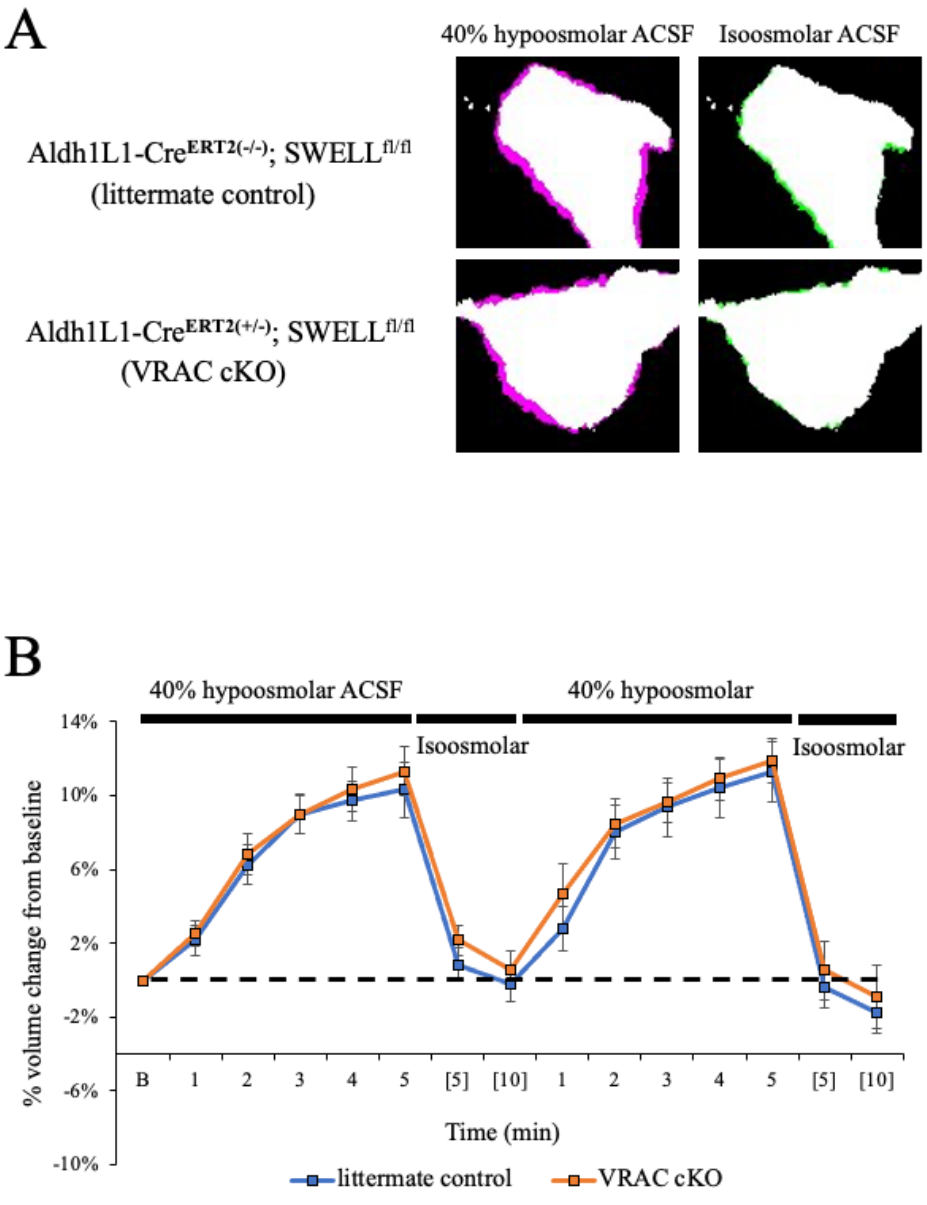
A
40% hypoosmolar ACSF
Isoosmolar ACSF
Aldh1L1-Cre^ERT2(-/-); SWELL^fl/fl
(littermate control)
Aldh1L1-Cre^ERT2(+/-); SWELL^fl/fl
(VRAC cKO)
B
40% hypoosmolar ACSF
40% hypoosmolar
Isoosmolar
Isoosmolar
% volume change from baseline
14%
10%
6%
2%
-2%
-6%
-10%
B
1
2
3
4
5
[5]
[10]
1
2
3
4
5
[5]
[10]
Time (min)
littermate control
VRAC cKO

Figure 4.5: Osmotic-driven astrocyte volume changes are not affected by the ablation of VRAC in *Aldh1l1-Cre^{ERT2};SWELL$^{fl/fl}$* mice. (A) Pseudocolor images of SR-101 labeled astrocytes from *Aldh1l1-Cre^{ERT2};SWELL$^{fl/fl}$* mice showcase swelling (magenta) and shrinkage (green) of astrocytic soma. Representative astrocytes from control (Cre$^{(-/-)}$, top left) and VRAC knockout (Cre$^{(+/-)}$, bottom left) brain slices show little visual variation in their degree of soma area increase in 40% hypoosmotic ACSF after 5 min of exposure. After 5 min of reperfusion in isoosmotic ACSF, both control (top right) and knockout (bottom right) astrocytes shrink back to their approximate baseline soma area. **(B)** Quantitative analysis of this imaging data reveals no significant differences in the volume changes of control (n=11) or knockout (n=9) astrocytes during exposure to hypoosmotic or isoosmotic ACSF. Astrocytes of both groups swell to ~10% greater than their baseline volumes after 5 minutes of hypoosmotic ACSF exposure. The 1st reperfusion of isoosmotic ACSF brings the volume of astrocytes back to their approximate baseline volume after 10 min of exposure. In the 2nd application of hypoosmotic ACSF, astrocytes of both groups swell closer to 11% beyond their baseline volumes, while the last reperfusion of isoosmotic ACSF triggers volume reduction of astrocytes to ~99% of their baseline volume. Only one astrocyte was imaged per brain slice.

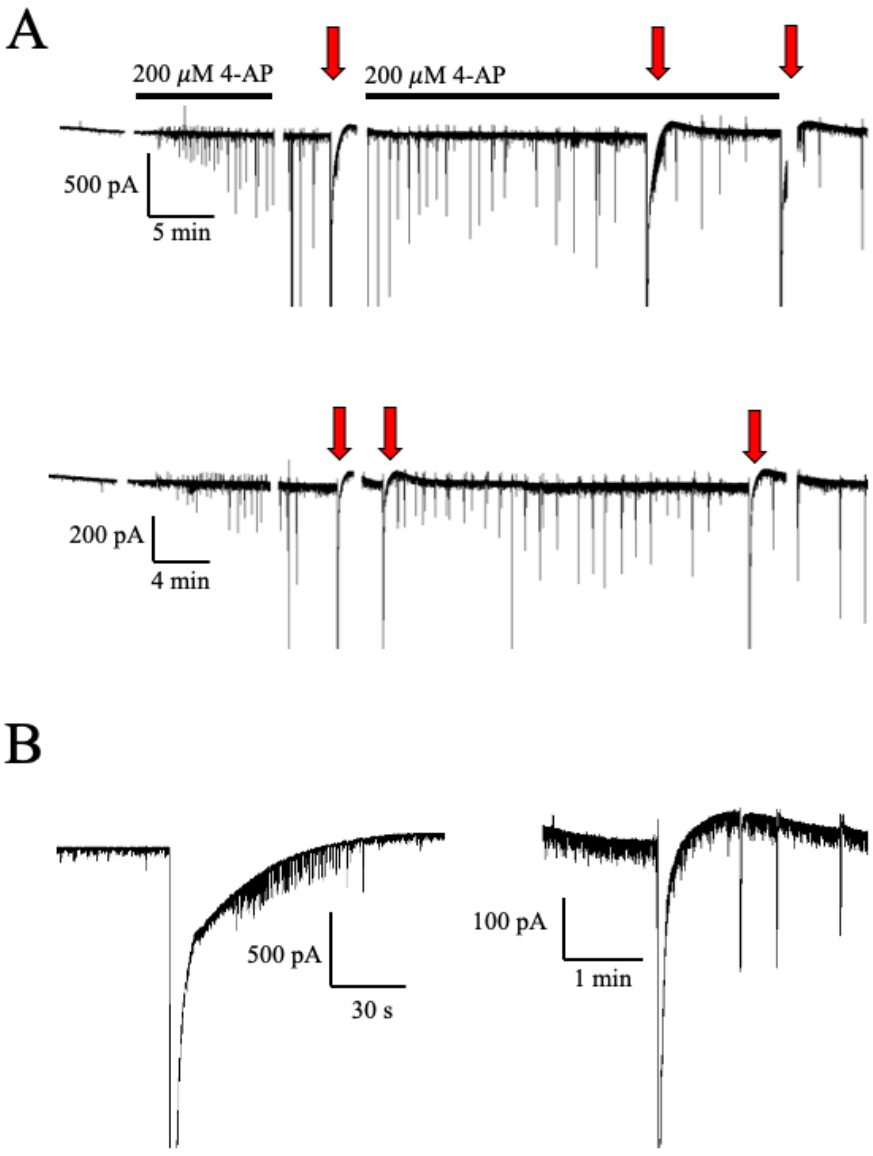
A
200 μM 4-AP
200 μM 4-AP
500 pA
5 min
200 pA
4 min
B
500 pA
30 s
100 pA
1 min

Figure 4.6: Representative epileptiform activity in *Aldh1l1-Cre^{ERT2};SWELL$^{fl/fl}$* hippocampal slices exposed to 200 μM 4-AP. (A) Whole-cell voltage clamp recordings of CA1 pyramidal neurons (clamped at -70 mV) exposed to alternating applications of control ACSF with or without 200 μM 4-AP. Baseline activity was recorded in the 1st 5-min application of control ACSF before being exposed to 10 min of ACSF containing 4-AP (black bar). The second 5-min washout period preceded a 30-min application of 4-AP, which was followed by a final 5-min washout period. Note the variety of events occurring throughout the recordings, but only large epileptiform events (denoted by red arrows) were selected for analysis. Sometimes events occurred during recording gaps when treatment solutions were alternated. Neuron recording from a control brain slice (Cre$^{(-/-)}$, top trace) includes three large epileptiform events that occurred during washout periods and direct perfusion of 4-AP. In comparison, three large epileptiform events are also recorded in a neuron from a VRAC knockout slice (Cre$^{(+/-)}$, bottom trace). **(B)** Higher magnification of single large epileptiform events recorded in neurons from control (left) and VRAC knockout (right) brain slices. Note that these events have amplitudes in the range of thousands of picoamperes and durations often lasting hundreds of seconds. Only a single neuron recording was obtained per brain slice.

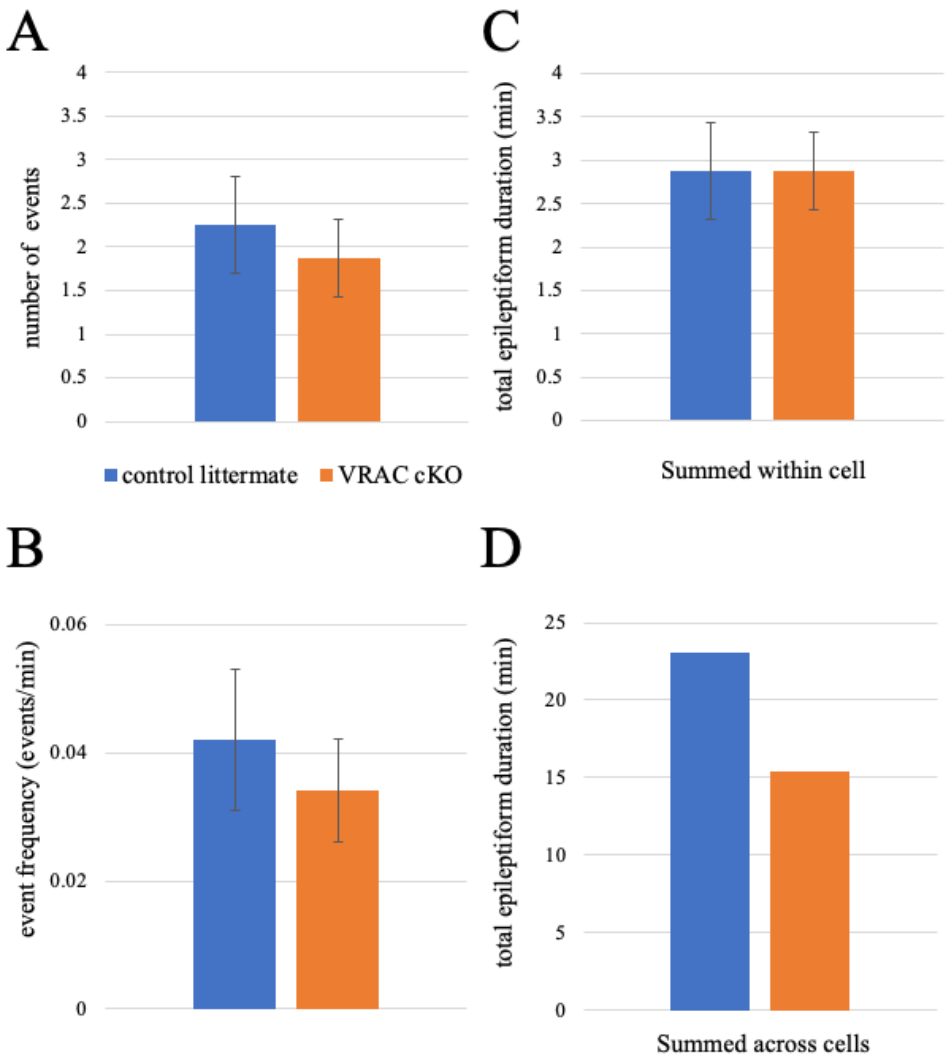
A
number of events
4
3.5
3
2.5
2
1.5
1
0.5
0
control littermate
VRAC cKO
C
total epileptiform duration (min)
4
3.5
3
2.5
2
1.5
1
0.5
0
Summed within cell
B
event frequency (events/min)
0.06
0.04
0.02
0
D
total epileptiform duration (min)
25
20
15
10
5
0
Summed across cells

Figure 4.7: Astrocyte-specific VRAC ablation has no effect on the severity of 200 μM 4-AP-evoked epileptiform activity in *Aldh1l1-Cre^{ERT2};SWELL$^{fl/fl}$* brain slices. Analysis of large epileptiform events from whole-cell voltage clamp recordings of neurons from control (Cre$^{(-/-)}$, blue) and VRAC knockout (Cre$^{(+/-)}$, orange) slices exposed to 200 μM 4-AP. **(A)** The average large epileptiform event number occurring during a 55-min neuron recording (~2 events) was not significantly different between control and knockout slices. **(B)** Average frequency of large epileptiform events (~0.035 events per minute) during these recordings was also not significantly different between groups. **(C)** The average total epileptiform duration of a single cell was slightly less than 3 minutes long and did not significantly differ between groups. **(D)** When every cell's total epileptiform duration was summed across the entire group (control n=8 cells, knockout n=8 cells), the control group's duration (~23 minutes) outlasted the knockout group duration (~15 minutes). Note the total epileptiform duration "across cells" is not a comparison of group averages, but rather a summation of each cell's epileptiform duration within the group.

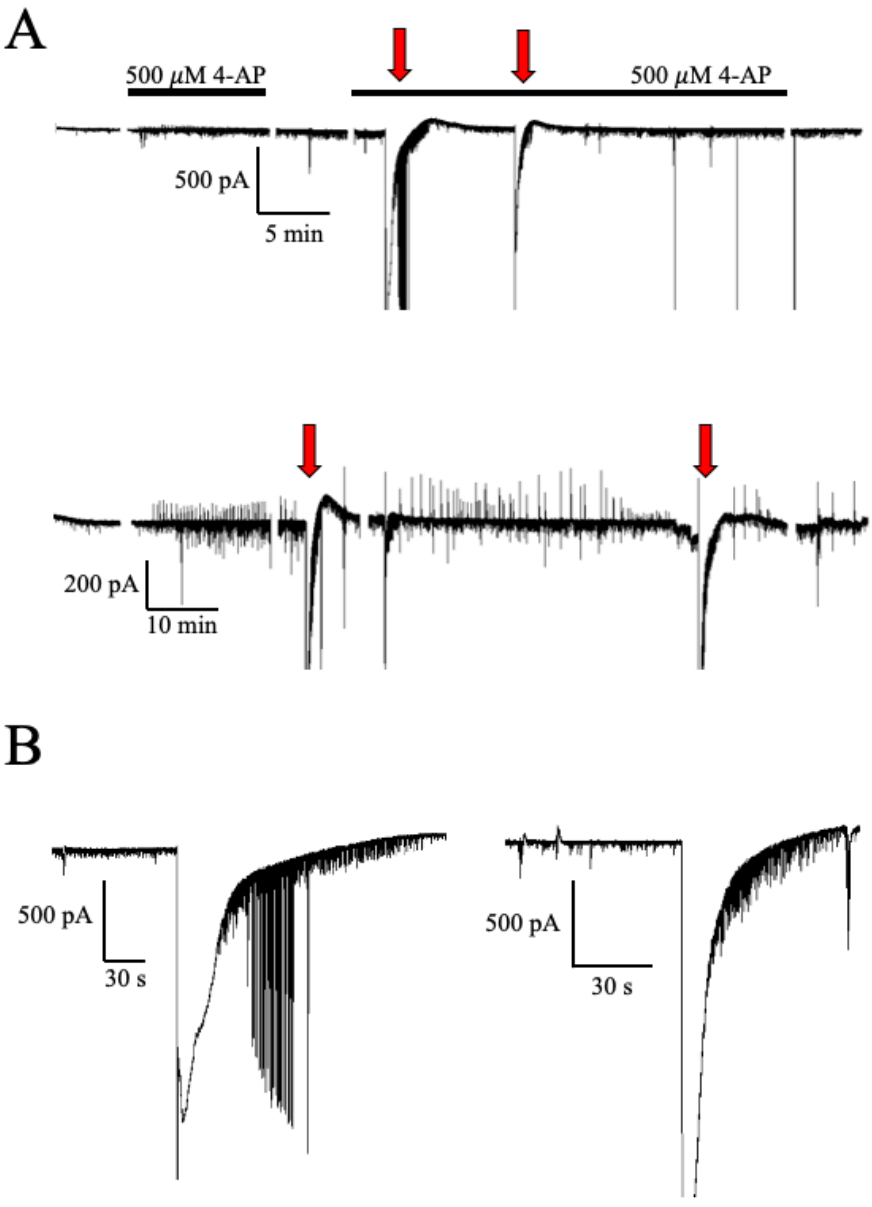
A
500 μM 4-AP
500 μM 4-AP
500 pA
5 min
200 pA
10 min
B
500 pA
30 s
500 pA
30 s

Figure 4.8: Representative epileptiform activity in *Aldh1l1-Cre^{ERT2};SWELL$^{fl/fl}$* hippocampal slices exposed to 500 μM 4-AP. (A) Whole-cell voltage clamp recordings of CA1 pyramidal neurons (clamped at -70 mV) exposed to alternating applications of control ACSF with or without 500 μM 4-AP. Control ACSF was applied intermittently between applications of ACSF with 4-AP (black bar). Large epileptiform events (red arrows) occurred during both treatments. Note these events in the representative neuron recordings from control (Cre$^{(-/-)}$, top trace), as well as VRAC knockout (Cre$^{(+/-)}$, bottom trace) brain slices. **(B)** Individual large epileptiform events are shown at increased scale from control (left) and knockout (right) slice recordings. Note the lack of apparent differences in epileptiform activity between groups. Only a single neuron recording was obtained per brain slice.

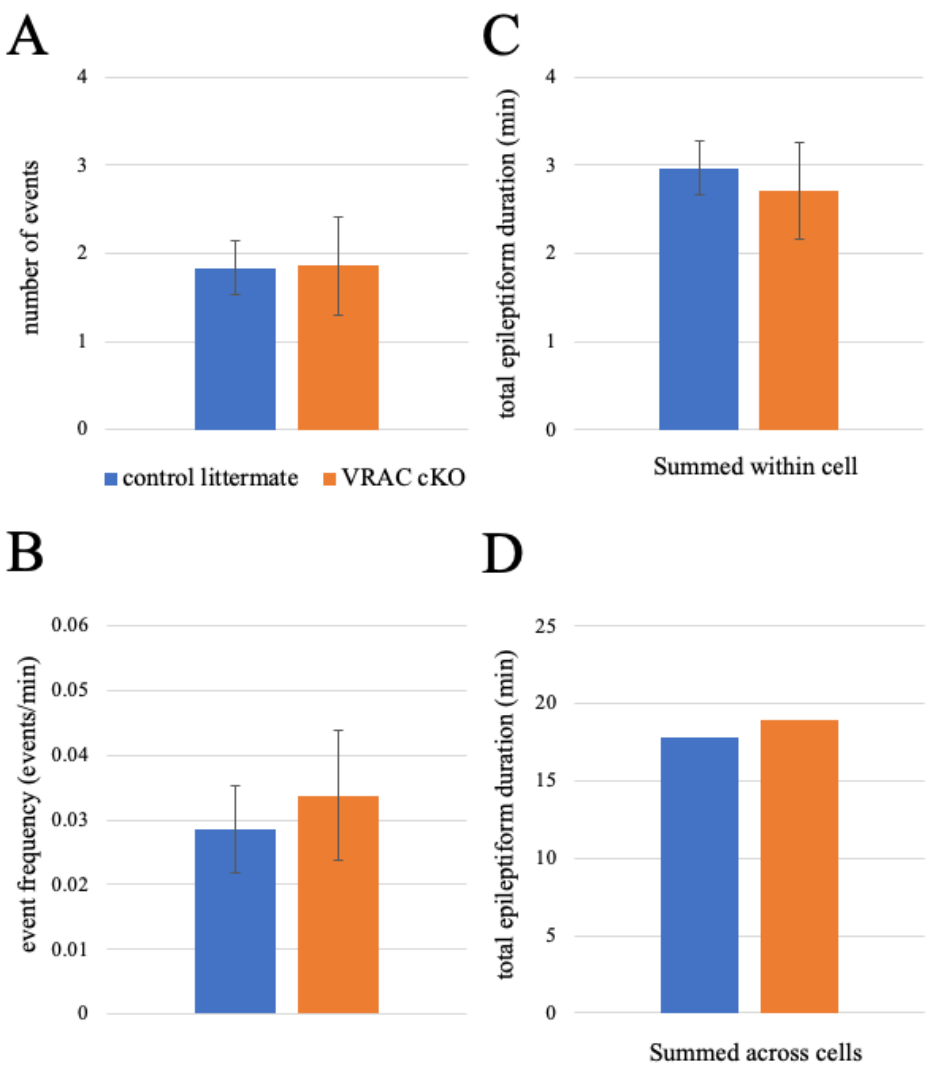
A
number of events
4
3
2
1
0
control littermate
VRAC cKO
C
total epileptiform duration (min)
4
3
2
1
0
Summed within cell
B
event frequency (events/min)
0.06
0.05
0.04
0.03
0.02
0.01
0
D
total epileptiform duration (min)
25
20
15
10
5
0
Summed across cells

Figure 4.9: Astrocyte-specific VRAC ablation has no effect on the severity of 500 μM 4-AP-evoked epileptiform activity in *Aldh1l1-Cre^{ERT2};SWELL$^{fl/fl}$* brain slices. Analysis of large epileptiform events from whole-cell voltage clamp recordings of neurons from control (Cre$^{(-/-)}$, blue) and VRAC knockout ((Cre$^{(+/-)}$, orange) slices exposed to 500 μM 4-AP. **(A)** The average large epileptiform event number occurring during a 55-min neuron recording (~1.8 events) was not significantly different between control and knockout slices. **(B)** Average frequency of large epileptiform events (~0.03 events per minute) during these recordings was also not significantly different between groups. **(C)** The average total epileptiform duration of a single cell was slightly less than 3 minutes long and did not significantly differ between groups. **(D)** When every cell's total epileptiform duration was summed across the entire group (control n=7 cells, knockout n=7 cells), the control group's duration (~18 minutes) was slightly less than the knockout group duration (~19 minutes). These data indicate that ablation of astrocytic VRAC did not influence 4-AP-evoked epileptiform activity and are in agreement with data collected in the same transgenic mouse line (*Aldh1l1-Cre^{ERT2};SWELL$^{fl/fl}$*) at a lower concentration of 4-AP (200 μM, Figure 7).

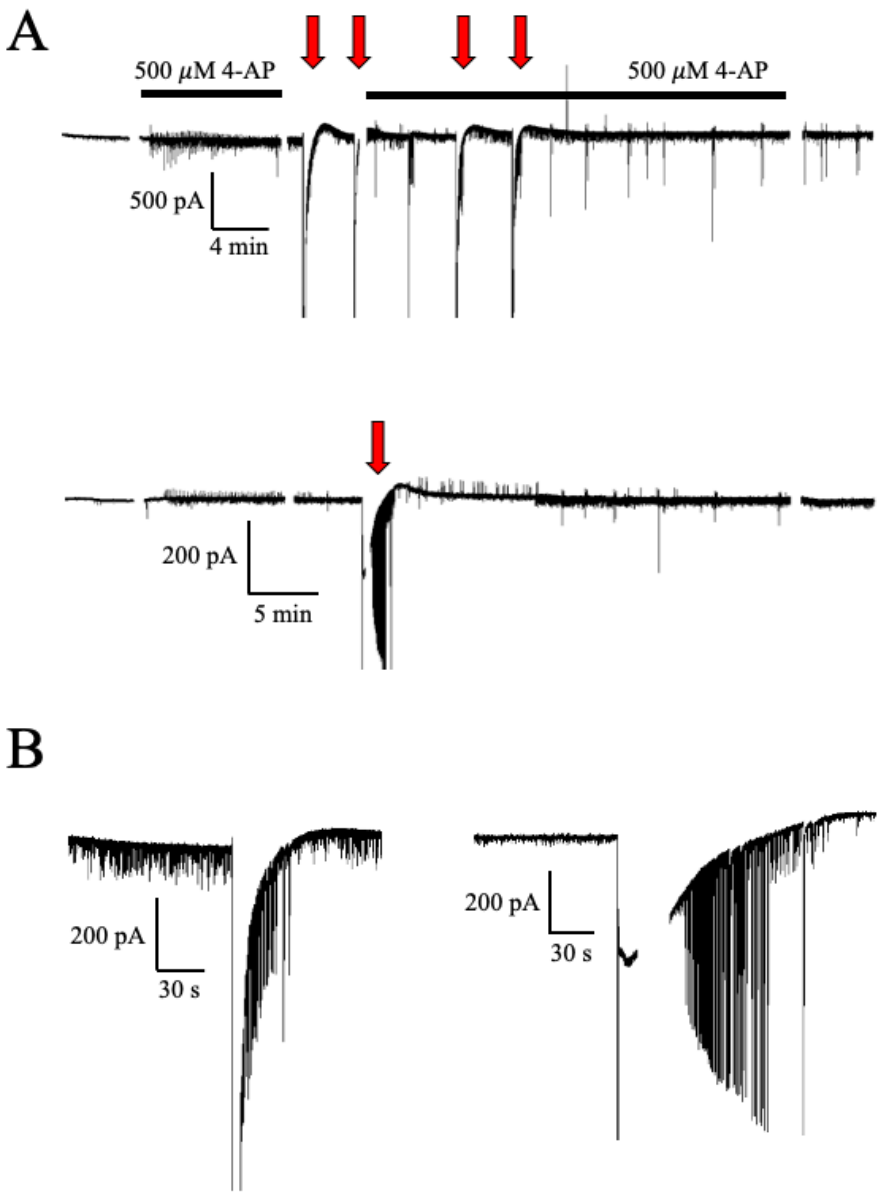
A
500 μM 4-AP
500 μM 4-AP
500 pA
4 min
200 pA
5 min
B
200 pA
30 s
200 pA
30 s

Figure 4.10: Representative epileptiform activity in *Nestin-Cre;SWELL$^{fl/fl}$* hippocampal slices exposed to 500 μM 4-AP. (A) Whole-cell voltage clamp recordings of CA1 pyramidal neurons (clamped at -70 mV) exposed to alternating applications of control ACSF with or without 500 μM 4-AP. Control ACSF was applied intermittently between applications of ACSF with 4-AP (black bar). Large epileptiform events (red arrows) occurred during both treatments. Note these events in the representative neuron recordings from control (Cre$^{(-/-)}$, top trace), as well as VRAC knockout (Cre$^{(+/-)}$, bottom trace) brain slices. **(B)** Individual large epileptiform events are shown at increased scale from control (left) and knockout (right) slice recordings. Although individual epileptiform events look similar between groups, there is an evident increase in large epileptiform event frequency in neurons from control slices in comparison to knockout slices. Only a single neuron recording was obtained per brain slice.

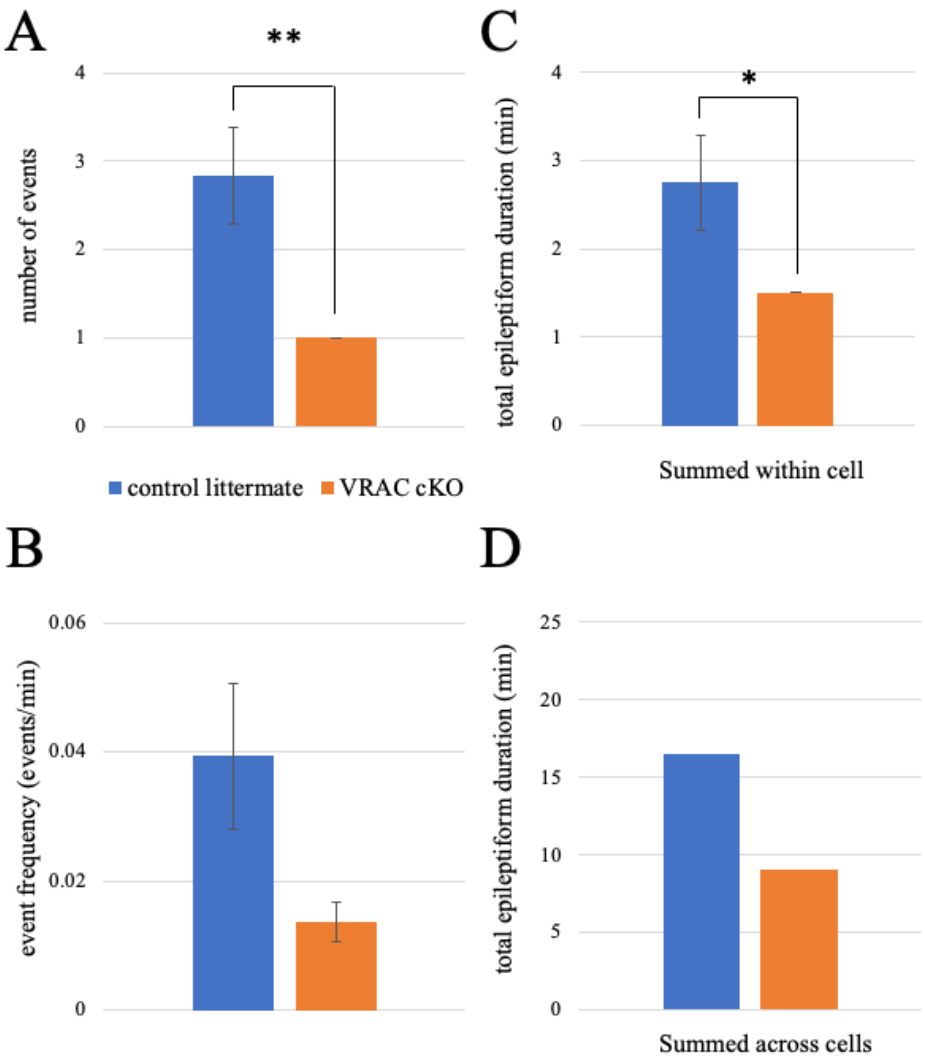
A
**
number of events
4
3
2
1
0
control littermate
VRAC cKO
C
*
total epileptiform duration (min)
4
3
2
1
0
Summed within cell
B
event frequency (events/min)
0.06
0.04
0.02
0
D
total epileptiform duration (min)
25
20
15
10
5
0
Summed across cells

Figure 4.11: Broad VRAC ablation in the CNS significantly reduces the severity of 500 μM 4-AP-evoked epileptiform activity in *Nestin-Cre;SWELL$^{fl/fl}$* brain slices. Analysis of large epileptiform events from whole-cell voltage clamp recordings of neurons from control (Cre$^{(-/-)}$, blue) and VRAC knockout ((Cre$^{(+/-)}$, orange) slices exposed to 500 μM 4-AP. **(A)** Average event number was significantly increased ($p<.01$) in control slice recordings (~2.8 events) compared to knockout slices (~1 event). **(B)** Accordingly, average frequency of large epileptiform events trended toward an increase in control slices (~0.04 events per minute) in comparison to the knockout (~0.015 events per minute). **(C)** Given this increased event frequency, it is unsurprising that average total epileptiform duration per cell was significantly higher ($p<.05$) in neurons from control slices (~2.75 minutes) in comparison to the knockout slices (~1.5 minutes). **(D)** The effects of neuronal VRAC ablation are most prominently observed when total epileptiform duration is summed across cells (control n=8, knockout n=8). Collectively, neurons from control slices endured over 15 min of epileptiform activity in comparison to the much quieter knockout-slice neurons (less than 10 minutes in total duration). Note the minimal variability in knockout slice data values (error bars depict standard error of the mean), reinforcing the significant reduction in epileptiform activity in comparison to littermate controls. *$p < .05$, **$p < .01$, and ***$p < .001$.

Chapter 4

Future Directions

Although this work focused primarily on the volume changes of astrocytes and thus water movement between the intra- and extra-cellular spaces, we largely ignored the intravascular space. This might be a critical oversight when it comes to translating our findings *in vivo*. After all, astrocytes have specialized endfoot processes that envelop the vasculature and have high subcellular localization of AQP4. Despite mounting evidence that AQP4 is uninvolved or largely redundant in the process of astrocyte volume change (Murphy et al., 2017; Walch et al., 2020), ablation of AQP4 has tangible consequences in models of brain edema and ischemia (Manley et al., 2000; Haj-Yasein et al., 2011). These findings suggest that water movement intra- and extra-cellularly is not selectively-gated by AQP4, but volume transmission through the astrocytic endfeet may be dominated by it. Disruption of AQP4 function leads to decreases in brain water content in models of water intoxication (Manley et al., 2000), while AQP4 overexpression drives tissue swelling harder (Yang et al., 2008). Given that $AQP4^{-/-}$ mice have no overt phenotype (Haj-Yasein et al., 2011), the role of AQP4 is likely emphasized under pathologic conditions rather than physiological ones.

To understand the role of AQP4 in mediating water movement between astrocytes and the vasculature, I would propose running water intoxication experiments on three

AQP4-inhibited mouse models, two of which are transgenic and already created ($AQP4^{-/-}$ and α-$syntrophin^{(-/-)}$ mice) and one which needs to be generated. Aquaporin localization in the cell membrane is known to be associated with the dystrophin protein complex (Waite, Brown and Blake, 2012) which is highly expressed in skeletal muscle and more sparingly in the brain (Barnea et al., 1990). Within the dystrophin complex, the syntrophin protein is needed to bind to both dystrophin and a candidate protein to form larger structures. Astrocytes express the α-syntrophin isoform which was found to be important for tethering of AQP4 channels at the astrocytic endfeet (Neely et al., 2001). Interestingly, α-$syntrophin^{(-/-)}$ mice do not display an overt phenotype, but similarly to $AQP4^{(-/-)}$ animals they exert neuroprotective effects under pathological conditions (Mahmood Amiry-Moghaddam et al., 2003).

In order to determine which population of AQP4 channels are essential for water movement through astrocytes, I would generate a third "knockout" approach, where AQP4 channels are selectively targeted on the soma and perisynaptic processes of astrocytes. Targeting this subset of AQP4 channels would be difficult to accomplish with Cre/lox technology. An alternative approach might involve intraventricular injection of an AQP4 blocker such as AER-271 (Wallisch et al., 2019). AQP4 channels expressed on the astrocytic soma and processes would be exposed to this pharmacologic inhibitor, while AQP4 channels wedged in between the astrocytic and endothelial membranes would be far less accessible. If the AQP4-inhibitor can stay bound to channels in a wild-type animal for long periods of time or even days, the animal could then be used as a third AQP4 "knockout" model to compare to $AQP4^{(-/-)}$ and α-$syntrophin^{(-/-)}$ mice. All

mice would be subjected to a commonly used water intoxication model where water is intravenously infused in mice (Manley et al., 2000). The severity of brain edema would be measured by brain tissue water content, intracranial pressure, and histological assessment (Manley et al., 2000). Outcomes of water intoxication would be closely compared between the three mouse models, and the results would provide valuable information regarding the subset of AQP4 channels that are more important in mediating brain edema. Hypothetically, AQP4$^{(-/-)}$ mice would likely be the most protected from edema, because astrocytes would have zero functioning AQP4 channels. If α-syntrophin$^{(-/-)}$ mice had decreased severity of edema in comparison to mice that sustained an intraventricular injection of an AQP4-inhibitor, it would suggest that water movement through AQP4 channels expressed on the astrocytic soma and perisynaptic processes are less important in mediating changes in brain water content in comparison to perivascular AQP4 channels expressed on the astrocytic endfeet. In contrast, less severe edema in AQP4-inhibitor injected animals in comparison to α-syntrophin$^{(-/-)}$ mice would indicate that the opposite. From these studies, the field would gain a better understanding of which subset of astrocytic AQP4 channels are essential for water movement and which are redundant.

References

Amiry-Moghaddam M, Otsuka T, Hurn PD, Traystman RJ, Haug FM, Froehner SC, Adams ME, Neely JD, Agre P, Ottersen OPT, Bhardwaj A (2003) An alpha-syntrophin-dependent pool of AQP4 in astroglial end-feet confers bidirectional water flow between blood and brain. Proceedings of the National Academy of Sciences of the United States of America 100:2106-2111.

Barnea E, Zuk D, Simantov R, Nudel U, Yaffe D (1990) Specificity of expression of the muscle and brain dystrophin gene promoters in muscle and brain cells. Neuron 5:881-888.

Haj-Yasein NN, Vindedal GF, Eilert-Olsen M, Gundersen GA, Skare O, Laake P, Klungland A, Thoren AE, Burkhardt JM, Ottersen OP, Nagelhus EA (2011) Glial-conditional deletion of aquaporin-4 (Aqp4) reduces blood-brain water uptake and confers barrier function on perivascular astrocyte endfeet. Proceedings of the National Academy of Sciences of the United States of America 108:17815-17820.

Manley GT, Fujimura M, Ma TH, Noshita N, Filiz F, Bollen AW, Chan P, Verkman AS (2000) Aquaporin-4 deletion in mice reduces brain edema after acute water intoxication and ischemic stroke. Nature Medicine 6:159-163.

Murphy TR, Davila D, Cuvelier N, Young LR, Lauderdale K, Binder DK, Fiacco TA (2017) Hippocampal and Cortical Pyramidal Neurons Swell in Parallel with Astrocytes during Acute Hypoosmolar Stress. Front Cell Neurosci 11:275.

Neely JD, Amiry-Moghaddam M, Ottersen OP, Froehner SC, Agre P, Adams ME (2001) Syntrophin-dependent expression and localization of Aquaporin-4 water channel protein. Proc Natl Acad Sci U S A 98:14108-14113.

Waite A, Brown SC, Blake DJ (2012) The dystrophin-glycoprotein complex in brain development and disease. Trends Neurosci 35:487-496.

Walch E, Murphy TR, Cuvelier N, Aldoghmi M, Morozova C, Donohue J, Young G, Samant A, Garcia S, Alvarez C, Bilas A, Davila D, Binder DK, Fiacco TA (2020) Astrocyte-Selective Volume Increase in Elevated Extracellular Potassium Conditions Is Mediated by the Na. ASN Neuro 12:1759091420967152.

Wallisch JS, Janesko-Feldman K, Alexander H, Jha RM, Farr GW, McGuirk PR, Kline AE, Jackson TC, Pelletier MF, Clark RSB, Kochanek PM, Manole MD (2019) The aquaporin-4 inhibitor AER-271 blocks acute cerebral edema and improves early outcome in a pediatric model of asphyxial cardiac arrest. Pediatr Res 85:511-517.

Yang BX, Zador Z, Verkman AS (2008) Glial cell aquaporin-4 overexpression in transgenic mice accelerates cytotoxic brain swelling. Journal of Biological Chemistry 283:15280-15286.

Appendix

A juvenile mGFAP-Cre;Rosa26$^{lsl\text{-}tdTomato}$ mice

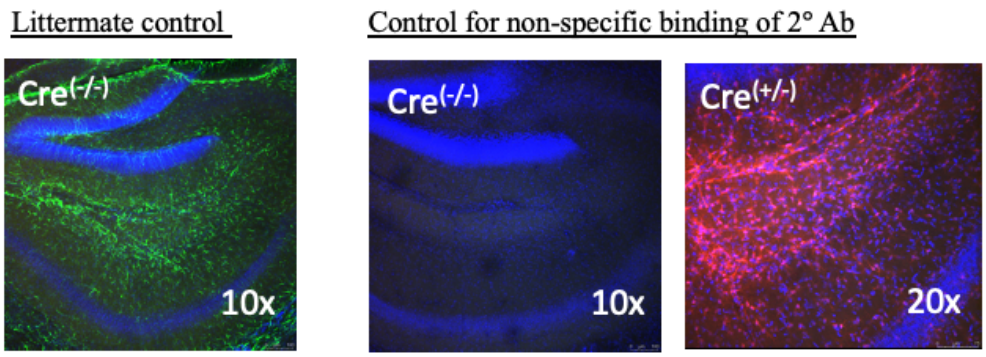

B adult mGFAP-Cre;Rosa26$^{lsl\text{-}tdTomato}$ mice

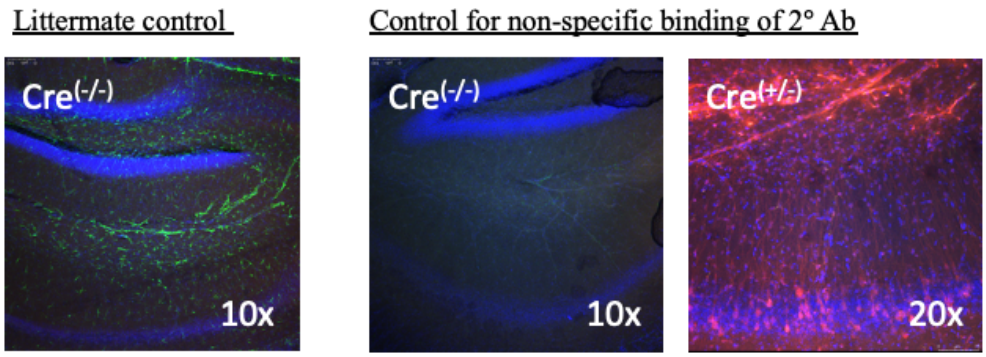

C adult Nestin-Cre;Rosa26$^{lsl\text{-}tdTomato}$ mice

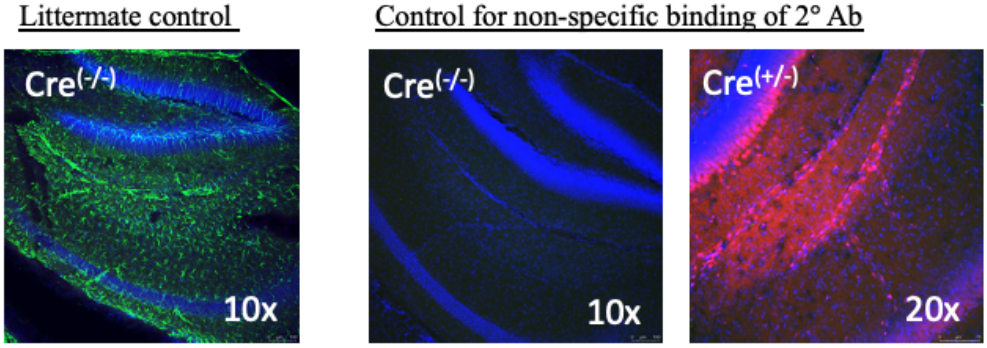

Figure 5.1: IHC from littermate controls and internal controls for non-specific binding of secondary antibody. When all antibodies are applied, the absence of Tdtomato signal in a littermate control confirms $Cre^{(-/-)}$ genotype (left image). In a test for non-specific binding of the secondary antibody (used for Tdtomato amplification), only the secondary antibody was applied to both genotypes (middle and right image). Only $Cre^{(+/-)}$ tissue should contain red signal from endogenous fluorescence (right image). Hippocampal tissue from **(A)** juvenile *mGFAP-Cre;Rosa26*$^{lsl\text{-}tdTomato}$ mice, **(B)** adult *mGFAP-Cre;Rosa26*$^{lsl\text{-}tdTomato}$ mice, and **(C)** adult *Nestin-Cre;Rosa26*$^{lsl\text{-}tdTomato}$ mice are shown.